Diogo Manuel Videira Quintela

SPECTROSCOPIC APPROACHES FOR FORENSIC PROBLEMS

Identification of pre-blast explosive residues and energetic materials by Raman spectroscopy

Dissertação apresentada para provas de Mestrado em Química Forense

Orientador(s)

Prof. Doutor Mário Túlio dos Santos Rosado

Prof. Doutor Carmen García Ruiz

Mestre Félix Zapata Arráez

Julho 2017

Universidade de Coimbra

Acknowledgments

First of all, I give special thanks to my family, my parents, brother and sisters, for the way they have always supported and guided me throughout my life.

It is a great pleasure to acknowledge my deepest thanks for all the guidance, availability and encouragement transmitted by the phD student Félix Zapata Arráez. Thanks also to Professor Carmen García Ruiz and Professor Mário Túlio dos Santos Rosado for all the contribution and availability.

I would also like to thank INQUIFOR group (Research Group in Forensic Chemistry), for the availability in always to help and support.

I would like to express my sincere gratitude to my friends from Portugal, but also to the new friends from Alcalá de Henares, for all the support and good moments spent during this stage.

I leave a huge thank you to my girlfriend Isabel Carolina for the support and encouragement, for the friendship and love.

I could not fail to thank all the colleagues, professors, and friends who supported me directly or indirectly since my entrance to the University, allowing me to remember one of the best phases of my life.

Diogo Quintela

Resumo

Esta tese descreve a aplicação de microscopia Raman confocal para a deteção e identificação de quantidades vestigiais de explosivos orgânicos (trinitrotolueno (TNT), hexogeno (RDX), pentrita (PETN), e hexametileno-triperóxido-diamina (HMTD)), explosivos inorgânicos ("*ammonal*" (AlAN), pólvora negra, "*chloratite*", e pólvora "*flash*"), e sais oxidantes (nitrato de amónio, nitrato de potássio, nitrato de sódio, nitrato de bário, clorato de potássio, clorato de sódio, e perclorato de potássio) presos entre as fibras de tecidos naturais e sintéticos, tingidos ou não. Os espectros Raman foram obtidos a partir das partículas dos explosivos/sais oxidantes por análise "*in situ"* (ou seja, dentro do laboratório) usando o instrumento "*Thermo Scientific DXR Raman microscope*", e por análise imitando situações reais (ou seja, fora do laboratório) usando um Raman portátil ("*portable BWTEK i-Raman pro*") acoplado a um microscópio ótico, usados com os parâmetros instrumentais de origem (sem modificações). As análises tiveram como duração entre 3 - 40 segundos, permitindo obter dimensões de partículas de 2 μm (sais oxidantes), 3 μm (explosivos orgânicos), e 6 μm (explosivos inorgânicos) para o "*Thermo Scientific DXR Raman microscope*", e entre 7 μm (sais oxidantes), 7 μm (explosivos orgânicos), e 18 μm (explosivos inorgânicos) para o instrumento de Raman portátil. Os resultados demonstram que, apesar da contribuição dos tecidos em termos de fluorescência e bandas Raman provenientes das próprias fibras e corantes, foi possível detetar e identificar as partículas de sais oxidantes/explosivos presos nessas superfícies de alta interferência. Além disso, realizou-se uma análise estatística e de quimiometria dos espectros Raman e dados das dimensões das partículas detetadas, que permitiu uma discriminação dos tecidos. No segundo estudo realizado, a identificação e deteção de nitrato de potássio misturado com dez diferentes substâncias interferentes (que atuam como combustíveis em explosivos caseiros) foi possível usando ambos os instrumentos Raman.

Palavras-chave: espectroscopia Raman, microscopia Raman confocal, deteção vestigial, artefacto explosivo improvisado ("*Improvised explosive device, IED*"), explosivos caseiros ("*Homemade explosives, HMEs*"), sais oxidantes, explosivos orgânicos e inorgânicos, têxteis.

Abstract

This thesis reports the application of confocal Raman microscopy to the detection and identification of trace amounts of organic explosives (trinitrotoluene (TNT); hexogen (RDX); penthrite (PETN); and hexamethylene triperoxide diamine (HMTD)), inorganic explosives (ammonal (AlAN); black powder; chloratite; and flash powder), and oxidizing salts (ammonium nitrate, potassium nitrate, sodium nitrate, barium nitrate, potassium chlorate, sodium chlorate, and potassium perchlorate) trapped between the fibres of dyed and undyed synthetic and natural textile clothing fabrics. Raman spectra were obtained from the explosive/oxidizing salt particles by in situ and on-field analysis using the Thermo Scientific DXR Raman microscope, and a portable BWTEK i-Raman pro system attached to an optic microscope, respectively, both with the standard instrument components (with no instrument modifications). Analysis were made within 3 to 40 s given particle dimensions as small as 2 μm (oxidizing salts), 3 μm (organic explosives), and 6 μm (inorganic explosives) for the Thermo Scientific DXR Raman microscope, and 7 (oxidizing salts), 7 μm (organic explosives), and 18 μm (inorganic explosives) for the portable BWTEK i-Raman pro. The results show that, despite the contribution of the textile fabric in terms of fluorescence and vibrational bands coming from the fibres and dyes, detection and identification of the explosive/oxidizing salt particles trapped on highly interfering surfaces was possible. Furthermore, by doing a statistic and chemometric analysis of the Raman spectra and particle size data, discrimination of the textile fabrics was made. In addition, a second study was made in which identification and detection of the potassium nitrate mixed with ten different interfering substances (that act as fuels in homemade explosives), was possible using both the Raman instruments.

Keywords: Raman spectroscopy, confocal Raman microscopy, trace detection, improvised explosive devices (IEDs), homemade explosives (HMEs), oxidizing salts, organic explosives, inorganic explosives, clothing textiles.

"Ever tried. Ever failed. No matter.
Try again. Fail again. Fail better."

Samuel Beckett

Table of Contents

List of Tables

List of Figures

Abbreviations

α – Polarizability

π – Dipole moment

AN – Ammonium nitrate

AP – Ammonium perchlorate

ANFO – Ammonium nitrate with fuel oil

AlAN – Aluminium powder with ammonium nitrate

C-4 – Composition C-4

CCD – Charge-coupled device

DNT – 2,4-Dinitrotoluene

E – Electronic field

EOD – Explosive Ordnance Disposal

FT – Fourier transform

GC-MS – Gas chromatography-mass spectrometry

HMX – Octogen

HMTD – Hexamethylene triperoxide diamine

HPLC-MS – High-performance liquid chromatography-mass spectrometry

HME – Homemade explosive

IED – Improvised explosive device

LOD – Limit of detection

LWP – Long-wave-pass

MeV-SIM – Mega-electron volt-secondary ionization mass spectrometry

NIR – Near infrared

PETN – Pentaerythritol tetranitrate

PBX – Polymer-based explosive

PCA – Principal component analysis

PC1 – Principal component 1

PC2 – Principal component 2

PERC – Perchloroethylene

PMT – Photomultiplier detector

PDA – Photodiode array detector

RRS – Resonance Raman spectroscopy

RDX – Hexogen

SEM – EDS/WDS

SERS – Surface-enhanced Raman spectroscopy

SERRS – Surface-enhanced resonance Raman spectroscopy

SORS – Spatially offset Raman spectroscopy

SWP – Short wave-pass

SEM-FIB – Focussed ion bean scanning electron microscope

TNT – 2,4,6-Trinitrotoluene

TATP – Triacetone triperoxide

TRRS – Time-resolved Raman spectroscopy

TEDAX – "*Técnico especialista en desactivación de artefactos explosivos*"

UV – Ultraviolet

XRF – X-Ray fluorescence

XRD – X-Ray diffraction

Chapter 1

Introduction

1.1 Introduction to explosives

Explosives are energetic chemical substances (either liquid, solid or gaseous, alone or mixed), that are capable of undergoing a rapid chemical reaction without the participation of external reactants such as atmospheric oxygen (i.e. because the substance has its own supply of oxygen). On application of a suitable stimulus (e.g. by mechanical means, heat, or detonating shock), they are properly ignited and subjected to certain phases which result in a chemical explosion including growth of deflagration, the transition to detonation, the propagation of detonation, and the liberation of a large amount of heat and gases. [1-5]

In brief, any explosion is the result of a sudden release of large quantities of energy in a violent manner, accompanied by noise, heat and pressure (blast waves). [1-5] According to Figure 1, every explosion might be classified into a physical/mechanical, atomic/nuclear explosion or chemical explosion.

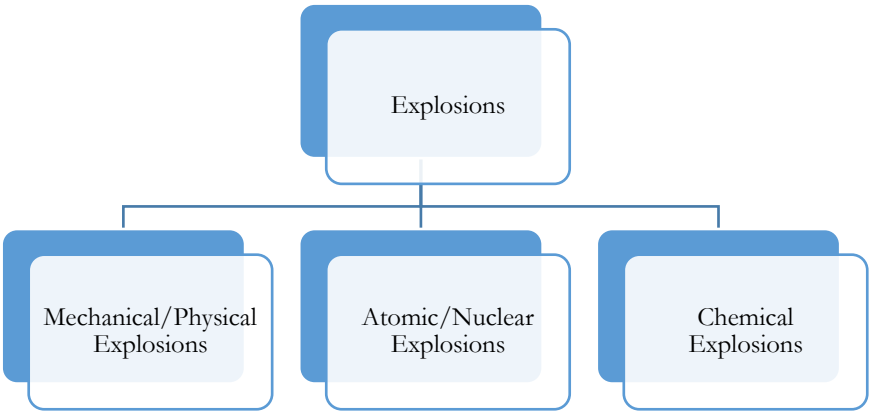

Figure 1. Classification of explosions according to their nature.

The chemical explosions are the result of the sudden release of energy caused by an extremely fast chemical reaction (exothermic transformation), normally between substances with explosive properties, resulting in the generation of large quantities of gases, and heat.

The high temperatures and pressures is responsible for producing a pressure wave that causes damage to the surrounding medium. If these pressure waves are subsonic (i.e. the speed of the propagation wave is lower than the speed of sound in medium), the explosion is characterized as deflagration (i.e. rapid combustion), in which the explosive substance decomposes at a rate below the sonic velocity of the unreacted material, and is propagated by the released heat of reaction. [1, 2, 3, 5] If the pressure wave is supersonic (i.e. referred as shockwave), the explosion is named as detonation, where the explosive substance decomposes at a rate greater than the sonic velocity of the unreacted material producing a shockwave, that may cause the detonation of adjacent explosive substances (contained in the explosive train as explained in section 1.2 - B). These concepts are used to classify the chemical explosives as high or low explosives, being the first subjected to detonation and the second to deflagration as explained in section 1.1.1.2.1. [1, 2, 3, 5]

Chemical explosives can be either pure compounds or a mixture of several compounds. Pure explosive compounds, generally contain both an oxidizer group (e.g. nitrogen groups, peroxide groups, etc.) and a fuel group (e.g. hydrocarbon chain) in the same molecule (e.g. the organic explosives: TNT, RDX, HMX, PETN, etc.). Explosive mixtures are usually the combination of two or more components that separately are oxidizer and fuel compounds (e.g. the inorganic explosives: ANFO, ammonal, chloratite, black powder, etc.). [1, 2, 6]

1.1.1 Classification of explosives

1.1.1.1 Classification of explosives based on their molecular structure

Explosives may be classified according to the chemical nature of the bonds present in certain molecular groups, responsible for their explosive properties. There is not a standard classification regarding the molecular structure of the explosives. Over the years, there has been a couple of classifications that can be accounted for. One classification was done by Plets in 1953 [1, 2], that explains that the explosive properties depend upon the presence of "explosophores" (i.e. molecular groups with explosive properties) and "auxoploses" (i.e. used to fortify or modify the explosive properties), classifying the explosives into eight classes as shown in Table 1.

Table 1. Plets classification of explosive substances by their molecular groups. [1, 2]

Molecular Group	Explosive compounds
$-NO_2$ and $-ONO_2$	Organic and inorganic compounds (e.g. $C_6H_3(NO_2)_3$, HNO_3 etc.)
–N=N- and –N=N=N–	Inorganic and organic azides and diazo compounds (e.g. CH_3N_3 etc.)
$-N-X_2$	X is a halogen;
–C=N–	Fulminates ($Hg(ONC)_2$) and fulminic acid (HONC)
–O–O– and –O–O–O–	Inorganic and organic peroxides and ozonides, respectively
$-OClO_2$ and $-OClO_3$	Inorganic and organic chlorates and perchlorates respectively (e.g. $KClO_3$, $KClO_4$, NH_4ClO_4 etc.)
–C≡C–	Acetylene and metal acetylides;
M–C	Metal bonded with carbon in some organometallic compound

In another classification, Paul W. Cooper [7], given the different molecular substituent groups found in explosive substances, classifies them in four different substituent groups regarding their contribution in terms of oxygen, fuel, both or the ones that only contribute with energy (e.g. azides). Table 2 shows the different molecular substituent groups found in pure explosives.

Table 2. Molecular substituent groups found in explosives by Paul W. Copper. [7]

Name	Molecular substituent groups
Oxidizer contributors	$-ONO_2$, $-NO_2$, –NO, $-NF_2$, –OH, –COOH etc.
Fuel contributors	Alkyl, $-NH_2$, $-NH_4$
Combined fuel and oxidizer contributors	–ONC (fulminate), $-NH-NO_2$ (nitramines)
Other bond energy contributors	$-N_3$ (azides)

A limitation of the classification given in Table 2 is that it does not consider that only few compounds that have hydrocarbon chains combined with those substituent groups are explosives. Explosive substances respect a special set of characteristics, such as stability, toxicity, handling and other factors, that diminishes the structures considered as explosive compounds. [1, 2, 7] Given this, Paul W. Cooper [7] divided the explosives as shown in Figure 2.

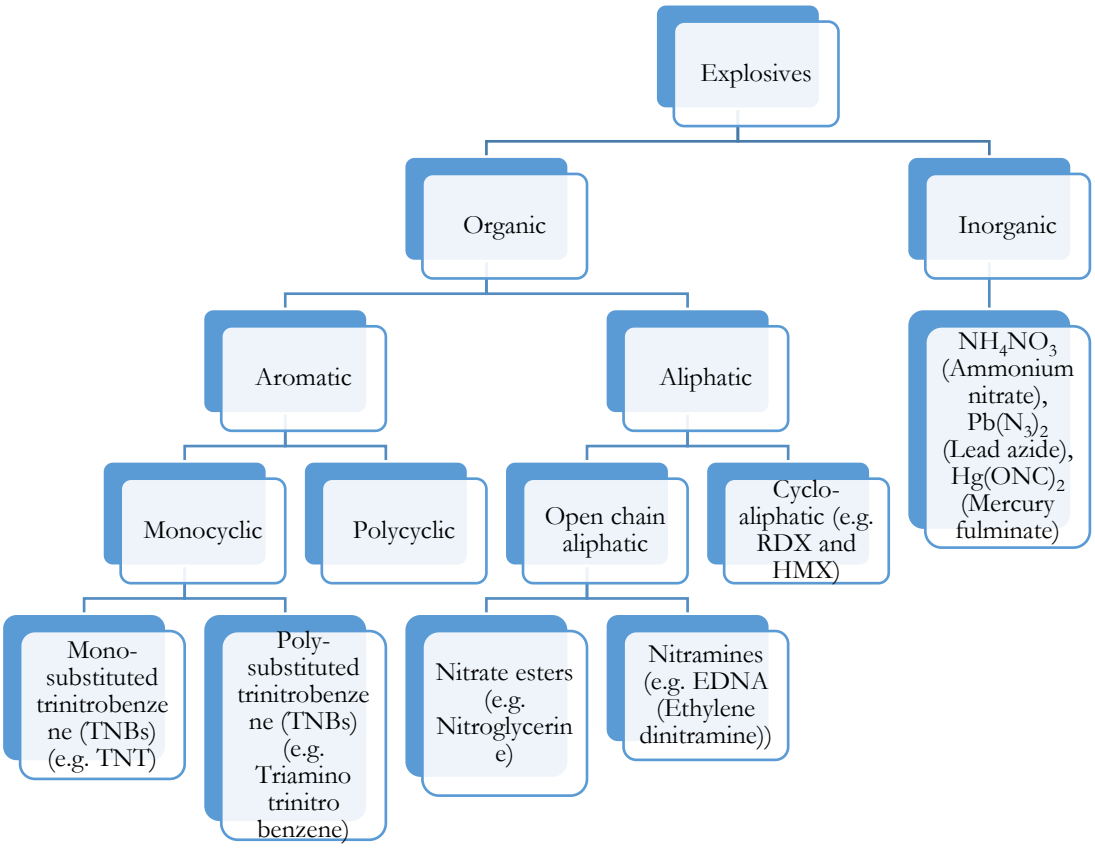

Figure 2. Classification of explosives based on their molecular structures by Paul W. Copper. [1, 2, 7]

1.1.1.2 Classification of explosives based on their performance and uses

The explosives may be classified according to their end-use (see appendix 1), as military explosives used for military applications (e.g. guns, warheads, and rockets), civilian explosives used for commercial applications (divided by demolitions and pyrotechnics), and homemade explosives. Figure 3 displays the classification of the military explosives, as high- and low-explosives (propellants). High-explosives are said to detonate, while low-explosives deflagrate. High-explosives can be further sub-categorized according to their sensitivity, as either primary, secondary or tertiary explosives, and low-explosives as gun or rocket propellants. [1-3, 5, 8]

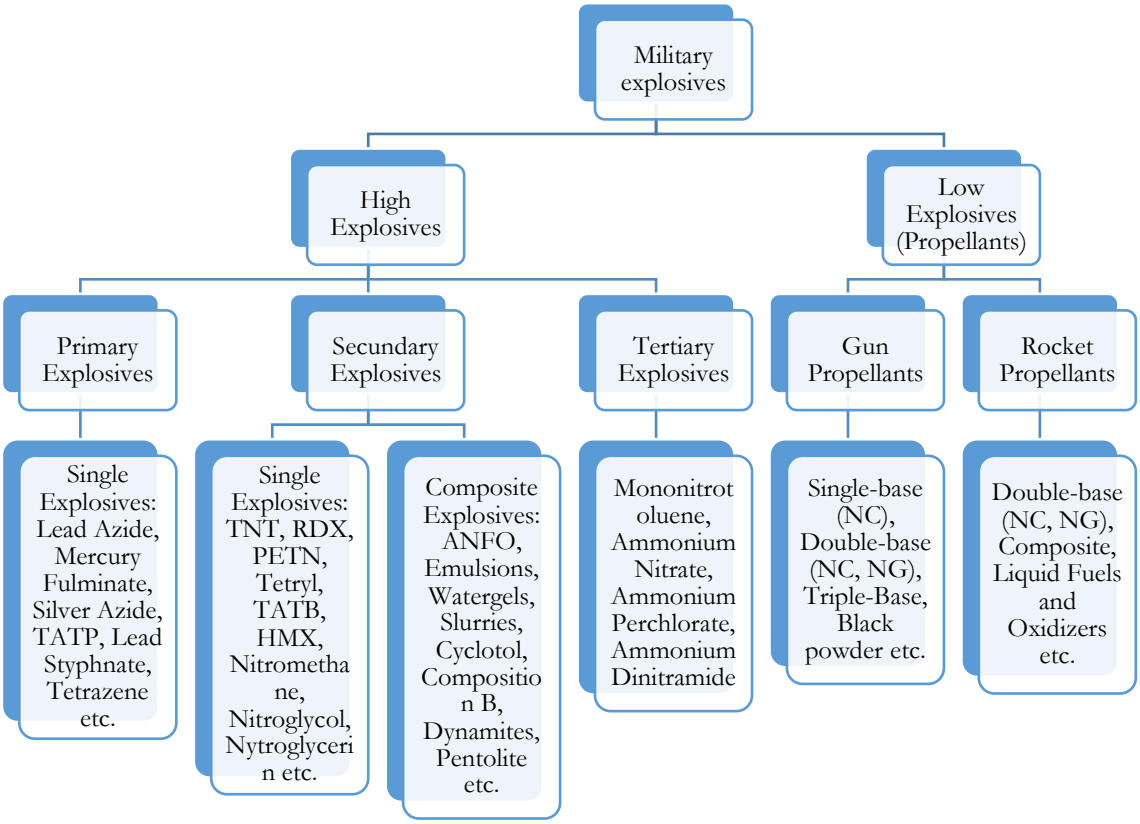

Figure 3. Classification of the military explosives. [1, 2, 5, 8]

1.1.1.2.1 Military explosives

Military explosives are normally used in military ammunitions such as, mines, bombs, rocket warheads, grenades, etc. The main charge used in most of these ammunition devices consists in insensitive secondary explosives triggered by means of an explosive train (see section 1.2 - B). The main characteristics of the military explosives are represented in Appendix 2. In general, this type of explosives needs to fulfil certain quality requirements, such as high performance, insensitivity regarding firing/impact safety, stability in terms of temperature and humidity, good storage life and transportation stability, rendering them valid and functional during battlefield conditions. Apart from these requirements, the availability of raw materials, ease of manufacture and cost, are also important factors. [2, 3, 8]

1.1.1.2.1.1 High or detonating explosives

These explosives suffer detonation and disintegrate at the molecular level as a shockwave travels through them. According to their sensitivity, they are sub-divided into: A. primary high explosives or initiatory explosives (usually used as initiators or primers), B. secondary high explosives, and C. tertiary explosives, the first being the most sensitive and the third the least.

A. Primary or initiatory explosives

Primary explosives are extremely sensitive, detonating when subjected to heat, spark, friction, shock or mechanical impact. They are also very unstable being generally used in small quantities. They undergo a very rapid deflagration-to-detonation transition and are normally used in initiating devices (e.g. initiator or primer in an explosive train), because of their ability to transmit the detonation to less sensitive explosives (e.g. secondary explosives). [1-3, 8] Figure 4 shows examples of primary explosives.

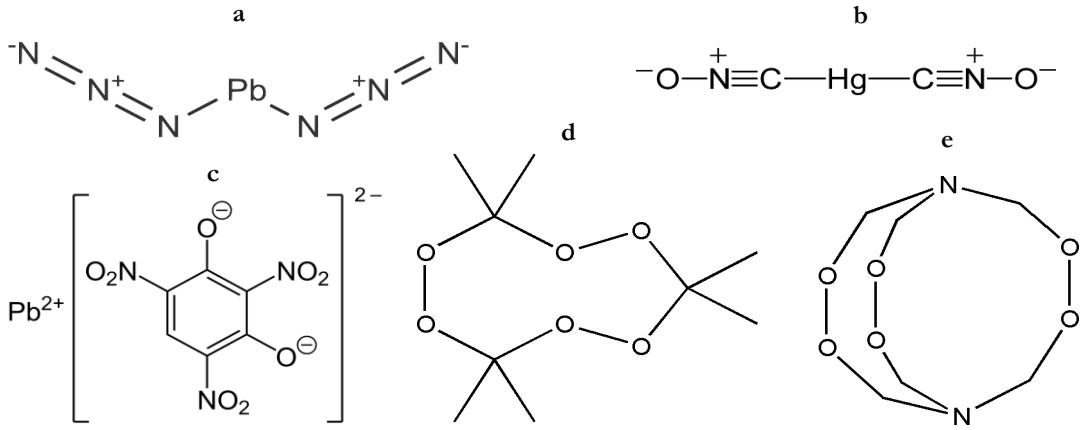

Figure 4. Chemical structure of the (a) lead azide, $Pb(N_3)_2$ (b) mercury fulminate, $Hg(ONC)_2$ (c) lead styphnate, $C_6HN_3O_8Pb$ (d) Triacetone triperoxide (TATP), $C_9H_{18}O_6$ (e) Hexamethylene triperoxide diamine (HMTD), $C_6H_{12}N_2O_6$.

B. Secondary explosives

The secondary explosives are less sensitive to stimulus (e.g. impact or friction), powerful, stable and generally initiated by shockwaves. When subjected to heat, impact or friction they do not detonate, instead they are initiated (or detonated) by the shockwave of the detonated primary explosive in an explosive train. Inside this explosive category we can

divide them into single (e.g. TNT, RDX, HMX and CL-20) or composite explosives. The latter are composed of mixtures of several explosives (e.g. composition B, cyclotol and octol); mixture of single explosives with inert plastic binders (mostly polymers) called plastic explosives (e.g. C-4, and semtex); or mixture of single explosives with energetic plastic binders (i.e. they have an energetic functional group that improves the explosive charge performance) and energetic or non-energetic plasticizers (i.e. capable of improve safety characteristics and modifying the mechanical proprieties of the final composition) called polymers-based explosives (PBX). [2, 3, 8]

They can also be classified regarding the type of element bonded to the NO_2 radical and the type of nitration involved in their synthesis (classification by molecular structure). [1, 2] Secondary explosives can be classified as nitramines with a N–NO_2 bond (e.g. RDX, HMX, tetryl), nitro-aromatics with a C–NO_2 bond (e.g. TNT, DNT) and nitric-esters with a O–NO_2 bond (e.g. nitroglycerine, nitroglycol, PETN, nitrocellulose). Figure 5 shows some examples of secondary explosives. [1, 2]

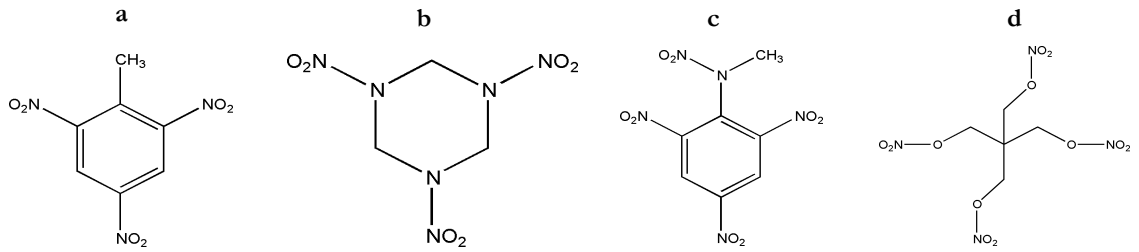

Figure 5. Chemical structure of the (a) 2,4,6-Trinitrotoluene (TNT), $C_7H_5N_3O_6$ (b) Hexogen (RDX), $C_3H_6N_6O_6$ (c) Tetryl, $C_7H_5N_5O_8$ (d) Pentaerythritol tetranitrate (PETN), $C_5H_8N_4O_{12}$.

C. Tertiary explosives

Tertiary explosives when compared to primary or secondary explosives are more difficult to be initiated by any mechanical or heat stimulus. They, besides the primary explosive, require a booster with secondary explosive to detonate. They are relatively low-sensitive explosives usually based on oxidizing salts such as ammonium nitrate (AN) (NH_4NO_3), ammonium perchlorate (AP) (NH_4ClO_4), ammonium dinitramide ($NH_4N(NO_2)_2$) or ammonium nitrate fuel oil (ANFO). [2, 8]

1.1.1.2.1.2 Low or deflagrating explosives

Also, called propellants, the low explosives differ from high explosives because they undertake deflagration instead of detonation. They are combustible materials that do not explode or detonate. When initiated by a flame or spark they burn at a very high rate, resulting in large volumes of high pressure and hot gases. Therefore, these explosives when confined in a closed container may lead to an explosion, because of the pressure formed during the production of the hot gases, making these explosives ideal to expel projectiles from weapons. Without containment, the gases merely dissipate as a cloud of smoke. [2, 3, 8] Examples of propellants are black powder or smokeless powders. The first is a mixture of potassium nitrate, charcoal, and sulphur, and the latter are nitrocellulose based propellants commonly used in military and civil ammunition. The smokeless powders can be divided into single-base powders containing mainly nitrocellulose, double-base powders containing nitrocellulose and nitroglycerine, and triple-base powders containing nitrocellulose, nitroglycerine and nitroguanidine. [8, 9] In appendix 3, the propellants are classified based on their end-use: small arms, mortar, gun, and rocket propellant. The compounds named composite propellants are mainly inorganic oxidizers (e.g. AN or AP) dispersed in a polymeric fuel-binder matrix. [2, 5] It should be noticed that these types of explosives are easily obtained and are likely to be encountered in IEDs, making them important in explosive detection of IEDs.

1.1.1.2.2 Civil or commercial explosives

Contrary to military explosives, the applications of commercial explosives include mining, quarrying, construction or tunnel building (i.e. demolitions), and pyrotechnics. Commercial explosives also have different characteristics in terms of explosive performance, sensitivity, stability on storage, and thermal behaviour, making them valid commercial explosives for industrial applications. For demolitions, they are mostly low-velocity high explosives (e.g. dynamite) because of their ability to break without shattering materials, such as rocks. They include ethylene glycol dinitrate with ammonium nitrate-based explosives (e.g. dynamites), ammonium nitrate-based formulations (e.g. ANFO), emulsion explosives (water

in oil with oxidizers like nitrates) and slurry explosives (mixtures of inorganic nitrates, gum, water, sensitizing agents, etc.). [2-4]

Pyrotechnics are mixtures used to produce different effects than those produced by high or low explosives. These effects can be categorized into four groups: light (for illumination, tacking or signalling), heat (for igniters and incendiaries), smoke (for signalling) and sound (for signalling or distraction). [5] Regarding their chemical structure, they are a powdered mixture of an oxidizer and a fuel, together with other additives such as binders or colour-giving metals (see appendix 4) for given them stability and the corresponded special effects. [5, 8] An example is the flash powder that is a mixture of potassium perchlorate ($KClO_4$) and aluminium powder, used in firecrackers for commercial applications.

1.1.1.2.3 Homemade explosives (HMEs)

These latter include the homemade explosives used in improvised explosive devices (IEDs). Normally, homemade explosives are manufactured from purchased reagents (i.e. energetic materials), such as mixtures of powdered oxidizing salts with fuel. The full explosive used as HME, cannot be bought since no company sells it (i.e. they are not commercialized) because of their instability.

In their composition, they may have liquid or solid homemade explosives, or liquid/solid explosive mixtures that contain energetic materials (see Table 3). [10, 11] Most of the explosives used as HMEs are unsuitable for commercial and military use, because of their unfavourable properties, such as low performance (nitromethane), high sensitivity (TATP), thermally instability (nitrourea), or chemically instability (urea nitrate). [10, 11] Peroxide-based IEDs are becoming a major threat to public safety because of their ease of manufacture and initiation, and the difficulty to be detected due to their high volatility and vapour pressure. One downside for the bomb makers is that the synthesis of peroxide explosives (e.g. TATP and HMTD) and the corresponding manipulation into an explosive device is very dangerous because of their high sensitivity (they are classified as primary explosives) and lack of stability. They can be synthesized using highly aqueous H_2O_2 (hydrogen peroxide) concentrations, which are nevertheless much more concentrated than normally used for commercial or domestic purposes. Thus, the detection of hydrogen

peroxide in high concentration would be very indicative of IED peroxide-based manufacture. [3, 12]

Regarding energetic materials (Table 3) used in homemade explosives, they may have explosive properties or not, are generally easy to obtain, and have the main role of enhancing the explosive power of the device. Oxidizing salts are usually used in combination with fuels (e.g. petrol/gasoline, diesel/fuel oil, alkanes, kerosene, charcoal, sugar, alcohols, etc.), which are flammable materials. [10, 13]

Table 3. Energetic materials that may be found in liquid and solid HMEs. [10, 11, 13]

Energetic materials found in liquid and solid HMEs	Observations
Hydrogen peroxide, H_2O_2	Oxidizer, used in disinfection applications, etc.
Nitric acid, HNO_3	Oxidizer, used as nitrating agent in the manufacture of explosives.
Methyl ethyl ketone peroxide (MEKP), $C_4H_8O_2$	Curing agent in diluted form;
Isopropyl nitrate (IPN), $C_3H_7NO_3$	Used as fuel.
Nitrocellulose (NC), $[C_6H_7N_3O_{11}]_n$ (n=1000-3000)	Component of smokeless powders; In pure form is an explosive.
Potassium chlorate (PC), $KClO_3$	Oxidizer used in pyrotechnics; SC is the main component of chloratite;
Sodium chlorate (SC), $NaClO_3$	
Ammonium perchlorate (AP), NH_4ClO_4	Oxidizer used in rocket motors or in the pyrotechnics; PP is the main component of flash powder
Potassium perchlorate (PP), $KClO_4$	
Ammonium nitrate (AN), NH_4NO_3	Components of commercial liquid explosives (e.g. ANFO, dynamites). Used in fertilizers, pyrotechnics, etc; AN is the main component of ammonal.
Sodium nitrate (SN), $NaNO_3$	
Potassium nitrate (PN), KNO_3	Used as fertilizer; Main component of black powder.

1.2 Improvised explosive devices (IEDs)

In recent years, several terrorist attacks, including those in Madrid (2004), London (2005), Paris (2015), Brussels (2016) and Manchester (2017), as well as, attacks in active warzones such as, Afghanistan, Syria and Iraq, have led to greater concern towards IEDs. According to the Department of defence dictionary of military terms [14], IED is "a weapon that is fabricated or emplaced in an unconventional manner incorporating destructive, lethal, noxious, pyrotechnic, or incendiary chemicals designed to kill, destroy, incapacitate, harass,

deny mobility, or distract". They consist of liquid/solid explosives or mixtures made of either commercial, military or homemade explosives (HMEs), easily synthesized in homemade conditions using readily available chemicals (with kitchen and other household materials replacing laboratory grade equipment without proper security protocols or hygiene). [3, 10] Normally, this type of device is placed at public places, such as roadsides or streets, city squares or confined spaces (e.g. airports, train stations, etc.). [15, 16] Thus, the concealment or masking of the device is often necessary, making the detection of IEDs extremely difficult. Figure 6 represents a general schematic of an improvised explosive device and the corresponding components, which are explained in more detail below.

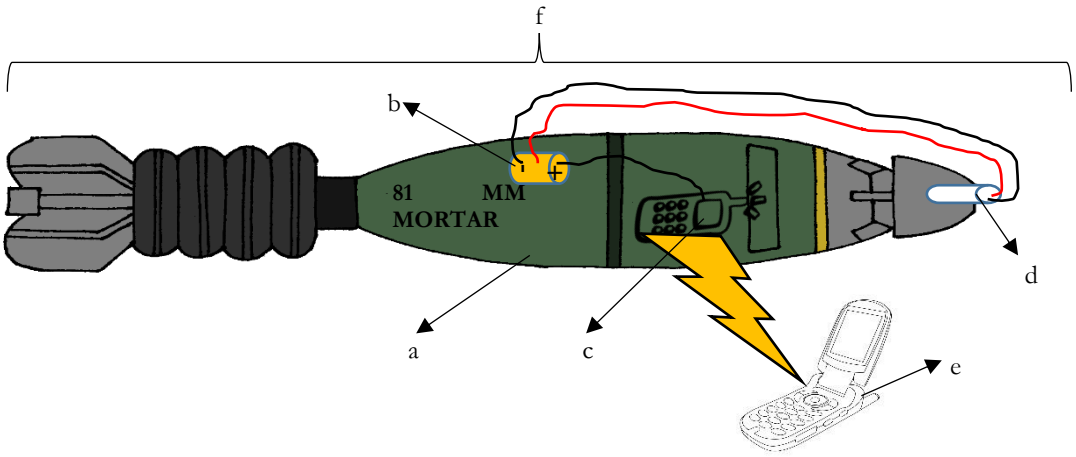

Figure 6. Schematic representation of an improvised explosive device (IED): (a) main charge (b) power source (c) switch (receiver) (d) initiator (e) trigger (transmitter) (f) container.

A. Main charge

Depending on the availability of the pure explosives or the ingredients necessary for their manufacture, IEDs may contain commercial, military or homemade explosives as main charge (see appendix 5). For commercial and military explosives, low explosives such as black powder or smokeless powder are usually encountered in IEDs because of their availability by disassembling of commercial fireworks or military ammunition. [16-19] Although low explosives are more easily to be obtained, most IEDs use high explosives (e.g. C-4, Semtex, etc.). These are more difficult to obtain (in pure forms) because of their stringent controls by governments all over the world. However, they are sometimes subjected to burglary from storage containers of military facilities. Since commercial and military explosives are more

controlled, nowadays, the main charge of the IEDs shifts to the use of HMEs (explained in the section 1.1.1.2.3). [5, 19]

Although IEDs can be manufactured from a large variety of explosive materials including military, commercial, or homemade explosives, they generally contain explosive mixtures based on energetic oxidants including nitrate, chlorate or perchlorate salts. The simplicity of combining these energetic salts with fuels, the large availability found in multiple commercial explosives (e.g. black powder), and ease of manufacture, makes them suitable for IEDs production. [10, 17] Thus, the analytical analysis of IEDs mainly involves the detection of these oxidizing salts.

B. Initiating system and initiation techniques

Commercial or military type explosive devices are initiated or detonated using an explosive train (or firing train), which is an arrangement of explosive components, namely, a detonator (initiator), a booster, and a main charge, that has the capability to transmit and intensify the initial force giving by the initiator, until it reaches and sets off the main charge. [2, 3, 17]

Depending on the type of explosive used as the main charge, initiators are classified as detonator or igniter (Figure 7). The detonators are mainly used for the initiation of low-sensitive explosives (e.g. secondary explosives), by the propagation of a shockwave. Due to their sensitivity, primary explosives are normally the first component, which, by the presence of a stimulus, will burn to initiation, producing the shockwave that will detonate the secondary main explosive. That stimulus can be provided by electrical discharge, friction, stabbing, percussion or flash. The igniters/initiators differ from the detonators in the type of explosive substance used in the main charge and the initiation system. The chemical explosives used as initiators are low deflagrating explosives (or propellants), that only require a flame, spark or flash to be initiated, instead of a shock (shockwave) produced by detonators. In the category of the igniters, a fuse (or burning fuse) which is designed to carry a spit of flame to initiate low explosives and the electric match (or squib) normally filed with an explosive that deflagrates, are the most common ones. [2, 15, 17]

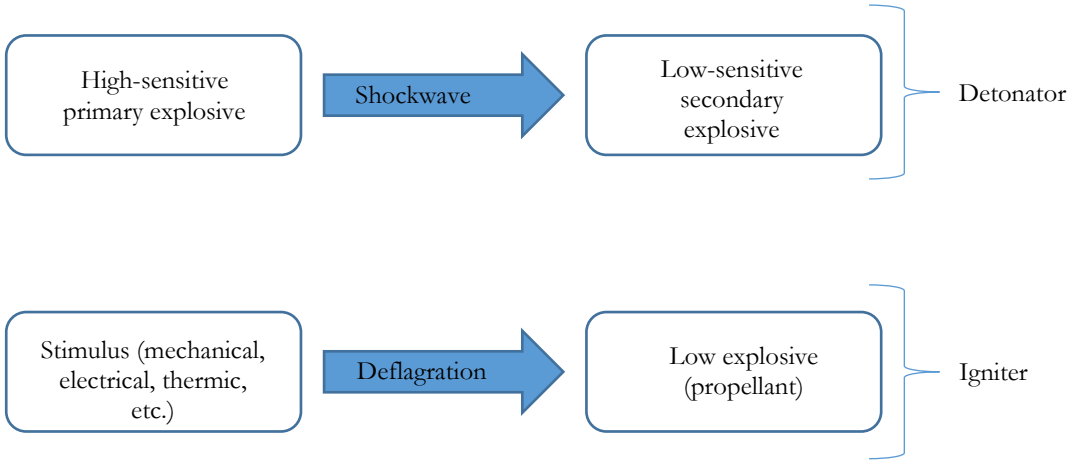

Figure 7. Types of initiators: detonators and igniters/initiators.

Like the explosive devices for military or industrial application, which use a logical placement of components (firing train) to give the detonation, the IEDs also use a similar process (Figure 8). In IEDs the initiating system normally comprises an initiator (Figure 6 – (d)), a power source (Figure 6 – (b)), and a switch (Figure 6 – (c)). As initiators, electrical matches (electric initiation), fuses, squibs, and detonators are frequently used in IEDs. It is also common to find improvised methods, involving, for example, improvised firing pin systems (e.g. rat traps). The power source refers to any energy source used for a device, being the most common the battery, normally associated with electric initiation of a detonator or electric match. The switch is a simple or highly complex component responsible for the activation of the initiation system of the device. This component is limited by the terrorist imagination and his electronic/mechanical skills, and classifies the devices by time-delayed devices (electronic timers), temperature-based devices (thermometers), light-based devices (photo resistors), movement-based devices (infrared sensors) or pressure-based devices etc. [11, 15, 17]

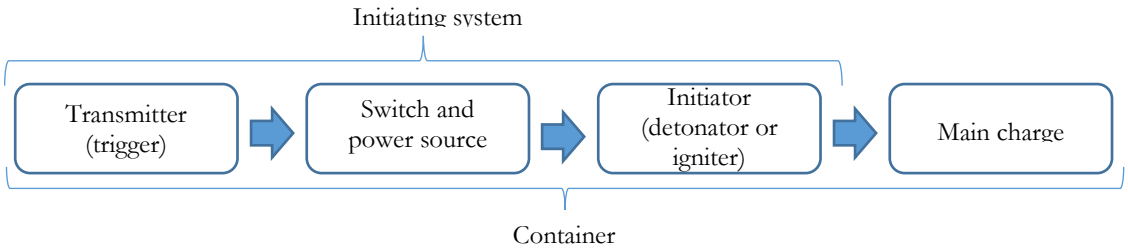

Figure 8. Common initiating system of an IED.

It is important to notice that the initiation of the explosive device depends upon the nature of the main charge/explosive. Low explosives and peroxide-based explosives are extremely heat sensitive, where a burning fuse, electric match or a spark may be used to the initiation. Most high explosives require a detonator of sufficient strength or booster charges (normally using a fully completed firing train). A tertiary explosive such as ANFO often requires a firing train consisting of a detonator and a secondary explosive booster to provide sufficient shock to achieve detonation. [1, 16, 17]

C. Containers

Since one of the main characteristics of IEDs is the concealment, the containers used are mainly materials that we use in our daily basis, such as briefcases, backpacks, drink cans, etc. of various forms and sizes. Depending on the size of the container, the IED may contain other materials like, glass or metal fragments with the purpose of promoting more damage to the target. Besides that, as we see in countries like Afghanistan or Iraq, car bombs are being frequently used to conceal IEDs. [11, 15] There is not a specific pattern of containers used as improvised explosive devices, because it depends on the imagination of the bomb maker/suicide bombers.

Today, the detection and identification of IEDs in real environments is a very challenging and dangerous task. Their diverse nature poses great challenges to the detection methods, since they can contain almost any available explosive (commercial, military or homemade explosives). The varied designs and appearances of IEDs, responsible for their concealment, also complicates their detection, limiting the number of analytical methods used in real situations. Thus, the understanding of the properties of the different explosives types, can be useful in their detection. [10, 13, 19, 20]

1.3 Experimental techniques

1.3.1 Vibrational spectroscopy

The interaction of electromagnetic radiation (photons) with a molecular system can lead to transitions between their rotational-vibrational energy levels. These transitions occur at well-defined frequencies that are related to the vibrational movements of the molecule, also called vibrational modes. The molecular movements that result from characteristic modes of vibration, are described in terms of degrees of freedom (see Table 4). [21-23, 94]

Table 4. Vibrational degrees of freedom of linear and non-linear molecules. [94]

	Total degrees of freedom	**Translational degrees of freedom**	**Rotational degrees of freedom**	**Vibrational degrees of freedom**
Linear molecules	3N	3	2	3N-5
Non-linear molecules	3N	3	3	3N-6

The vibrational degrees of freedom correspond to different types of vibrational modes (see appendix 6) that a molecule can have. These modes can be distinguished between stretching (change in bond length) and deformation (change in bond angles) vibrations. This latter is subdivided into bending, wagging, twisting, torsion, and rocking modes. The symmetry of the vibration is also important, dividing the modes between symmetric or antisymmetric, in-plane or out-of-plane. Each mode has a well defined vibrational frequency that gives rise to bands in the IR and Raman spectrum, in both or none. [21, 24, 94]

Not all vibrational modes are Raman or IR active. This is related to the selection rules, where the change in polarizability (discussed in the section 1.3.2) will give Raman-active modes, and a change in the dipole moment gives IR-active modes. [21, 22, 24] The relative intensities of specific bands and their position, in Raman and IR spectra, are assigned to vibrational modes of certain molecular groups, allowing the study of the chemical structures to identify the substances (qualitative analysis).

1.3.2 Raman spectroscopy

Raman spectroscopy is a vibrational technique involving an instantaneous inelastic scattering of photons (also called Raman effect or Raman scattering). When monochromatic radiation strikes a sample, some of the light is scattered. Much of the scattering is elastic (i.e., with the same frequency and wavelength as the incident light), known as Rayleigh scattering. A smaller fraction (approximately 1 photon in 10^6 or 10^8) suffers an inelastic scattering process, known as Raman scattering. Simultaneously, its frequency shifts towards lower frequencies (Stokes or redshifted scattering), or higher frequencies (anti-Stokes or blue shifted scattering) regarding the incident light. The incident photon interacts with the molecular vibrations, and loses vibrational energy (Stokes scattering) or gains it (anti-Stokes scattering), from the analyte molecule (see Figure 9). The resulting scattered light has different wavelengths (because of the energy difference between the incident and scattered photons), corresponding to the energy of vibrational modes. This allows the identification of a variety of species based on their vibrational "fingerprints". [25-31]

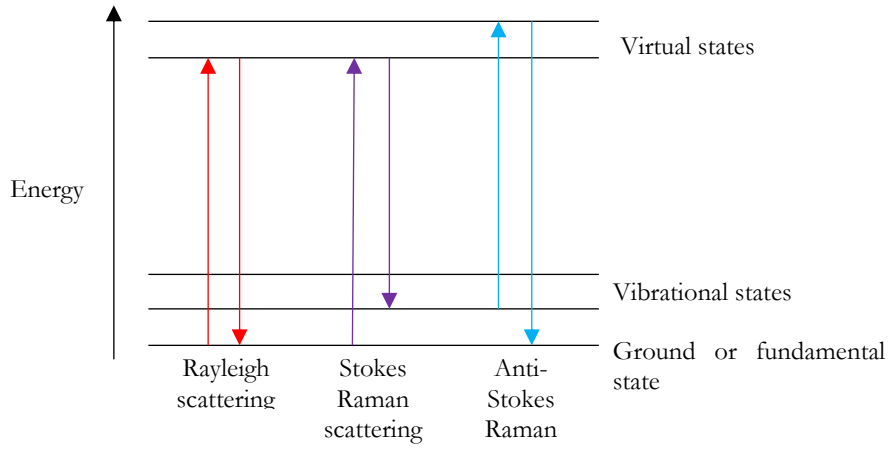

Figure 9. Diagram of the Rayleigh and Raman scattering processes: Stokes and anti-Stokes Raman scattering. The energy changes correspond to the vertical arrows, and the different states the horizontal lines.

These scattering processes involve a two-photon transition between the "virtual states" (high-energy state) and the ground or excited states, causing the release of photons with either the same energy (Rayleigh scattering), lower energy and longer wavelength (Stokes Raman scattering) or higher energy and shorter wavelength (anti-Stokes Raman scattering), than the incident photons. The relative intensity of the Raman lines in the Stokes and anti-

Stokes-shifted Raman spectra is different. The Stokes side has higher intensity than the anti-Stokes. This is related to the fact that, most molecules at room temperature are likely to be in the ground vibrational state (i.e. the relative intensities are dependent on the population of molecules in the ground and excited vibrational levels) associated with the Stokes Raman transition. [21, 22, 25, 26]

As previously discussed in section 1.3.1, not all vibrational modes are Raman-active. The strength of a Raman transition is determined by the selection rule that says that, for a molecular vibration to be Raman active, a change in the polarizability of the molecule must occur during the interaction between the photons and the molecule. The polarizability (α) is a measure of an applied electronic field (E) ability, to generate a dipole moment (π) in the molecule. In other words, it is the ability of the electrons to polarize (deform or displace the molecule electron cloud) resulting in an induced electric dipole. [21, 24, 25]

The result of this technique is the Raman spectra. Vibrations of atoms (vibrational modes) occur in the frequency value ranges of the spectra, which correspond to functional groups present in the molecule. These values vary from functional group to another, due to the different type of atoms present, chemical bonds strength, geometric arrangement, and interactions with neighbouring atoms. [21, 24, 25] Appendix 7, shows the Raman band wavenumber ranges for different vibrational modes of various functional groups. The major drawbacks of the Raman spectroscopy are the weakness of the signal intensity leading to a low sensitivity, the fluorescence (that occurs when the virtual energy levels overlap an upper electronic level), photo-fragmentation, degradation of the sample due to the laser power, and sensitivity to ambient light. [9, 26, 30]

1.3.3 Raman instrumentation

The Raman spectrometer consists of four basic components: an excitation source, an optical sampling system, a wavelength separator, and a detector. A block diagram of the generic components making up a Raman system is displayed in Figure 10.

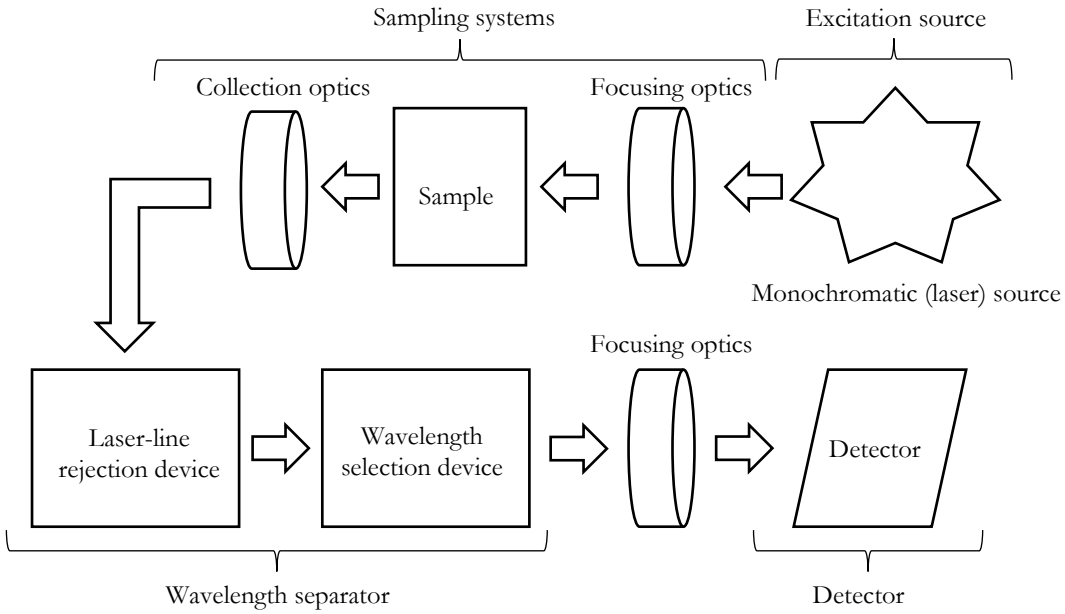

Figure 10. Block diagram of the components making up a Raman spectrometer (adapt from [25]).

Excitation source

The most convenient high-intensity monochromatic light used for the excitation source is the laser. There are continuous wave and pulsed (quasi-continuous) lasers, used in wavelength ranges that can be in the ultraviolet (e.g. 288-nm), visible (e.g. 457, 488, 514, 633, 660, 780 and 785 nm) or near-infrared (NIR) regions (e.g. 830, 980, and 1064 nm). The choice of the laser wavelength is related to the Raman intensity and sensitivity (since Raman efficiency increases by a fourth order function as the laser frequency is increased ($1/\lambda^4$)), fluorescence, which is excitation wavelength dependent (i.e. a sample that fluoresces at one wavelength may not at another, and in general, the shorter the wavelength the bigger the risk of fluorescence), sample photodegradation (observed more in shorter wavelengths) and spatial resolution (related to the confocal Raman microscopy). [22, 23, 31] The use of UV-lasers has the advantages of producing both high Raman signal intensity and sensitivity and, in some cases, are unaffected by fluorescence (i.e. the fluorescence lies outside the Raman spectral range), but can cause sample photodegradation. [22, 27, 31, 32] For NIR lasers, the low fluorescence interferences obtained are the main advantage (the lower laser energies required to generate a Raman spectrum do not give rise to fluorescence). [22, 28, 32] Besides the wavelength region, the laser power (normally in mW) needs to be adjusted to the type of Raman experiment.

Optical sampling system

The optical sampling system includes the sample illumination system and light collection optics. The types of sample illumination systems for the collection of Raman scattered light includes: the conventional optics such as lenses and mirrors, the use of fibre optics (remote or non-invasive sampling via fibre optic-probes), optical microscopes (confocal Raman microscopy), or telescopes (stand-off detection). [22, 23] The sampling collection geometries for Raman scattered light can be of 180º (the most common, and referred to as back-scattering collection geometry, where the scattered light is collected in the reverse direction), 90º (also called right angle scattering, where the scattered light is collected at 90º) or 0º (referred to as transmission Raman). [19]

Wavelength separator

This component includes the laser-line rejection devices and wavelength selection/dispersion devices. Laser-line rejection devices have the role of preventing the weak scattered Raman light from being overlapped by the intense elastically scattered radiation (i.e., the Rayleigh scattering), before it enters the spectrometer, spectrograph or interferometer. The most common laser rejection devices are the holographic notch filters (allow measurements for both Stokes and anti-Stokes Raman scattering) and edge filters (divided in long-wave-pass (LWP) edge filter for Stokes measurements and short wave-pass (SWP) for anti-Stokes measurements). [23-25] Besides those, double or triple stage instruments which suppress the Rayleigh light by an intermediate slit between monochromators (called zero-dispersion double monochromator laser-line filter) are also available. [24, 25] For the wavelength dispersion devices, their role is to separate the wavelengths that comprise the Raman signal and present them to the detector. The most common device used in dispersive Raman spectroscopy is the spectrograph, which is a dispersive polychromator, that contains a diffraction (or dispersion) grating responsible for the angularly separation of the Raman signal into their individual wavelength components, projecting them into the detector. [23-25]

Detector

The detectors used in Raman spectroscopy instruments can be either single- or multi-channel detectors. As single-channel detectors, the photomultiplier tubes (PMTs) are used.

Multi-channel detectors may include the photodiode arrays (PDA), or the charge-coupled device (CCD). The detector of choice for most commercial Raman spectrometers, in the visible, UV, and near-infrared light, is the CCD (charge-coupled device) silicon based multichannel array cooled detectors. [22-25] They consist of thousands of pixels (light-sensitive elements), that act as an individual (or grouped) detector for each dispersed wavelength. They are sensitive to the weak Raman light and capable of measuring the entire Raman spectrum in a single acquisition (multiplex advantage). Other classes of detectors are the non-silicon detectors, such as the germanium (Ge), and indium gallium arsenide (InGaAs) detectors. They differ from silicon detectors in the fact that these are more sensitive in the NIR region, thus appropriate for FT-Raman spectroscopy. [22-25]

According to the type of modification or alteration made in any of the four basic components, we can have multiple advanced techniques that enhance the Raman sensitivity and reduce the interference effects. Some of these techniques include: the FT-Raman (Fourier Transform) instrumentation, that employs a neodymium-doped yttrium aluminium garnet (Nd:YAG) solid state laser operating at 1064 nm, a scanning interferometer (Michelsen interferometer), an laser-line rejection device (normally a notch filter), and a high-sensitivity NIR detector such as the Ge or InGaAs detector. This system allows non-resonant enhancement conditions (i.e., the band intensities in the spectra are more likely to be representative of the concentrations of the chemical species), and fluorescence is decreased. However, the low sensitivity and intensity problem due to the $1/\lambda^4$ dependence effect of operating with 1064 nm excitation wavelength, is present. [22, 33] Other important techniques are the resonance Raman scattering (RRS**)** [34-38], surface-enhanced Raman scattering (SERS) or surface-enhanced resonance Raman scattering (SERRS) [30, 39-42], coherent anti-Stokes Raman scattering (CARS**)** [24, 43], time-resolved Raman spectroscopy (TRRS) [44, 45]**,** spatially offset Raman spectroscopy (SORS) [46-49], stand-off Raman spectroscopy [19, 20, 26, 28, 29, 32, 49-54], and confocal Raman microscopy [6, 9, 13, 55-60].

Confocal Raman microscopy was the methodology used in this thesis, where the Raman spectrometer is combined with a standard optical microscope allowing spatial resolution (i.e., the sample is distinguished from its surroundings). The use of optical microscopes allows the excitation laser beam to be focused in the sample, creating a micro-spot with small diameters. In addition, the incorporation of a confocal pinhole aperture

(small aperture, see Figure 11), allows the separation of the rays from the surrounding regions of the sample (i.e., blocked by the aperture), and those from the optical focal point. [22, 61, 62]

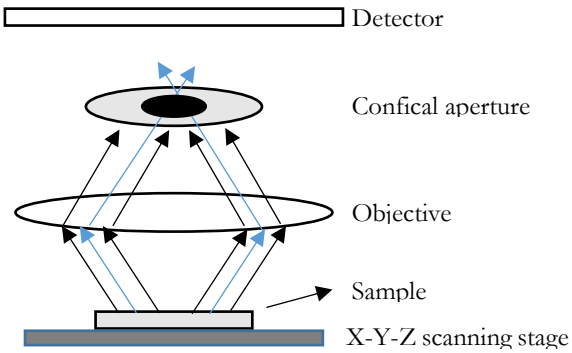

Figure 11. Confocal pinhole aperture.

The use of an X-Y-Z scanning stage allows to perform different mapping techniques, such as X-Y optical sectioning (surface scan), X-Z cross-sectioning (depth profiling or multiple layers of the sample), Z-series (X-Y-Z scan), and surface profiling. Besides that, no preparation of the sample is required, small sample volume measurements are possible, and allows the acquisition of Raman chemical imaging. [24, 26, 62, 63]

The two Raman instruments used in this work are the Thermo Scientific DXR Raman microscope (Waltham, MA, USA) and the portable BWTEK i-Raman Pro instrument (BWTEK Inc., Newark, Delaware). They both are dispersive Raman systems, with an excitation source (laser of 780 nm for the Thermo Scientific DXR Raman microscope, and of 785 nm for the portable Raman), bandpass filters, an optical sampling system to focus the laser onto the sample and collect the Raman scattered light (in both cases, the optical microscope was used), a laser-line rejection device to block residual reflected or scattered laser light, a beamsplitter or dichroic mirror to pass the laser wavelength and reflect longer wavelengths (the Stokes Raman lines), a spectrometer (with gratings) to disperse the Raman spectrum, multichannel detectors (CCD), and several lens and mirrors to focus and reflect the light.

The main differences between them, are that the BWTEK i-Raman Pro instrument is a portable Raman coupled with a fibre optic probe in combination with an optical microscope, suitable for out-of-field analysis. The use of optical fibres normally makes the size of the focal area much larger than laboratory instruments. [64] In addition, to overcome

the various external interferences when used in out-of-field environments, they are more robust, what makes them having less resolution and sensitivity when compared to laboratory instruments. To compensate this lack of resolution, they normally have high power excitation sources (in the Thermo Scientific DXR Raman microscope the maximum laser power is 14 mW and in the BWTEK i-Raman pro is 320 mW). [64]

According to Figure 12, the pathway of the Raman laser in the Thermo Scientific DXR Raman microscope can be described as follows: the laser beam is reflected in a first mirror and passes through the first pair of lenses and through the bandpass filter into the beamsplitter or dichroic mirror, where half of the beam is transmitted to a second mirror that reflects it into the microscope objective. The light strikes the sample, and is scattered by the sample. The scattered light is collected by the microscope objective at 180º degrees, and passes through the second mirror and the beamsplitter or dichroic mirror, to the filter. The resulted filtered light passes through the second pair of lenses and is reflected by a third mirror to the spectrograph. This dispersive spectrometer contains a grating that diffracts the light and directs it to the cooled CCD detector, connected to a computer for data treatment. The pathway for the portable BWTEK i-Raman pro is similar, except for the fact that the laser needs to pass first through a fibre optic probe, connected to the confocal microscope.

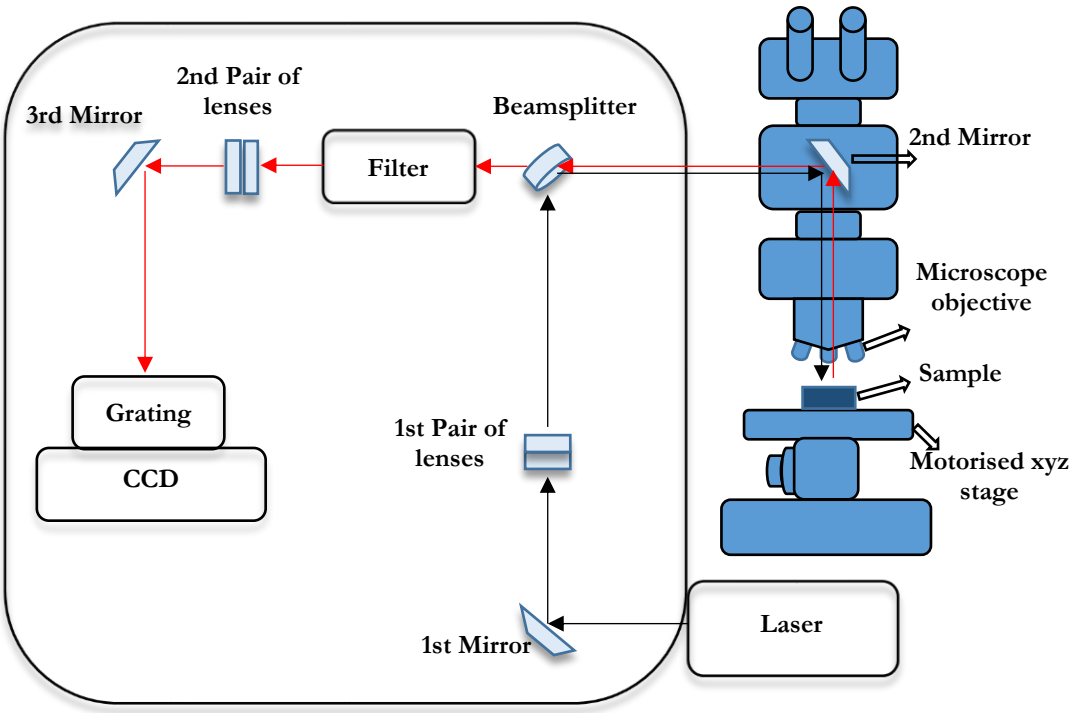

Figure 12. Schematic diagram of the Thermo Scientific DXR Raman microscope.

1.4 Explosive detection techniques and the role of vibrational spectroscopy

The detection and prevention of terrorism has never been more relevant in current present world climate. These concerns have become more intense due to the ease by which an improvised explosive device (IED) can be made from readily available ingredients. In the explosives detection, there are various drawbacks that need to be overcome, such as concealment, interferences, low volatility of explosive vapours, explosive nature of the analyte, very small amounts of explosive substance, and their complexity. This has generated a great demand for sensitive, selective, reliable, low cost, rapid, portable, miniaturized, low false alarm rates, robust, accurate, and minimally invasive detection and identification instruments, for use by law enforcement and security agencies. The use of analytical techniques on explosives detection, will depend on the field at which they will be applied (e.g. for environmental monitoring laboratories, complex instrumentation like the GC-MS may be applied, where for counter-terrorism applications, laser-based techniques are more adequate). [12, 39, 65, 66] Figure 13, represents the fields where the detection and identification of explosives and explosive-related compounds is often required.

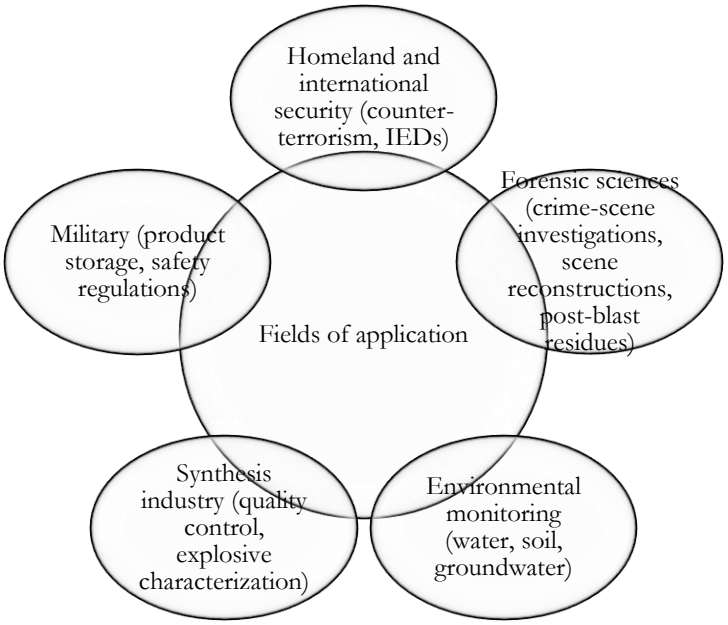

Figure 13. Fields of application where the detection and identification of explosives and explosive-related compounds is often required. [12]

Conventional approaches, such as metal detectors in combination with X-ray machines, usually found at airport security points, are not the most effective devices to detect explosive compounds, and are becoming easy "preys" for terrorists, in a way that, they can avoid being detected. [12, 66] In general, the identification and detection of concealed explosives (energetic compounds) and their precursors/degradation products, is based on their chemical and physical proprieties, such as vapour pressure, density, performance, elemental composition, detonability, ignitability, sensitivity, stability, colour reaction, UV absorbance, mass spectrum, IR and Raman absorbance, dielectric constant, purity, viscosity, particle adhesion and size, and others. [3, 10, 66] Properties such as high nitrogen, carbon and/or oxygen content, high density or fast energetic release in the analysed sample is indicative of the presence of an explosive/energetic substance. [10, 66] The study of these properties helps in the development and improvement of the analytical techniques, dividing them into trace, bulk or vapour detection techniques. [3, 67] Bulk detection is related to the techniques able to detect high quantities of explosive substances. The detection of very low amounts of explosive substance is regarded as trace detection, where high sensitive techniques are normally used (i.e., with very low limit of detection, LOD). The detection of traces of explosives in the air (vapour detection) depends on the vapour pressure of the explosives. Explosives that have a relatively high vapour pressure (e.g. TATP) can be detectable by vapour detection techniques (i.e., they have detectable concentrations in air), however, in real scenarios, external conditions (rain, drafts, etc.) affect the amount of detectable explosive. [3, 36, 68] For low vapour pressure explosives (e.g. octogen (HMX)), they are not detectable with vapour techniques and are best detected in their solid form. [3, 26, 32, 36, 68] Appendix 9 demonstrates numerous analytical techniques that have been utilized for the detection of explosives in various matrices (e.g. air, soil, water, etc.).

The trace detection techniques are very important in the forensic field, since they allow the quantification with very low LOD of pre- and post-blast explosion residues. The detection of pre-blast particles in human fingerprints and clothes or other materials of a suspect (e.g. glasses, gloves, etc.), is one of the most direct ways of associating the suspect with the handling of explosives. There is a high variability in the amount of explosive residues and particle size distribution found in various fingerprints, depending on which explosive or explosive mixture is used, the particle adhesion to the surface, the surface material, fingertip properties (roughness, greasiness), the presence of contamination, sweat, etc. Thus, in order

to analyse explosive pre-blast particles, it is essential to understand the adhesion of those particles, and the particle size distribution to different surfaces (e.g. clothes, skin, paint, metal surfaces, building materials, etc.). [10, 13, 26, 65]

Regarding the post-blast explosion residues, their analysis is very important in forensic science, when investigating a crime scene where an explosion occurred, to identify what type of explosive compound was used. That information will help the police investigations, enabling crime reconstruction, to find the terrorists (or criminals) behind the attack. The detection and analysis of post-blast residues is very difficult, because the explosive that is inside the IED is completely consumed and destroyed during the explosion. However, in some cases it is possible to find trace post-blast unreacted (or undetonated) particles from the original explosive in the surface of the materials present in the post-blast crime scene. This happens mostly for the explosive mixtures based on inorganic oxidizing salts and combustible compounds (e.g. ANFO), where a badly made mixture of those two, may not react to the combustion reaction, and the resultant shock-wave will spread those unreacted particles all around. [57, 69, 70] For pure explosives (e.g. TNT, RDX, PETN, TATP, HMTD), where the same molecule acts as a combustible and as an oxidizer, the explosion is more effective and powerful, making the detection of post-blast unreacted particles more difficult, but nonetheless possible. [57, 69, 70]

If there are any post-blast particles in the crime scene, they generally result from incomplete or partial detonation of the explosive device (i.e. particularly interesting, when considering the presence of IEDs, where their construction is usually made with cheap materials and in unstable conditions), and are usually found spread out over large areas along the various materials burnt and devastated by the explosion. Other problem is that, the amount of post-blast particles remaining is usually very small (trace amounts) and is often mixed with impurities or contaminants due to the high contamination present in open air environments (e.g. particles of the ground). [22, 39, 57, 65, 69] Various techniques are used as confirmatory techniques for the analysis of pre- and post-blast explosion particles, such as ion chromatography (IC), capillary electrophoresis, SEM-EDS/WDS, XRF for inorganic phase; high-performance-liquid chromatography (HPLC-MS), GC-MS, GC-MS/MS for organic phase; XRD for both; and, mega-electron volt-secondary ionization mass spectrometry (MeV-SIMS) or SEM-FIB. [57, 65] Although most of these methods give good sensitivities and positive chemical confirmation, they require isolation (separation) and/or

destruction of the analyte, (causing the alteration and/or destruction of the evidential material), and are time and reagent consuming, what can lead to delays in a crime scene investigation. They also require complex laboratory instruments making their portability not so easy for out of field and real-time analysis (routine field use), and require that the personnel come in contact with the explosive evidence, placing workers at risk. [27, 30, 33, 39, 55, 59, 60, 66, 71]

To overcome these difficulties, the use of spectroscopic techniques (such as Raman spectroscopy), recognized for being rapid, non-destructive and solvents-free, can be considered as a positive alternative for the analysis of pre- and post-blast particles in trace detection, avoiding sampling and separation methods (see Table 5).

Table 5. Advantages of Raman spectroscopy. [12, 22, 27-29, 51, 63]

Advantages of Raman spectroscopy
Is a robust, reproducible, very reliable and non-destructive technique with minimal instrumental maintenance, that allows for highly selective identifications (qualitative analysis) considering the specific molecular fingerprints;
Possibility to analyse samples with different physical states (solids, liquids or gases), composition (organic, inorganic or biological), as well as samples inside transparent or non-transparent containers;
Requires minimal or no sample preparation (non-invasive characteristic);
Offers different detection configurations, such as microscope-based systems or stand-off systems with fibre-optics (noncontact characteristic), that accommodate different target sizes and ranges;
Allows the use of different laser excitation wavelengths, such as UV, IR, and visible region lasers, having multiple advantages on reducing the fluorescence and increase of Raman intensity;
It has a portability feature, important in the development of fully portable systems for field analysis, where detections can be done during the day and night;
Allows quantitative analysis, since the relative band intensities within a spectrum are linearly proportional to the density number of species giving rise to the target band;
In vibrational spectroscopy, the Raman spectra are generally simpler than IR spectra, since overtones and combination bands are usually very weak and are complementary.

Regarding the trace detection of explosives using Raman spectroscopy, it is necessary to increase the Raman signal of the analyte somehow. One of the simplest and fastest ways is to use confocal Raman microscopy, which enhances the signal from the analyte over the background by focusing the microscopic spot on the surface of the explosive particle. [57, 60]

In explosives detection, it was used for the discrimination of different types of smokeless gunpowders [9], the detection of explosive particles trapped between clothing fibres [55, 59, 60, 72, 73], the identification of the different components that constitute the dynamites [58], and for the direct detection of microscopic residues that ranged below 5 μm, 10 – 30 μm and 60 – 100 μm depending on the region analysed, of smokeless gunpowder, black powder and dynamite on human fingerprints with little interference [13]. This trace detection technique provides a useful way to analyse trace amounts of pre- and post-blast explosives residues [13, 57]. Almeida et al. [63], used Raman hyperspectral imaging and chemometric methods for identification of pre- and post-blast explosive residues of PETN, RDX, HMX, TNT, ANFO, trinitrophenol (TNP), perchloroethylene (PERC), and black powder on banknote surfaces with a detection limit of 50 μg cm^{-2}.

In addition, the spectra of an unknown sample may be correlated with reference spectra from a library or from the literature, considering the characteristic frequency groups present or absent and relative band intensities. [31, 64, 74] Besides libraries, the use of chemometric tools, like supervised and unsupervised neural networks, fuzzy and statistical networks as well as PCA, can be used for the proper classification of the measured spectra. [75]

1.5 Motivation

This thesis attempts to address the detection of pre-blast explosive residues, such as oxidizing salts, organic and inorganic explosives, on high interfering surfaces (i.e., clothing fabrics). The difficulty in the detection of trace explosive residues on textile fabrics of a giving suspect is known, resulting in a delay in the criminal investigation. Thus, this thesis will investigate the feasibility of using vibrational spectroscopy, more precisely confocal Raman microscopy, to detect those trace particles. The hypothesis is that a positive identification and detection can be made using this analytical technique, allowing its use on criminal cases involving explosive contaminated cloth fabrics from a suspect.

In addition, a second study was made, in which confocal Raman microscopy was also used, to prove its feasibility in the analysis of energetic materials (e.g., oxidizing salts) in the presence of multiple interference substances that act as fuels. This type of mixtures, classified as homemade explosives (HMEs), is often seen in IEDs.

1.6 Hypothesis and Objectives

According to Edmond Locard, when two objects come into contact with one another, a cross-transfer of evidence occurs. This statement is known as Locard's Exchange Principle and is the foundation for the use of physical evidence to link or at least associate a suspect to a crime scene or victim. We can apply this principle regarding the manipulation of IEDs or other explosive devices or substances. This means that in the manufacture, handling or transportation of IEDs, there is a possibility of pre-blast residues (trace amounts of particles) to be easily deposited or transferred onto other surfaces present in the contaminated area, such as car handles, gear sticks, suit cases, human fingerprints, human nails, fibres of clothes, pressure-sensitive tapes, etc. [13, 53, 63]

In a criminal case, when the suspect is identified, evidential material is needed to convict him. This evidential material can include a wide range of materials that can go from personal stuff (e.g., clothes, etc.) to very small particulates (e.g., explosive particles, etc.). The combination of these two kinds of evidential material is possible when the suspect is connected to a crime scene involving explosive devices. During the manufacture of IEDs, manual handling, packaging or transportation of the explosive material, direct or cross-contamination of the explosives, clothing and other possessions of the suspect, may occur. In the case of clothing, microscopic particles of the explosives get physically trapped between the fibres. [59, 60] This leads to an evidence that can serve as a powerful indicator for linking those materials that belong to the suspect and the crime scene. Considering the advantages of Raman spectroscopy (see Table 5), such as an ability to detect very small particles, prevent sample contamination, preserve the evidence (non-destructive technique), with minimal sample preparation, and high speed of analysis, makes it the ideal analytical instrument to detect those explosive particles on surfaces. Raman spectroscopy combined with confocal microscopy follows those principles. Taking this into account, the hypothesis and objectives were formulated as shown in Figure 14.

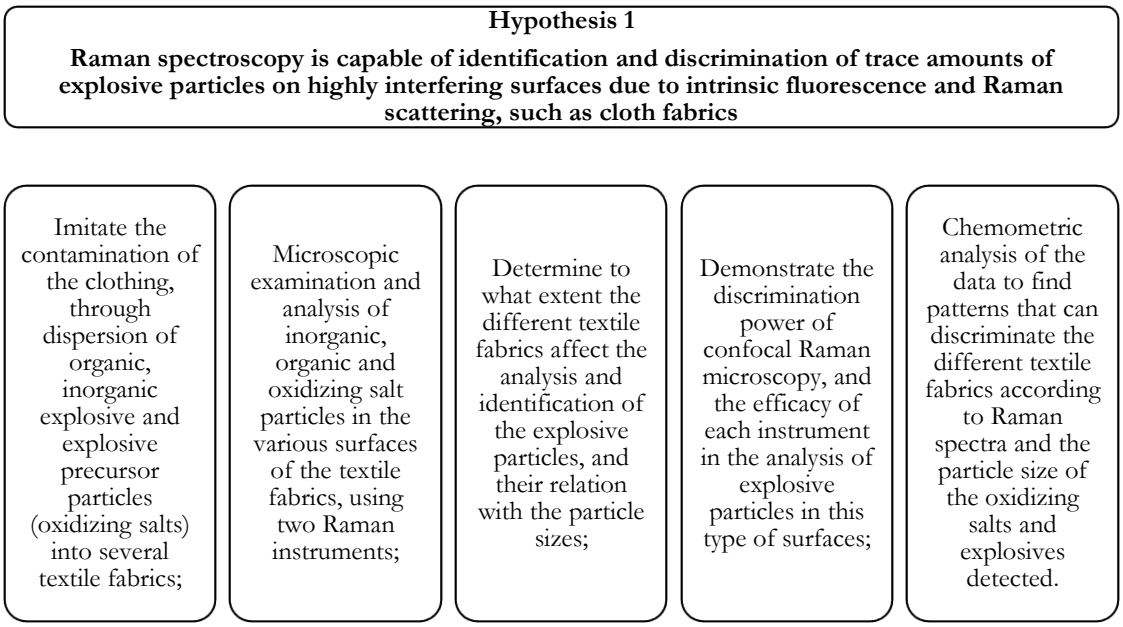

Figure 14. Schematic representation of the hypothesis and objectives corresponding to the first part of the thesis.

The second part of this thesis is related to the fact that energetic substances, such as oxidizing salts, can be used in combination with various materials that act as fuels (here regarded as interfering substances), to produce explosive mixtures often encountered in IEDs. [10, 55] These interfering substances (fuels) can be easily purchased at supermarkets or other similar outlets, providing means for a low cost and rapid way for terrorists to do explosion attempts and crimes related to explosive devices. Given this, the second hypothesis and the respective objectives are indicated in Figure 15.

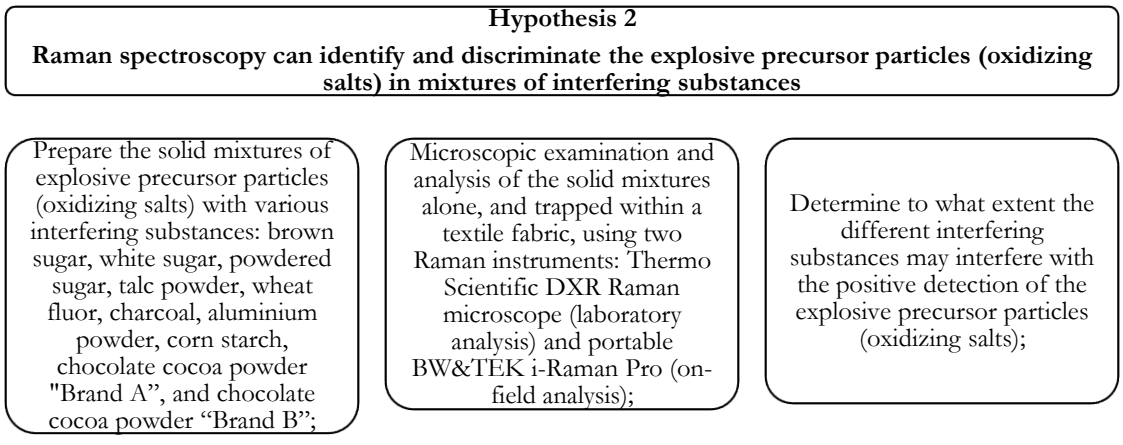

Figure 15. Schematic representation of the hypothesis and objectives corresponding to the second part of the thesis.

1.7 Thesis organization

Chapter 1 provides information about what is an explosive, the different classifications of explosive substances, and the constitution and/or mechanisms applied to an improvised explosive device. In addition, information about the Raman spectroscopy and instrumentation is also referred. Chapter 2 presents the materials and the experimental methodology used for the performance of the two studies. Chapter 3 talks about the experimental results and their discussion. Chapter 4 presents the conclusion.

Chapter 2

Experimental

2.1 Materials and methods

2.1.1 Explosive samples and oxidizing salts

Table 6 represents the composition of the 8 explosives used in this thesis. Most of these explosives were obtained from previous studies done in the INQUIFOR investigation group in collaboration with TEDAX, the Spanish Explosive Ordnance Disposal (EOD). Flash powder is the only exception since it was acquired from commercial bought firecrackers. The information about their physical properties is presented in Appendix 10.

Table 6. Composition of the explosives studied.

Explosives	Composition
Ammonal (AlAN)*	Ammonium nitrate (85%) + aluminium (15%)
Black powder	Potassium nitrate (75%) + charcoal (15%) + sulfur (10%)
Chloratite	Sodium chlorate (80%) + sugar (10%) + sulfur (10%)
Flash powder	Potassium perchlorate (80-90%) + aluminium (10-20%)
Trinitrotoluene (TNT)	2,4,6-trinitrotoluene (100%)
Hexogen (RDX)	Cyclotrimethylene trinitramine (91%) + bis(2-ethylhexyl)phthalate (5.3%) + polyisobutylene (2.1%) + motor oil (1.6%)
Penthrite (PETN)	Pentaerythritol tetranitrate (100%)
Hexamethylene triperoxide dyamine (HMTD)	Hexamethylene triperoxide diamine (100%)

*The military ammonal explosive normally contains ammonium nitrate, aluminium and TNT. But in this case, the TNT is not present. Thus, the proper name is AlAN which is classified as homemade explosive.

These explosives can be divided as inorganic and organic explosives. The inorganic ones contain inorganic salts (or oxidizing salts) in combination with fuels, and are here

represented by the explosives: black powder, flash powder, chloratite, and ammonal (AlAN) (Figure 16).

Figure 16. Inorganic explosives studied. From left to right: black powder, flash powder, chloratite, and ammonal (AlAN).

Apart from these explosives, the oxidizing salts used in their composition (also called explosive precursors) including ammonium, sodium, potassium and barium nitrates, sodium and potassium chlorate and potassium perchlorate, were separately analysed (Figure 17).

Figure 17. Oxidizing salts studied. From left to right: ammonium nitrate (NH_4NO_3), sodium nitrate ($NaNO_3$), potassium chlorate ($KClO_3$), sodium chlorate ($NaClO_3$), potassium perchlorate ($KClO_4$), barium nitrate ($Ba(NO_3)_2$), and potassium nitrate (KNO_3).

These salts act as oxidizers and are characterized as white crystals. The organic explosives contain both the oxidizer and fuel groups in the same molecule, and are here represented by the explosives: TNT, RDX, PETN, and HMTD. Regarding their characteristics, TNT is a nitroaromatic compound (C-CO_2). It is the most important explosive used for blasting charges of all weapons, is stable, and insensitive (secondary explosive); [2, 3, 8, 11] RDX is an aliphatic nitramine (N-NO_2), used as high-brisance explosive due to their high density and explosive velocity. It is insensitive, stable, and used as plastic explosive; [2, 3, 8, 11] PETN is a nitrate ester (CH_2-O-NO_2), mostly used for booster charges due to its high brisance, power, and moderate sensitivity; [2, 3, 8, 11] HMTD

is a peroxide explosive (i.e. prepared from highly concentrated hydrogen peroxide, H_2O_2), effective at initiating explosives, due to their high sensitivity to any stimulus. [3, 8, 11] In Figure 18 the chemical structures of the organic explosives and the corresponding images are displayed. The RDX used, was in a plastic explosive composition (i.e. with energetic plasticizers and binders), and the TNT was in a solid form. To obtain powdered particles of these explosives, the procedure explained in section 2.2.2 was performed.

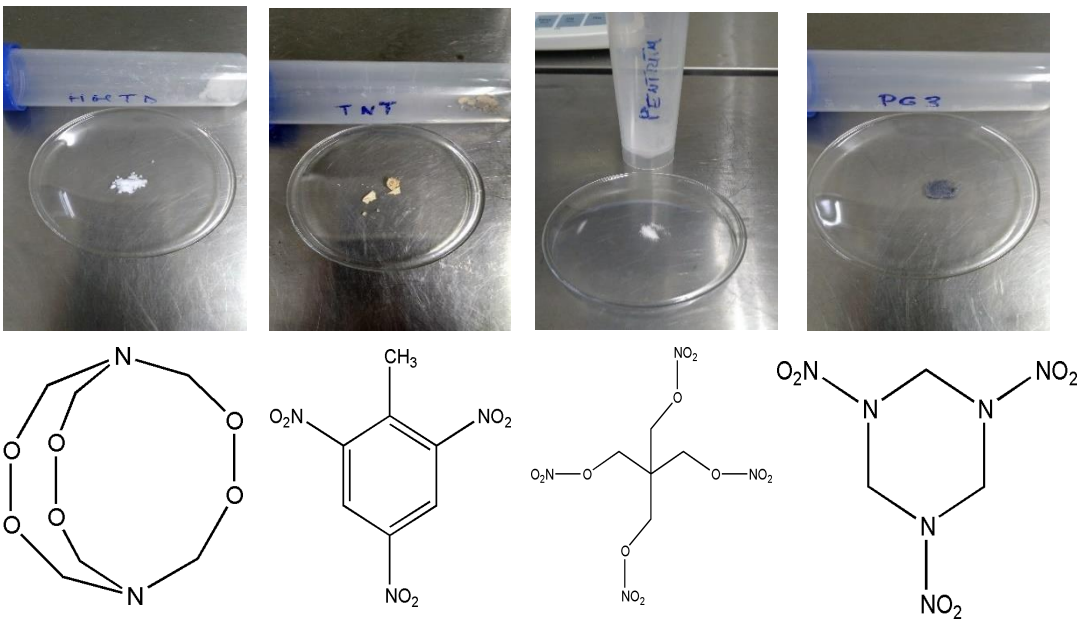

Figure 18. Organic explosives used. From left to right: HMTD, TNT, PETN and RDX.

2.1.2 Textile samples and interfering substances

In the first step of the experimental work, a large set of natural and synthetic fibres was used to cover the large variety of textile fabrics available in daily life. The natural fibres included: cotton, wool, and two blue denim jeans. As representative synthetic fibres, two white polyester, polyskin, laboratory latex and two nitrile gloves, were used. These were divided in dyed clothing, which included red, green, black, and blue cotton; blue and black polyester; two blue nitrile laboratory gloves; two blue denim jeans; polyskin; and dyed wool. Figure 19 shows the textile fibres used in this experimental work.

Figure 19. Textile fabrics used in the experimental work. From left to right (top to bottom): white cotton, blue cotton, green cotton, red cotton, black cotton, white polyester A, white polyester B, blue polyester, black polyester, wool, jeans B, jeans A, polyskin, latex glove, nitrile A glove, and nitrile B glove.

In the second study, regarding the mixture of the interfering substances with an explosive precursor (oxidizing salt), the substances used are displayed and indicated in Figure 20. In appendix 11 is described the complete composition of those substances.

Figure 20. Interfering substances used in the second step of the experimental work. From left to right: talc powder, corn starch, wheat flour, chocolate cocoa powder "Brand 2", chocolate cocoa powder "Brand 1", brown sugar, powdered sugar (or confectioners sugar), white normal sugar, aluminium powder, and charcoal.

2.2 Support and samples preparation

2.2.1 Support preparation

Several cardboard supports coated with the different textile fabrics were prepared. For this, the textile materials where attach with the use of office-clips to a support made of small square pieces of cardboard wrapped with aluminium (Figure 21). The aluminium was used to avoid the Raman signal from cardboard. The size of these supports was in accordance with the area of dispersion (the affected area by the explosive particles), that corresponded to the area of the circle in the end of the card roll cylinder, that was approximately 23.8 cm^2.

Figure 21. Image of the cardboard support with aluminium foil.

2.2.2 Samples preparation: explosives and oxidizing salts on textiles and laboratory gloves

The objective was to disperse and trap the particles of the explosives and oxidizing salts, that are in a dust/powder composition, on the textiles and laboratory gloves, to mimic the direct transfer that happens during the handling of explosives (e.g. during the manufacture of IEDs). Before the dispersion, the oxidizing salts were crushed/grinded with the help of a pestle and mortar, to obtain small particles sizes. The inorganic explosives, and the organic explosives HMTD and PETN were already in powder form and used as they were. In order to disperse TNT and RDX, they had to be recrystallized by evaporation after dissolution, since they were not presented in powder form. The solvent used was acetonitrile, because in most of the explosive standards vendors (e.g. AccuStandard and LGC standards) those explosives are dissolved in acetonitrile. Two solutions of 1000 ppm were prepared (Figure 22), and after the precipitation, a final mass of 0.11747g for the TNT and 0.11260g for the RDX was obtained (see appendix 12). The TATP was also submitted to this method, but since it is a very unstable explosive under ambient conditions it was not possible to obtain any measurable mass (0 g).

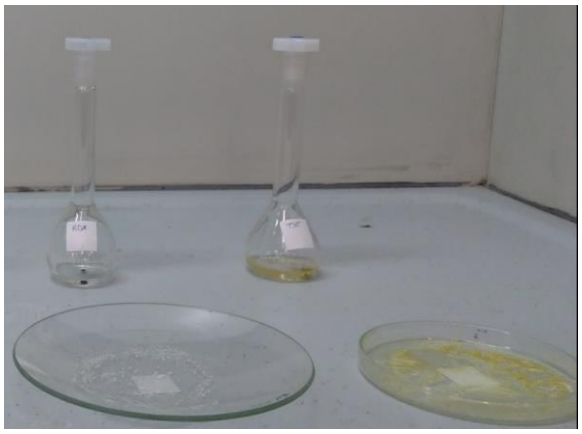

Figure 22. In the back: solutions with 1000 ppm concentration of the RDX and TNT; In front: precipitated RDX and TNT explosive.

To disperse the particles onto the textiles, the experimental setup presented in Figure 23 was used.

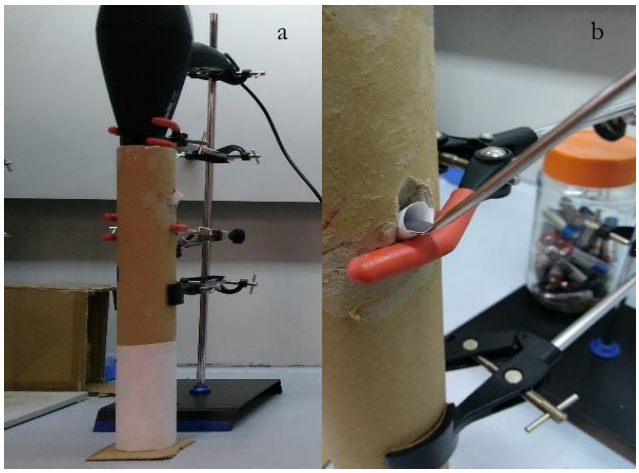

Figure 23. (a) Experimental setup used for the dispersion of the explosives and oxidizing salts onto the textile fabrics; (b) how the explosives and oxidizing salts were putted inside the card roll.

The process can be explained in the following steps: 1) weight the amounts of explosive materials or oxidizing salts on a watch glass or petri dish; 2) transfer the weighed amount to the spatula; 3) put the spatula inside the cardboard cyllinder (Figure 23 - (b)); 4) turn on the air dryer; 5) dispersion of the particles. In detail, the air coming from the air dryer passes through a card roll, where the spatula with the explosive/oxidizing salt is. Then the particles are dispersed onto the textile fabrics and laboratory gloves covering an area of 23.8 cm^2, obtaining a good homogeneity of distribution (Figure 24).

Figure 24. Particle distribution on the various textile fabrics.

The inside of the card roll was wrapped with wax paper, to prevent the contact of the particles with the card roll, because they can be trapped. To avoid losses to the exterior, because the particles bounced off upon hitting the textile, the end of the card roll was also wrapped. The "vegetal paper" was always changed to avoid contamination between the explosive materials.

The weighed quantities for the dispersion of the different explosive materials (see appendix 13, 14, and 15) were between 25 - 35 mg for the oxidizing salts, 5 – 10 mg for the inorganic explosives, and 3 – 5 mg for the organic explosives. These quantities were established considering the amount of explosive material available, losses to the exterior, and to ensure that explosive particles could be found on the textile fabrics and gloves. After the dispersion, the explosive particles were analysed by confocal Raman microscopy.

2.2.3 Samples preparation: mixtures of potassium nitrate with various interfering substances on red cotton textile

For this step, mixtures of the interfering substances with potassium nitrate were made, using a pestle and mortar. The potassium nitrate is one of the most encountered salt in the composition of inorganic explosives, thus it was chosen to do this study. The total quantity of the mixtures is approximately 100 mg (see appendix 16, 17 and 18) in which, 70% corresponds to the potassium nitrate and 30% to the interfering substance. These

percentages were considered because in the existing inorganic explosives those are the percentages of the oxidizing salt and fuel used to fabricate them.

These mixtures were also dispersed in the textile fabric, red cotton, using the same process explained in the step 1. The use of only this textile was because, it allows for a better visualization of the particles, more precisely, the white crystal potassium nitrate particles.

2.3 Instrumentation

2.3.1 Raman instrumentation

Thermo Scientific DXR Raman microscope (Figure 25)

Figure 25. Thermo Scientific DXR Raman microscope (Waltham, MA, USA).

The Raman microscope analysis was performed with a Thermo Scientific DXR Raman microscope (Waltham, MA, USA) with a 780 nm near-infrared laser wavelength with a maximum laser power of 14 mW. The textile fabrics and gloves were microscopically observed using 10x, 20x, 50x and 100x microscope objectives giving a laser spot diameter of 3.1, 1.9, 1.6, and 0.9 μm, respectively. After finding a potential explosive/precursor particle, its Raman spectrum was recorded. The Raman spectra were obtained at approx. 2 cm^{-1} resolution, in the wavenumber region of 3200 to 200 cm^{-1}, using an aperture of 50 μm slit and grating of 400 lines mm^{-1}. The Raman measurements and acquisition options were

different for each explosive material (Table 7). These parameters were fixed considering the behaviour of the textile and the amount of fluorescence.

Table 7. Raman acquisition options used in the Thermo Scientific DXR Raman microscope.

Explosives	Laser power (mW)	Accumulations (scans)	Acquisition time (seconds)	Total acquisition time (seconds)
Oxidizing salts	14, 5*, 1*	8	5	40
Inorganic explosives	10, 5*, 1*	5	6	30
Organic explosives	10, 5*, 1*	5	6	30

*Black cotton and polyskin textiles were analysed with 5 mW and 1 mW, respectively, due to their sensitivity to the laser.

Portable BW&TEK i-Raman Pro (Figure 26)

Figure 26. Portable BWTEK i-Raman Pro (BWTEK Inc., Newark, Delaware).

The Raman microscope analysis was also performed with a portable BWTEK i-Raman Pro (BWTEK Inc., Newark, Delaware) instrument able to exciting the samples with a 785-nm excitation laser and with adjustable power in the range 1% to 100% of a maximum power of 320 mW. With a confocal microscope attached, the samples were microscopically observed using 20x and 40x microscope objectives, giving a laser spot diameter of approximately 87 and 56 μm, respectively. After finding a potential explosive/precursor particle, that spot was analysed by Raman spectroscopy. The Raman spectra were obtained at approx. 3 - 4 cm^{-1} resolution, measured from 3200 to 200 cm^{-1} in the dark subtracted option (i.e. removing the background signal from the instrument). Considering the sensitivity

of each textile in relation to the laser power, the spectra parameters were different for each explosive and textile (Table 8). Some textile samples suffered from burning degradation when submitted to the laser power (blue and black cotton, jeans 1 and jeans 2).

Table 8. Raman acquisition options used in the portable BWTEK i-Raman Pro.

Explosives	Laser power (%) of 320 mW	Accumulations (scans)	Acquisition time (seconds)	Total acquisition time (seconds)
Oxidizing salts	20, 1*	10	0.3	3
Inorganic explosives	1	10	1	10
Organic explosives	5, 1*	5	3	15

*Laser power for the textiles black cotton, blue cotton, jeans 1, and jeans 2.

2.3.2 Data treatment and chemometric software

The Raman spectra of the particles detected in the fabric samples were compared with the spectral library previously created from the standards of the explosives and oxidizing salts, which were analysed prior to being dispersed onto the fabrics. The comparison of the spectra recorded from both instruments were made using the Thermo Scientific Omnic for dispersive Raman 8 software.

The program used to do the chemometric and statistical analysis was the "The Unscrambler X" (version 10.1, CAMO, Oslo, Norway). Two statistic tests were performed. One descriptive statistical analysis of the particle size data from both Raman instruments, and a principal component analysis (PCA) for the acquired Raman spectra by the Thermo Scientific DXR Raman microscope.

Descriptive statistics provides a quantitative analysis, that summarizes the sample data. In this case, the use of a univariate statistical analysis to describe the distribution of a single variable (i.e. the particle size data), its central tendency (including the mean, median, and mode), and dispersion (including the range and quartiles of the dataset, variance and standard deviation), was performed. [76] The specific statistic test used, was the box plot (or box-and-whisker diagram). This test provides the distribution of the variable through their quartiles (first, second (median), and third quartiles). In addition, the maximum and minimum of all the data can also be visualized. The distribution is divided in three parts: 25% between the minimum and the first quartile, 50% between the first and third quartile, and

25% between the third quartile and the maximum. [76] To do this univariate statistic test, three of the smallest particles for each explosive material (oxidizing salt, organic and inorganic explosive), detected in each textile fabric were selected. This was made to evaluate the smallest particle size (LOD) detected for each explosive on each material.

A multivariate statistical (or chemometric) technique, such as principal component analysis (PCA) was performed on the Raman spectra of each particle analysed in each textile fabric by the Thermo Scientific DXR Raman microscope. In a brief explanation, the PCA is used for screening, extracting and compressing multivariate data (i.e., diminishes the variability of the dataset). PCA provides new variables that best explain the variation of the possible correlated variables present in a certain dataset. These new variables are called the principal components (non-correlated variables). Normally the first component explains the most variation, the second component the second most, etc. There are four fundamental parts of a PCA model: the data, the scores, the loadings, and the residuals. The data is here represented by the variables present on the Raman spectra dataset matrix. The residuals are used to calculate the explained or unexplained variation (i.e., what spectral variation has not been explained). The scores correspond to the new values of each sample to the different variables now combined in the principal components. The scores plot provide means to see certain grouping in the data, and/or the tendency of the scores (negative or positive) related to the corresponding principal component. Finally, the loadings define what a principal component represents, more precisely the linear combination of the variables. [77-81]

For the execution of the PCA model, five positive (i.e., the characteristic vibrational bands of the explosive were detected) Raman spectra of each oxidizing salt, and organic explosive, analysed in each textile fabric, were selected. It should be noted that as an example, only one oxidizing salt (potassium chlorate), and one organic explosive (RDX) were used to perform the chemometric analysis. The objective pursued by performing the PCA was to statistically evaluate the fluorescence of the different textile fabrics. Before performing the PCA model, the matrix of the Raman spectra was normalized (i.e., a pre-processing method to avoid differences due to the intensity, which is affected by the size of the particle and the focusing). [82]

Chapter 3

Results and Discussion

3.1 Raman spectral library of the explosives and oxidizing salts

The reference Raman spectra of the oxidizing salts, organic explosives, and inorganic explosives in the spectral wavenumber region 2000-200 cm^{-1}, taken by the Thermo scientific DXR Raman microscope, are displayed in Figures 27, 28, and 29, respectively. In appendix 22, 23, and 24 the reference Raman spectra taken by the portable BWTEK i-Raman Pro are displayed. These spectra were useful for the prior comparison and identification of the spectra from the explosive and salt particles trapped on the textile fabrics.

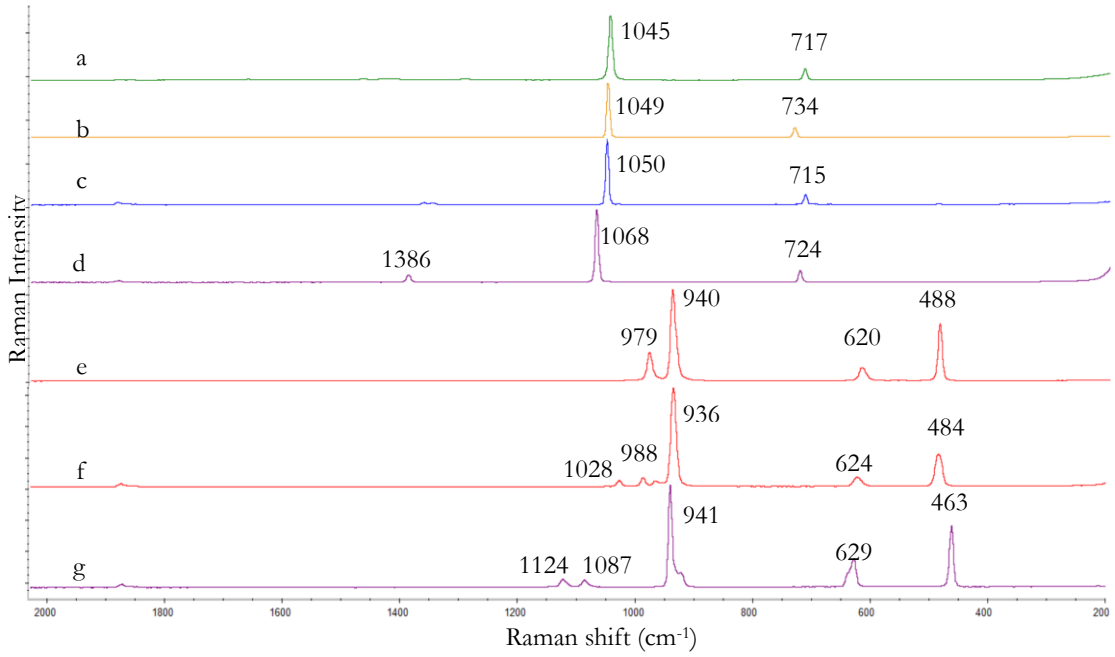

Figure 27. Reference Raman spectra of (a) ammonium nitrate (b) barium nitrate (c) potassium nitrate (d) sodium nitrate (e) potassium chlorate (f) sodium chlorate (g) potassium perchlorate (Thermo scientific DXR Raman microscope 780 nm, 14 mW, 5 s exposure, 8 accumulations).

The spectra of the oxidizing salts (Figure 27) mainly display those bands corresponding to the molecular compounds that conform each ionic salt, i.e. mainly the

anion. Positively, the distinction of these salts by their Raman shift shows the high specificity of the Raman spectroscopy in the differentiation of similar compounds due to the specific cation-anion interaction. The ammonium nitrate, barium nitrate, potassium nitrate and sodium nitrate are distinguished by the difference in Raman shift of the NO_3^- symmetric stretching and NO_3^- in-plane deformation. In addition, for the sodium nitrate, the appearance of a band at 1386 cm^{-1}, corresponding to the antisymmetric stretching vibration, allow it to be distinguished from the other nitrate salts. The sodium chlorate and potassium chlorate are very well differentiated from the nitrates and from themselves by the slight difference in Raman shift of the ClO_3^- symmetric stretching (940 cm^{-1} vs 936 cm^{-1}), and the appearance of only one band at 979 cm^{-1} on potassium chlorate for the antisymmetric stretching, and two bands at 1028 cm^{-1} and 988 cm^{-1} for the sodium chlorate. The potassium perchlorate is easily distinguished from the other spectra due to the difference Raman shift corresponding to the bands 941, 629, and 463 cm^{-1}, and the presence of two far away bands 1124 and 1087 cm^{-1}.

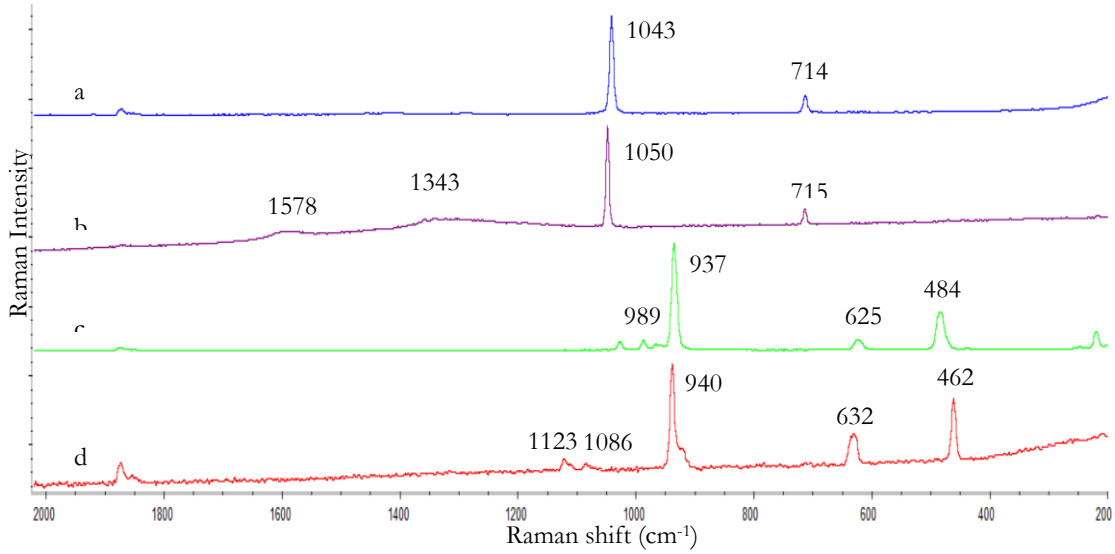

Figure 28. Reference Raman spectra of (a) ammonal (AlAN) (b) black powder (c) chloratite (d) flash powder (Thermo scientific DXR Raman microscope 780 nm, 10 mW, 6 s exposure, 5 accumulations).

Regarding the inorganic explosives, these are heterogenous mixtures of ionic compounds (i.e., the oxidizing salts), leading to spectra (see Figure 28) characterized by the presence of bands corresponding to the oxidizing salts (i.e., their major component). [57] The Raman spectra of ammonal (AlAN) displays bands at 1043 and 714 cm^{-1} that correspond to the ammonium nitrate. The bands located at 1050 and 715 cm^{-1} in the Raman spectra of

black powder correspond to the potassium nitrate. Flash powder displayed a Raman spectrum dominated by the bands of potassium perchlorate, located at 1123, 1086, 940, 632, and 462 cm^{-1}. In addition, the Raman spectra of chloratite showed characteristic bands of sodium chlorate, located at 989, 937, 625, and 484 cm^{-1}.

Although most of the spectra of inorganic explosives correspond to the oxidizing salts, the analysis of these explosives depends on the component of the mixture focused on the spot laser. This can be seen in appendix 25 for the inorganic explosive, chloratite, where different particles were analysed, that correspond to different components of the explosive mixture (sodium chlorate, sugar, and sulphur). For the black powder, this can also be seen by the appearance of two wide and weak bands at 1578 and 1343 cm^{-1} attributable to the charcoal fluorescence [57], and the spectra of sulphur in appendix 26. For flash powder and ammonal (AlAN), the same analysis was not possible, because the aluminium, which constitute these explosives, is inactive in Raman (i.e. aluminium does not contain covalent bonds).

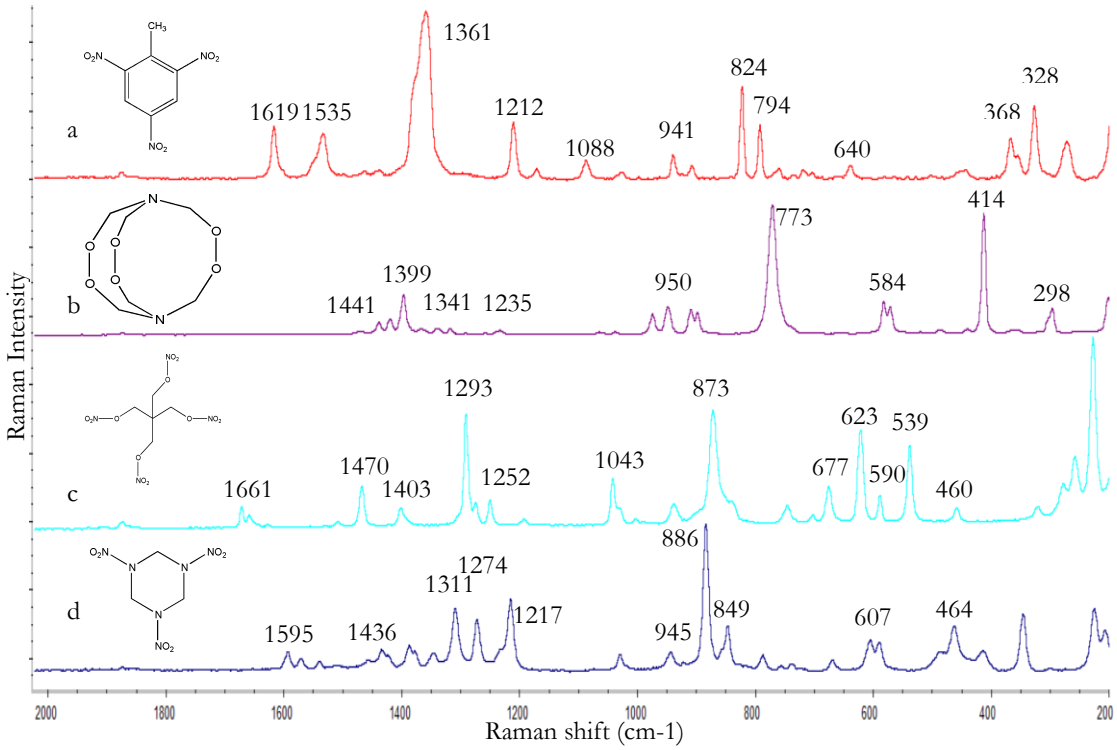

Figure 29. Reference Raman spectra of (a) TNT (b) HTMD (c) PETN (d) RDX (Thermo scientific DXR Raman microscope 780 nm, 10 mW, 6 s exposure, 5 accumulations). TNT and RDX were submitted to fluorescence correction.

The small number of bands that represent the spectra of the oxidizing salts and inorganic explosives, are in contrast with the spectra of the organic explosives (Figure 29). These explosives are organic homogeneous compounds with multiple covalent bonds that give a numerous display of bands, corresponding to their characteristic molecular vibrations. [57] TNT, PETN and RDX contain the nitro (NO_2) group and so, are classified as nitro-compounds. Despite all being nitro-compounds, they belong to distinct chemical families: the aliphatic nitrate ester (R-O-NO_2), the nitro-aromatic (Ar-NO_2), and the cycloaliphatic nitramine (>N-NO_2) family groups. [71, 75] This is due to the different type of bonds and the interaction with their neighbouring groups, resulting in Raman spectra with different characteristic bands. TNT is characterized by the bond C-NO_2, and thus classified as nitro-aromatic, has a Raman spectra where the most prominent band is located at 1361 cm^{-1}, that correspond to the NO_2 symmetric stretching vibration. The Raman spectrum of PETN, classified as nitrate ester (bond O-NO_2), is dominated by the bands located at 1293 and 873 cm^{-1} corresponding to the NO_2 symmetric stretching, and O-N stretching vibrations, respectively. In addition, the Raman spectra of RDX classified as nitramine (bond N-NO_2), has as the most intense band located at 886 cm^{-1} corresponding to the C-N or N-N stretching vibrations (appendix 20). The literature values of the positions of the symmetric and the antisymmetric NO_2 stretching vibrations of the organic explosives are given in appendix 8. Comparing with that table, the Raman shifts shown in the analysed spectra, are within the range of the literature values. This permits the discrimination of nitro-explosives.

Although, in these three organic explosives, the identification or detection is done mostly by the identification of the -NO_2 vibrational bands, there are a wide variety of explosives that do not have that oxidizer group. The HMTD is different from the nitro explosives, because it does not have the NO_2 group in his chemical structure. It is a peroxide explosive characterized by the O-O bond. The Raman spectra of HMTD is dominated by the bands located at 773 and 414 cm^{-1} corresponding to O-O stretching and N-C-O deformation (Figure 29 – (d)). Appendix 19, 20, and 21, lists the Raman shift and vibrational assignments of the principal characteristic bands in the spectra of the explosives and oxidizing salts.

3.2 Raman spectra taken from explosive and oxidizing salt particles trapped in the textile fabrics

Considering a real scenario where contamination of textile fabrics by explosives occurred, only trace or very small amounts of explosive residues will be trapped on the textile fabrics (Table 9). Thus, when using the Raman spectroscopy, the predominant spectral signatures will be from the background material (i.e., the textile fabrics). [72] After finding the alleged explosive/oxidizing salt particles trapped on the surface of the cloth fabrics, the laser was focused on it, and the Raman analysis was performed providing its characteristic Raman spectrum. To confirm that the analyte (i.e., the explosive and oxidizing salt particles) is present, the intensity of the Raman peak corresponding to the analyte, must be three times higher than the background noise (i.e., the fluorescence coming from the textile fabrics) at the proximity of the peak. In addition, the Raman spectra obtained from the analysis, was compared with the standard spectra of the explosives/oxidizing salts (Figures 27, 28, and 29 in section 3.1). In this section are represented and explained the Raman spectra of the oxidizing salts, inorganic explosives, and organic explosives particles trapped in the textile fabrics analysis by the Thermo Scientific DXR Raman microscope and the portable BWTEK i-Raman pro. It is important to notice that these Raman spectra did not undergo pre-processing methods, like baseline correction, smoothing or background fluorescence correction. This allow to see, if the interferences coming from the textile fabric hinder or not the positive chemical identification of the explosive.

Table 9. Classification of the textile fabrics.

Classification	Textile fabrics
Undyed natural fibre	White cotton
Undyed synthetic fibre	White polyester A, and White polyester B
Dyed natural fibre	Green, red, blue, black cotton; wool (beige colour)
Dyed synthetic fibre	Black, and blue polyester
Dyed natural/synthetic fibre	Blue denim jeans A, and jeans B.
Synthetic material	Latex, nitrile B, and nitrile B gloves; Polyskin

3.2.1 Explosives and oxidizing salts on undyed natural and synthetic fibres (white cotton and white polyester)

The Raman spectra obtained from oxidizing salt, inorganic and organic explosive particles trapped between white cotton natural fibres (Figure 30) are shown in Figures 31, 32, and 33, respectively.

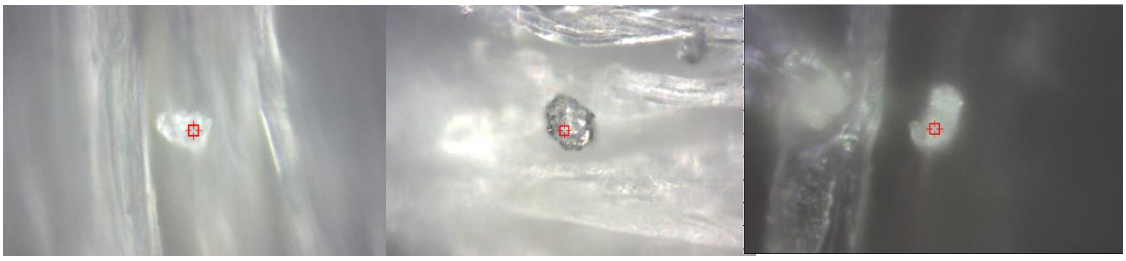

Figure 30. Left to right: particle of barium nitrate (100x), flash powder (50x), and TNT (100x) trapped in the white cotton fibres.

The comparison of these spectra with the reference spectra collected for the explosives standards shows that they are easily identified by their intense Raman bands. In Figures 32 and 33, corresponding to the inorganic and organic explosives trapped on white cotton, no characteristic Raman bands from the cotton fibres appeared, due to the precise confocal sampling of the particles. Regarding the oxidizing salts (Figure 31), some contain bands attributable to the cotton fibres (positive match to cotton fibres was made by a search in the Thermo Scientific DXR Raman microscope library, see appendix 98). Nevertheless, positive identification of the salt was still possible, since none of those bands interfered with the characteristic bands of the oxidizing salts. One exception was potassium perchlorate, whose bands located at 1124 and 1087 cm^{-1} are overlapped by the bands of the white cotton fibres. In the portable BWTEK i-Raman pro, the same analysis was made, providing similar results (see appendix 27, 28, and 29).

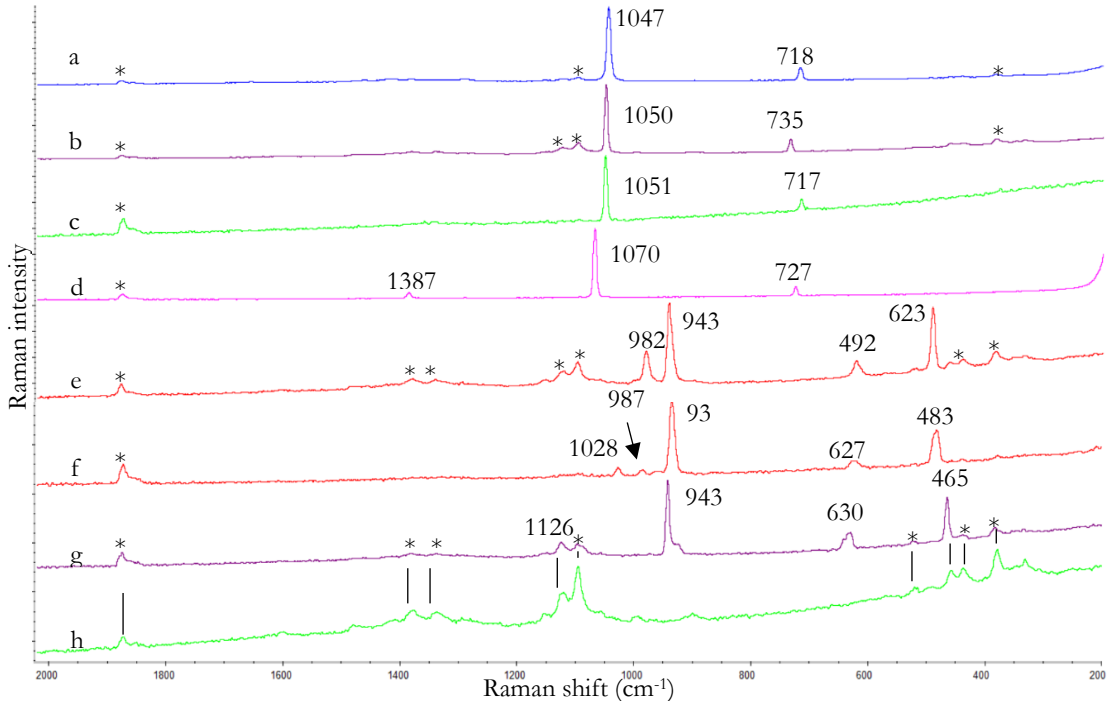

Figure 31. Raman spectra of (a) ammonium nitrate (b) barium nitrate (c) potassium nitrate (d) sodium nitrate (e) potassium chlorate (f) sodium chlorate (g) potassium perchlorate particles on white cotton fibres (h) white cotton fibres (asterisks indicate white cotton bands) (Thermo Scientific DXR Raman microscope, 780 nm, 14 mW, 5 s exposure, 8 accumulations).

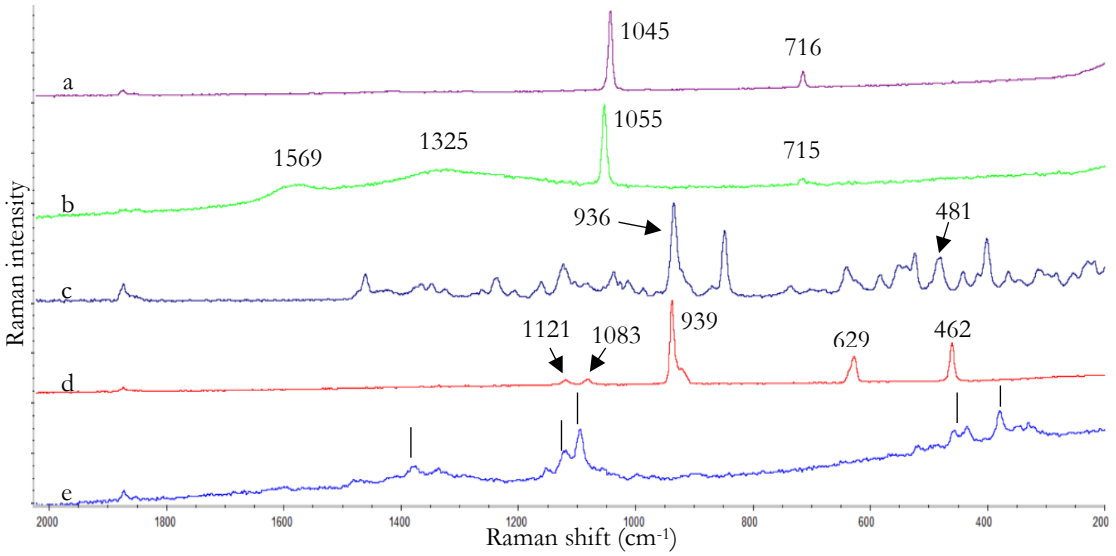

Figure 32. Raman spectra of (a) ammonal (b) black powder (c) chloratite (d) flash powder particles on white cotton fibres (e) white cotton fibres (Thermo Scientific DXR Raman microscope, 780 nm, 10 mW, 6 s exposure, 5 accumulations).

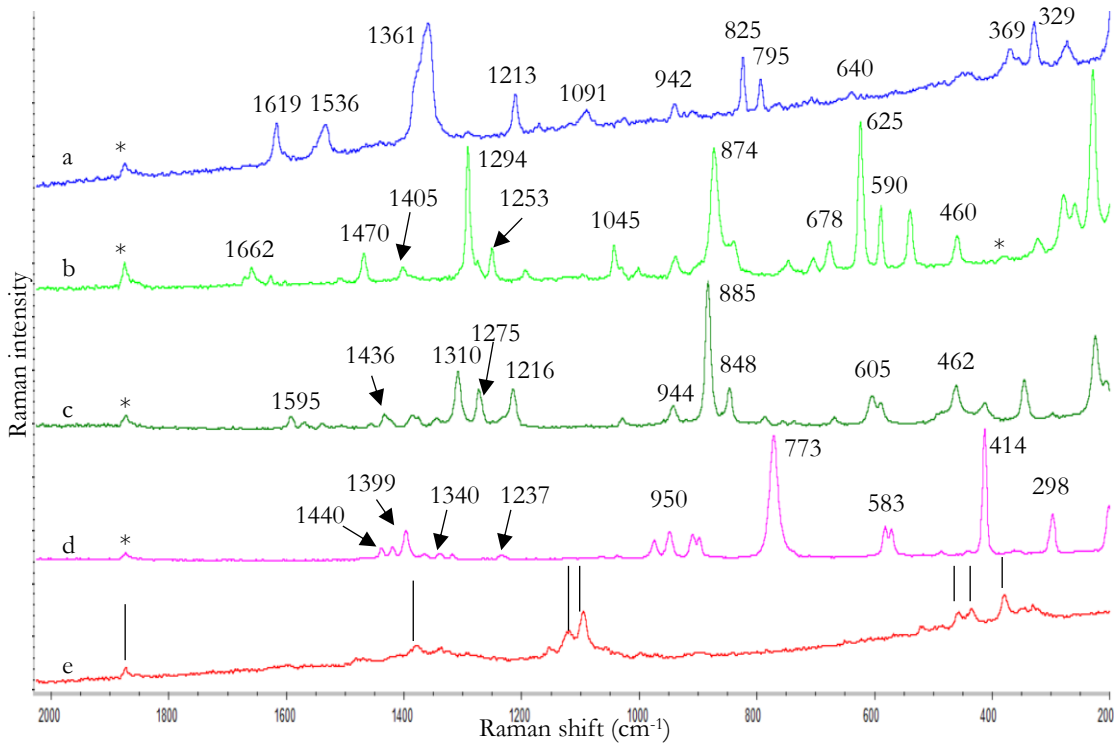

Figure 33. Raman spectra of (a) TNT (b) PETN (c) RDX (d) HMTD particles on white cotton fibres (e) white cotton fibres (asterisks indicate white cotton bands) (Thermo Scientific DXR Raman microscope, 780 nm, 10 mW, 6 s exposure, 5 accumulations).

The other undyed textiles analysed were the two-white polyester synthetic fibres. The Raman spectra of both is identical, but they differentiate in the organization of the polyester fibres (Figure 34).

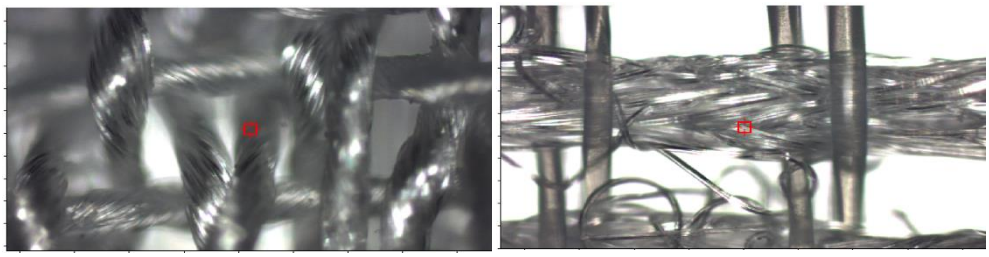

Figure 34. Left to right: white polyester 1 and 2 (Thermo Scientific DXR Raman microscope, 10x microscopic objective).

The Raman spectra of the oxidizing salt, inorganic and organic explosives particles trapped in the white polyester fibres (Figure 35) are represented in Figures 36, 37, and 38, (and appendix 33, 34, 35 for white polyester 1), respectively, for the Thermo Scientific DXR Raman microscope.

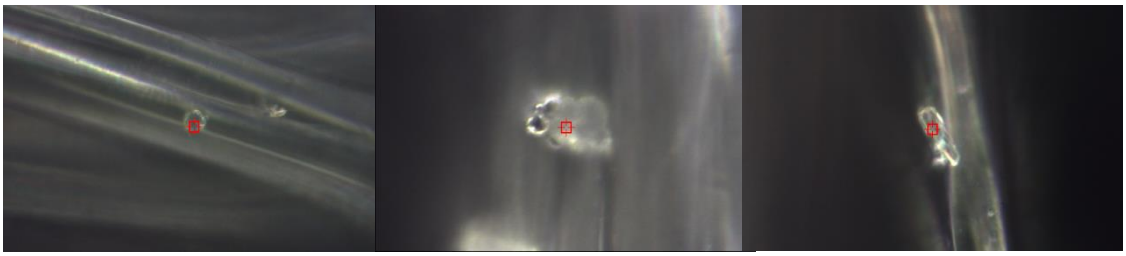

Figure 35. Left to right: particle of potassium chlorate (100x), ammonal (ALAN) (100x), and HMTD (100x) trapped in the white polyester fibres.

Besides the bands from the explosive/oxidizing salt, the resulting spectra also showed many bands assigned to the polyester fibre (marked with asterisks in the figures), making this textile a Raman active one. Even though some of the white polyester bands did overlapped with the ones of the analyte (e.g. the bands 627 cm^{-1} for sodium chlorate (f) and 631 cm^{-1} for potassium perchlorate (g), or the band 1274 cm^{-1} of RDX explosive in Figure 38 – (c)), the most intense bands arising from the explosive/oxidizing salt were always very well distinguished and visible, allowing a positive identification.

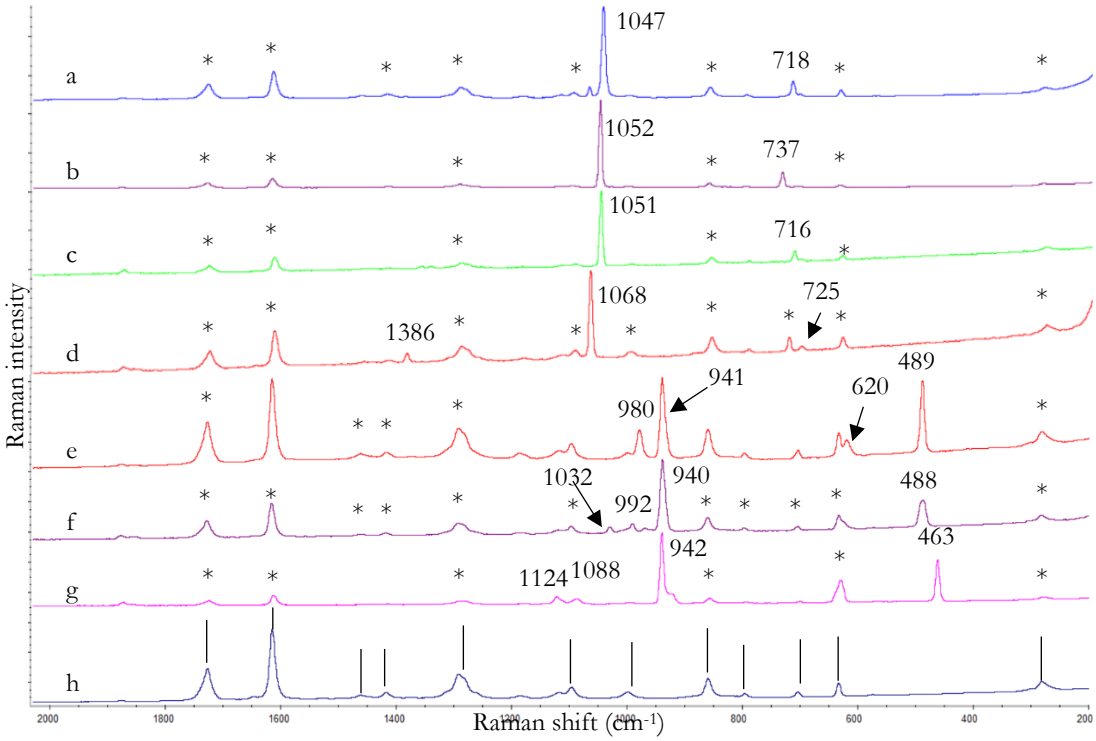

Figure 36. Raman spectra of (a) ammonium nitrate (b) barium nitrate (c) potassium nitrate (d) sodium nitrate (e) potassium chlorate (f) sodium chlorate (g) potassium perchlorate particles on white cotton fibres (h) white polyester 2 fibres (asterisks indicate white polyester 2 bands) (Thermo Scientific DXR Raman microscope, 780 nm, 14 mW, 5 s exposure, 8 accumulations).

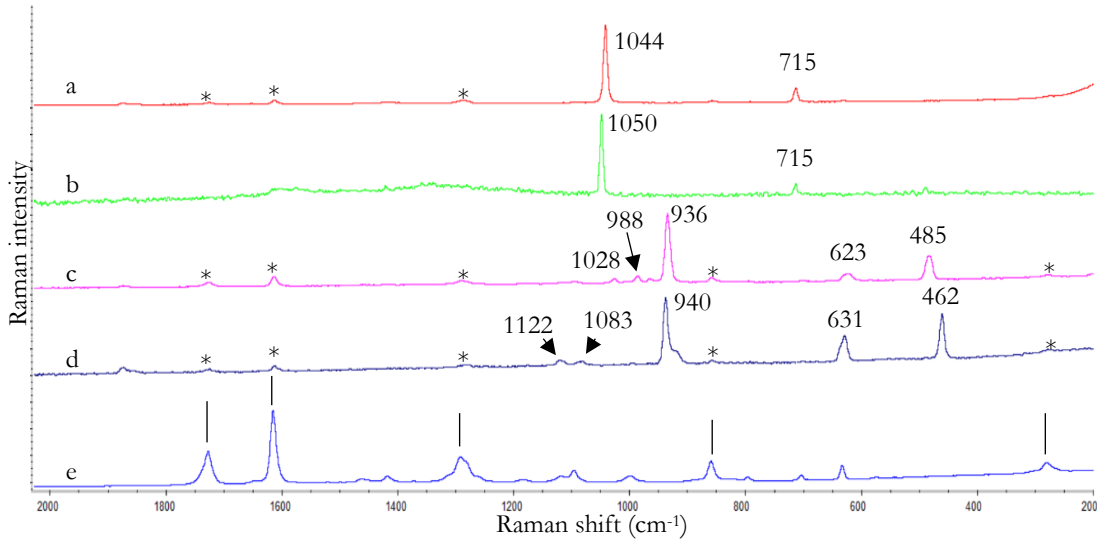

Figure 37. Raman spectra of (a) ammonal (b) black powder (c) chloratite (d) flash powder particles on white polyester 2 fibres (e) white polyester 2 fibres (asterisks indicate white polyester 2 bands) (Thermo Scientific DXR Raman microscope, 780 nm, 10 mW, 6 s exposure, 5 accumulations).

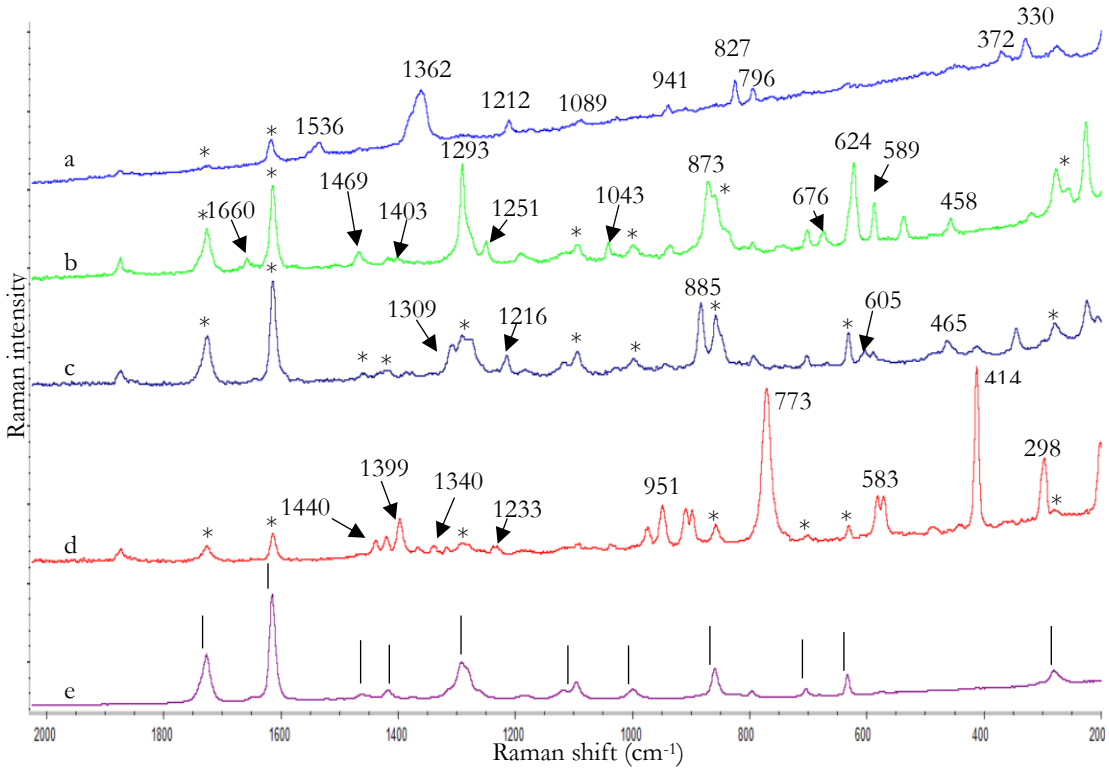

Figure 38. Raman spectra of (a) TNT (b) PETN (c) RDX (d) HMTD particles on white polyester 2 fibres (e) white polyester 2 fibres (asterisks indicate white polyester 2 bands) (Thermo Scientific DXR Raman microscope, 780 nm, 10 mW, 6 s exposure, 5 accumulations).

The same results were observed for the white polyester analysed by the portable BWTEK i-Raman pro (appendix 30, 31, 32, 36, 37, and 38), where the bands of the polyester fibres do not overlap the most characteristic bands of the explosives/oxidizing salts.

3.2.2 Explosives and oxidizing salts on dyed natural and synthetic textiles (green, red, blue, and black cotton; black, and blue polyester; blue denim jeans; polyskin; and wool)

Green, red, blue, and black cotton

Most of the textiles encountered in daily life are dyed, and it is necessary to determine how this will affect the Raman spectra of the explosive particles trapped between fibres of dyed clothing textiles (see Figure 39). In Raman spectroscopy, the characteristic vibrations arising from the dye molecules and the high levels of fluorescence may conceal the spectral features of the explosives/oxidizing salts. [60] Thus, in most Raman spectra of the analysed dyed textiles, the bands corresponding to the original textile fabrics usually do not appear. Instead, they may correspond to the different dyes, and sometimes only fluorescence is seen in these Raman spectra.

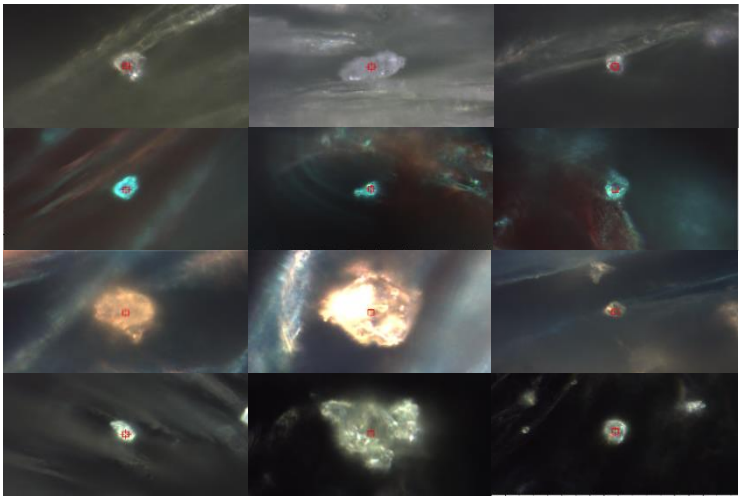

Figure 39. Left to right: particles of potassium perchlorate, chloratite, and PETN trapped in the (top to bottom) green, red, blue, and black cotton fibres (100x).

In blue cotton fibres (Figures 40, 41 and 42 for the oxidizing salts, inorganic and organic explosives analysed in the Thermo Scientific DXR Raman microscope), the chemical identification was easily made by comparing their characteristic Raman bands to those of the

standards. Bands that may correspond to the dye (marked with asterisks) superimposed on a fluorescence background, were also observed, as they do not overlap with the bands of the explosives/oxidizing salts. In appendix 39, 40, and 41 the same results for the Raman spectra analysed by the portable Raman are shown.

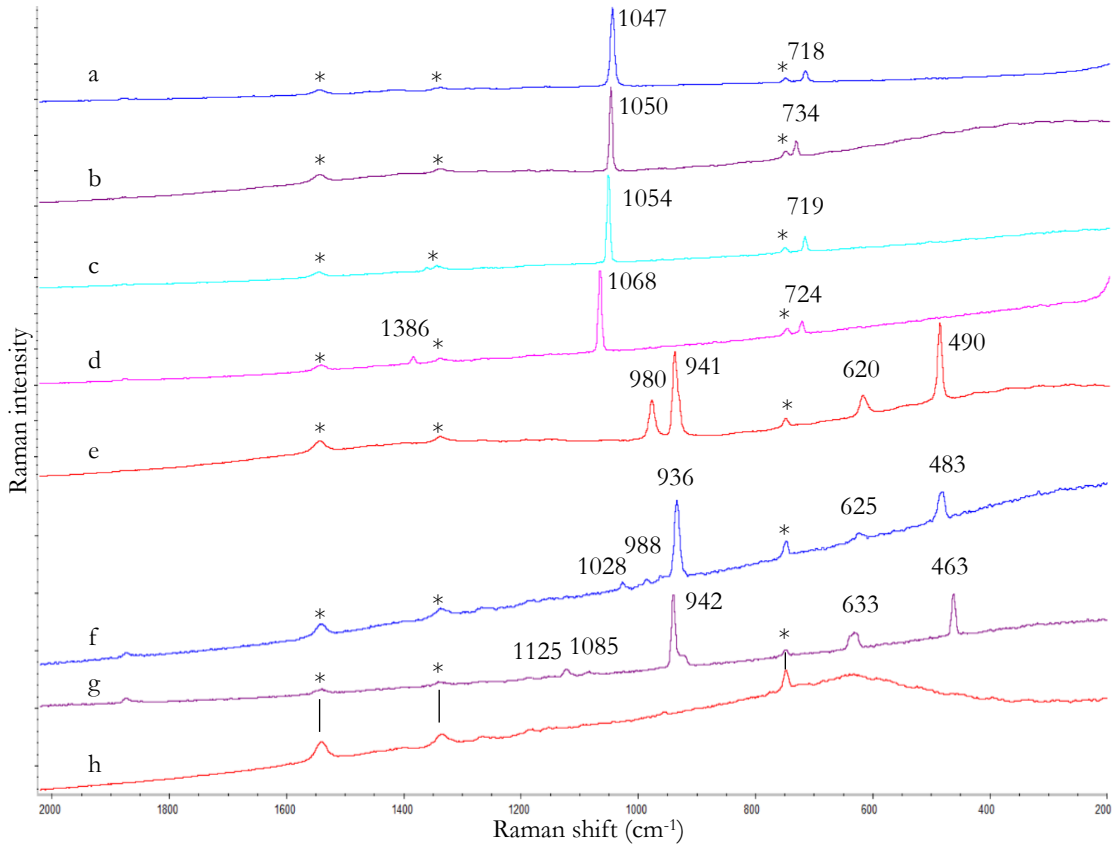

Figure 40. Raman spectra of (a) ammonium nitrate (b) barium nitrate (c) potassium nitrate (d) sodium nitrate (e) potassium chlorate (f) sodium chlorate (g) potassium perchlorate particles on blue cotton fibres (h) blue cotton fibres (asterisks indicate blue cotton bands) (Thermo Scientific DXR Raman microscope, 780 nm, 14 mW, 5 s exposure, 8 accumulations).

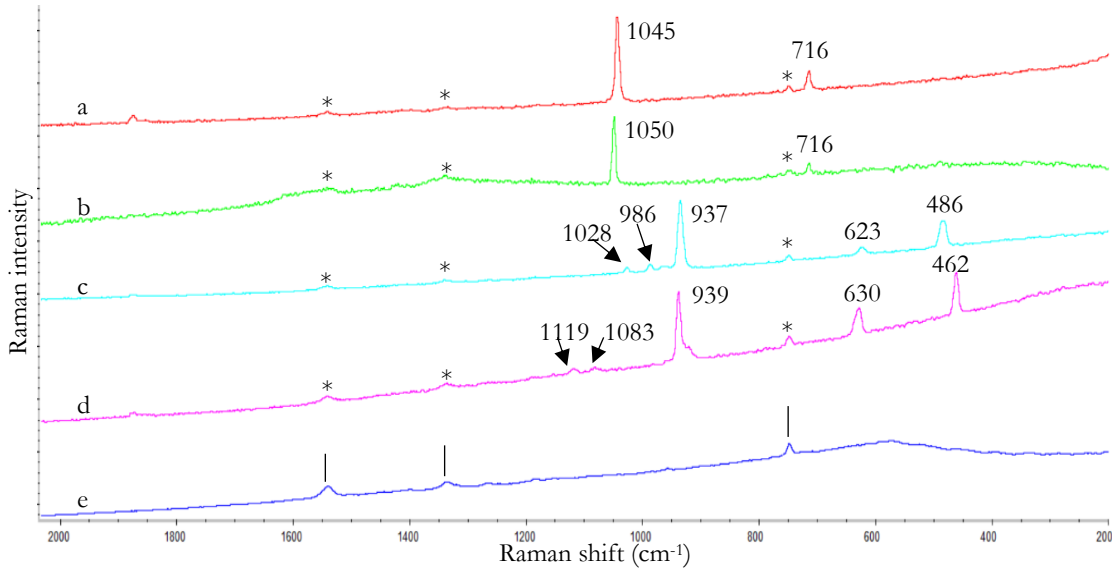

Figure 41. Raman spectra of (a) ammonal (b) black powder (c) chloratite (d) flash powder particles on blue cotton fibres (e) blue cotton fibres (asterisks indicate blue cotton bands) (Thermo Scientific DXR Raman microscope, 780 nm, 10 mW, 6 s exposure, 5 accumulations).

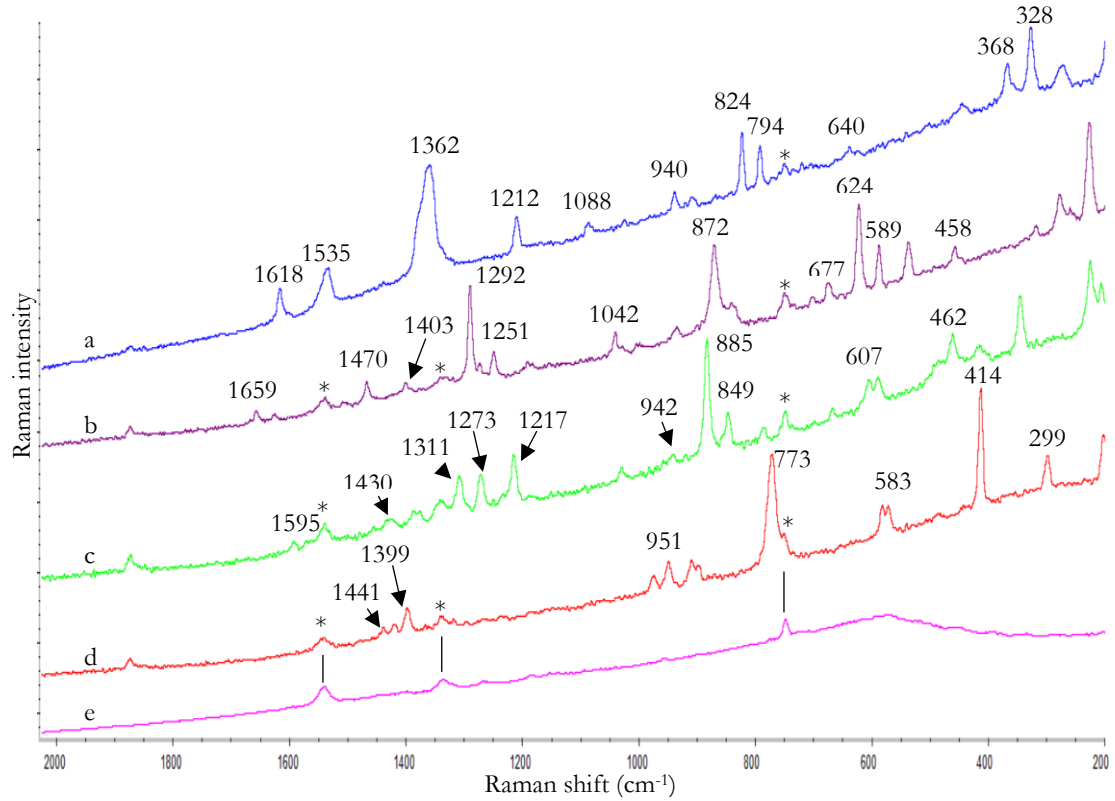

Figure 42. Raman spectra of (a) TNT (b) PETN (c) RDX (d) HMTD particles on blue cotton fibres (e) blue cotton fibres (asterisks indicate blue cotton bands) (Thermo Scientific DXR Raman microscope, 780 nm, 10 mW, 6 s exposure, 5 accumulations).

For red (appendix 42, 44, and 46 for the Thermo Scientific DXR Raman microscope, and appendix 43, 45, and 47 for the portable Raman), and green cotton (appendix 48, 50, and 52 for the Thermo Scientific DXR Raman microscope, and appendix 49, 51, and 53 for the portable Raman), positive chemical identification of explosives was also possible. The analysis of these textiles showed some bands that may correspond to the dye or to the original fibres (i.e. cotton fibres). In the case of green cotton, those bands gave a partial match to the Raman spectra of cotton fibres (see appendix 99). For red cotton, a partial match to a Raman spectra of "cibracon brilliant red 3B-A" dye was observed (see appendix 100). In addition, in the Raman spectra of red cotton, also bands of the cotton fibres were seen, in conjunction with the ones of the red dye (see appendix 100). Nevertheless, those bands did not interfere with the characteristic bands of explosives/oxidizing salts.

Regarding black cotton (appendix 54, 56, and 58 for the Thermo Scientific DXR Raman microscope, and appendix 55, 57, and 59 for the portable Raman), most of the Raman spectra presented high levels of fluorescence with no band corresponding to the dye or cotton fibres. By focusing the laser spot directly on the particle, it was possible to obtain the Raman spectra of the analytes, ignoring the fluorescence from the textile fabric. The analysis of this textile posed some problems. In some cases, textile burned when subjected to the Raman laser (see appendix 97). Even so, by reducing the laser power (5 mW for the Thermo Scientific, and 1% of the 320 mW for the portable Raman), and focusing the laser at big particles (see section 3.3, for the relation of the particle sizes with black cotton), positive identification was possible.

Black and blue polyester

Explosives/oxidizing salt particles trapped in black and blue polyester are displayed in the Figure 43. The Raman spectra of the explosive/oxidizing salt particles analysed in blue polyester are shown in Figures 44, 45, and 46 for the Thermo Scientific DXR Raman microscope, and appendix 60, 61, and 62 for the portable Raman. For black polyester, the spectra are represented in appendix 63, 65, and 67 for the Thermo Scientific DXR Raman microscope, and appendix 64, 66, and 68 for the portable Raman.

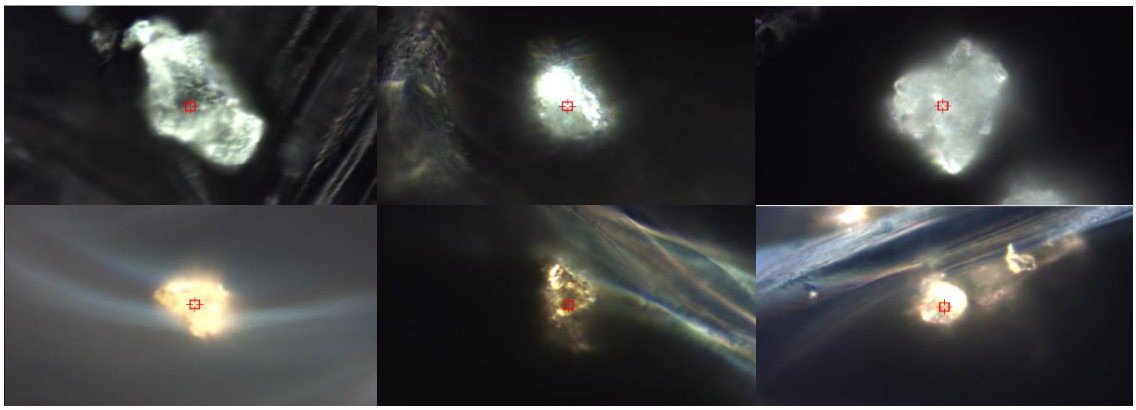

Figure 43. Left to right: particles of potassium nitrate, flash powder, and RDX trapped in the (top to bottom) black and blue polyester fibres (100x).

By carefully focusing the laser into the particles, Raman spectra were obtained and compared to the spectra of standards to identify the bands related to the explosives/oxidizing salts. This provided positive identification of each particle. Most of the resulting spectra contained high levels of background fluorescence that did not allow the visualization of the bands corresponding to the dye and/or polyester fibres. However, the Raman spectral bands from explosives are clearly identifiable above the background. In some cases, background fluorescence swamped the Raman signals from the explosive particles (see appendix 61 and 62 for organic and inorganic particles analysed in blue polyester fibres by the portable Raman). This occurred more frequently when using the portable Raman and for organic and inorganic explosives, due to the fluorescence-giving components that constitute the inorganic explosives (i.e. charcoal and aluminium), and the colour (e.g. TNT crystals have a weak yellow colour). This can lead to the conclusion that the portable Raman is not the ideal instrument when analysing inorganic and organic explosives on very fluorescent textiles (i.e. blue polyester). A solution was the targeting of large particles, to minimize the influence from the textile fabric. Despite fluorescence, good results for the black polyester were observed for both instruments (see appendix 63, 65, and 67 for the Thermo Scientific DXR Raman microscope, and appendix 64, 66, and 68 for the portable BWTEK i-Raman pro).

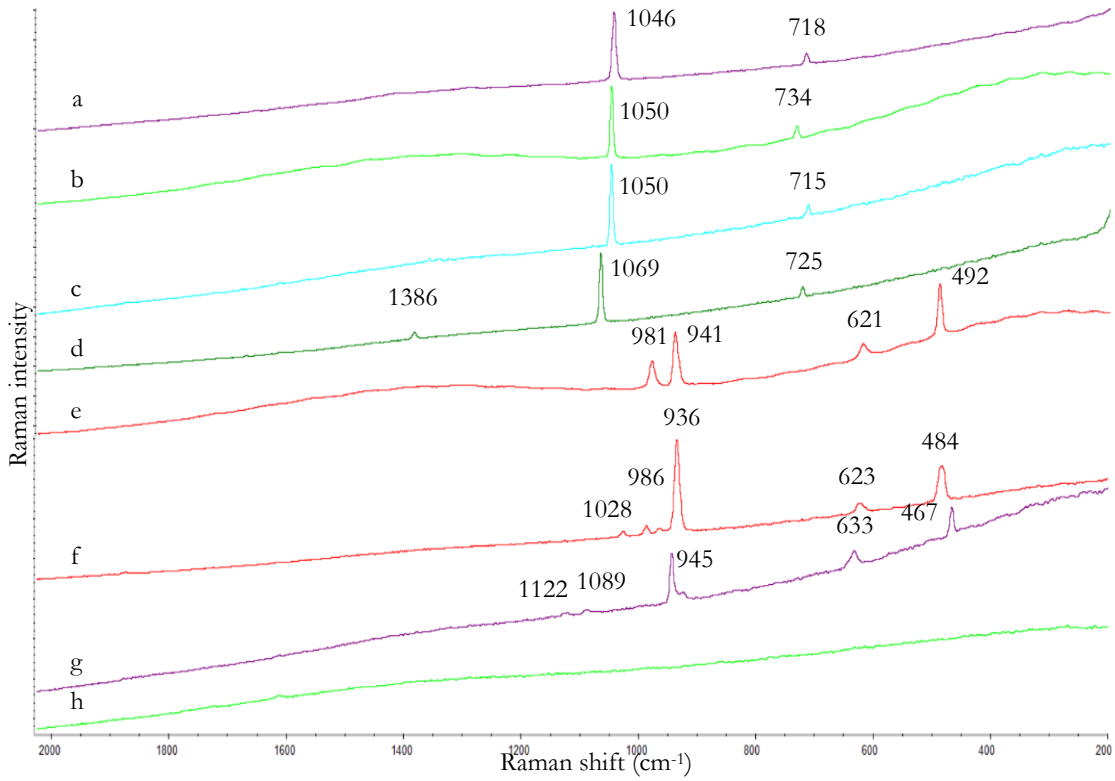

Figure 44. Raman spectra of (a) ammonium nitrate (b) barium nitrate (c) potassium nitrate (d) sodium nitrate (e) potassium chlorate (f) sodium chlorate (g) potassium perchlorate particles on blue polyester fibres (h) blue polyester fibres (asterisks indicate blue polyester bands) (Thermo Scientific DXR Raman microscope, 780 nm, 14 mW, 5 s exposure, 8 accumulations).

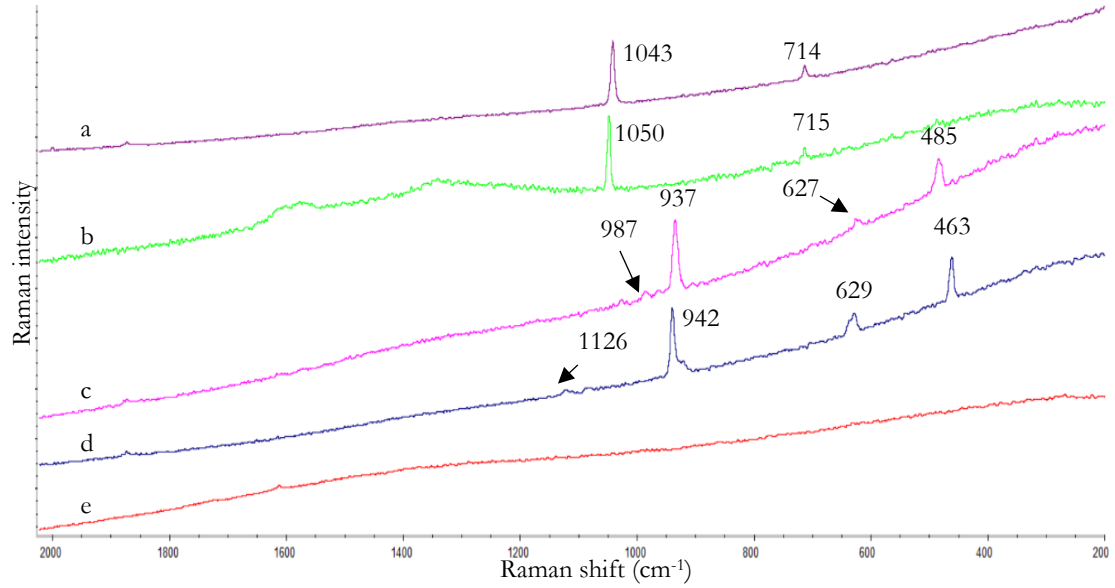

Figure 45. Raman spectra of (a) ammonal (b) black powder (c) chloratite (d) flash powder particles on blue polyester fibres (e) blue polyester fibres (asterisks indicate blue polyester bands) (Thermo Scientific DXR Raman microscope, 780 nm, 10 mW, 6 s exposure, 5 accumulations for (a-d), 1 mW for (e)).

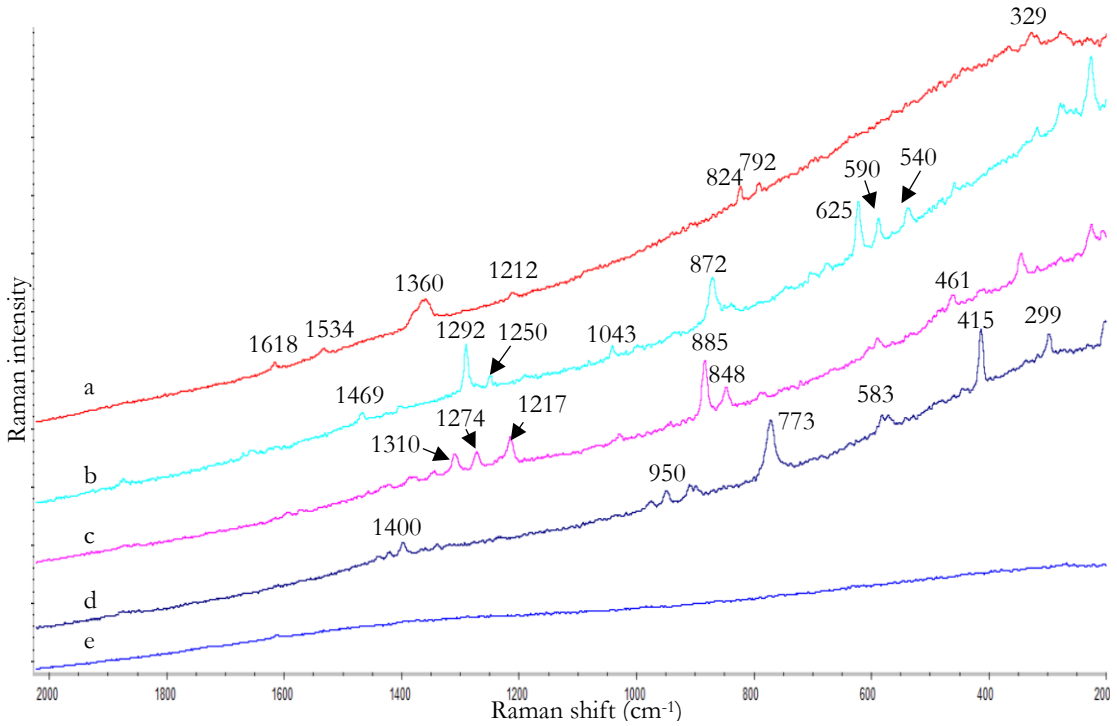

Figure 46. Raman spectra of (a) TNT (b) PETN (c) RDX (d) HMTD particles on blue polyester fibres (e) blue polyester fibres (asterisks indicate blue polyester bands) (Thermo Scientific DXR Raman microscope, 780 nm, 10 mW, 6 s exposure, 5 accumulations).

Blue denim jeans

The explosives particles trapped on two different blue denim jeans were analysed (Figure 47).

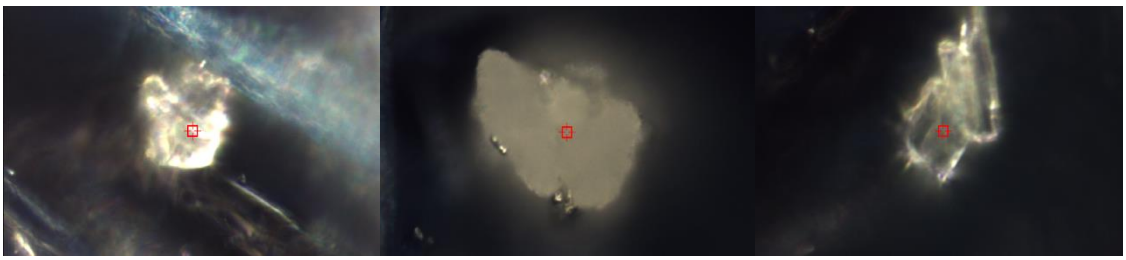

Figure 47. Left to right: particles of sodium chlorate (100x), ammonal (50x), and HMTD (100x) trapped in the blue denim fibres.

The Raman spectra of the oxidizing salts, inorganic and organic explosives trapped in the jeans B textile fabric, are displayed in Figures 48, 49, and 50 for the Thermo Scientific DXR Raman microscope, and appendix 69, 70, and 71 for the portable Raman. Regarding the jeans A textile, the Raman spectra of the analysed particles are included in appendix 72, 74, and 76 for the Thermo Scientific DXR Raman microscope, and appendix 73, 75, and 77

for the portable Raman. Similarly, to blue and black polyester, the spectra of the particles trapped on blue denim jeans showed high levels of fluorescence from the dye. Thus, targeting the larger particles and with a correct focusing of the laser, the Raman spectral bands of the explosives/oxidizing salts were clearly identifiable above the background. By comparison with the standard spectra, positive identification was made. In jeans B, besides the high level of fluorescence, it was possible to detect bands that did not interfere with the characteristic vibrations of the particles analysed. Those bands corresponded partially to the "blue indigo" dye (see appendix 101), whose main band is located at 1570 cm^{-1}, generally present in blue denim textiles. [60] On the contrary, in jeans A, only fluorescence was observed. Another problem when analysing these textiles with the portable Raman, was that they burned even when the laser power (see appendix 97) used was the lowest.

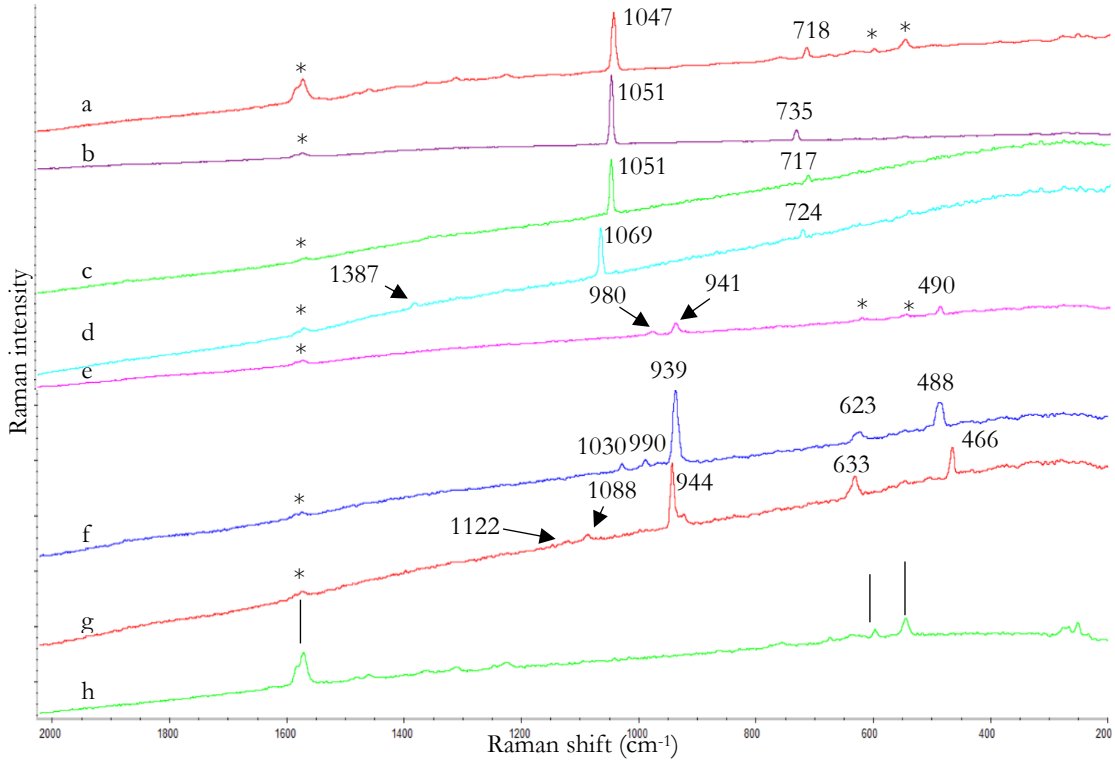

Figure 48. Raman spectra of (a) ammonium nitrate (b) barium nitrate (c) potassium nitrate (d) sodium nitrate (e) potassium chlorate (f) sodium chlorate (g) potassium perchlorate particles on jeans 2 fibres (h) jeans 2 fibres (asterisks indicate jeans 2 bands) (Thermo Scientific DXR Raman microscope, 780 nm, 14 mW, 5 s exposure, 8 accumulations for (a-g), 1 mW, 6 s exposure, 5 accumulations for (h)).

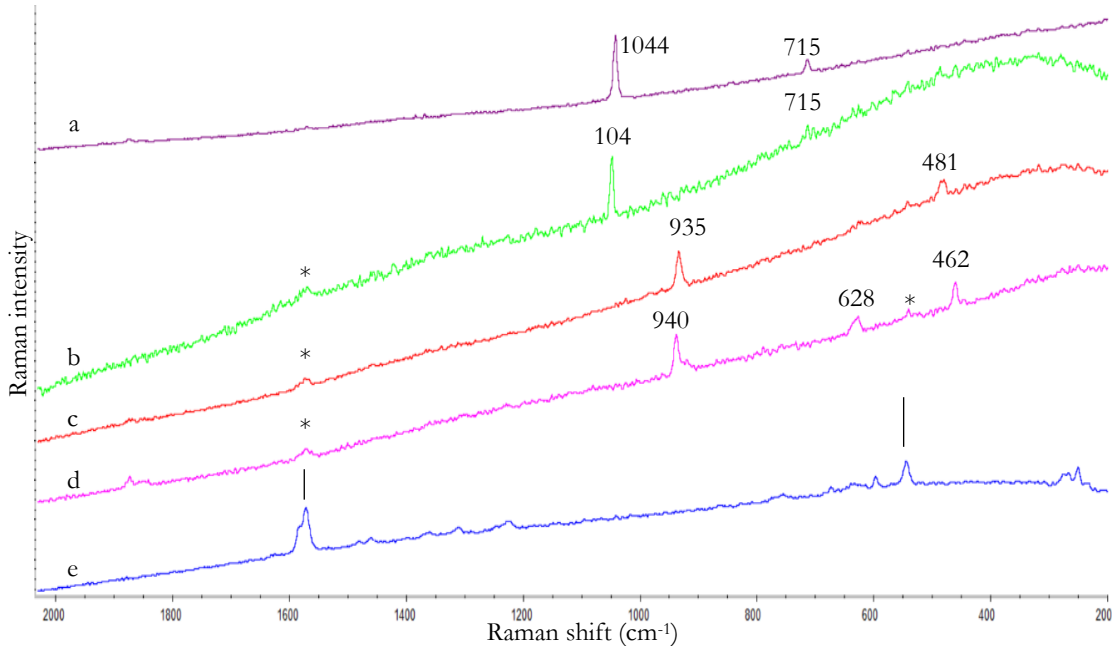

Figure 49. Raman spectra of (a) ammonal (b) black powder (c) chloratite (d) flash powder particles on jeans 2 fibres (e) jeans 2 fibres (asterisks indicate jeans 2 bands) (Thermo Scientific DXR Raman microscope, 780 nm, 10 mW, 6 s exposure, 5 accumulations for (a-d), 1 mW, 6 s exposure, 5 accumulations for (e)).

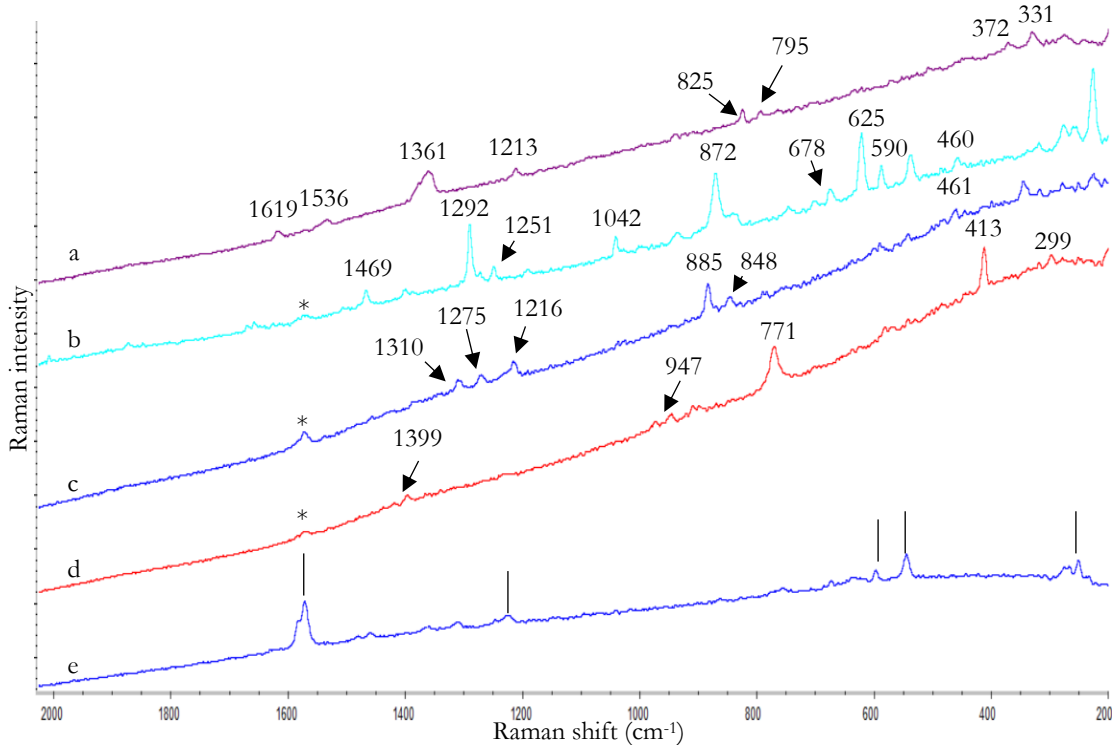

Figure 50. Raman spectra of (a) TNT (b) PETN (c) RDX (d) HMTD particles on jeans 2 fibres (e) jeans 2 fibres (asterisks indicate jeans 2 bands) (Thermo Scientific DXR Raman microscope, 780 nm, 10 mW, 6 s exposure, 5 accumulations for (a-d), 1 mW, 6 s exposure, 5 accumulations for (e)).

Wool

The wool is here classified as a dyed natural textile, since it showed a beige dye. The spectra represented in Figures 52, 53 and 54 for the inorganic explosives, oxidizing salts, and organic explosives particles analysed by the Thermo Scientific DXR Raman microscope trapped in the wool textile (Figure 51), show that, with the corrected focusing, the analytes are very well identified by their characteristic bands above the background fluorescence.

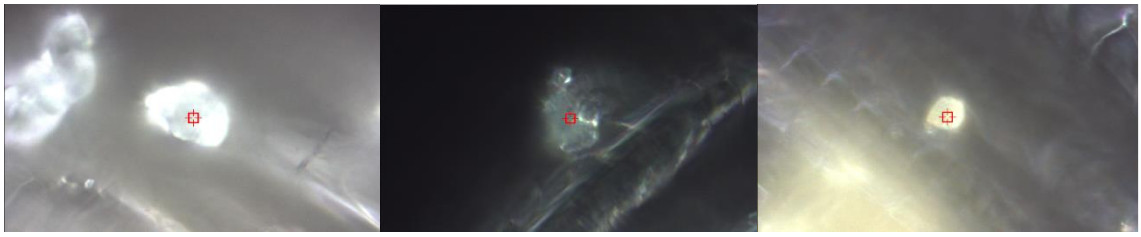

Figure 51. Left to right: particles of ammonium nitrate (100x), chloratite (50x), and TNT (100x) trapped in the wool fibres.

By comparison with the standard spectra, the identification was positive. The spectra analysed from both instruments (in appendix 78, 79, 80 the spectra analysed by the portable Raman may be found) presented some fluorescence due to the dye present in the textile fabric. In addition, in the case of the spectra analysed in the Thermo Scientific DXR Raman microscope, some bands that do not interfere with the bands of explosives are seen (marked as asterisks), that may correspond to the dye or to the original wool fibres.

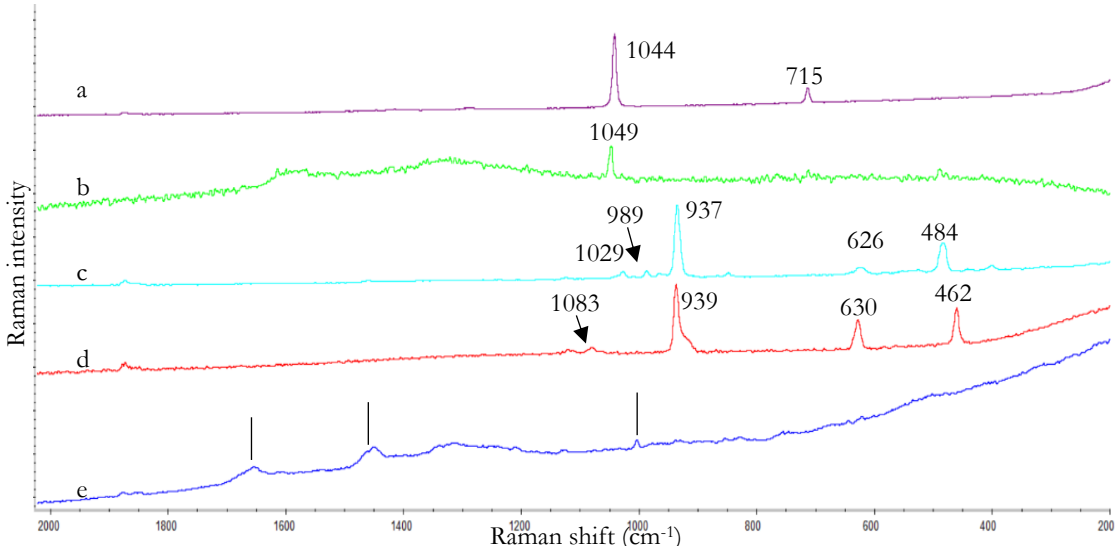

Figure 52. Raman spectra of (a) ammonal (b) black powder (c) chloratite (d) flash powder particles on wool fibres (e) wool fibres (asterisks indicate wool bands) (Thermo Scientific DXR Raman microscope, 780 nm, 10 mW, 6 s exposure, 5 accumulations).

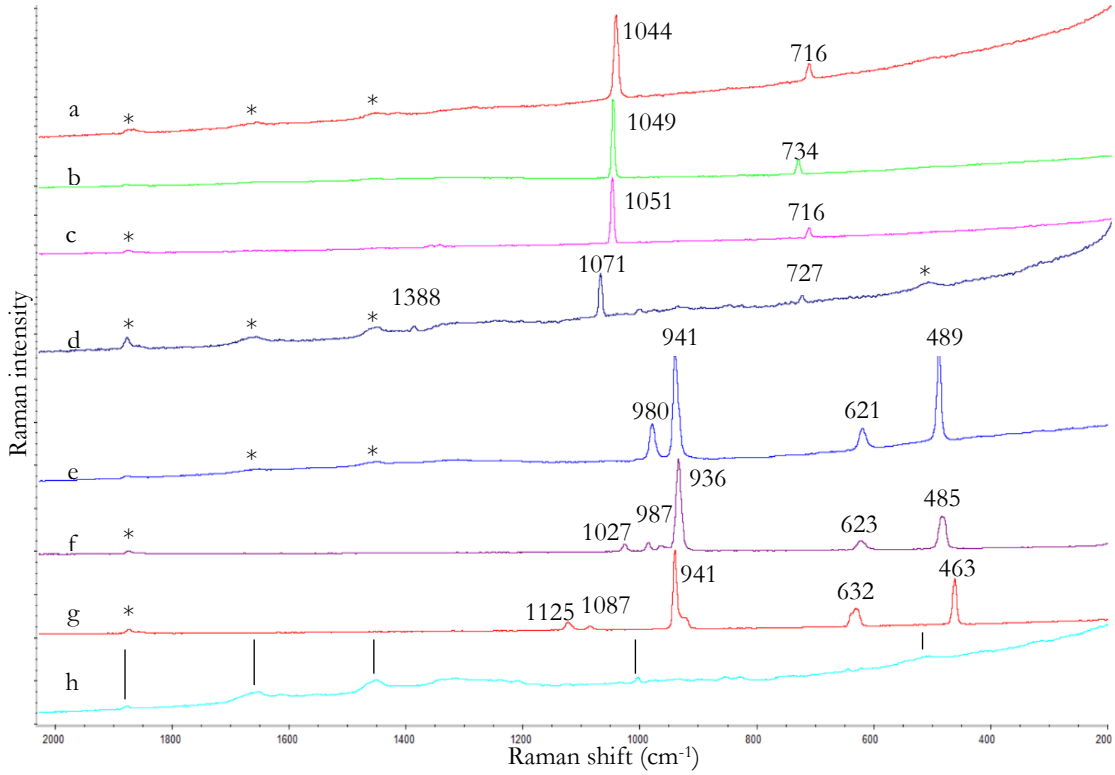

Figure 53. Raman spectra of (a) ammonium nitrate (b) barium nitrate (c) potassium nitrate (d) sodium nitrate (e) potassium chlorate (f) sodium chlorate (g) potassium perchlorate particles on wool fibres (h) wool fibres (asterisks indicate wool bands) (Thermo Scientific DXR Raman microscope, 780 nm, 14 mW, 5 s exposure, 8 accumulations).

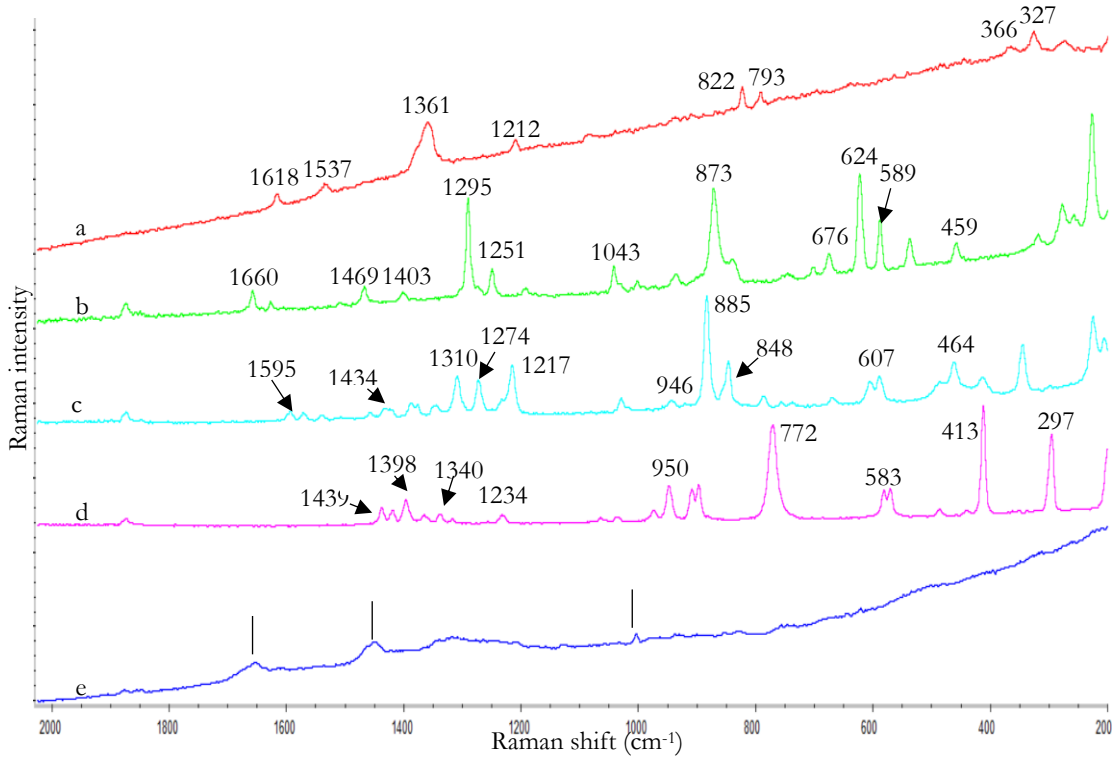

Figure 54. Raman spectra of (a) TNT (b) PETN (c) RDX (d) HMTD particles on wool fibres (e) wool fibres (asterisks indicate wool bands) (Thermo Scientific DXR Raman microscope, 780 nm, 10 mW, 6 s exposure, 5 accumulations).

3.2.3 Explosives and oxidizing salts on synthetic materials: laboratory gloves (nitrile and latex), and polyskin

In this case, particles were no longer trapped, since these materials do not have fibres (see Figure 55). Instead, they are smooth surface materials, allowing rapid visualization of the particles. The latex and nitrile laboratory gloves were used in this study, thinking that during the construction of an IED or bombing device, the terrorist may use these kind of gloves (i.e. if he has minimal knowledge of chemistry).

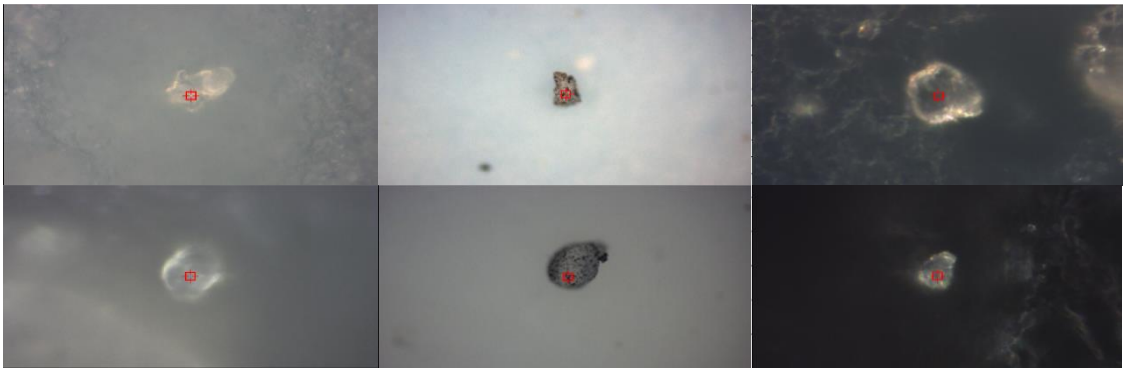

Figure 55. Left to right: particles of sodium nitrate (100x), black powder (10x), and PETN (100x) trapped in the (top to bottom) nitrile and latex materials.

The results are shown in Figures 56, 57, and 58 for the Thermo Scientific DXR Raman analysis (and appendix 84, 85, and 86 for the portable Raman) for the nitrile A. Results for nitrile B are included in appendix 87, 89, and 91 for the Thermo Scientific DXR Raman analysis (and appendix 88, 90, and 92 for the portable Raman). In both nitrile gloves, positive identification of the oxidizing salts/explosive particles was possible by matching the characteristic bands to the standards. Bands (marked as asterisks) corresponding to the polymeric materials that compose these gloves were also observed for both nitrile materials. In the case of nitrile A, between 400 -650 cm^{-1} two peaks were observed that were not present in nitrile B. Thus, besides their different colours, differentiation of their Raman spectra is also possible, differences which seem to be due to the different dyes. The most intense bands of both nitrile samples are above 1200 cm^{-1} Raman shift, thus they did not interfere with the bands of the inorganic explosives (Figure 57) and oxidizing salts (Figure 56), but they partially overlapped the bands of organic explosive particles (see Figure 58 – RDX (c), HMTD (d)). Nevertheless, positive identification of the explosive was still possible.

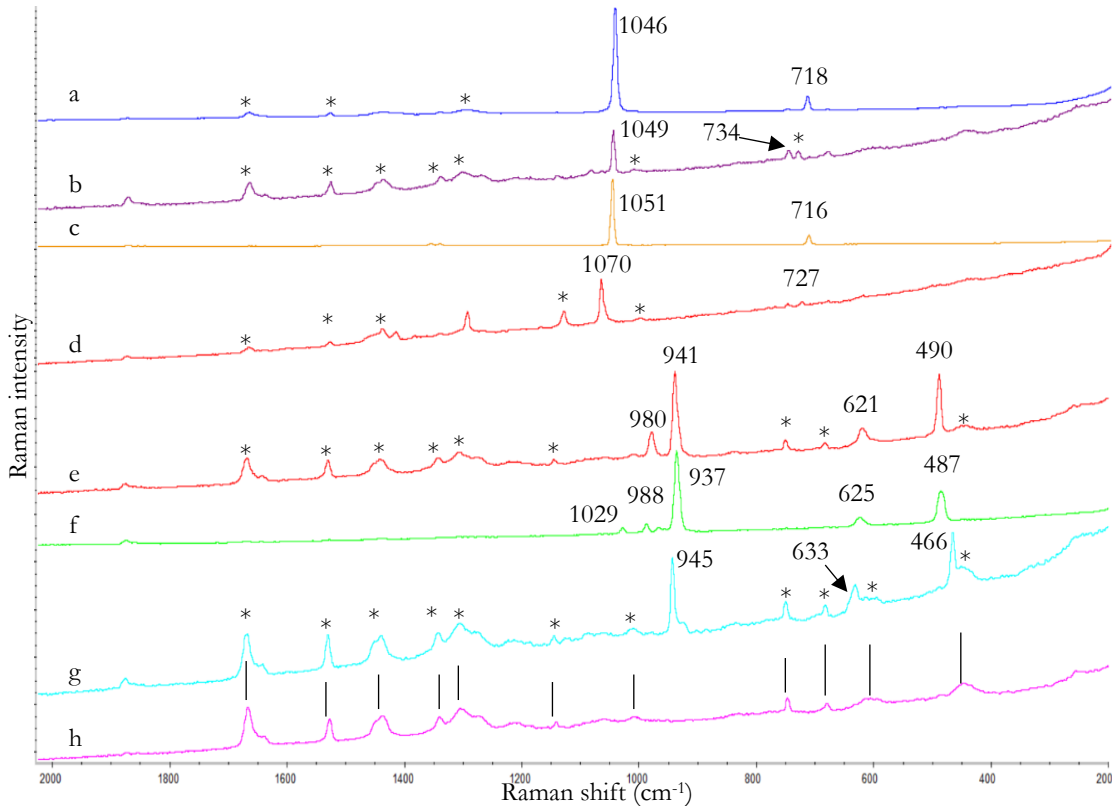

Figure 56. Raman spectra of (a) ammonium nitrate (b) barium nitrate (c) potassium nitrate (d) sodium nitrate (e) potassium chlorate (f) sodium chlorate (g) potassium perchlorate particles on nitrile 1 (h) nitrile 1 (asterisks indicate nitrile 1 bands) (Thermo Scientific DXR Raman microscope, 780 nm, 14 mW, 5 s exposure, 8 accumulations).

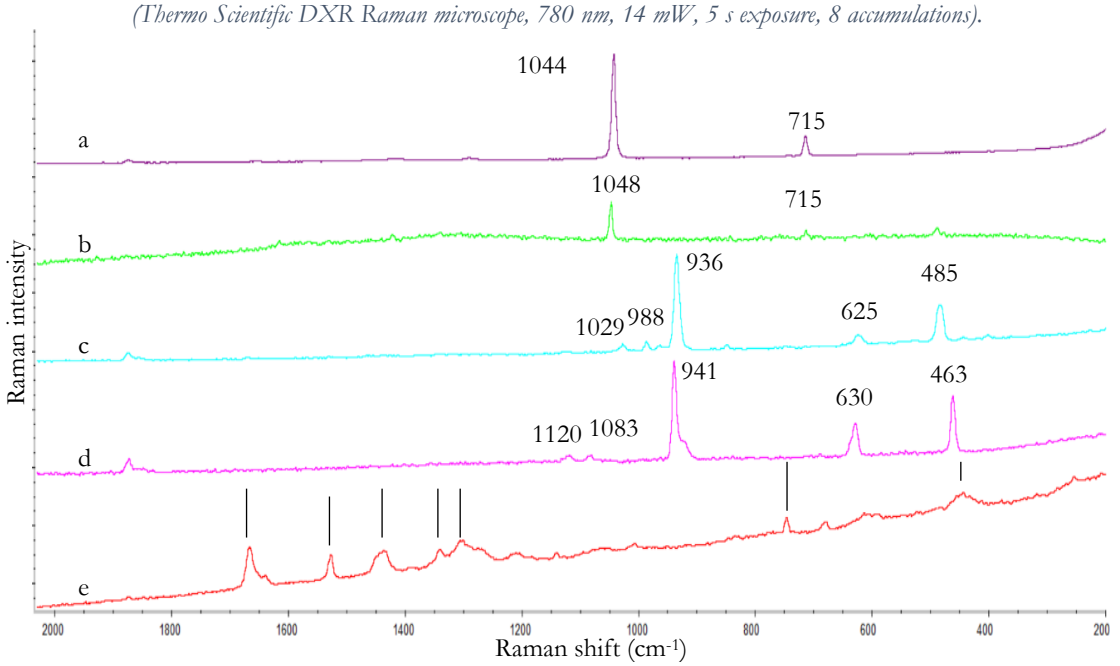

Figure 57. Raman spectra of (a) ammonal (b) black powder (c) chloratite (d) flash powder particles on nitrile 1 (e) nitrile 1 (asterisks indicate nitrile 1 bands) (Thermo Scientific DXR Raman microscope, 780 nm, 10 mW, 6 s exposure, 5 accumulations).

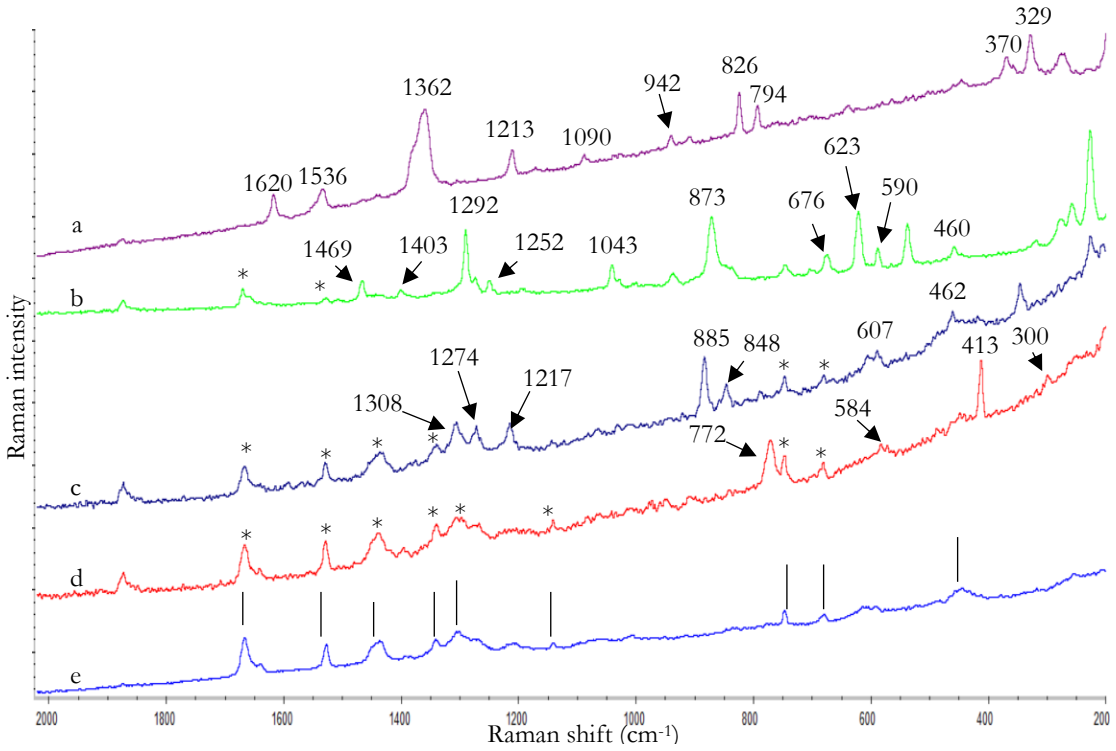

Figure 58. Raman spectra of (a) TNT (b) PETN (c) RDX (d) HMTD particles on nitrile 1 (e) nitrile 1 (asterisks indicate nitrile 1 bands) (Thermo Scientific DXR Raman microscope, 780 nm, 10 mW, 6 s exposure, 5 accumulations)

Regarding the latex glove, similar results were obtained. The positive identification of the explosive/oxidizing salt particles was possible despite the high fluorescence (see Figures 59, 60 and 61 for the Thermo scientific DXR Raman microscope, and appendix 93, 94, and 95 for the portable Raman). The Raman spectra of latex is clearly different from the nitrile one, but the bands are located within similar Raman shift ranges. Almost no interference with the vibrational bands of the oxidizing salts and explosive particles was observed for both instruments.

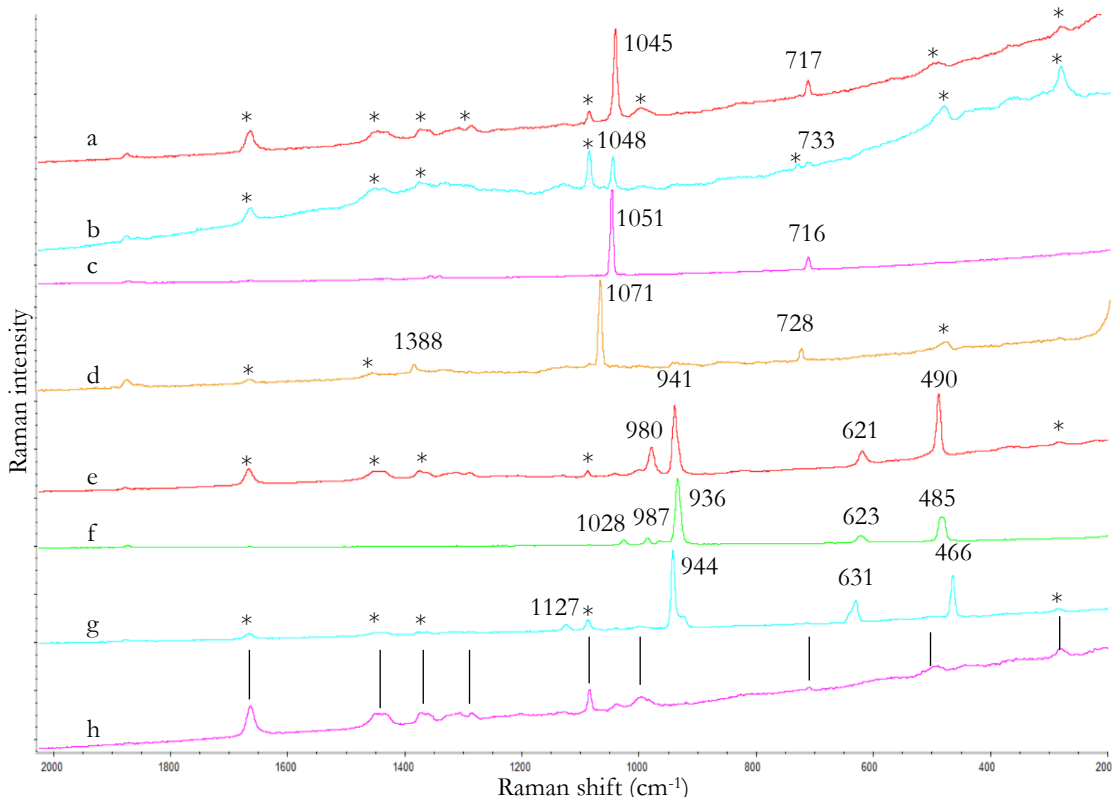

Figure 59. Raman spectra of (a) ammonium nitrate (b) barium nitrate (c) potassium nitrate (d) sodium nitrate (e) potassium chlorate (f) sodium chlorate (g) potassium perchlorate particles on latex (h) latex (asterisks indicate latex bands) (Thermo Scientific DXR Raman microscope, 780 nm, 14 mW, 5 s exposure, 8 accumulations)

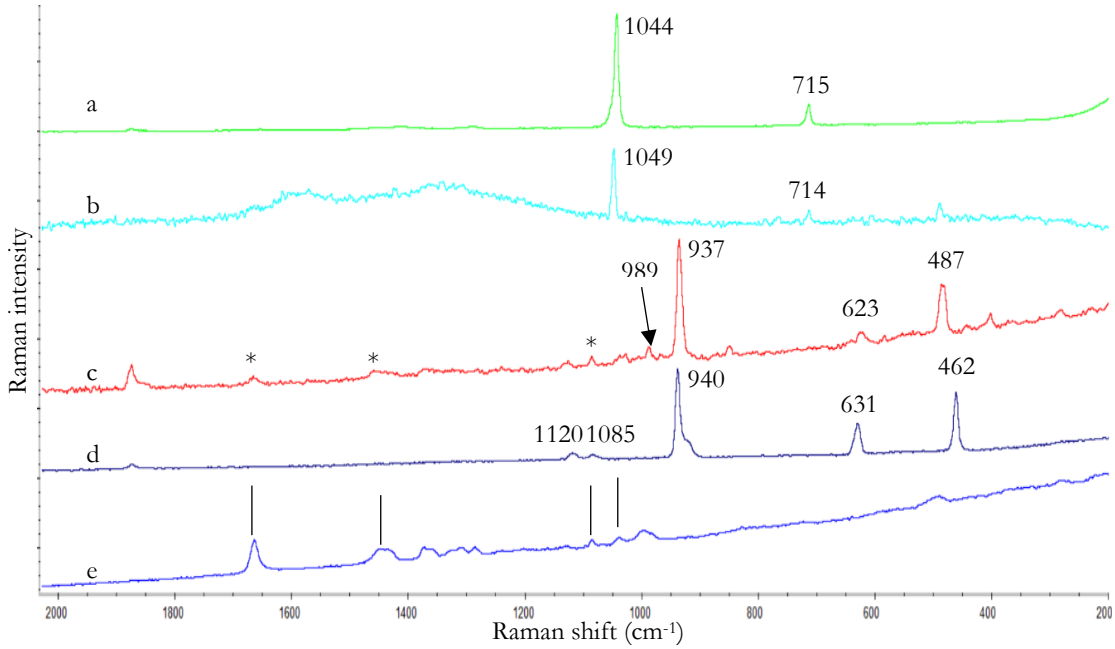

Figure 60. Raman spectra of (a) ammonal (b) black powder (c) chloratite (d) flash powder particles on latex (e) latex (asterisks indicate latex bands) (Thermo Scientific DXR Raman microscope, 780 nm, 10 mW, 6 s exposure, 5 accumulations).

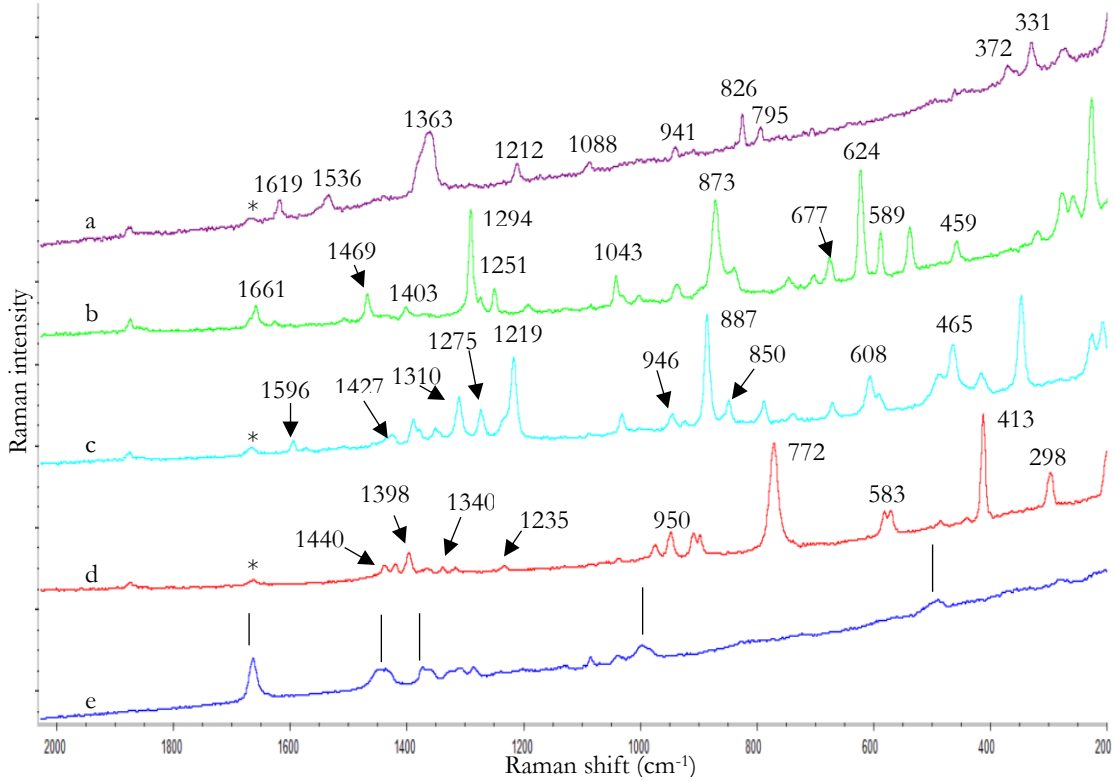

Figure 61. Raman spectra of (a) TNT (b) PETN (c) RDX (d) HMTD particles on latex (e) latex (asterisks indicate latex bands) (Thermo Scientific DXR Raman microscope, 780 nm, 10 mW, 6 s exposure, 5 accumulations).

At last, particle analysis on the surface of polyskin was made. This fabric is characterized as a black smooth surface synthetic material. The Raman spectra of the oxidizing salt/explosive particles analysed on the surface of this fabric are shown in appendix 81, 82, and 83 for the Thermo scientific DXR Raman microscope. No bands from polyskin that could interfere with the particle bands were observed. Thus, positive identification was done by matching the characteristic bands of the particles to those of the standards. However, one major problem of this material was that it burned very easily under the Raman laser. For the Thermo scientific DXR Raman microscope, minimum laser power of 1 mW was used to prevent the photodegradation of the polyskin material. This in turn resulted in spectra with high levels of instrumental noise background. The analysis using the portable Raman was not possible, because it burned even when using the minimum laser power, 1% of the 320 mW (see appendix 97).

Overall, the Raman spectra of particles of oxidizing salts and explosives trapped on the studied textile fabrics, presented no difficulty in identifying them. As major difficulties, one can highlight the difficult visualization and focusing of the particles, due to the white

coloured crystalline characteristics of most of them (more for the oxidizing salts and some organic explosives (RDX, PETN and HMTD)) when trapped in textiles with similar colours, such as white and green cotton. This resulted in a more time-consuming analysis around 10 to 15 minutes (analysing only the smallest particles). Another difficulty was the high background fluorescence coming from the textile fabric, more observed in dyed ones. Even using a 780 nm (in the Thermo scientific DXR Raman microscope) and 785-nm (in the portable Raman) red excitation laser, known for their reduction of fluorescence, high levels were still observed for some textiles. Nevertheless, the use of these wavenumber excitation lasers did not provide intense signals from the textile material, as it may be seen by using other wavenumbers [83], preventing more overlapping with the particle bands. To solve this, the interference background fluorescence coming from the surrounding material, was overcome by the careful focusing of the tightly confocal bean on the particles. This enabled the differentiation of the particle vibration bands from the textile background fluorescence. In addition, the Raman scattering from the oxidizing salt and explosive particles was usually more active (i.e. have a significantly stronger signal) compared to that from the fibres. It is important to notice that the fluorescence was more visible in the Raman spectra analysed with the portable Raman instrument. This is due to the larger laser spot (40x microscopic objective), in such a way that, when focusing on the particle, most of the spot also focused on the surrounding substrate. Thus, small particle sizes were impossible to be analysed using this instrument standard components (40x and 20x microscopic objective). On the contrary, the Thermo scientific DXR Raman microscope had much smaller laser spot (100x microscopic objective), which allowed the correct targeting of the molecule, and in most cases, positive detection of smaller particles (see section 3.3). When analysing small particle sizes the appearance of the vibrational bands coming from the textiles on the Raman spectra of the particles is more prominent, but, positively, they did not overlap the more intense bands of explosive particles.

Burning the textile fabrics was also a difficulty when analysing the oxidizing salt/explosive particles. Basically, the dark or highly coloured textiles fabrics, which can lead to strong absorption of the excitation laser, burned. The dark textiles referred here are: black cotton, black polyester, polyskin, jeans A, and jeans B. Appendix 97 presents the burning of these textiles under the Raman laser of the portable Raman. For the Thermo scientific DXR Raman microscope only black cotton and polyskin evidenced photo-degradation. One

possible explanation for the easy burning of polyskin in relation to the other black fabrics, is that, since it is a smooth material with no fibres, the laser rapidly burns the unique layer that polyskin has. In the case of textiles with black fibres, the laser encounters many layers, and so the burning is retarded. Regarding the highly coloured textiles, only blue cotton burned. In addition, in the analysis of the inorganic explosives, since they also have highly dark components in their composition (e.g. charcoal), burning of the particles trapped in those dark or highly coloured textiles fabrics was a constant. Thus, the analysis of these particles must be made carefully, considering the level of contamination of each oxidizing salt particle by charcoal or other inorganic explosive components, and reducing the power of the laser if necessary.

Also, one of the major problems in searching and identifying explosive particles in cloth matrices is the high contamination that these surfaces had, resulted from the constant direct contact with the exterior environment. Thus, contamination by dust particles, more specifically calcium carbonate ($CaCO_3$) which is a constituent of the soil, was observed. As an example, Figure 62 shows two particles of HMTD, and one of calcium carbonate trapped in the green cotton. The positive identification for calcium carbonate was made by comparison with the standard spectra of $CaCO_3$, whose main bands are 1087 cm^{-1} and 714 cm^{-1}. As shown in Figure 62, these dust particles have shapes and sizes similar to the particles of explosive, in such a way that might mislead the identification of explosive particles. Thus, when searching explosive particles in textile surfaces, one must be aware of the presence of contamination particles like calcium carbonate.

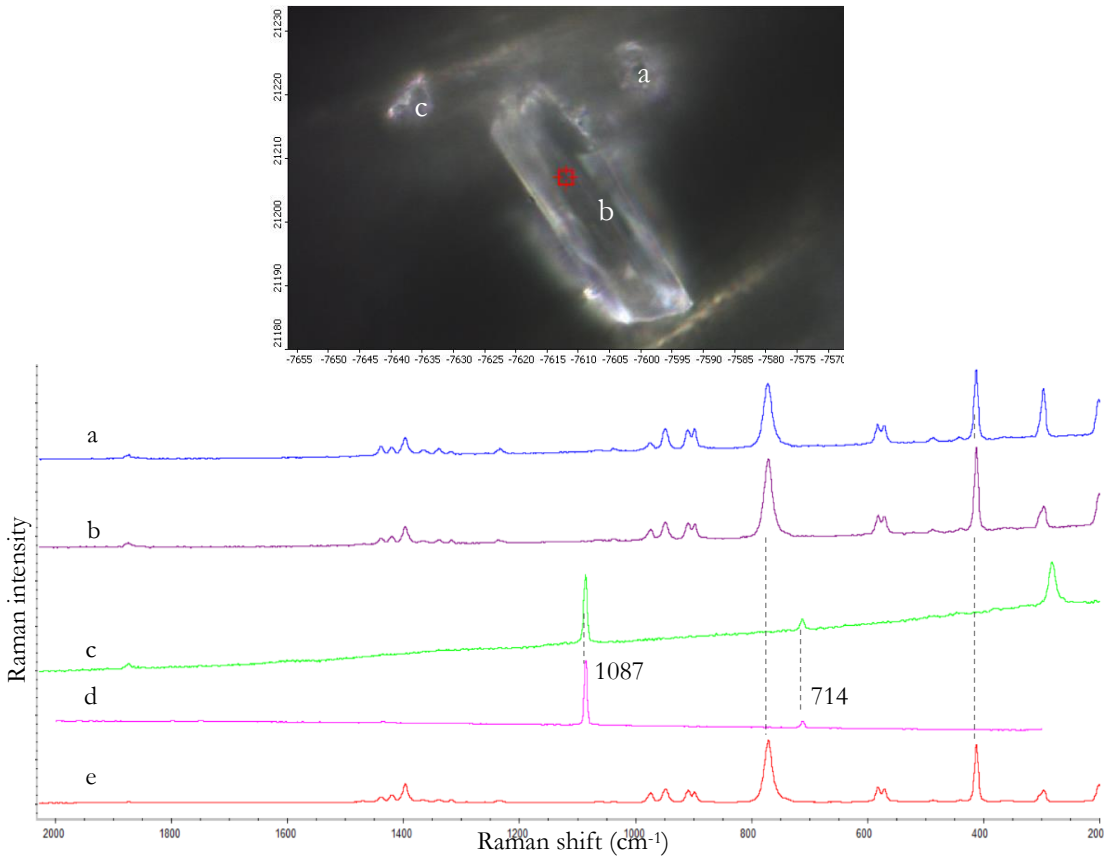

Figure 62. Raman spectra of (a), (b) HMTD (c) calcium carbonate, CaCO3 (d) calcium carbonate standard (e) HMTD standard on green cotton (Thermo Scientific DXR Raman microscope, 780 nm, 10 mW, 6 s exposure, 5 accumulations for (a) – (c) and (e), 5 s exposure, 6 accumulations, 3 mW for (d)).

One interesting aspect in the analysis of the inorganic explosive ammonal (AlAN), which was observed in some cases, involved the deviation of the Raman shift value of the ammonium nitrate band from 1044 to approximately 1052 cm^{-1}. Figure 63 represents one particle of the inorganic explosive, ammonal (i.e. one particle of ammonium nitrate in combination with aluminium particles). Two spectra were collected, one in the centre of the ammonal (AlAN) particle and the other near the aluminium particles. The results show that the spectra (b) (the one taken near the aluminium particles), is beginning to deviate from 1044 cm^{-1} to 1052 cm^{-1}, due to the interaction with aluminium. This deviation could be explained by the interaction of ammonium nitrate with the aluminium particles through some kind of SERS effect. [30, 39]

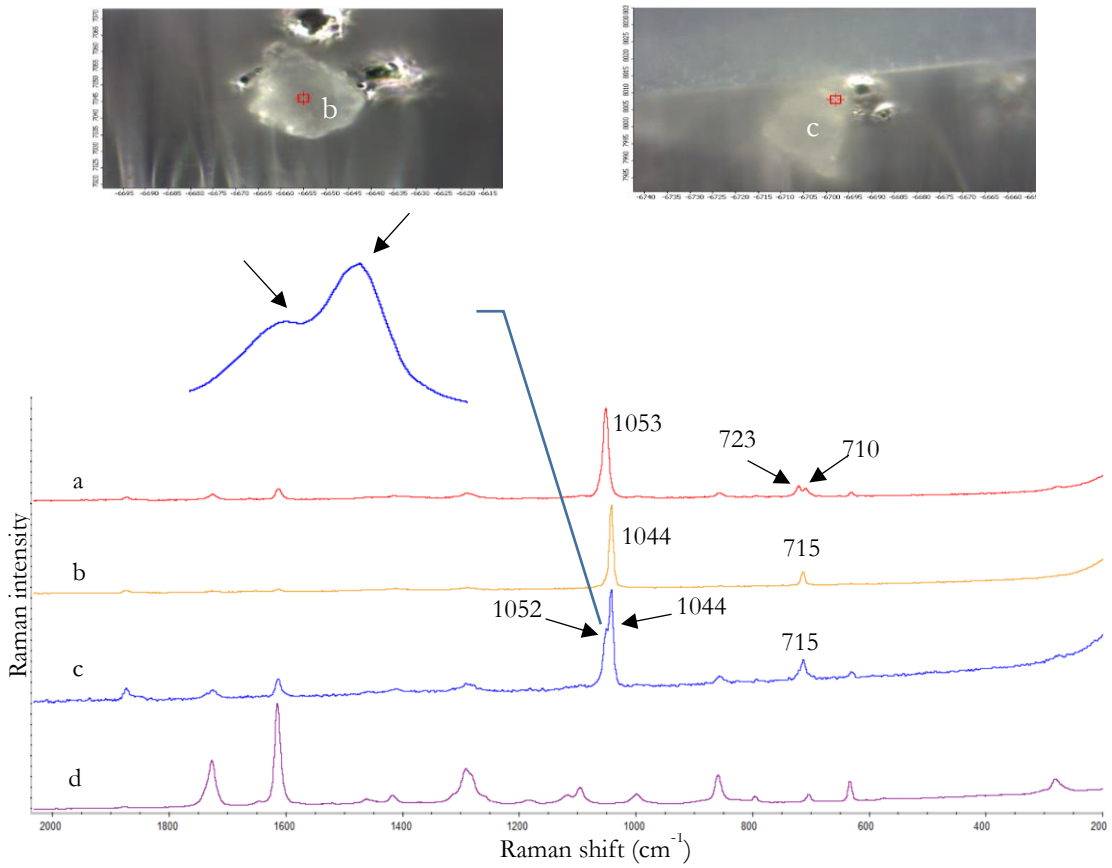

Figure 63. Raman spectra of (a) ammonal (AlAN) deviated (b) ammonal (centre) (c) ammonal (near aluminium particles) (d) white polyester B standard (Thermo Scientific DXR Raman microscope, 780 nm, 10 mW, 6 s exposure, 5 accumulations).

The AN band deviation was more often observed in the Raman spectra of ammonal (AlAN) taken by the portable Raman because of the bigger laser spot compared to the Thermo Scientific, by which no correct focusing of AN particles away from the aluminium particles could be performed. Nevertheless, the confirmation of ammonium nitrate could be dubious since there are no studies confirming this theory. Actually, besides some kind of SERS effect, another possibility, is the occurrence of a chemical reaction between the oxidizing salt and the fuel (burning textile under the influence of the portable Raman laser) resulting in a possible degradation product of AN with the band at 1052 cm^{-1} (see appendix 96).

3.3 Particle sizes and its correlation with their detection in textiles

3.3.1 Particles sizes

The particle sizes for each instrument, were calculated using a program called "ImageJ", that allows the determination of the distance in pixels of a certain marked line. This marked line corresponded to the wider diameter of each particle, as shown in Figure 64, where the size of a particle of sodium nitrate is being determined in pixels.

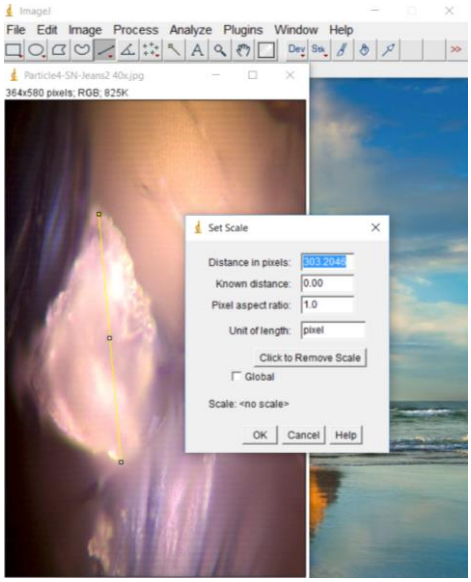

Figure 64. Determination of the distance in pixels that corresponds to the widest diameter on the sodium nitrate particle, by using the "ImageJ" program.

Using this distance, and considering the correlation pixels-distance previously calculated for that scale (see appendix 102 and 103), the particle size was calculated using cross-multiplication (Equation 1). This method provided a better approximation to the real size of the particle, since by using the program one can draw the line that corresponds to the widest diameter of each particle.

Equation 1. Cross-multiplication process used for the determination of the particle sizes.

$$\text{particle size} = \frac{(\text{distance in pixels corresponding to the wider diameter of the target particle}) \times (\text{scale in } \mu\text{m})}{\text{distance in pixels corresponding to the scale in } \mu\text{m}}$$

For the analysis using the Thermo scientific DXR Raman microscope a total of 1075, 442 and 357 particles of oxidizing salts, organic and inorganic explosives, respectively, trapped in the 16 different textile fabrics were analysed. Of these, only 762 (71%), 366 (83%), and 294 (82%) of the 1075, 442, and 357 analysed particles were positively identified as the oxidizing salt, organic or inorganic explosive. The reason for the 452 non-identified particles was mostly due to the background interference from textile fabrics, and the miss-identification with contaminating particles (e.g. calcium carbonate). The particle size ranges of the positively identified particles using the Thermo Scientific DXR Raman microscope are summarized in the histograms showed in Figure 65. They are divided by oxidizing salt (Figure 65 – (a.1, a.2)), organic explosive (Figure 65 – (b.1, b.2)), and inorganic explosive (Figure 65 – (c.1, c.2)).

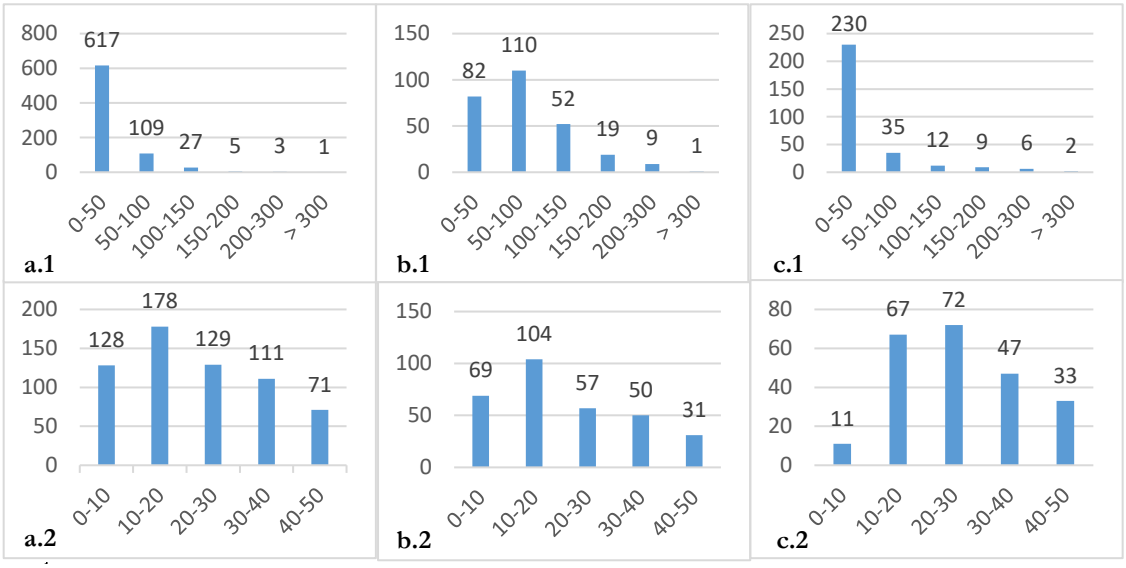

Figure 65. Histograms that represent the number of particles (y-axis) divided in their particle size ranges (x-axis) between 0 to more than 300 µm, and between 0 to 50 µm, of the 1422 positively analysed (a.1, a.2) oxidizing salt, (b.1, b.2) organic, and (c.1, c.2) inorganic explosive particles by the Thermo Scientific DXR Raman microscope.

The size of most positively identified particles ranged between 0 – 50 µm (Figures 65 (a.1, c.1)), except for most organic explosive particles, whose range was 50 – 100 µm (Figure 65 (b.1)). Regarding the histograms comprising the particle size range of 0 to 50 µm (Figure 65 (a.2, b.2, c.2)), very small particle sizes from 1 to 20 µm were positively detected, showing the power of this technique. Despite the high level of fluorescence from the surrounding fibres, very small particle sizes were detected by using the Thermo Scientific DXR Raman

microscope. This was due to the advantage of focusing the laser directly onto the particle using a 100x microscope objective.

For the analysis using the portable BWTEK i-Raman pro coupled to an optic microscope, a total of 668, 412, and 458 particles of oxidizing salts, organic and inorganic explosives, trapped in the 15 different textiles, (polyskin was not included because of burning problems), were analysed. Of these, only 613 (92%), 257 (62%), and 273 (60%) of the 668, 412, and 458 analysed particles were positively identified as the oxidizing salt, organic or inorganic explosive. The reason for the 395 non-identified particles was due to the high fluorescence of the textile fabrics that saturated the Raman spectra, the high particle contamination of other substances, and the burning of most of the smaller particles by the powerful portable Raman laser. Figure 66 represents the histograms of the number of positively identified particles of oxidizing salt (Figure 66 – (a.1, a.2)), organic (Figure 66 (b.1, b.2)) and inorganic explosive (Figure 66 (c.1, c.2)), in function of their size ranges.

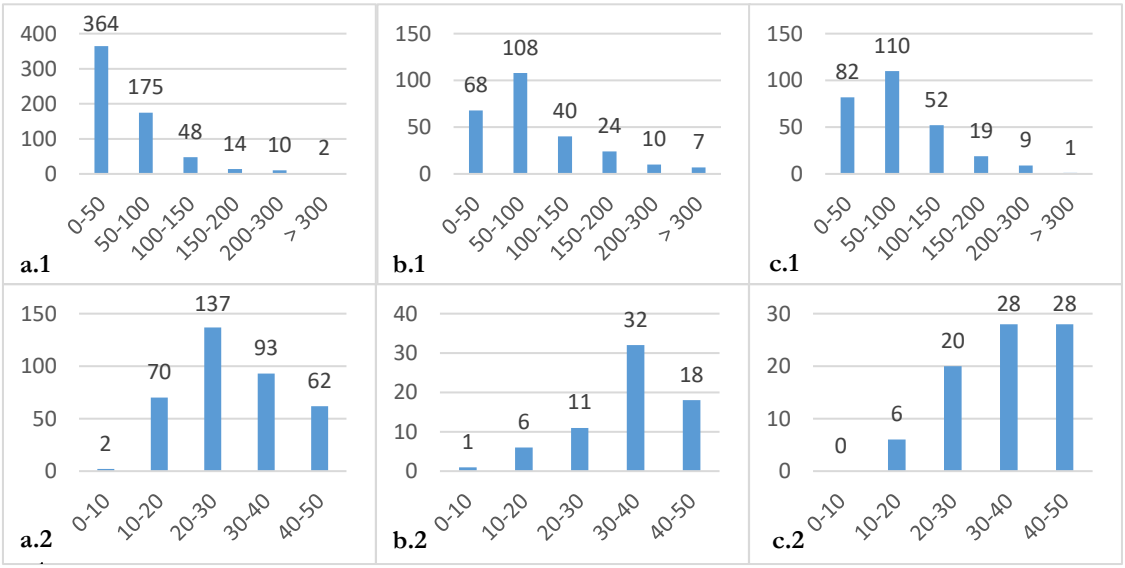

Figure 66. Histograms that represent the number of particles (y-axis) divided in their particle size ranges (x-axis) between 0 to more than 300 µm, and between 0 to 50 µm, of the 1143 positively analysed (a.1, a.2) oxidizing salt, (b.1, b.2) organic, and (c.1, c.2) inorganic explosive particles by the portable BWTEK i-Raman pro.

The results evidenced that for the portable Raman, bigger particles were identified in comparison to the Thermo Scientific DXR Raman microscope. Nevertheless, the particle ranges of 0 – 50 µm and 50 – 100 µm for the three types of energetic substances (Figure 66 (a.1, b.1, c.1)) were still the most encountered ones. The difference was most notable in the

histograms comprising the particle size ranges of 0 to 50 μm. In the portable BWTEK i-Raman pro, almost no particle in the 0 – 10 μm range was observed for the three energetic substances. In addition, particles between 10 – 30 μm were observed, but in less quantity when compared to the Thermo Scientific DXR Raman microscope. Overall, bigger particles could be identified using the portable Raman, due to the large size of the portable laser spot, (i.e. since the maximum microscopic objective available was 40x), that also comprised most of the surrounding fibres when analysing small particles giving high levels of fluorescence. In the case of inorganic explosives (black powder, ammonal (AlAN) and flash powder particles), it was noticed that the laser had a destructive effect (burning), mostly seen with the smaller particles. To solve this, bigger and less contaminated particles with aluminium or charcoal, had to be analysed to achieve a positive chemical identification.

3.3.2. Particle sizes and LOD (limit of detection)

The LOD (that corresponds to the lowest amount (mass) detected) can be determine using the smallest particle size. The Thermo Scientific DXR Raman microscope enabled the identification of particles with dimensions of 2 μm for the oxidizing salts, 3 μm for the organic explosive particles, and 6 μm for the inorganic explosive particles. For the portable BW&TEK i-Raman Pro, particles sizes of 7 μm for the oxidizing salts, 7 μm for the organic explosive particles, and 18 μm for the inorganic explosive particles were identified. According to Zapata and García-Ruiz [57], the LOD can be estimated by multiplying the density of the explosive substance (oxidizing salt, organic or inorganic explosive) by the volume of the particle detected, assuming always a range since the shape of the particle might be between a spherical or cubic shape (e.g. for a cubic or spherical particle with a diameter of 10 μm, its volume is 1000 μm^3, if cubic, or 524 μm^3 if spherical).

The smallest particle identified using the Thermo Scientific DXR Raman microscope for each explosive substance are given in Table 10. In the knowledge that barium nitrate, HMTD, black powder (potassium nitrate), and chloratite (sodium chlorate) have a density of 3.24 g/cm^3 [84], 0.38 or 0.88 g/cm^3 [11, 85], 2.11 g/cm^3 [57], and 2.50 g/cm^3 [57], respectively, the mass of the smallest particles determined using the Thermo Scientific DXR

Raman microscope was 0.03 ng, 0.01 - 0.02 ng, 0.5 ng, and 0.5 ng if cubic particles, and 0.01 ng, 0.005 - 0.01 ng, 0.2 ng, and 0.3 ng if spherical.

Table 10. LOD of the smallest particles analysed by the Thermo DXR Raman microscope.

Thermo Scientific DXR Raman microscope			
Particle identification	**Particle size (μm)**	**Volume (μm³)**	**LOD (ng)**
Barium nitrate particle trapped in white cotton (oxidizing salt)	2	8, if cubic 4.19, if spherical	0.03, if cubic 0.01, if spherical
HMTD particle trapped in latex (organic explosive)	3	27, if cubic 14.14, if spherical	0.01 or 0.02, if cubic 0.005 or 0.01, if spherical
Black powder particle trapped in white polyester B (inorganic explosives)	6	216, if cubic 113.10, if spherical	0.5, if cubic 0.2, if spherical
Chloratite particle trapped in nitrile B (inorganic explosive)	6	216, if cubic 113.10, if spherical	0.5, if cubic 0.3, if spherical

For the portable BW&TEK i-Raman Pro, the LOD of the smallest particles analysed are shown in Table 11. Considering that barium nitrate, TNT, and chloratite (sodium chlorate) have a density of 3.24 g/cm^3 [84], 1.654 g/cm^3 [6], and 2.50 g/cm^3 [57], respectively, the mass of the smallest particles determined using the portable BW&TEK i-Raman Pro was 1.11 ng, 0.57 ng, and 14.58 ng if cubic particles, and 0.58 ng, 0.30 ng, and 7.63 ng if spherical particles.

Table 11. LOD of the smallest particles analysed by the portable BWTEK i-Raman pro

Portable BWTEK i-Raman pro			
Particle identification	**Particle size**	**Volume (μm3)**	**LOD (ng)**
Barium nitrate particle trapped in green cotton (oxidizing salt)	7	343, if cubic 179.59, if spherical	1.11, if cubic 0.58, if spherical
TNT particle trapped in white cotton (organic explosive)	7	343, if cubic 179.59, if spherical	0.57, if cubic 0.30, if spherical
Chloratite (sodium chlorate) particle trapped in latex (inorganic explosive)	18	5832, if cubic 3053.63, if spherical	14.58, if cubic 7.63, if spherical

The limits of detection estimated (LOD) were in the nanogram range, even in the presence of high interfering surfaces, which proves that Raman microscopy is a high efficient

technique, comparable with other high sensitive and specific analytical techniques with low LOD, such as mass spectrometry (e.g. GC-MS or HPLC-MS). [12, 66]

3.4 Comparison of the discrimination power of the Thermo Scientific DXR Raman microscope and Portable BWTEK i-Raman Pro.

The Thermo Scientific DXR Raman microscope is a laboratory equipment with more sensitivity and spatial resolution than the portable BW&TEK Raman i-Pro. This last one, is characterized by being a very robust equipment capable of making measurements in the most varied environments (e.g. active crime scenes or warzones). Combined with a optic microscope, this equipment can be used to detect minute traces of explosive particles.

The detection of explosive and oxidizing salt particles trapped in textile fabrics was studied with both instruments. The results, which are summarized in Table 12, showed that both could detect and identify very small particle sizes in highly interfering surfaces. Regarding particle sizes, the ones identified by the portable BW&TEK Raman i-Pro were, in general, bigger than those detected by the Thermo Scientific DXR Raman microscope, due to the large laser spot, provided by the 40x microscope objective. Fluorescence was detected in every textile fabric except for white polyester and polyskin (this last was measured at 1 mW because of burning problems). Nevertheless, for a portable Raman device, the particle sizes detected, the corresponding LOD (see section 3.3.2), and the quick analysis were very good considering the standard characteristics (or components) available for this instrument, making it suitable for using in an active crime scene.

One problem that appeared, when analysing explosives and oxidizing salts in the studied textile fabrics, was the effect of the excitation laser in those materials. With the portable BW&TEK Raman i-Pro, the textiles: black cotton, blue cotton, both blue denim jeans and polyskin burned when irradiated with different laser powers. Even when using the minimum laser power (1% of 320 mW), black cotton and polyskin burned. This last (polyskin), could not be at all, analysed by the portable Raman. Regarding the Thermo Scientific DXR Raman microscope, only black cotton and polyskin had problems with the laser. Reduction of the laser power was necessary, and in the case of polyskin, a laser power of 1 mW was used. It should be highlighted that the destruction of textile fabrics (criminal

evidence), will cause a huge bow to the criminal investigation, since it can no longer be further analysed by other analytical technique, and can not be admitted in the criminal proceedings. Standard (i.e. with no modifications) portable Raman devices, have very strong laser powers to compensate their lack of sensitivity, care must be taken when using them in the analyses of these sensitive materials. Sensitivity tests of the different textile fabrics when subjected to the laser power need to be performed for a proper understanding of the power to be used.

Regarding the analysis of the inorganic explosives it was noticed that for black powder, ammonal (AlAN) and flash powder particles, the laser of the portable Raman device had a destructive effect, mostly observed in smaller particles. This was because these explosives have in their composition substances, like charcoal and aluminium powder, that heat up very fast when subjected to the laser, causing the destruction of the explosive particle. In the Thermo Scientific DXR Raman microscope, black powder was the only explosive that posed difficulties due to the reasons discussed and the fluorescence resulting from charcoal. Both instruments had the same behaviour regarding the acquisition of Raman spectra with the vibrational peaks of the textile fibre or present dye. Only for wool, the portable Raman was not capable of providing any vibrational bands from either the fibre or the dye.

Table 12. Summary of the smallest particle sizes for each energetic materials, fluorescence, burning/ destruction, and vibrational peaks of the fibres/ dyes, verified in each textile fabric for both instruments (A – Thermo Scientific DXR Raman microscope; B – Portable BWTEK i-Raman Pro).

	Oxidizing salts		**Organic explosives**		**Inorganic explosives**		**Fluorescence**		**Burning/destruction**		**Vibrational peaks of the fibres/dyes**	
	Smallest particle sizes (µm)		Smallest particle sizes (µm)		Smallest particle sizes (µm)							
Instrument	A	B	A	B	A	B	A	B	A	B	A	B
White cotton	2	14	5	7	6	18	Yes	Yes	No	No	Yes	Yes
Blue cotton	3	25	5	36	12	34	Yes	Yes	No	Yes*	Yes	Yes
Red cotton	4	13	5	27	9	23	Yes	Yes	No	No	Yes	Yes
Green cotton	6	7	4	26	15	27	Yes	Yes	No	No	Yes	Yes
Black cotton	4	30	9	47	14	40	Yes	Yes	No (at 5 mW)	Yes*	No	No
Black polyester	7	15	6	44	11	46	Yes	Yes	No	No	No	No
Blue polyester	8	29	7	76	14	54	Yes	Yes	No	No	No	No
White polyester	3	10	6	25	9	27	No	Yes	No	No	Yes	Yes
White polyester B	5	12	4	23	14	20	No	Yes	No	No	Yes	Yes
Wool	3	11	4	16	6	18	Yes	Yes	No	No	Yes	No
Jeans A	3	39	6	79	17	22	Yes	Yes	No	Yes*	No	No
Jeans B	5	35	6	49	12	33	Yes	Yes	No	Yes*	Yes	Yes
Latex	4	12	3	30	7	18	Yes	Yes	No	No	Yes	Yes
Nitrile A	3	9	4	30	14	21	Yes	Yes	No	No	Yes	Yes
Nitrile B	3	11	3	48	6	23	Yes	Yes	No	No	Yes	Yes
Polyskin	7	-	8	-	11	-	No	-	No (at 1mW)	Yes	No	-

*Although they burned when subjected to the laser, it was possible to analyse them using a powder of 1% of 320 mW (but even so they sometimes burned).

3.5 Chemometric and statistical analysis

3.5.1 Descriptive analysis of the particle size data

In this section, descriptive analysis in the form of box plots was made for the particle size data from both Raman instruments. By doing a manual search by visualization of the particles trapped in the textile fabrics, the three smallest particles detected for each oxidizing salt, organic and inorganic explosive in each textile fabric were selected to perform this analysis. Due to lack of Raman imaging system, it was not possible to automatically detect and determine the average size of the explosive particles, thus the search was made manually, and with the purpose of finding always de smallest particles, to get the corresponding LOD for each explosive, in each instrument.

Thermo Scientific DXR Raman microscope

Figure 67 – (a) represents the distribution of the oxidizing salts according to their detected particle size. For ammonium nitrate, potassium perchlorate, potassium chlorate, and barium nitrate, 50% (the blue box) of the particles detected are in the same range, in contrast to sodium nitrate, sodium chlorate and potassium nitrate. These different particle size ranges, may be due to the distinct Raman activity of each oxidizing salt.

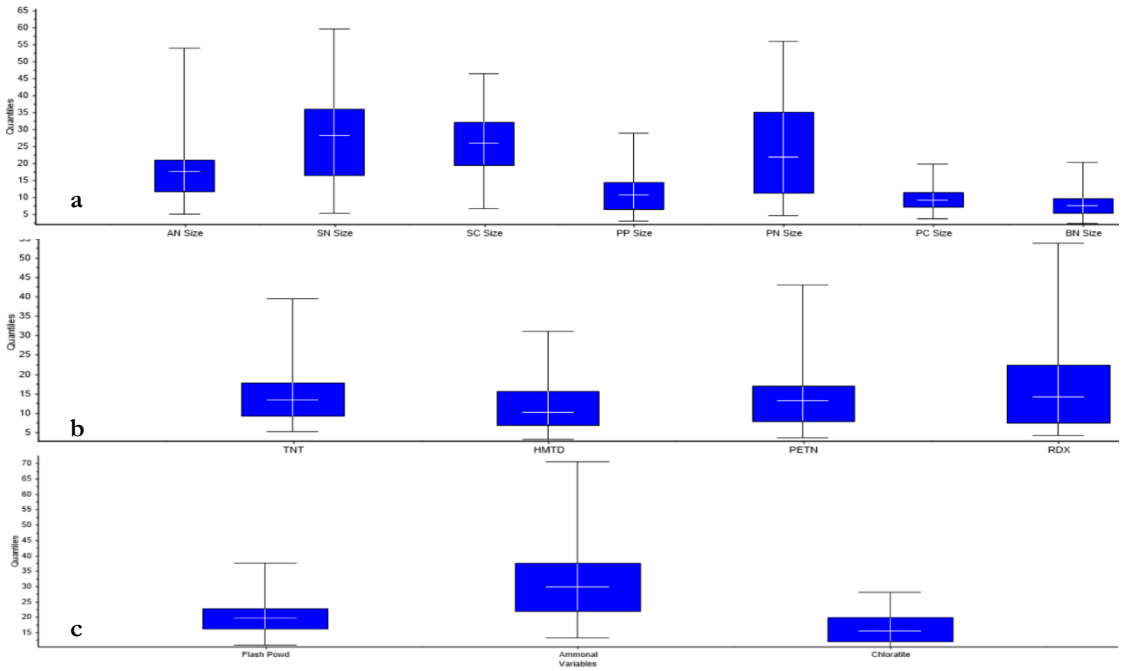

Figure 67. Y-axis: particle size ranges; X-axis: energetic substances; Box plot of the (a) oxidizing salt (b) organic explosive (c) inorganic explosive particle sizes (Thermo Scientific DXR Raman microscope, 780 nm, 14 mW, 5 s exposure, 8 accumulations (oxidizing salts) and 10 mW, 6 s exposure, 5 accumulations (organic and inorganic explosives)).

Figure 68 shows the total Raman intensity of the most intense Raman band for each of the standard oxidizing salt. As can be seen, the ammonium nitrate, potassium chlorate, and barium nitrate have a bigger Raman intensity regarding their most intense Raman band. This means that smaller particles of these salts will provide still a detectable Raman signal in contrast to the less Raman intensity salts (regarding their most intense band) as evidenced in the box plot (Figure 67 – (a)). The only exception was potassium perchlorate, where small particle sizes were also detected. This is not explained by what is seen in Figure 68, since the most intense band of potassium perchlorate has a low Raman intensity.

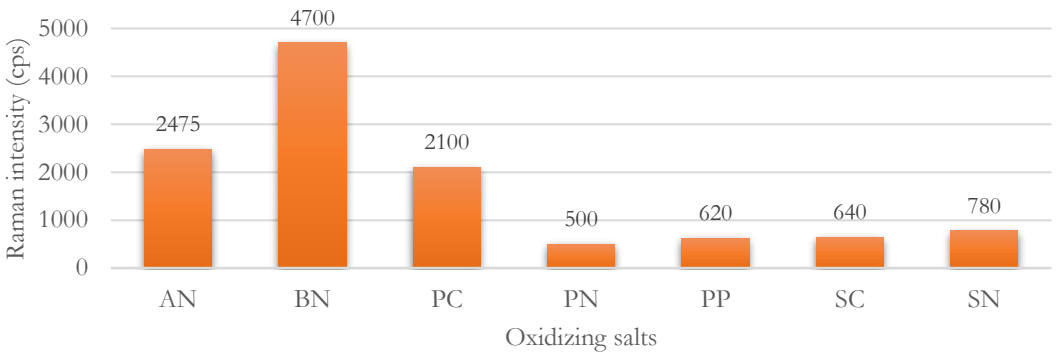

Figure 68. Raman intensity of the most intense Raman band for the different oxidizing salt standards (Thermo Scientific DXR Raman microscope, 780 nm, 14 mW, 5 s exposure, 8 accumulations).

Figure 67 – (b) displays the results for organic explosives. HMTD showed the smallest particle size range, while RDX the largest detected. According to the Raman intensity of the most intense Raman bands of each organic explosive standard (Figure 69) the same correlation was difficult to be made. Only a difference of 400 cps is seen between the most intense Raman band of HMTD and PETN, which is very small in comparison to the values observed for the oxidizing salts.

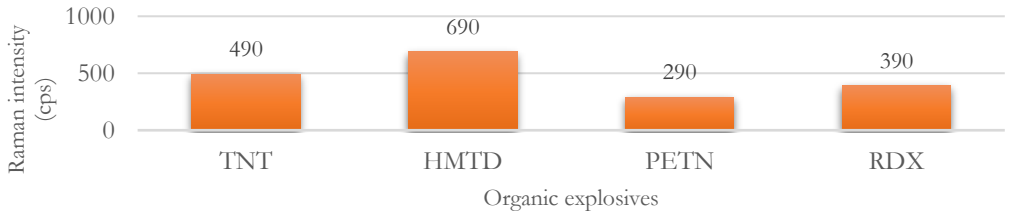

Figure 69. Raman intensity of the most intense Raman band for the different organic explosive standards (Thermo Scientific DXR Raman microscope, 780 nm, 10 mW, 6 s exposure, 5 accumulations).

As previously said, the analysis of inorganic explosives posed difficulties, since they are composed with very high interfering components, such as aluminium and charcoal. In Figure 67 – (c), we can see that for ammonal (AlAN) and flash powder, 50% of the particle sizes detected are bigger than those of chloratite. This is because this last does not have in its composition aluminium or charcoal that interferes and causes high fluorescence. Black powder is not present because the number of analysed particles was not big enough to be included in the box plot statistic test. This was due to the difficulties when submitted to the laser at 100x microscope objective, which most of the black powder particles burned when in contact with the laser.

Regarding the particle sizes of oxidizing salts in each textile fabric (Figure 70 – (a)), because of the micro-spot that the laboratory instrument provided, the fluorescence coming from the textile fabric could be reduced. Large and homogeneous variations of the particle sizes were verified in most of the textile fabrics. The exception, was that for the two white polyester fibres, in which small particle sizes were detected. This is related to the fact that these fibres have no or less fluorescence in comparison to the other fabrics. The box plot of the organic explosive particle sizes detected in each textile fabric (Figure 70 – (b)), showed that for black cotton, blue polyester, black polyester, both blue denim jeans, and polyskin, large particle size ranges were detected. In addition, for blue cotton and jeans A, large variation in the particle size ranges was evidenced. No major differences were seen in the box plot regarding the inorganic explosives (Figure 70 – (c)).

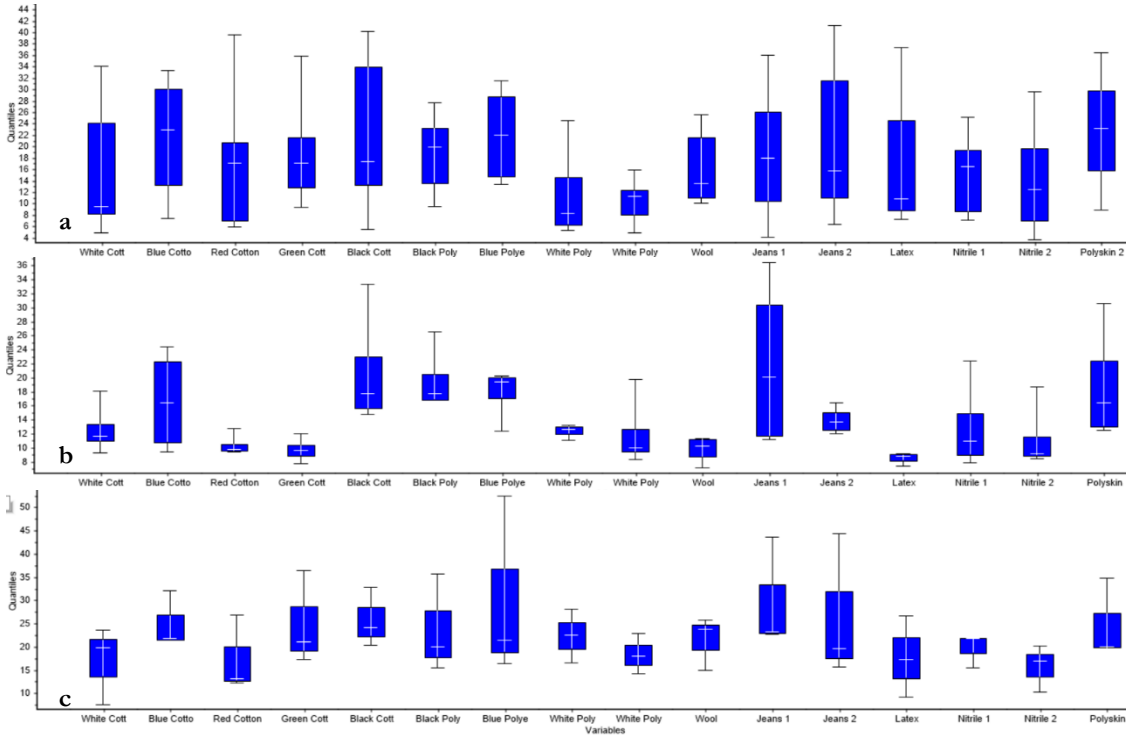

Figure 70. Y-axis: particle size ranges; X-axis: textile fabrics; Box plot of the (a) oxidizing salt (b) organic explosive (c) inorganic explosive particle sizes in each textile fabric (Thermo Scientific DXR Raman microscope, 780 nm, 14 mW, 5 s exposure, 8 accumulations (oxidizing salts) and 10 mW, 6 s exposure, 5 accumulations (organic and inorganic explosives)).

Portable Raman

For the portable Raman, the box plots of the particle size ranges identified in all textile fabrics are represented in Figure 71. Regarding the oxidizing salts (Figure 71 – (a)), no

major differences are verified, as the same variation is seen. The particle sizes of the organic explosives (Figure 71 – (b)) are in accordance with the Raman intensity of the corresponding standards (Figure 69). PETN has the largest particle sizes, and TNT the lowest. For inorganic explosives (Figure 71 – (c)), black powder and ammonal (AlAN) showed larger particle sizes, due to the high interference substances that compose them, in comparison to chloratite. Thus, the same conclusion previously said about the particles sizes detected by the Thermo Scientific DXR Raman microscope, can be taken. Flash powder is not present because the number of analysed particles was not big enough to be included in the box plot statistic test. This was due to the difficulties in the analysis by the Raman portable laser (i.e. most of the flash powder particles burned when in contact with the laser).

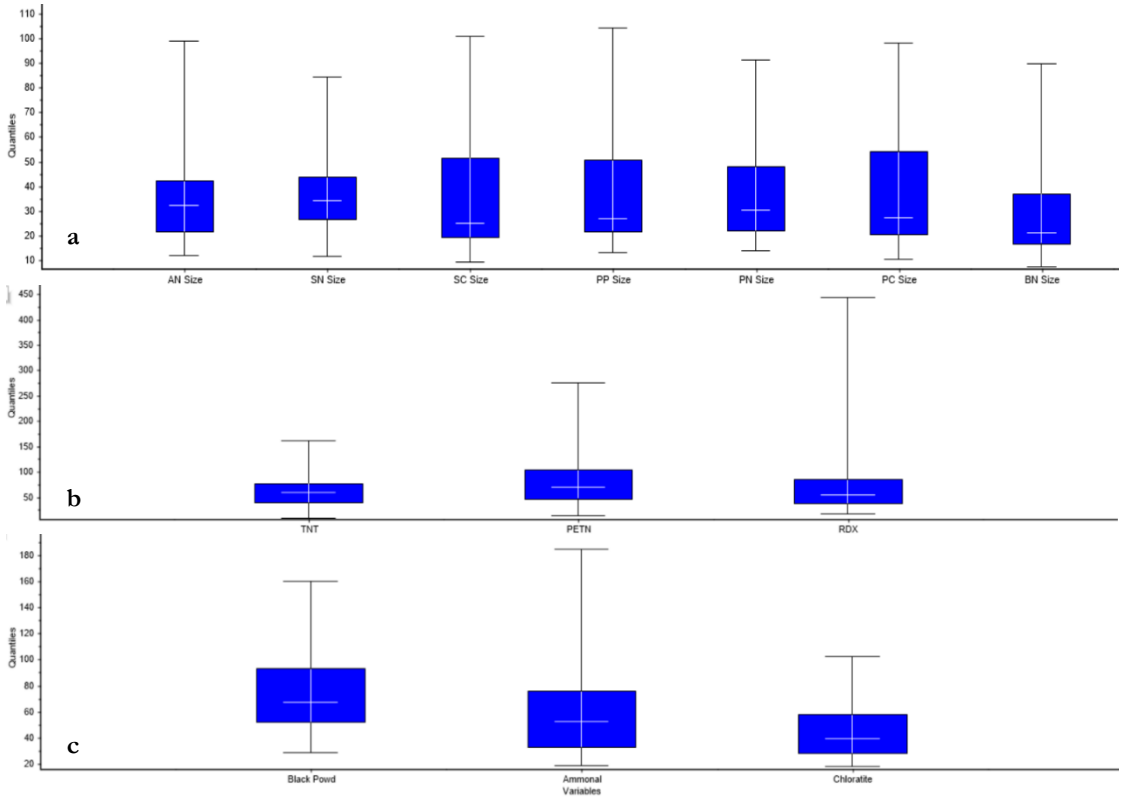

Figure 71. Y-axis: particle size ranges; X-axis: energetic substances; Box plot of the (a) oxidizing salt (b) organic explosive (c) inorganic explosive particle sizes (Portable BWTEK i-Raman Pro, 785 nm, 20%, 0.3 s exposure, 10 accumulations (oxidizing salts), 5%, 3 s exposure, 5 accumulations (organic explosives), and 1%, 1 s exposure, 10 accumulations (inorganic explosives;) For the textiles black cotton, blue cotton, jeans 1, and jeans 2 a 1% power was used).

In Figure 72 - (a), (b), and (c), we can see the patterns relating the particle size ranges to the type of textile fabric in which they were analysed. Either for the oxidizing salts, organic or inorganic explosives, higher particle sizes were detected in black cotton, blue polyester,

black polyester and both blue denim jeans. This is explained by the high fluorescence of these textiles, where larger particles needed to be analysed so that the laser spot comprised only the particle, given good and identifiable Raman spectra. Also, blue cotton when detecting oxidizing salts and organic explosives (Figure 72 – (a), and (b)), provided high particle sizes. In addition, large variation in wool, (Figure 72 – (c)) red cotton (Figure 72 – (c)), and white polyester B (Figure 72 – (b)) was verified.

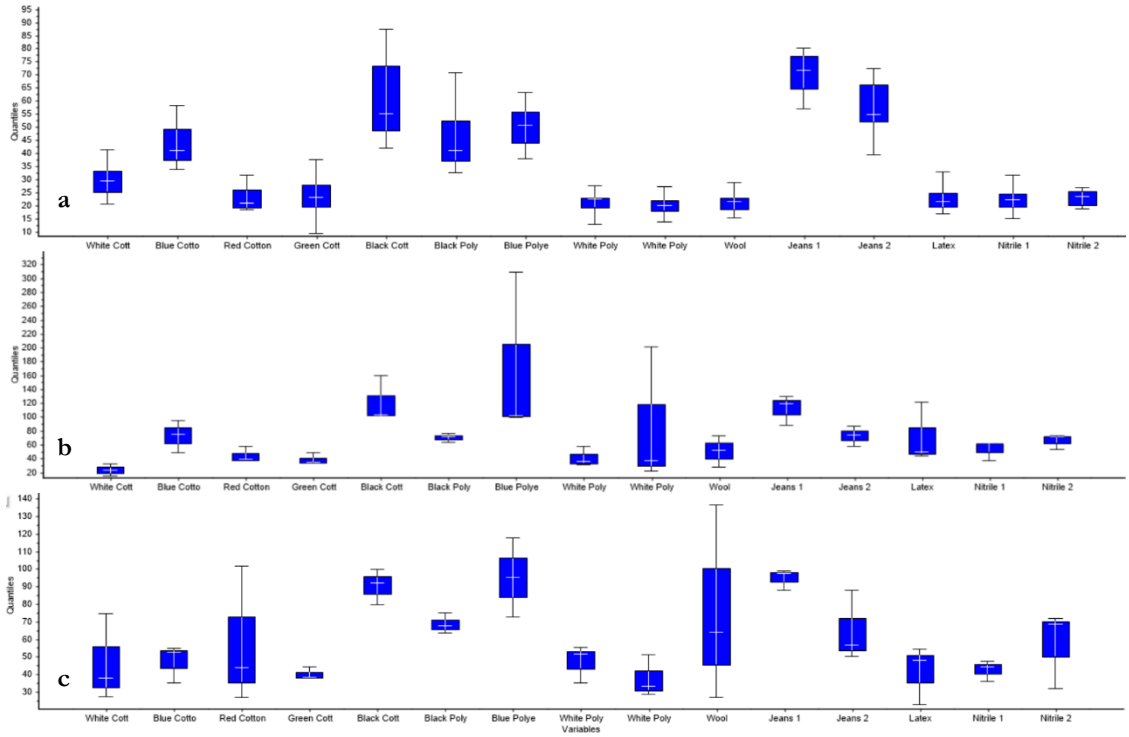

Figure 72. Y-axis: particle size ranges; X-axis: textile fabrics; Box plot of the (a) oxidizing salt (b) organic explosive (c) inorganic explosive particle sizes in each textile fabric (Portable BWTEK i-Raman Pro, 785 nm, 20%, 0.3 s exposure, 10 accumulations (oxidizing salts), 5%, 3 s exposure, 5 accumulations (organic explosives), and 1%, 1 s exposure, 10 accumulations (inorganic explosives;) For the textiles black cotton, blue cotton, jeans 1, and jeans 2 a 1% power was used)

3.5.2 PCA analysis of the Raman spectra

Chemometric analysis allow the simultaneous processing of large amounts of complex data (e.g., Raman spectra) enabling the extraction of the information. Principal component analysis (PCA) of the Raman spectra of five positively identified potassium chlorate particles trapped in each textile fabric were used as input data. In this PCA model, since the PC1 can explain 89% of the data (i.e. 89% of the variability), only this new variable

was used to plot the graphic in the x- and y-axis. Before explaining the PCA, one needs to know what represents this new variable. For this, the loading of PC1 is provided (Figure 73). According to the loading, the negative bands that correspond to the well-defined Raman spectrum of the potassium chlorate, means that for negative values of PC1 in the scores plot (Figure 74), the Raman spectrum of potassium chlorate was easily identified with no or low fluorescence. Regarding the positive bands seen in the loading (i.e. the peaks facing upwards), they correspond to fluorescence. Thus, for positive values of PC1, high fluorescence is seen in the Raman spectra of the potassium chlorate.

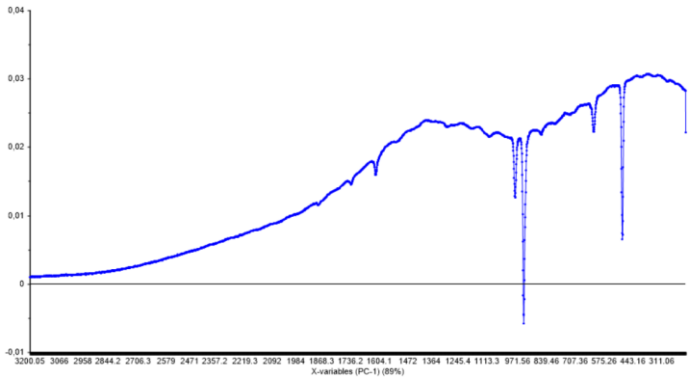

Figure 73. Loading of the PC1 principal component, regarding the Raman spectra of the potassium chlorate in each textile fabric.

In brief, two zones can be highlighted in this model (Figure 74), zone A and B. The zone A corresponds to the textiles encountered in high positive values of PC1, thus they represent high levels of fluorescence in the Raman spectra of the potassium chlorate: both blue denim jeans, black cotton, black polyester, and blue polyester. Zone B corresponds to the textiles positioned in negative values of PC1: white cotton, both white polyesters, wool, nitrile A, and polyskin. Polyskin is easily explained since the power used was 1 mW to avoid burning it, so there was no fluorescence. In these textile fabrics, the potassium chlorate was easily identified with no or low fluorescence in the spectra.

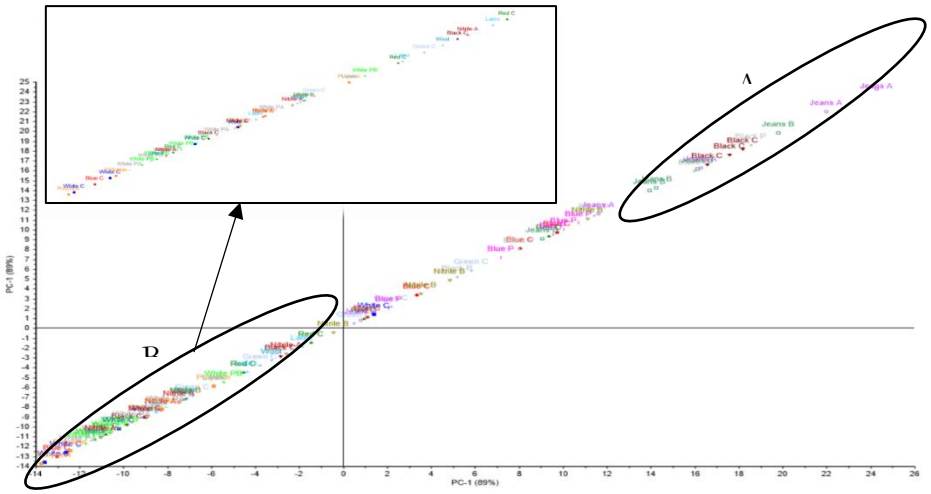

Figure 74. PCA model of five (5) positively identified potassium chlorate Raman spectra in each textile fabric (total of 80 particles).

A second PCA analysis was performed including the Raman spectra of five positively identified RDX particles trapped in each textile fabric. In this PCA, two principal components were used to plot the graphic of the scores, the PC1 (72% of data variability), and PC2 (22% of data variability). In Figures 75 - (a) and (b) are represented the loadings for the PC1 and PC2, respectively.

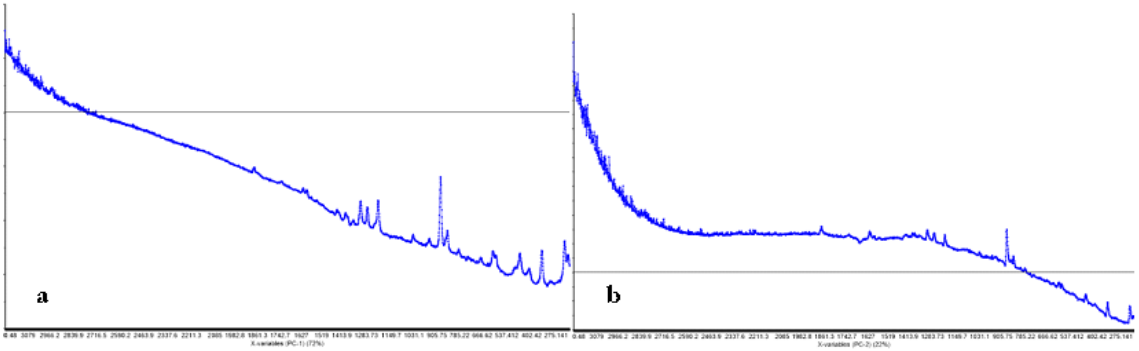

Figure 75. (a) Loading of the PC1 (b) loading of the PC2, regarding the Raman spectra of the RDX in each textile fabric.

The loading of PC1 (Figure 75 –(a)) demonstrates that the upward bands correspond to the well-defined RDX Raman spectra. Thus, in the positive values of PC1 (scores in Figure 77), RDX was detected with no or low fluorescence. For the negative values of PC1, the RDX is detected with some fluorescence (since the line goes down in the loading of the PC1). Regarding the loading of PC2, it displays similar behaviour of PC1, but with more fluorescence according to the higher decrease of baseline.

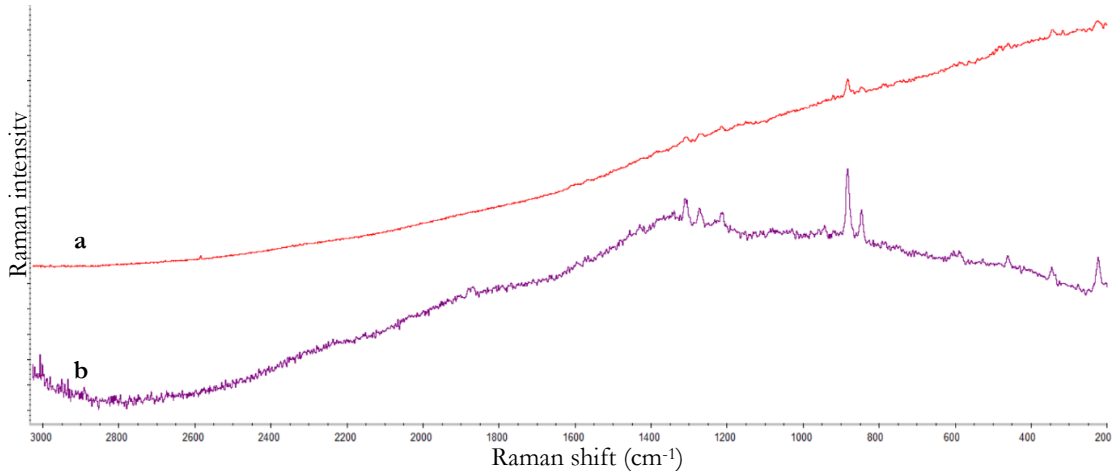

Figure 76. (a) Raman spectra of an RDX particle trapped in Jeans 1 fibres (b) Raman spectra of an RDX particle trapped in black cotton fibres (Thermo Scientific DXR Raman microscope, 780 nm, 10 mW, 6 s exposure, 5 accumulations).

In this second PCA (Figure 77), we can highlight four zones: A, B, C, and D. The zone A represents the textile fibres where the RDX Raman spectra was well distinguished and identified with no or very low fluorescence, since it is close to zero in PC2 (i.e. they have plane baselines). These textiles corresponded to polyskin, both white polyesters, white cotton, and nitrile A. Zone B corresponds to latex and nitrile B fabrics where the RDX spectra was well defined (PC1 positive values), but it showed fluorescence with the baseline going up, since they are positioned in the negative values of PC2. Both blue denim jeans, blue cotton, blue polyester, and black polyester are encountered in zone C, with negative values for both PC1 and PC2. This means that the Raman spectra of RDX was almost covered by the high fluorescence verified with the baseline going up. Distinction between textiles was also observed. Jeans A showed more fluorescence in comparison to the others. Black cotton is very well isolated from the other textiles in zone D. This fabric was the one that showed the highest fluorescence (negative values of PC1), with the baseline going down as seen in Figure 76. This was due to the saturation of the Raman spectra. The separating groups, can be explained by the two kinds of baseline observed (Figure 76): one with increasing baseline (see Figure 76 – (a) for jeans A), and other with decreasing baseline (see Figure 76 – (b) for black cotton).

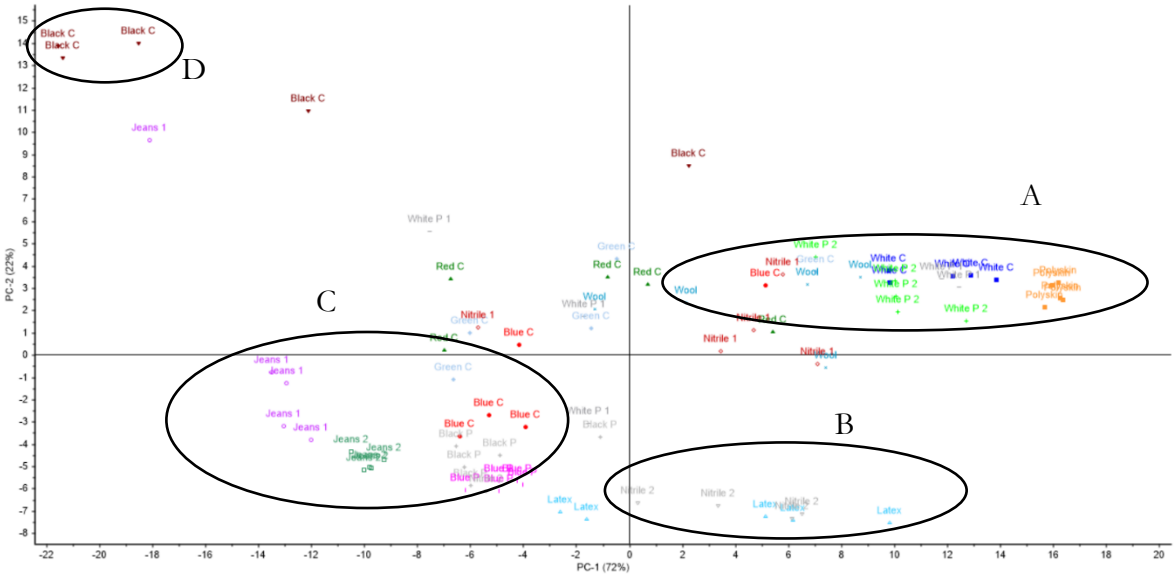

Figure 77. PCA model of five (5) positively identified RDX Raman spectra in each textile fabric (total of 80 particles).

3.6 Raman spectra of the potassium nitrate in the presence of interfering substances (fuels)

Figure 78 and appendix 104 shows the Raman spectra of the ten interfering substances analysed by the Thermo Scientific DXR Raman microscope and portable BW&TEK Raman i-Pro, respectively. The images of those substances are displayed in appendix 105. We can see that the Raman spectra of brown sugar, charcoal, and aluminium are overtaken by fluorescence. The rest of the interfering substances show Raman spectra with multiple bands. Most interfering substances were characterized by one kind of particle (mostly white particles), except in the case of both chocolate cocoa powders, in which there were two kinds of particles: white particles that gave the spectra h) and i), and brown particles that gave the spectra with fluorescence j) and k).

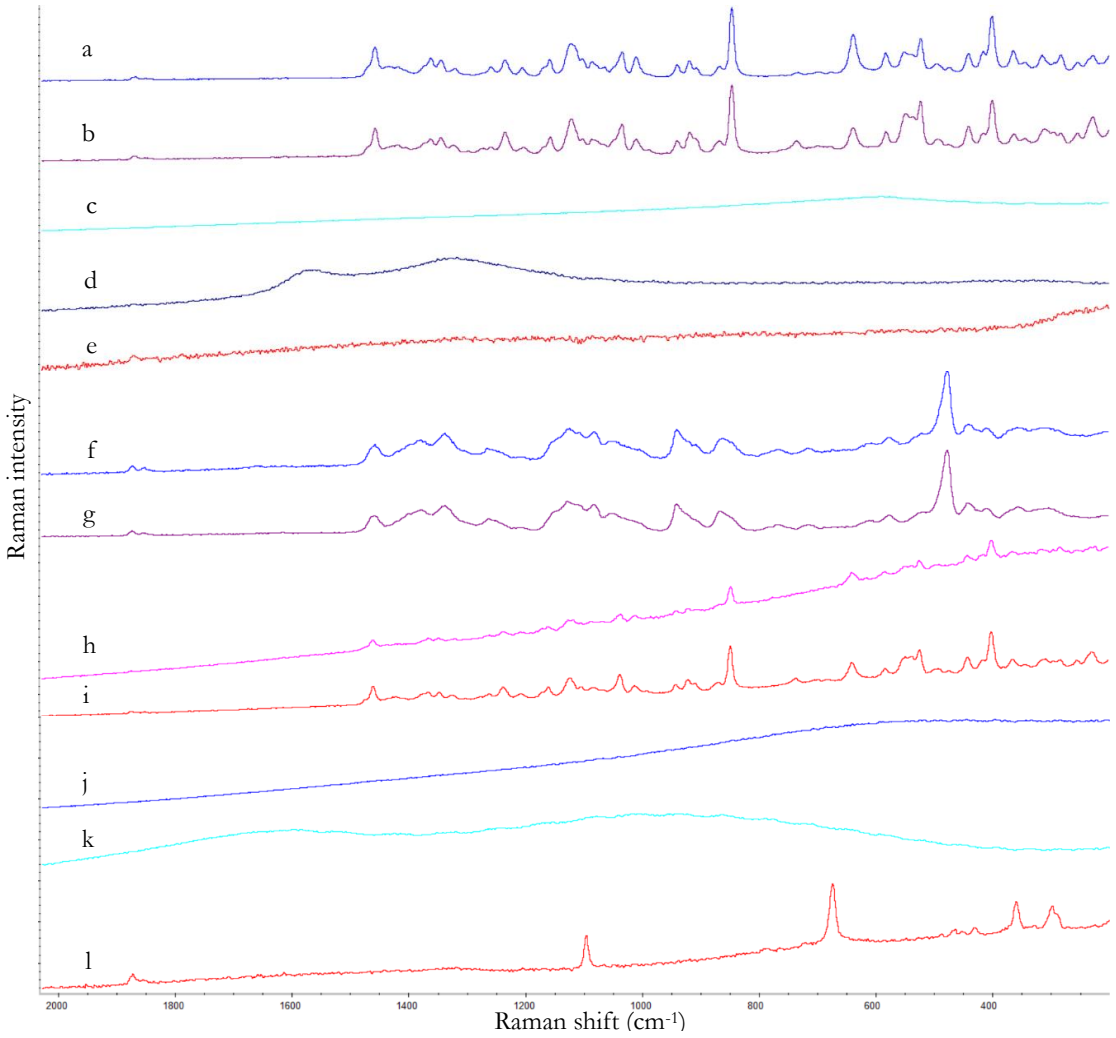

Figure 78. Raman spectra of the 10 interfering substances: (a) white sugar, (b) powdered sugar, (c) brown sugar, (d) charcoal, (e) aluminium, (f) wheat flour, (g) corn starch ("Maizena"), (h) chocolate cocoa powder "Brand 2" white particles, (i) chocolate cocoa powder "Brand 1" white particles, (j) chocolate cocoa powder "Brand 2" brown particles, (k) chocolate cocoa powder "Brand 1" brown particles, and (l) talc powder (Thermo Scientific DXR Raman microscope, 780 nm, 14 mW, 5 s exposure, 8 accumulations for (a), (b), (f) – (l); 1 mW for (c); 5 mW for (d) and (e)).

The Raman spectra of these substances were submitted to a search in the Thermo Scientific DXR Raman microscope database. The results provided positive identification for some of the main components of the interfering substances (see appendix 106, and 107): sucrose in white sugar, powdered sugar, both chocolate cocoa powders, and corn starch for wheat flour, and corn starch "Maizena".

Regarding the analysis of the mixtures, a positive identification and detection of the potassium nitrate was always possible. The detection of potassium nitrate in the mixtures with white sugar, powdered sugar, and brown sugar can be seen in Figure 79 (appendix 108 for the potable BW&TEK Raman i-Pro), together with the respective images of the particles.

Despite the numerous bands that sucrose spectra contains, the bands of potassium nitrate (1050 cm^{-1} and 715 cm^{-1}) were easily identified.

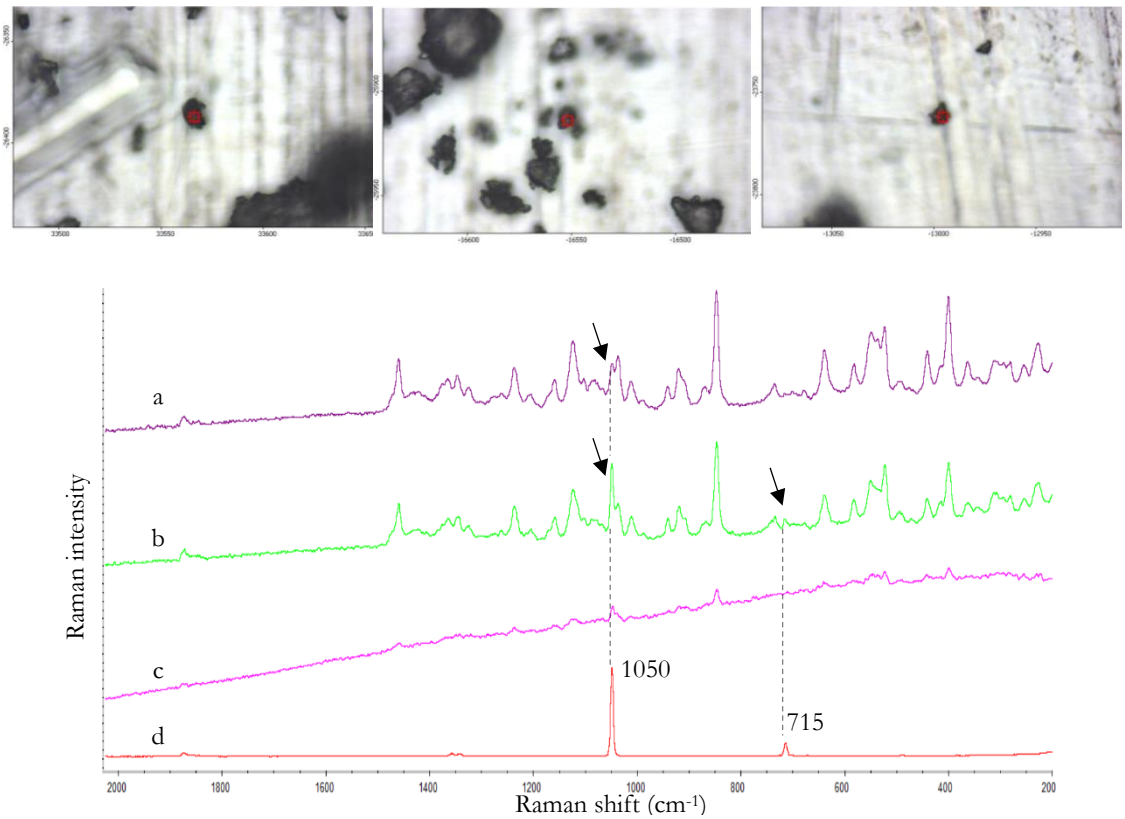

Figure 79. (Right to left, and top to bottom) Images (10x) and Raman spectra of the potassium nitrate mixed with white, powdered, and brown sugar (Thermo scientific DXR Raman microscope 780 nm, 14 mW, 5 s exposure, 8 accumulations).

The Raman spectra of potassium nitrate mixed with the white and brown particles of both chocolate cocoa powders are represented in Figure 80 (appendix 110 for the portable BW&TEK Raman i-Pro). Positive identification of potassium nitrate was possible by focusing the potassium nitrate particles (Figure 80 – (a), and (b)). The results for the portable Raman, were also the same as those obtained in the mixtures with sugars (appendix 108), since the main component of the chocolate is also sucrose. Besides the presence of sucrose, other particles are present (brown particles). The Raman spectra of these particles gave high fluorescence making impossible the identification of either sucrose or potassium nitrate particles when they were very closed to those brown particles (Figure 80 – c) and d)).

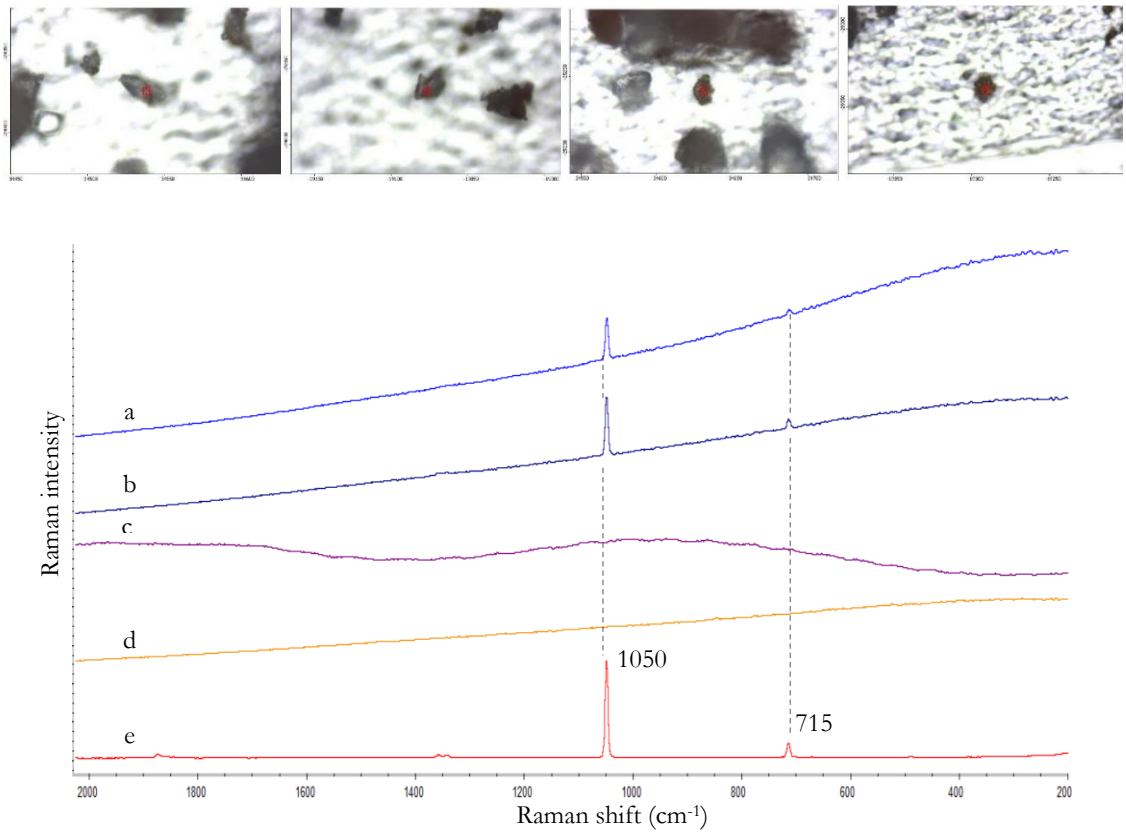

Figure 80. (Right to left, and top to bottom) Images (10x) and Raman spectra of the potassium nitrate mixed with the white particles of chocolate "Brand 1", and chocolate "Brand 2", and brown particles of the chocolate "Brand 1" and "Brand 2" (Thermo scientific DXR Raman microscope 780 nm, 14 mW, 5 s exposure, 8 accumulations).

The mixtures of wheat flour, corn starch, and talc powder with potassium nitrate gave the Raman spectra showed in Figure 81 (appendix 109 for the portable BW&TEK Raman i-Pro). For the mixtures with wheat flour and corn starch, the Raman bands of the potassium nitrate are positively identified, even with some overlapping bands of the interfering substance spectrum. Regarding the talc powder mixture, the characteristic bands of potassium nitrate, 1050 cm^{-1} and 715 cm^{-1}, are very well distinguished and identified, and do not overlap the bands of talc powder.

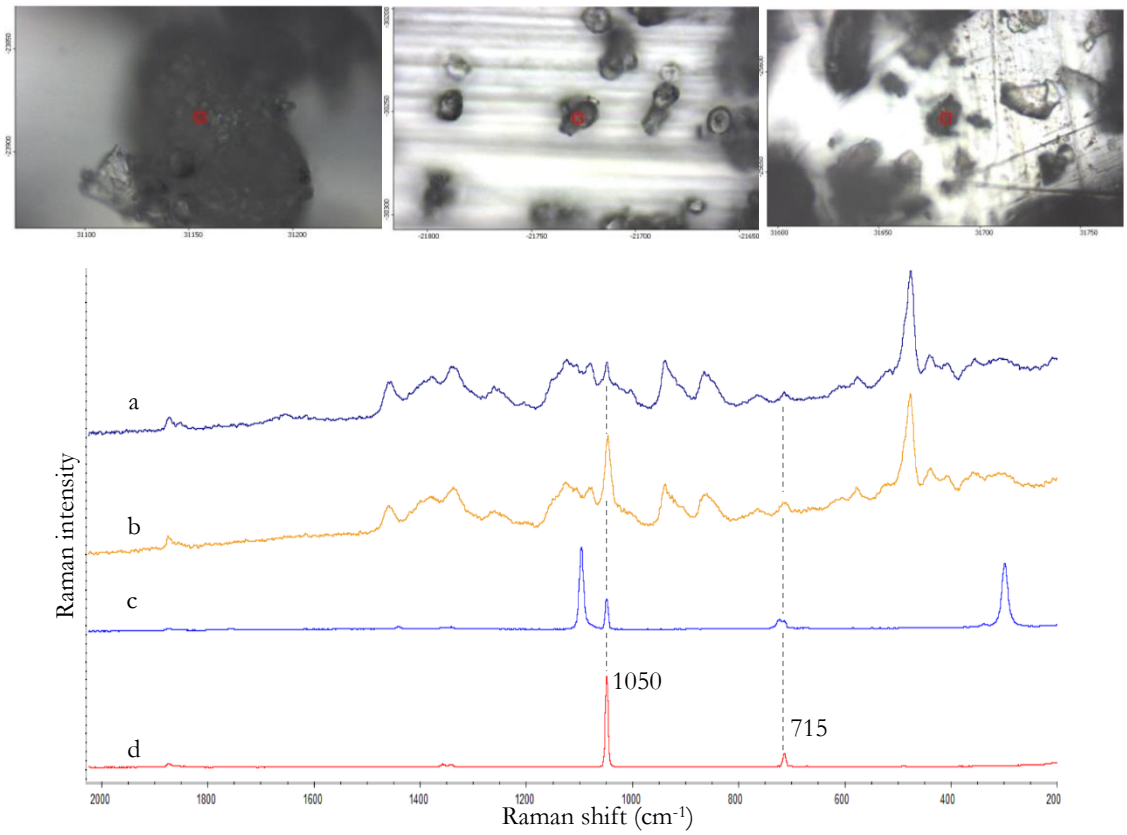

Figure 81. (Right to left, and top to bottom) Images (10x) and Raman spectra of the potassium nitrate mixed with wheat flour, corn starch, and talc powder (Thermo scientific DXR Raman microscope 780 nm, 14 mW, 5 s exposure, 8 accumulations).

At last, the mixtures of potassium nitrate with aluminium powder and charcoal were also analysed by Raman spectroscopy. In Figure 82 (appendix 111 for the portable BW&TEK Raman i-Pro), the bands of potassium nitrate are easily distinguished, since no bands from interfering substances may overlap. They only gave fluorescence. The problem of analysing these mixtures, is that potassium nitrate particles are easily covered with charcoal and aluminium powder, which give rise to spectra with high levels of fluorescence, not being possible to detect the oxidizing salt. Thus, small particle sizes were difficult to be detected.

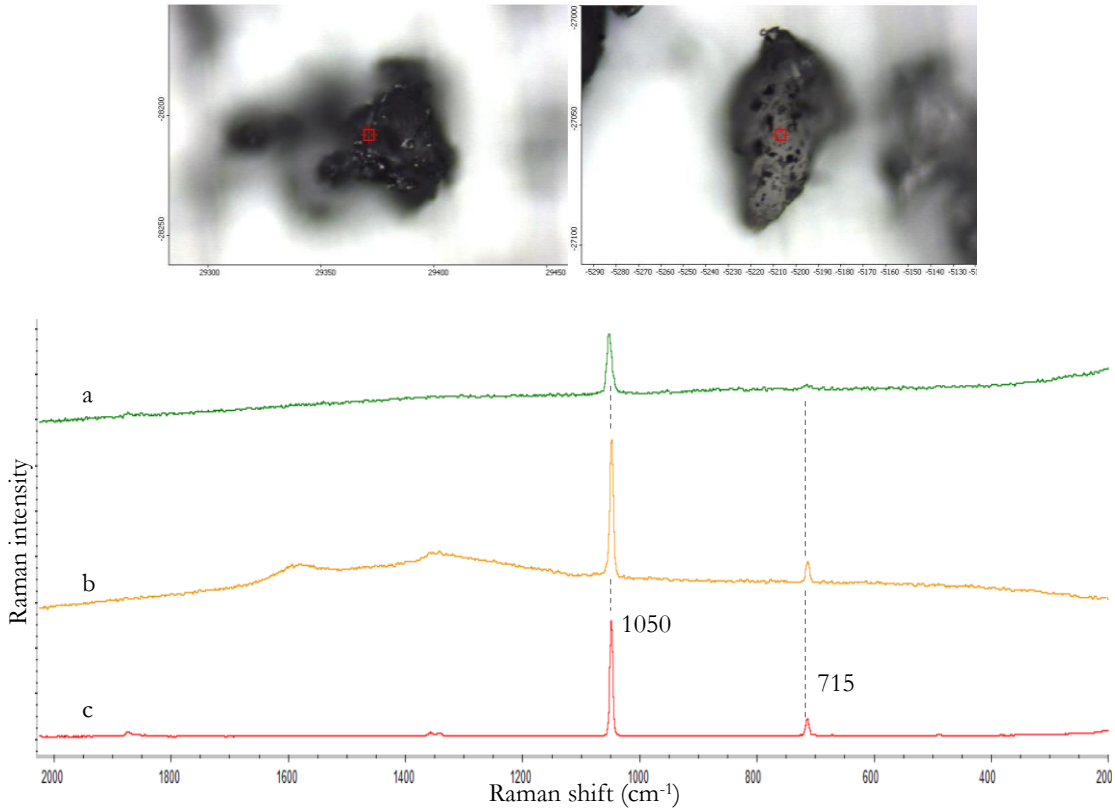

Figure 82. (Right to left, and top to bottom) Images (10x) and Raman spectra of the potassium nitrate mixed with aluminium powder and charcoal (Thermo scientific DXR Raman microscope 780 nm, 14 mW, 5 s exposure, 8 accumulations).

The mixtures were also analysed after being dispersed in a textile fabric, particularly the red cotton fabric. The results are shown in appendix 112, 113, 114, and 115 for the portable BW&TEK Raman i-Pro. Despite the fluorescence coming from the textile fabric, the potassium nitrate was positively detected and identified no matter what interfering substance (fuel) was used to make the mixture.

Chapter 4

Conclusions

The advantage and capability of confocal Raman microscopy to obtain Raman spectra by focusing the incident laser radiation in small particles of explosive and energetic salts, even when embedded within highly fluorescence interfering surfaces (i.e. textile fabrics), is demonstrated in the first study. With the right focus, the fluorescence coming from the surrounding material (i.e. the textile fabrics) was minimized or even removed, enabling the positive identification of the energetic material. Doing manual searching, particles with the size of 2 μm for the oxidizing salts, 3 μm for the organic explosives, and 6 μm for the inorganic explosives were detected using the Thermo Scientific DXR Raman microscope. For the portable BW&TEK i-Raman Pro, particles of 7 μm for the oxidizing salts, 7 μm for the organic explosives, and 18 μm for the inorganic explosives were detected. Considering the smallest particles detected (i.e. particle size of 2, 3, 6, and 6 μm for barium nitrate, HMTD, black powder, and chloratite particles), the LOD were estimated by using the density of the corresponding explosives/oxidizing salt, being 0.03 ng, 0.01 or 0.02 ng, 0.5 ng, and 0.5 ng if cubic particles, and 0.01 ng, 0.005 or 0.01 ng, 0.2 ng, and 0.3 ng if spherical for the Thermo Scientific DXR Raman microscope. The estimated mass of the smallest particles (i.e. particle size of 7, 7, and 18 μm for barium nitrate, TNT, and chloratite particles) determined by the portable BW&TEK i-Raman Pro was 1.11 ng, 0.57 ng, and 14.58 ng if cubic particles, and 0.58 ng, 0.30 ng, and 7.63 ng if spherical particles. This gives a sensitivity comparable to mass spectrometric and chromatography techniques.

Nevertheless, it was observed that some spectral bands arising from the fibres (natural or synthetic) and/or dyes, and mostly, a high fluorescence was observed in most cloth fabrics (except for white polyester and polyskin in the Thermo Scentific DXR Raman microscope). Fortunately, those bands from the fabric did not interfere with the identification of the particle since they did not overlap the characteristic bands of the explosive/energetic salt. In addition, the fluorescence was overcome by carefully focusing the confocal beam into the small particles. Furthermore, the use of a red laser is an added

advantage, as the generation of fluorescence is reduced. The analysis with the portable BWTEK i-Raman pro provided difficulties regarding the high fluorescence (due to the large laser spot), and burning/degradation of some of the textile fabrics (such as black cotton, blue cotton, blue denim jeans and polyskin). Besides the fluorescence, and the burning of the textile fabrics, the visual searching and location of the particles trapped within the cloth fibres posed difficulties (mostly on white coloured textiles), increasing the time for spectra scanning (10 to 15 minutes more) and a delay in the forensic investigation.

Correlation between the particle sizes and the type of cloth textile in which they were detected was demonstrated. Generally, for the textiles with high fluorescence, higher particle sizes needed to be analysed to give an identifiable Raman signal. Separation of the different textile fabrics according to their fluorescence was also demonstrated by performing a PCA analysis on the Raman spectra of potassium chlorate and RDX. Textiles such as blue denim jeans, black cotton, blue polyester, and black polyester provided high fluorescence, contrary to white cotton, and white polyester that showed much less.

In the second study, regarding the interfering substances, positive identification of the potassium nitrate was possible in all of them. This might be explained by the fact that potassium nitrate is more Raman active than those interfering substances. Thus, even when the bands from those substances overlapped with the ones from the oxidizing salt, positive identification was still made. Since the other oxidizing salts (sodium nitrate, ammonium nitrate, potassium chlorate, sodium chlorate, potassium perchlorate, and barium nitrate) have the same behaviour as potassium nitrate, it might be assumed also a positive identification for those oxidizing salts when mixed with different fuel interfering substances.

Overall, confocal Raman microscopy provided high discrimination of the explosive particles on cloth fabrics, leaving the particle unaltered. However, for inorganic explosives, since they are composed with high heat-sensitive compounds (such as aluminium powder and charcoal), some the particles burned. This problem was enhanced when analysing these explosives in the textiles that also burned.

The rapid acquisition time for both instruments, no sample preparation, non-destructive nature, the easy discrimination of the analyte from the contaminant with the right focus of the laser and the high specificity and selectivity of this analytical technique, allows forensic scientists and police security agencies to screen the cloth fabrics with the aim of detecting explosive particles during initial inspections. However, attention regarding the

burning of textile fabrics, (mostly the black dyed ones) must be paid. In addition, the use of a portable Raman laser in these kind of matrices needs specially attention, because the laser is too strong, and destruction of the textiles may occur. Thus, sensitivity trials for the different textiles regarding the Raman laser need to be made, preventing the destruction of the evidential material in order to leave it intact for further analysis. The positive identification of explosives in clothing can be used as a strong forensic evidence to establish a link between these energetic materials and suspects involved in terrorist activities, because handling, transportation, and packaging of these materials will cause cross-contamination of the clothing belonging to the suspect.

Bibliography

[1] J. Akhavan, *The chemistry of explosives*, 2nd ed. Cambridge, UK: Royal Society of Chemistry, 2004.

[2] J. P. Agrawal, *High Energy Materials: Propellants, Explosives and Pyrotechnics*. John Wiley & Sons, 2010.

[3] M. Marshall and J. C. Oxley, *Aspects of explosives detection*, 1st ed. Amsterdam: Elsevier, 2009.

[4] S. Bhandari, *Engineering rock blasting operations*. Rotterdam: A.A. Balkema, 1997.

[5] S. Venugopalan and R. Sivabalan, *Demystifying explosives: concepts in high energy materials*. Oxford: Elsevier, 2015.

[6] J. Hwang et al., "Fast and sensitive recognition of various explosive compounds using Raman spectroscopy and principal component analysis," *J. Mol. Struct.*, vol. 1039, pp. 130–136, May 2013.

[7] P. W. Cooper, *Explosives engineering*. Wiley-VCH, 1996.

[8] R. Meyer, J. Köhler, and A. Homburg, *Explosives*, 6th ed. Weinheim: Wiley-VCH, 2007.

[9] M. López-López, J. L. Ferrando, and C. García-Ruiz, "Comparative analysis of smokeless gunpowders by Fourier transform infrared and Raman spectroscopy," *Anal. Chim. Acta*, vol. 717, pp. 92–99, Mar. 2012.

[10] D. Menning and H. Östmark, "Detection of liquid and homemade explosives: what do we need to know about their properties?," in *Detection of Liquid Explosives and Flammable Agents in Connection with Terrorism*, Springer, 2008, pp. 55–70.

[11] J. Siegel and P. Saukko, *Encyclopedia of Forensic Sciences*, 2nd ed. Academic Press, 2013.

[12] M. López-López and C. García-Ruiz, "Infrared and Raman spectroscopy techniques applied to identification of explosives," *Trends Anal. Chem.*, vol. 54, pp. 36–44, 2014.

[13] F. Zapata, M. Á. F. de la Ossa, E. Gilchrist, L. Barron, and C. García-Ruiz, "Progressing the analysis of Improvised Explosive Devices: Comparative study for trace detection of explosive residues in handprints by Raman spectroscopy and liquid chromatography," *Talanta*, vol. 161, pp. 219–227, Dec. 2016.

[14] United States Department of Defense (DOD), "DOD Dictionary of Military and Associated Terms." *Office of the Secretary of Defense, the Services, the Joint Staff, combatant commands, DOD agencies, and all other DOD components*, May-2017.

[15] J. Sundram and P. P. Sim, "Using Wireless Sensor Networks in Improvised Explosive Device Detection," M. S. Thesis, Naval Postgraduate School, Monterey, CA, 2007.

[16] H. Schubert and A. Kuznetsov, *Detection and disposal of improvised explosives*. Dordrecht: Springer, 2006.

[17] P. R. Laska, *Bombs, IEDs, and explosives: identification, investigation, and disposal techniques*. Boca Raton, FL: CRC/Taylor & Francis, 2016.

[18] J. Bevan et al., *Conventional ammunition in surplus: a reference guide*. Geneva: Small Arms Survey, Graduate Institute of International Studies, 2008.

[19] L. C. Pacheco-Londoño, W. Ortiz-Rivera, O. M. Primera-Pedrozo, and S. P. Hernández-Rivera, "Vibrational spectroscopy standoff detection of explosives," *Anal. Bioanal. Chem.*, vol. 395, no. 2, pp. 323–335, Sep. 2009.

[20] H. Östmark, M. Nordberg, and T. E. Carlsson, "Stand-off detection of explosives particles by multispectral imaging Raman spectroscopy," *Appl. Opt.*, vol. 50, no. 28, pp. 5592–5599, 2011.

[21] E. Smith and G. Dent, *Modern Raman spectroscopy: a practical approach*. Hoboken, NJ: J. Wiley, 2005.

[22] J. M. Chalmers, H. G. M. Edwards, and M. D. Hargreaves, Eds., *Infrared and Raman spectroscopy in forensic science*. Oxford: Wiley-Blackwell, 2012.

[23] G. Gauglitz and D. S. Moore, *Handbook of Spectroscopy*, 2nd ed., vol. 4. Weinheim, Germany: Wiley-VCH, 2014.

[24] J. Chalmers and P. R. Griffiths, *Handbook of Vibrational Spectroscopy*. Chichester: Wiley, 2001.

[25] I. R. Lewis and H. G. M. Edwards, *Handbook of Raman spectroscopy: from the research laboratory to the process line*. New York: Marcel Dekker, 2001.

[26] S. Wallin et al., "Possibilities for standoff Raman detection applications for explosives," in *2012 Proc. SPIE 8358, Chemical, Biological, Radiological, Nuclear, and Explosives (CBRNE) Sensing XIII*, pp. 83580P. doi:10.1117/12.919144

[27] E. L. Izake, "Forensic and homeland security applications of modern portable Raman spectroscopy," *Forensic Sci. Int.*, vol. 202, no. 1–3, pp. 1–8, Oct. 2010.

[28] A. J. Hobro and B. Lendl, "Stand-off Raman spectroscopy," *TrAC Trends Anal. Chem.*, vol. 28, no. 11, pp. 1235–1242, Dec. 2009.

[29] S. Sadate, "Standoff Raman Spectroscopy of Explosive Nitrates Using 785 nm Laser," *Am. J. Remote Sens.*, vol. 3, no. 1, p. 1, 2015.

[30] A. Hakonen, P. O. Andersson, M. S. Schmidt, T. Rindzevicius, and M. Käll, "Explosive and chemical threat detection by surface-enhanced Raman scattering: A review," *Anal. Chim. Acta*, vol. 893, pp. 1–13, 2015.

[31] N. R. Butt et al., "Classification of Raman Spectra to Detect Hidden Explosives," *IEEE Geosci. Remote Sens. Lett.*, vol. 8, no. 3, pp. 517–521, May 2011.

[32] A. Pettersson *et al.*, "Explosives standoff detection using Raman spectroscopy: from bulk towards trace detection," 2010, vol. 7664, p. 76641K–76641K–12.

[33] M. L. Lewis, I. R. Lewis, and P. R. Griffiths, "Raman spectrometry of explosives with a no-moving-parts fiber coupled spectrometer: A comparison of excitation wavelength," *Vib. Spectrosc.*, vol. 38, no. 1–2, pp. 17–28, Jul. 2005.

[34] D. D. Tuschel, A. V. Mikhonin, B. E. Lemoff, and S. A. Asher, "Deep ultraviolet resonance Raman excitation enables explosives detection," *Appl. Spectrosc.*, vol. 64, no. 4, pp. 425–432, 2010.

[35] M. Ghosh, L. Wang, and S. A. Asher, "Deep-Ultraviolet Resonance Raman Excitation Profiles of NH_4NO_3, PETN, TNT, HMX, and RDX," *Appl. Spectrosc.*, vol. 66, no. 9, pp. 1013–1021, Sep. 2012.

[36] A. Ehlerding, I. Johansson, S. Wallin, and H. Östmark, "Resonance-Enhanced Raman Spectroscopy on Explosives Vapor at Standoff Distances," *Int. J. Spectrosc.*, vol. 2012, pp. 1–9, 2012.

[37] W. A. Al-Saidi, S. A. Asher, and P. Norman, "Resonance Raman Spectra of TNT and RDX Using Vibronic Theory, Excited-State Gradient, and Complex Polarizability Approximations," *J. Phys. Chem. A*, vol. 116, no. 30, pp. 7862–7872, Aug. 2012.

[38] K. L. Gares, K. T. Hufziger, S. V. Bykov, and S. A. Asher, "Review of explosive detection methodologies and the emergence of standoff deep UV resonance Raman: Review of explosive detection methodologies," *J. Raman Spectrosc.*, vol. 47, no. 1, pp. 124–141, Jan. 2016.

[39] F. Zapata, M. López-López, and C. García-Ruiz, "Detection and identification of explosives by surface enhanced Raman scattering," *Appl. Spectrosc. Rev.*, vol. 51, no. 3, pp. 227–262, Mar. 2016.

[40] H. Wackerbarth et al., "Detection of explosives based on surface-enhanced Raman spectroscopy," *Appl. Opt.*, vol. 49, no. 23, pp. 4362–4366, 2010.

[41] B. D. Piorek, S. J. Lee, M. Moskovits, and C. D. Meinhart, "Free-Surface Microfluidics/Surface-Enhanced Raman Spectroscopy for Real-Time Trace Vapor Detection of Explosives," *Anal. Chem.*, vol. 84, no. 22, pp. 9700–9705, Nov. 2012.

[42] S. Almaviva et al., "Trace detection of explosives and their precursors by surface enhanced Raman spectroscopy," in *2012 Proc. SPIE 8546, Optics and Photonics for Counterterrorism, Crime Fighting, and Defence VIII*, pp. 854602-7. doi:10.1117/12.970300

[43] A. Portnov, I. Bar, and S. Rosenwaks, "Highly sensitive standoff detection of explosives via backward coherent anti-Stokes Raman scattering," *Appl. Phys. B*, vol. 98, no. 2–3, pp. 529–535, Feb. 2010.

[44] I. E. I. Petterson and F. Ariese, "Time-resolved Raman spectroscopy for non-invasive detection through non-transparent materials," *Spectroscopy Europe*, vol. 24, no. 1, pp. 19–21, 2012.

[45] I. E. I. Petterson, M. López-López, C. García-Ruiz, C. Gooijer, J. B. Buijs, and F. Ariese, "Noninvasive Detection of Concealed Explosives: Depth Profiling through Opaque Plastics by Time-Resolved Raman Spectroscopy," *Anal. Chem.*, vol. 83, no. 22, pp. 8517–8523, Nov. 2011.

[46] E. L. Izake, B. Cletus, W. Olds, S. Sundarajoo, P. M. Fredericks, and E. Jaatinen, "Deep Raman spectroscopy for the non-invasive standoff detection of concealed chemical threat agents," *Talanta*, vol. 94, pp. 342–347, May 2012.

[47] C. Eliasson, N. A. Macleod, and P. Matousek, "Non-invasive detection of powders concealed within diffusely scattering plastic containers," *Vib. Spectrosc.*, vol. 48, no. 1, pp. 8–11, Sep. 2008.

[48] C. Eliasson, N. A. Macleod, and P. Matousek, "Noninvasive Detection of Concealed Liquid Explosives Using Raman Spectroscopy," *Anal. Chem.*, vol. 79, no. 21, pp. 8185–8189, Nov. 2007.

[49] B. Zachhuber, C. Gasser, E. t.H. Chrysostom, and B. Lendl, "Stand-Off Spatial Offset Raman Spectroscopy for the Detection of Concealed Content in Distant Objects," *Anal. Chem.*, vol. 83, no. 24, pp. 9438–9442, Dec. 2011.

[50] S. Wallin, A. Pettersson, H. Östmark, and A. Hobro, "Laser-based standoff detection of explosives: a critical review," *Anal. Bioanal. Chem.*, vol. 395, no. 2, pp. 259–274, Sep. 2009.

[51] B. Zachhuber, G. Ramer, A. Hobro, E. t. H. Chrysostom, and B. Lendl, "Stand-off Raman spectroscopy: a powerful technique for qualitative and quantitative analysis of inorganic and organic compounds including explosives," *Anal. Bioanal. Chem.*, vol. 400, no. 8, pp. 2439–2447, Jun. 2011.

[52] M. Åkeson, M. Nordberg, A. Ehlerding, L.-E. Nilsson, H. Östmark, and P. Strömbeck, "Picosecond laser pulses improves sensitivity in standoff explosive detection," in *2011 Proc. SPIE 8017, Detection and Sensing of Mines, Explosive Objects, and Obscured Targets XVI*, pp.80171C-8. doi:10.1117/12.883351

[53] M. Nordberg, M. Åkeson, H. Östmark, and T. E. Carlsson, "Stand-off detection of explosive particles by imaging Raman spectroscopy," in *2011 Proc. SPIE 8017, Detection and Sensing of Mines, Explosive Objects, and Obscured Targets XVI*, pp.80171B-7. doi:10.1117/12.883179

[54] B. Zachhuber, G. Ramer, A. J. Hobro, and B. Lendl, "Stand-off Raman spectroscopy of explosives," in *2010 Proc. SPIE 7838, Optics and Photonics for Counterterrorism and Crime Fighting VI, and Optical Materials in Defence Systems Technology VII,* pp.78380F-10. doi:10.1117/12.864564

[55] S. Almaviva et al., "Application of micro-Raman spectroscopy for fight against terrorism and smuggling," *Opt. Eng.*, vol. 53, no. 4, pp. 44113–44113, 2014.

[56] E. M. A. Ali, H. G. M. Edwards, M. D. Hargreaves, and I. J. Scowen, "Detection of explosives on human nail using confocal Raman microscopy," *J. Raman Spectrosc.*, vol. 40, no. 2, pp. 144–149, Feb. 2009.

[57] F. Zapata and C. García-Ruiz, "Determination of Nanogram Microparticles from Explosives after Real Open-Air Explosions by Confocal Raman Microscopy," *Anal. Chem.*, vol. 88, no. 13, pp. 6726–6733, Jul. 2016.

[58] M. López-López, J. L. Ferrando, and C. García-Ruiz, "Dynamite Analysis by Raman Spectroscopy As a Unique Analytical Tool," *Anal. Chem.*, vol. 85, no. 5, pp. 2595–2600, Mar. 2013.

[59] E. M. A. Ali, H. G. M. Edwards, and I. J. Scowen, "In-situ detection of single particles of explosive on clothing with confocal Raman microscopy," *Talanta*, vol. 78, no. 3, pp. 1201–1203, May 2009.

[60] E. M. A. Ali, H. G. M. Edwards, and I. J. Scowen, "Raman spectroscopy and security applications: the detection of explosives and precursors on clothing," *J. Raman Spectrosc.*, vol. 40, no. 12, pp. 2009–2014, Dec. 2009.

[61] M. Diem, *Modern vibrational spectroscopy and micro-spectroscopy: theory, instrumentation, and biomedical applications*. Chichester, West Sussex, UK: John Wiley & Sons, Inc, 2015.

[62] R. S. Das and Y. K. Agrawal, "Raman spectroscopy: Recent advancements, techniques and applications," *Vib. Spectrosc.*, vol. 57, no. 2, pp. 163–176, Nov. 2011.

[63] M. R. Almeida, D. N. Correa, J. J. Zacca, L. P. L. Logrado, and R. J. Poppi, "Detection of explosives on the surface of banknotes by Raman hyperspectral imaging and independent component analysis," *Anal. Chim. Acta*, vol. 860, pp. 15–22, Feb. 2015.

[64] D. S. Moore and R. J. Scharff, "Portable Raman explosives detection," *Anal. Bioanal. Chem.*, vol. 393, no. 6–7, pp. 1571–1578, Mar. 2009.

[65] M. Kotrlý and I. Turková, "Analysis of nonstandard and home-made explosives and post-blast residues in forensic practice," in *2014 Proc. SPIE 9073, Chemical, Biological, Radiological, Nuclear, and Explosives (CBRNE) Sensing XV,* pp.90730U-10. doi:10.1117/12.2050121

[66] J. S. Caygill, F. Davis, and S. P. J. Higson, "Current trends in explosive detection techniques," *Talanta*, vol. 88, pp. 14–29, Jan. 2012.

[67] J. Yinon, Ed., *Counterterrorist detection techniques of explosives*. Amsterdam; Boston: Elsevier, 2007.

[68] H. Östmark, S. Wallin, and H. G. Ang, "Vapor Pressure of Explosives: A Critical Review," *Propellants Explos. Pyrotech.*, vol. 37, no. 1, pp. 12–23, Feb. 2012.

[69] N. Abdul-Karim et al., "Morphological Variations of Explosive Residue Particles and Implications for Understanding Detonation Mechanisms," *Anal. Chem.*, vol. 88, no. 7, pp. 3899–3908, Apr. 2016.

[70] N. Abdul-Karim, C. S. Blackman, P. P. Gill, E. M. M. Wingstedt, and B. A. P. Reif, "Post-blast explosive residue - a review of formation and dispersion theories and experimental research," *RSC Adv*, vol. 4, no. 97, pp. 54354–54371, Oct. 2014.

[71] I. R. Lewis, N. W. Daniel Jr, and P. R. Griffiths, "Interpretation of Raman spectra of nitro-containing explosive materials. Part I: Group frequency and structural class membership," *Appl. Spectrosc.*, vol. 51, no. 12, pp. 1854–1867, 1997.

[72] A. Tripathi et al., "Semi-Automated Detection of Trace Explosives in Fingerprints on Strongly Interfering Surfaces with Raman Chemical Imaging," *Appl. Spectrosc.*, vol. 65, no. 6, pp. 611–619, Jun. 2011.

[73] D. S. Moore, "Instrumentation for trace detection of high explosives," *Rev. Sci. Instrum.*, vol. 75, no. 8, pp. 2499–2512, Aug. 2004.

[74] T. J. Johnson et al., "Demonstrated Wavelength Portability of Raman Reference Data for Explosives and Chemical Detection," *Int. J. Spectrosc.*, vol. 2012, pp. 1–11, 2012.

[75] N. W. Daniel Jr, I. R. Lewis, and P. R. Griffiths, "Interpretation of Raman spectra of nitro-containing explosive materials. Part II: the implementation of neural, fuzzy, and statistical models for unsupervised pattern recognition," *Appl. Spectrosc.*, vol. 51, no. 12, pp. 1868–1879, 1997.

[76] K. Potter, H. Hagen, A. Kerren, and P. Dannenmann, "Methods for presenting statistical information: The box plot," *Vis. Large Unstructured Data Sets*, vol. 4, pp. 97–106, 2006.

[77] R. Bro and A. K. Smilde, "Principal component analysis," *Anal. Methods*, vol. 6, no. 9, p. 2812, 2014.

[78] R. G. Brereton, *Chemometrics: data analysis for the laboratory and chemical plant*. Chichester, West Sussex, England; Hoboken, NJ: Wiley, 2003.

[79] K. Kjeldahl and R. Bro, "Some common misunderstandings in chemometrics," *J. Chemom.*, vol. 24, no. 7–8, pp. 558–564, Jul. 2010.

[80] D. Cozzolino, W. U. Cynkar, N. Shah, and P. Smith, "Multivariate data analysis applied to spectroscopy: Potential application to juice and fruit quality," *Food Res. Int.*, vol. 44, no. 7, pp. 1888–1896, Aug. 2011.

[81] H. Mark and J. Workman, *Chemometrics in spectroscopy*. Academic Press, 2010.

[82] A. Rinnan, F. van den Berg, and S. B. Engelsen, "Review of the most common pre-processing techniques for near-infrared spectra," *TrAC Trends Anal. Chem.*, vol. 28, no. 10, pp. 1201–1222, Nov. 2009.

[83] P. P. Meleiro and C. García-Ruiz, "Spectroscopic techniques for the forensic analysis of textile fibers," *Appl. Spectrosc. Rev.*, vol. 51, no. 4, pp. 278–301, Apr. 2016.

[84] P. G. Zverev, T. T. Basiev, V. V. Osiko, A. M. Kulkov, V. N. Voitsekhovskii, and V. E. Yakobson, "Physical, chemical and optical properties of barium nitrate Raman crystal," *Opt. Mater.*, vol. 11, no. 4, pp. 315–334, 1999.

[85] V. V. Kuzmin, M. Y. Solov'ev, Y. B. Tuzkov, and G. D. Kozak, "Forensic investigation of some peroxides explosives," *Cent. Eur. J. Energ. Mater.*, vol. 5, no. 3–4, pp. 77–85, 2008.

[86] F. A. Miller, D. W. Mayo, and R. W. Hannah, *Course notes on the interpretation of infrared and Raman spectra*. Hoboken, N.J: Wiley-Interscience, 2004.

[87] B. Schrader and D. Bougeard, Eds., *Infrared and Raman spectroscopy: methods and applications*. Weinheim ; New York: VCH, 1995.

[88] P. Vandenabeele, *Practical Raman spectroscopy: an introduction*. The Atrium, Southern Gate, Chichester, West Sussex, United Kingdom: Wiley, 2013.

[89] P. A. Carson and C. J. Mumford, *Hazardous chemicals handbook*, 2nd ed. Oxford; Boston: Butterworth-Heinemann, 2002.

[90] S. K. Sharma, A. K. Misra, P. G. Lucey, R. C. F. Lentz, and C. H. Chio, "Stand-off Raman instrument for detection of bulk organic and inorganic compounds," in *2007 Proc. SPIE 6554, Chemical and Biological Sensing VIII*, pp.655405. doi:10.1117/12.719152

[91] A. K. Misra, S. K. Sharma, T. E. Acosta, J. N. Porter, and D. E. Bates, "Single-Pulse Standoff Raman Detection of Chemicals from 120 m Distance During Daytime," *Appl. Spectrosc.*, vol. 66, no. 11, pp. 1279–1285, Nov. 2012.

[92] C. Martín-Alberca, F. Zapata, H. Carrascosa, F. E. Ortega-Ojeda, and C. García-Ruiz, "Study of consumer fireworks post-blast residues by ATR-FTIR," *Talanta*, vol. 149, pp. 257–265, Mar. 2016.

[93] K. Nakamoto, *Infrared and Raman spectra of inorganic and coordination compounds*, 6th ed. Hoboken, N.J: Wiley, 2009.

[94] National Science Foundation University of California (2017, Jan). *Vibrational Modes,* [Online]. Available: https://chem.libretexts.org/Core/Physical_and_Theoretical_Chemistry/Spectroscopy/Vibrational_Spectroscopy/Vibrational_Modes

Appendix

Appendix 1. Classification of explosives per their end-use.

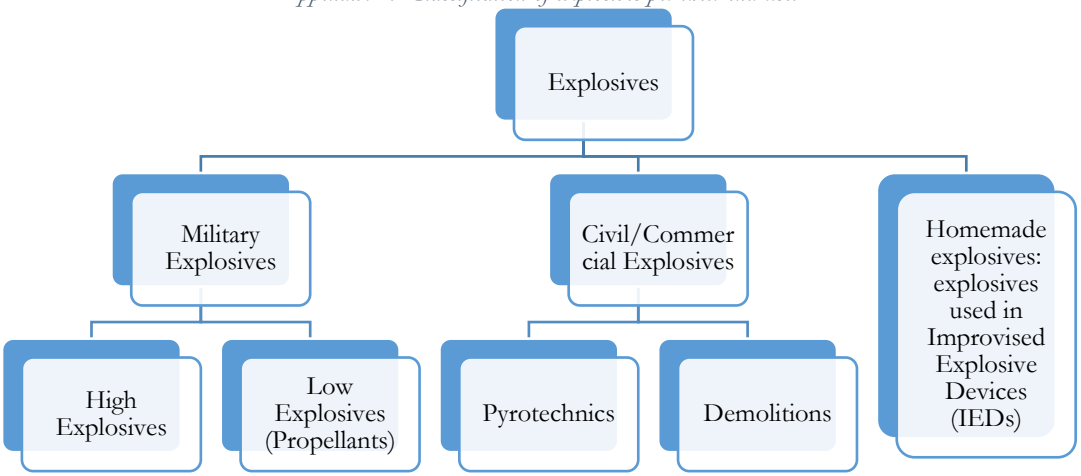

Appendix 2. Characteristics of military explosives. [2, 3, 8, 11]

Characteristics	Description
Stability	How well it stores before chemically breaking down. Measure of chemical stability, storage temperature, resistance to UV rays of the sun and electrostatic discharge;
Power (performance)	Measure of explosives ability to do work (how much energy is released);
Brisance	Measure of shattering effect (how fast the maximum detonation pressure is reached);
Availability and cost	Cheap, readily available material;
Sensitivity	Measure of the ease of initiation of detonation. Englobes sensitivity to impact, friction, shock, spark or heat;
Density	Weight of the explosive per unit volume. Higher density, more explosive can be packed in. Determines the method of loading: pellet loading, cast loading or press loading;
Volatility	How easily the explosive vaporizes. Very high volatility increases instability;
Hygroscopicity	Measure of a material's moisture-absorbing tendency. Hygroscopicity reduces the sensitivity, strength, stability and brisance and so is undesirable;
Toxicity	High toxicity is not desirable in military explosives.

Appendix 3. Classification of propellants based on their end-use. [2, 5]

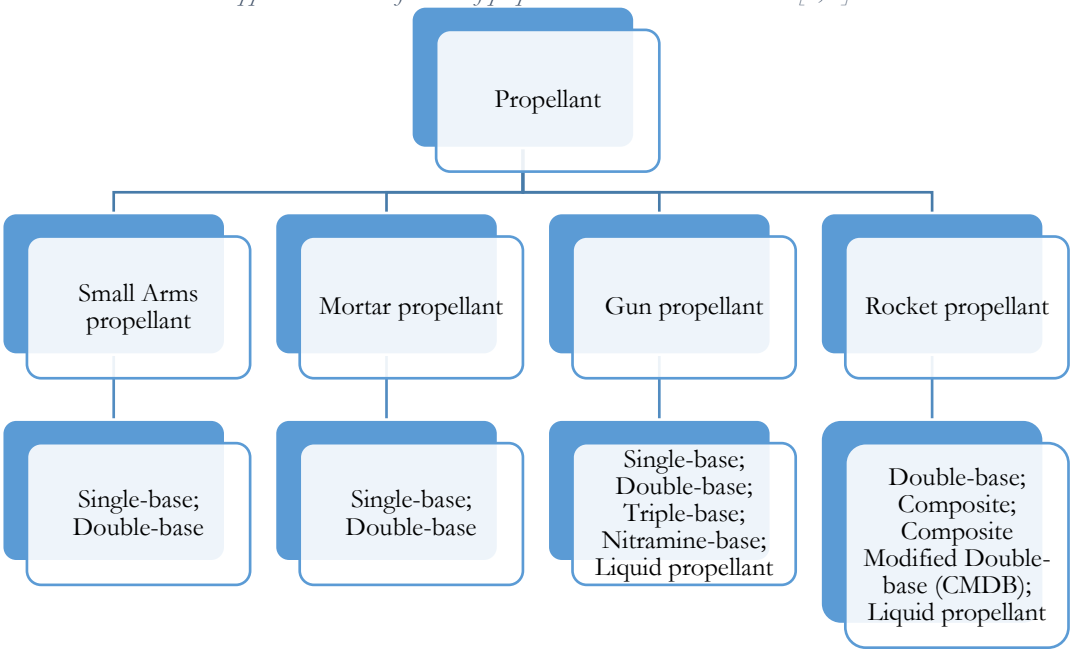

Appendix 4. Materials used to produce pyrotechnic devices. [5]

	Materials
Fuels (metallic/non-metallic)	Al, Cr, Mg, Mn, Ti, B, Si, S, etc.
Oxidizers	Chlorates, nitrates, perchlorates, chromates, etc.
Binders	Natural: paraffin wax, beeswax, etc. Man-made: polyester resin, PVC, epoxy resin.

Appendix 5. Examples of commercial, military explosives and homemade explosives encountered in IEDs at known places where explosions occurred. [3], [15], [17]

Explosive	**Observations**	**Chemical formula**	**Known IED used locations**
RDX-based (e.g. Semtex and C-4)	Military; Solid explosive;	$(O_2NNCH_2)_3$ (RDX)	Irish Republican Army bombings
TNT-based (e.g. cyclotol or tetryol)	Military; Solid explosives	$C_6H_2(NO_2)_3CH_3$ (TNT)	
Smokeless powder	Military (ammunition); Solid explosive	Single-base, double-base, triple-base powder	Olympic Park bombings
Black powder	Military (ammunition); Commercial (fireworks); Solid explosive;	Major component: KNO_3 (Potassium Nitrate)	Boston Marathon Bombing
Nitroglycerine (NG)	Composition of dynamites; Liquid explosives; Homemade or commercial;	$C_3H_5N_3O_9$	Madrid train bombings (2004)
Ethyleneglycol dinitrate (EGDN)		$C_2H_4N_2O_6$	
Nitromethane (NM)	Commercial (rocket propellant, etc.); Liquid explosive;	CH_3NO_2	Oklahoma City bombing

Triacetone triperoxide (TATP)	Peroxide explosives; TATP: no common uses; HMTD: primary explosive for detonators; Solid explosives;	$C_9H_{18}O_6$	London bombings, 2005; Brussels bombing 2016
Hexamethylene triperoxidediamine (HMTD)		$C_6H_{12}N_2O_6$	
Ammonium nitrate-based (e.g. ANFO)	Commercial (mining and blasting); Homemade; Solid explosive;	NH_4NO_3 (AN)	Oklahoma City bombing
Nitrourea	Solid explosive;	$CH_3N_3O_3$	-
Urea nitrate	Commercial (fertilizer); Solid explosive.	$CH_5N_3O_4$	Oklahoma City bombing

Appendix 6. Types of modes of vibration (the vibrational movements are indicated by arrows).

Modes of vibration	Vibrations	Description of the vibrations	Molecular representation
Stretching modes of vibrations (change in bond length)	Symmetric stretching (ν_s)	Change in bond length (the number of stretching modes is equal to the number of bonds in the molecule)	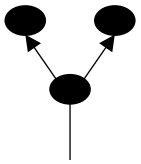
	Anti-symmetric stretching (ν_{as})		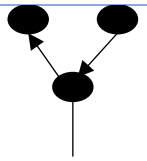
Bending or deformation modes of vibrations (change in bond angles)	Wagging (ϱ_w)	Change in angle between the plane of a group of atoms	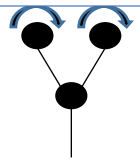
	Twisting (ϱ_t)	Change in angle between the planes of two groups of atoms	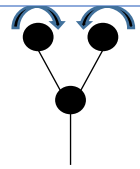
	Scissoring (δ)	Change in bond angle	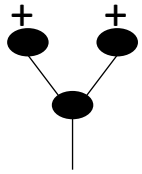
	Rocking (ϱ_r)	Change in angle between a group of atoms	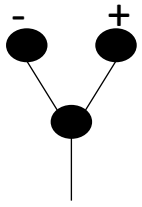

Appendix 7. Band wavenumber ranges for the different vibrational modes of the most common functional groups in chemistry. [86-88]

Wavenumber ranges (cm^{-1})	Functional groups
3650 – 3000	Stretching (v) O-H
1410 - 1350	Bending (ϱ) O-H
3500 – 3300	Stretching (v) N-H
1640 – 1550	Bending (ϱ) N-H
3000 – 2800	Stretching (v) C-H
900 - 730	Bending (ϱ) C-H
2250 - 2100	Stretching (v) C≡C
1820 – 1680	Stretching (v) C=O
1900 – 1500	Stretching (v) C=C
1600 - 1450	Stretching (v) C=C aromatic
1590 – 1530 (asym); 1380 – 1340 (sym)	Stretching (v) NO2
660 - 470	Bending (ϱ) NO2
1070 - 1015	Stretching (v) NO3-
770 - 700	Bending (ϱ) NO3-
1170 – 930	Stretching (v) ClO4-
630 - 420	Bending (ϱ) ClO4-
1100 – 900	Stretching (v) ClO3-
630 - 420	Bending (ϱ) ClO3-
1300 – 1000	Stretching (v) C-O
400 – 250	Bending C-C aliphatic chains

Appendix 8. Literature values of the positions of the symmetric and the antisymmetric NO_2 stretching vibrations. [71, 75]

Band	**Nitro-aromatic (cm^{-1})**	**Nitrate ester (cm^{-1})**	**Nitramine (cm^{-1})**
ν_s (NO_2)	1375-1315	1300-1270	1350-1250
N_{as} (NO_2)	1590-1457	1660-1610	1630-1500

Appendix 9. Multiple analytical techniques employed for explosives detection. [3, 12, 66, 67, 73]

Spectrometry techniques

- Ion mobility spectrometry (IMS)
- Mass spectrometry (including coupled techniques such as HPLC-MS, GC-MS, GC-MS/MS, etc.)
- Terahertz spectroscopy
- Cavity ring down spectroscopy
- Laser-induced breakdown spectroscopy (LIBS)
- Laser-induced fluorescence (LIF)
- Fluorescence spectroscopy
- Infra-red spectroscopy
- Raman spectroscopy
- Milimeter-wave imaging
- Dual-energy X-ray
- X-ray powder diffraction
- Photofragmentation combined with LIF (PF-LIF)
- Nuclear magnetic resonance (NMR)

Olfatory sensors

- Narural sensors: aninal detection (e.g. sniffer dogs, rats, insects, etc.);
- Artificial sensors: electronic or artificial noses

Sensor techniques

- Chemical sensors (change in color or conductivity)
- Electrochemical sensors (redox reaction; potenciometric, amperometric or conductimetric)
- Immunochemical sensors (antibody-antigen reaction)
- Luminescence sensors (fluorescence from the sample or from the material attached to the sample)

Nanotechnology

- Molecularly imprinted polymers (MIPs), Nanotubes, and Nanoparticles (associated with the enhancement of sensitivity and selectivity of other techniques, for example, electrochemical sensors)

Others

- Thermal neutron analysis (NAA)
- Surface acoustic waves
- Thin film sensors
- Elemental analysis
- Differential scanning calorimetry (DSC)

Appendix 10. Selected explosives and explosive precursors (oxidizing salts) and their physical properties. [1, 6, 8, 11, 89]

Compound (IUPAC name)	Abbreviation	Chemical formula	Density (g/cm^3)	Molecular weight (M)	Oxygen balance (%)	Nitrogen content (%)	Detonation velocity (m/s)
Ammonium nitrate	AN	NH_4NO_3	1.725	80.0	+19.99	36.98	6556; 1400 - 6000
Potassium nitrate	PN	KNO_3	2.10	101.1	+39.6	13.86	-
Sodium nitrate	SN	$NaNO_3$	2.265	85	+47.1	16.48	-
Barium nitrate	BN	$Ba(NO_3)_2$	3.24	261.4	+30.6	10.72	-
Sodium chlorate	SC	$NaClO_3$	2.48	106.4	+41.5	-	1300 - 4100
Potassium chlorate	PC	$KClO_3$	2.34	122.6	+39.2	-	1300 - 4100
Potassium perchlorate	PP	$KClO_4$	2.52	138.6	+46.2	-	1300 - 4100
Ammonal (AlAN)	AN + Al	NH_4NO_3	1.725	80.0	+19.99	36.98	6556
Chloratite	SC + Sugar + Sulfur	$NaClO_3$	2.48	106.4	+41.5	-	-
Black powder	PN + Charcoal + Sulfur	KNO_3	2.10	101.1	+39.6	13.86	-
Flash powder	PP + Al	$KClO_4$	2.52	138.6	+46.2	-	-
2-Methyl-1,3,5-trinitrobenzene	TNT	$C_7H_5N_3O_6$	1.654	227.1	-73.9	18.50	6735; 6900
[3-Nitrooxy-2,2-bis(nitrooxymethyl)propyl]nitrate	PETN	$C_5H_8N_4O_{12}$	1.76, 1.778	316.1	-10.1	17.72	8390; 8400; 8260
1,3,5-Trinitroperhydro-1,3,5-triazine	RDX	$C_3H_6N_6O_6$	1.816, 1.82	222.1	-21.6	37.84	8739; 8750; 8700
3,4,8,9,12,13-Hexaoxa-1,6-diazabicyclo[4.4.4]tetradecane	HMTD	$C_6H_{12}N_2O_6$	0.38; 0.88	208.1	-92.2	13.46	4500 (at 0.88 g/cm^3); 2820 (at 0.38 g/cm^3)

Appendix 11. Composition of the interfering substances.

Interfering substance	Composition
Talc powder	Talc, magnesium carbonate, perfume (fragrance)
Wheat flour	Wheat flour (contains gluten). May contain traces of egg and milk;
Corn starch	Corn starch
Chocolate cocoa powder "Brand 1"	Sugar, light cocoa powder (15%), emulsifier: sunflower lecithin. Cocoa: 15% minimum. May contain traces of gluten and milk;
Chocolate cocoa powder "Brand 2"	Sugar. Cocoa powder. "*Kda-malteado*" cereal cream (wheat flour; extract of barley malt; natural aroma: cola nut extract; mineral salts: calcium and phosphorus; Aromas; Salt. May contain milk.)
White (normal) sugar	Sugar (sacarose)
Brown sugar	Sugar (sacarose)
Powdered (confectioners) sugar	Sugar (sacarose) and corn starch
Charcoal	Charcoal
Aluminium powder	Aluminium

Appendix 12. Mass of the explosives during the dissolution and precipitation process.

Mass of the explosives during the precipitation process		
No precipitate (TATP)	35.12976 g	**0.00945g**
TATP	35.13921g	
No precipitate (TNT)	35.19795 g	**0.16655g**
TNT	35.36450g	
No precipitate (RDX)	92.5903 g	**0.11880g**
RDX	92.7091g	
Mass of the storage recipients (after the transfer from the petri dish and glass watch)		
No TATP	20.71256g	**0 g**
TATP*	20.71256g	
No TNT	20.54620g	**0.11747g**
TNT	20.66367g	
No RDX	20.72354g	**0.11260g**
RDX	20.83614g	

*TATP is a very unstable explosive under ambient conditions, and therefore degrades.

Appendix 13. Quantities of oxidizing salt measured for the dispersion onto the various textile fabrics from top to bottom: white, blue, red, black, and green cotton; blue, black, white 1, and white 2 polyester; wool, jeans 1, jeans 2, polyskin, latex, nitrile 1, and nitrile 2) between 25 –35 mg.

Oxidizing salts	Quantity (mg)		Oxidizing salts	Quantity (mg)	
Sodium chlorate	25.78	28.54	**Potassium chlorate**	26.06	29.92
	25.69	30.23		29.46	28.21
	27.18	29.54		29.90	29.98
	27.31	28.62		29.21	28.99
	26.88	28.62		27.10	28.10
	27.71	28.50		26.07	29.90
	26.90	28.05		28.66	28.00
	28.99	28.07		28.65	32.45
Sodium Nitrate	30.10	28.26	**Potassium Nitrate**	26.50	27.98
	31.54	29.62		27.06	27.10
	29.81	30.46		30.14	29.30
	31.71	29.43		26.57	28.30
	26.69	27.15		30.25	26.66
	30.86	29.32		26.11	30.59
	28.41	28.33		25.99	26.97
	28.79	27.93		27.72	29.11
Ammonium Nitrate	25.61	26.95	**Potassium perchlorate**	29.82	32.77
	27.67	27.71		26.34	29.15
	26.39	25.63		30.28	28.62
	25.64	27.71		27.60	27.98
	25.22	28.24		27.43	30.24
	25.49	25.68		28.96	29.96
	26.77	25.77		31.58	31.33
	26.93	25.36		27.56	33.20
Barium Nitrate	33.00			31.02	
	29.33			30.11	
	29.69			26.82	
	31.00			28.20	
	32.28			30.00	
	31.00			32.29	
	29.03			29.10	
	29.19			31.11	

Appendix 14. Quantities of organic explosive measured for the dispersion onto the various textile fabrics from top to bottom: white, blue, red, black, and green cotton; blue, black, white 1, and white 2 polyester; wool, jeans 1, jeans 2, polyskin, latex, nitrile 1, and nitrile 2) between 3 – 5 mg.

Organic Explosives	Quantity (mg)		Organic Explosives	Quantity (mg)	
PETN	3.82	4.62	**HMTD**	4.00	4.30
	3.33	5.38		3.40	3.77
	3.31	4.83		3.77	3.52
	3.77	4.13		4.53	4.34
	3.20	3.82		3.54	4.54
	3.43	5.83		3.90	4.11
	4.05	4.65		3.90	4.49
	4.18	4.42		3.94	3.33
RDX	3.88	4.28	**TNT**	3.75	4.95
	4.32	4.26		3.06	4.14
	5.49	4.05		3.76	4.48
	3.19	4.36		3.42	4.88
	3.09	5.02		4.16	4.06
	3.76	4.92		3.70	4.57
	4.58	5.04		3.62	4.61
	4.99	4.10		3.90	3.66

Appendix 15. Quantities of inorganic explosive measured for the dispersion onto the various textile fabrics (from top to bottom: white, blue, red, black, and green cotton; blue, black, white 1, and white 2 polyester; wool, jeans 1, jeans 2, polyskin, latex, nitrile 1, and nitrile 2) between 5 –10 mg.

Inorganic Explosives	Quantity (mg)		Inorganic Explosives	Quantity (mg)	
Black Powder	11.69	8.58	Flash Powder	8.11	8.51
	8.97	10.41		7.64	7.86
	8.85	9.24		7.77	7.55
	8.98	10.55		8.05	8.34
	9.68	9.34		7.78	7.35
	8.90	9.37		8.16	8.83
	8.24	9.52		7.91	8.93
	10.35	9.15		8.84	8.50
Chloratite	10.76	9.76	Ammonal (AlAN)	8.96	8.13
	8.26	10.30		11.99	8.34
	9.22	9.78		9.71	7.82
	8.33	10.51		10.00	8.68
	11.46	10.55		9.63	9.53
	8.28	9.58		9.42	8.01
	8.41	11.07		10.68	8.52
	8.49	11.90		8.87	8.44

Appendix 16. Quantities of the potassium nitrate and the interfering substances measured for the preparation of the solid mixtures (standard percentages: 70% of potassium nitrate and 30% of interfering substances of a total of 100 mg).

Interfering substances	Quantity (g)	Quantity (g)	Oxidizing salt
Charcoal	0.03280 (31.2%)	0.07224 (68.8%)	Potassium nitrate (KNO_3)
Aluminium powder	0.03478 (31.8%)	0.07445 (68.2%)	
Brown sugar	0.03255 (30.9%)	0.07288 (69.1%)	
White normal sugar	0.03259 (30.8%)	0.07313 (69.2%)	
Powdered sugar	0.03172 (30.5%)	0.07245 (69.5%)	
Chocolate cocoa powder "Brand 1"	0.03549 (31.9%)	0.07582 (68.1%)	
Chocolate cocoa powder "Brand 2"	0.03056 (30.3%)	0.07033 (69.7%)	
Wheat flour	0.03024 (30%)	0.07059 (70%)	
Corn starch	0.03087 (30.5%)	0.07037 (69.5%)	
Talc powder	0.03043 (30%)	0.07027 (70%)	

Appendix 17. Quantities of the solid mixtures inside the appropriate recipient for safe storage.

Solid mixtures	Quantity of the mixture inside the recipient (g)	Total quantity of the mixture (g)
PN + charcoal	recipient without mixture 20.72646 recipient with mixture 20.82258	0.09612
PN + aluminium powder	recipient without mixture 21.01052 recipient with mixture 21.11099	0.10047
PN + Brown sugar	recipient without mixture 20.32336 recipient with mixture 20.42254	0.09918
PN + white normal sugar	recipient without mixture 20.87618 recipient with mixture 20.97672	0.10054
PN + powdered sugar	recipient without mixture 20.81066 recipient with mixture 20.90999	0.09933
PN + chocolate "Brand 1"	recipient without mixture 21.30514 recipient with mixture 21.40701	0.10187
PN + chocolate "Brand 2"	recipient without mixture 20.81818 recipient with mixture 20.91531	0.09713
PN + wheat flour	recipient without mixture 21.34548 recipient with mixture 21.44276	0.09728
PN + Corn starch	recipient without mixture 20.69083 recipient with mixture 20.78616	0.09533
PN + talc powder	recipient without mixture 20.69400 recipient with mixture 20.78565	0.09165

Appendix 18. Quantities measured for the dispersion onto red cotton fibres between 15 – 20 mg.

Solid mixtures	Quantity (mg)
PN + charcoal	15.28
PN + aluminium powder	15.02
PN + brown sugar	15.22
PN + white normal sugar	14.99
PN + powdered sugar	15.56
PN + chocolate "Brand 1"	15.07
PN + chocolate "Brand 2"	15.17
PN + wheat flour	15.63
PN + Corn starch	15.20
PN + talc powder	15.16

Appendix 19. Wavenumbers and vibrational assignments of the main Raman bands from the spectra of the oxidizing salts; A – Thermo Scientific DXR Raman microscope; B – Portable BWTEK i-Raman pro.

Oxidizing salts	Raman shift (cm^{-1}) A	Raman shift (cm^{-1}) B	Vibrational assignments	References
Ammonium nitrate (NH_4NO_3)	1045 717	1043 714	NO_3 sym str NO_3 ip def	[56, 57, 90, 91]
Barium nitrate ($Ba(NO_3)_2$)	1049 734	1049 733	NO_3 sym str NO_3 ip def	[92, 93]
Sodium nitrate ($NaNO_3$)	1386 1068 724	1387 1069 725	NO_3 degenerate str NO_3 sym str NO_3 ip def	[93]
Potassium nitrate (KNO_3)	1050 715	1050 715	NO_3 sym str NO_3 ip def	[57, 91]
Sodium chlorate ($NaClO_3$)	988 936 624 484	988 936 624 482	ClO_3 asym str ClO_3 sym str ClO_3 sym def ClO_3 asym def	[57, 93]
Potassium chlorate ($KClO_3$)	977 940 620 488	978 939 619 488	ClO_3 asym str ClO_3 sym str ClO_3 sym det ClO_3 asym def	[57, 93]
Potassium perchlorate ($KClO_4$)	1124 1087 941 629 463	1124 1088 942 629 464	ClO_4 asym str ClO_4 asym str ClO_4 sym str ClO_4 asym bend ClO_4 sym bend	[91]

*asym, antisymmetric; bend, bending; def, deformation; ip, in-plane; oop, out-of-plane; rock, rocking; scis, scissoring; str, stretching; sym, symmetric; twist, twisting; wag, wagging.

Appendix 20. Wavenumbers and vibrational assignments of the main Raman bands from the spectra of the organic explosives; A – Thermo Scientific DXR Raman microscope; B – Portable BWTEK i-Raman pro.

Organic explosives	Raman shift (cm^{-1}) A	Raman shift (cm^{-1}) B	Vibrational assignments	References
TNT ($C_7H_5N_3O_6$)	1619	1617	C-C aromatic str or 2,6-NO_2 asym str	[55-57, 60, 71]
	1535	1534	NO_2 asym str	
	1361	1358	NO_2 sym str	
	1212	1210	Ring breathing or C_6H_2-C vibration	
	1088	1088	C-H ip bend	
	941	939	C-N str or C-H oop bend	
	824	822	NO_2 scis	
	794	792	C-CH_3 str, NO_2 scis or C-H oop bend	
	640	-	C-C ring bend	
	368	367	CH_3 def	
	328	326	2,4,6 C-N ip torsion	
HMTD ($C_6H_{12}N_2O_6$)	1441	1439	CH_2 scis	[57]
	1399	1398	CH_2 wag	
	1341	1341	CH_2 twist	
	1235	1236	C-N str	
	950	949	C-O str	
	773	771	O-O str	
	584	582	Ring str	
	414	413	NCO def	
	298	297	CN bend or O-O torsion	
PETN ($C_5H_8N_4O_{12}$)	1661	1659	NO_2 asym str	[55-57, 60, 75]
	1470	1468	NO_2 asym str or CH_2 scis	
	1403	1402	CH_2 wag or C-C str	
	1293	1291	NO_2 sym str or CH_2 wag	
	1252	1251	C-H bend	
	1043	1042	CH_2 torsion or C-C bend	
	873	872	O(ester)-N sym str or C-C str	
	677	675	O(ester)-N str, C-C str or NO_2 scis	
	623	622	C-C-C def or ONO_2 rock	
	590	588	ONO_2 rock or C-C bend	
	460	458	C-C-C def, O(ester)-N str or NO_2 rock	
RDX ($C_3H_6N_6O_6$)	1595	1594	NO_2 asym str	[57, 71, 72]
	1436	1435	H-C-N bend	
	1311	1310	CH_2 wag, CH_2 twist or N-N str	
	1274	1273	CH_2 scis or N-N str	
	1217	1216	CH_2 rock	
	945	943	C-N str, CH_2 rock or N-N str	
	886	884	C-N str or N-N str	
	849	847	N-N str or NO_2 scis	
	607	604	O-C-O str	
	464	462	Ip ring bend	

*asym, antisymmetric; bend, bending; def, deformation; ip, in-plane; oop, out-of-plane; rock, rocking; scis, scissoring; str, stretching; sym, symmetric; twist, twisting; wag, wagging.

Appendix 21. Wavenumbers and vibrational assignments of the main Raman bands from the spectra of the inorganic explosives; A – Thermo Scientific DXR Raman microscope; B – Portable BWTEK i-Raman pro.

Inorganic explosives	Raman shift (cm^{-1}) A	Raman shift (cm^{-1}) B	Vibrational assignments	References
Ammonal (NH_4NO_3)	1043	1043	NO_3 sym str	[56, 57, 90, 91]
	714	714	NO_3 ip def	
Black powder (KNO_3)	1578	-	Fluorescence from charcoal	[57, 90, 91]
	1343	-	Fluorescence from charcoal	
	1050	1050	NO_3 sym str	
	715	715	NO_3 ip def	
Chloratite ($NaClO_3$)	989	987	ClO_3 asym str	[57]
	937	936	ClO_3 sym str	
	625	623	ClO_3 sym det	
	484	472	ClO_3 asym def	
Flash powder ($KClO_4$)	1123	-	ClO_4 asym str	[91]
	1086	-	ClO_4 asym str	
	940	936	ClO_4 sym str	
	632	629	ClO_4 asym bend	
	462	462	ClO_4 sym bend	

*asym, antisymmetric; bend, bending; def, deformation; ip, in-plane; oop, out-of-plane; rock, rocking; scis, scissoring; str, stretching; sym, symmetric; twist, twisting; wag, wagging.

Appendix 22. Reference Raman spectra of (a) ammonium nitrate (b) barium nitrate (c) sodium nitrate (d) potassium nitrate (e) sodium chlorate (f) potassium chlorate (g) potassium perchlorate (Portable BW&TEK i-Raman Pro 785 nm, 20% of 320 mW, 0.3 s exposure, 10 accumulations).

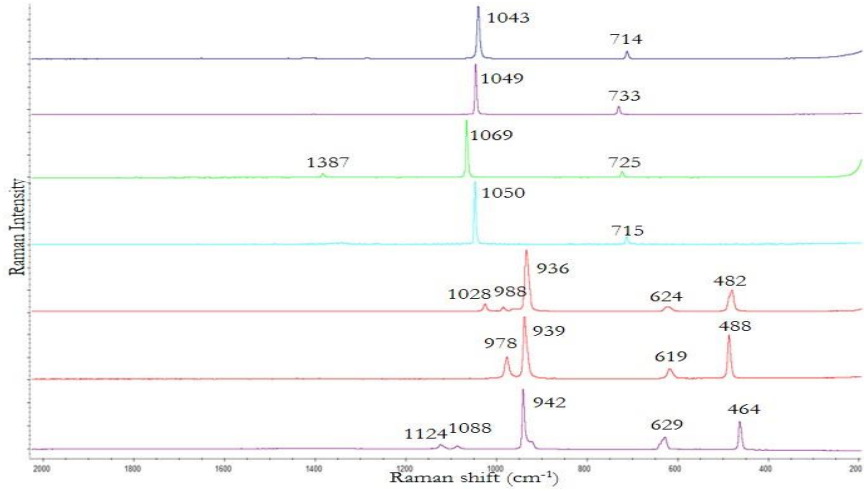

Appendix 23. Reference Raman spectra of (a) ammonal (AlAN) (b) black powder (c) chloratite (d) flash powder (Portable BW&TEK i-Raman Pro 785 nm, % of 320 mW, s exposure, accumulations).

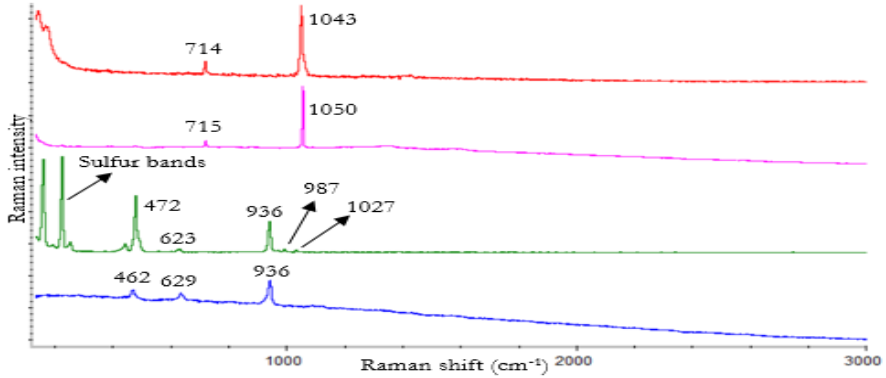

Appendix 24. Reference Raman spectra of (a) (b) (c) (d) (Portable BW&TEK i-Raman Pro 785 nm, % of 320 mW, s exposure, accumulations).

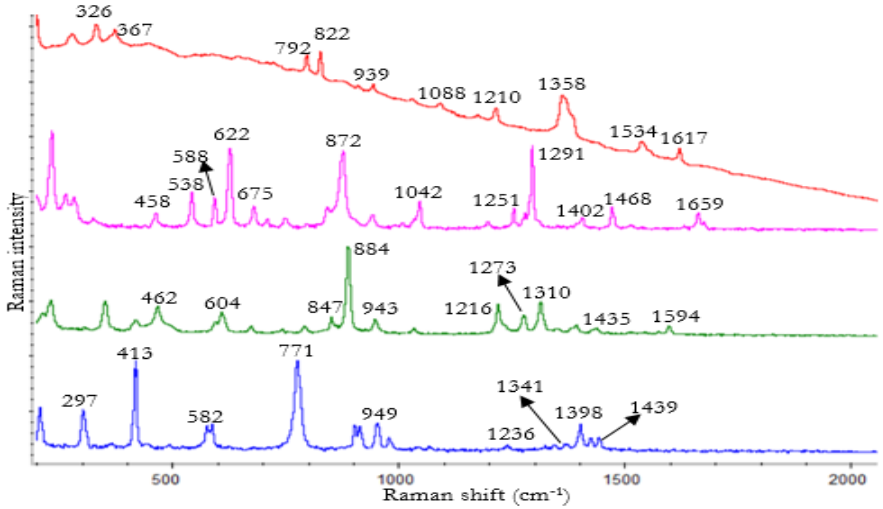

Appendix 25. Raman spectra of the chloratite components (a) sodium chlorate particle in chloratite (b) sulfur particle in chloratite (c) sugar particle in chloratite (d) sugar standard (Thermo scientific DXR Raman microscope 780 nm, 10 mW, 6 s exposure, 5 accumulations).

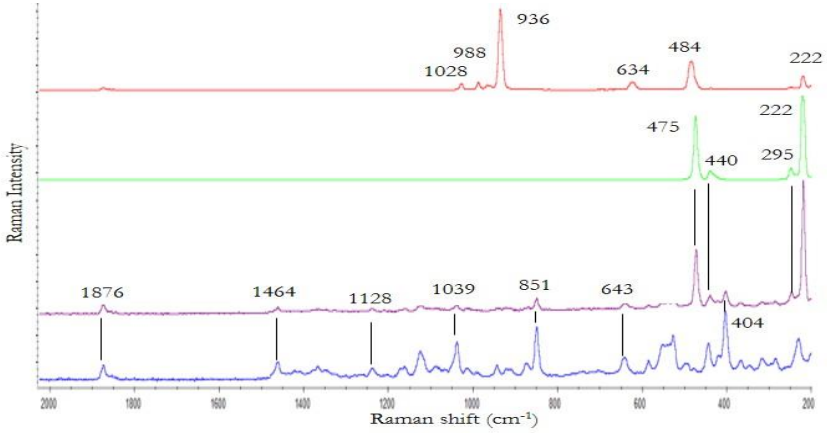

Appendix 26. Raman spectra of sulfur contained in the composition of black powder (Thermo scientific DXR Raman microscope 780 nm, 1 mW, 6 s exposure, 5 accumulations).

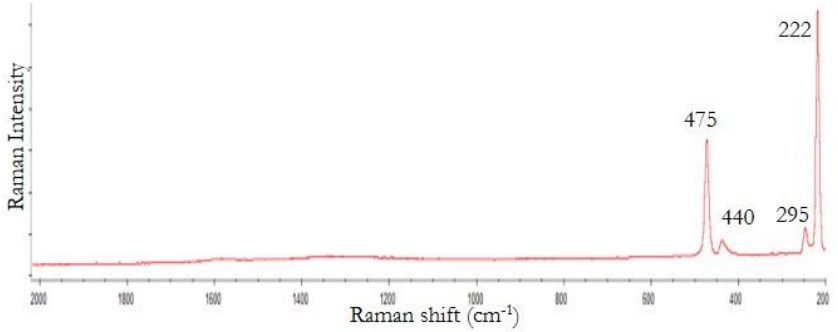

Appendix 27. Raman spectra of (a) ammonium nitrate (b) barium nitrate (c) potassium nitrate (d) sodium nitrate (e) potassium chlorate (f) sodium chlorate (g) potassium perchlorate particles on white cotton fibres (h) white cotton fibres (asterisks indicate white cotton bands) (Portable BWTEK i-Raman Pro, 785 nm, 20% of 320 mW, 0.3 s exposure, 10 accumulations).

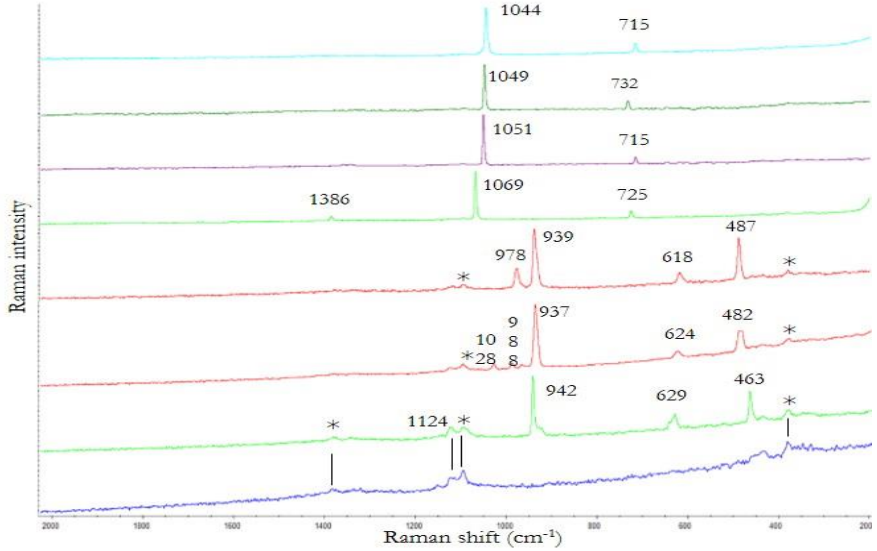

Appendix 28. Raman spectra of (a) TNT (b) PETN (c) RDX (d) HMTD particles on white cotton fibres (e) white cotton fibres (asterisks indicate white cotton bands) (Portable BWTEK i-Raman Pro, 785 nm, 5% of 320 mW, 3 s exposure, 5 accumulations).

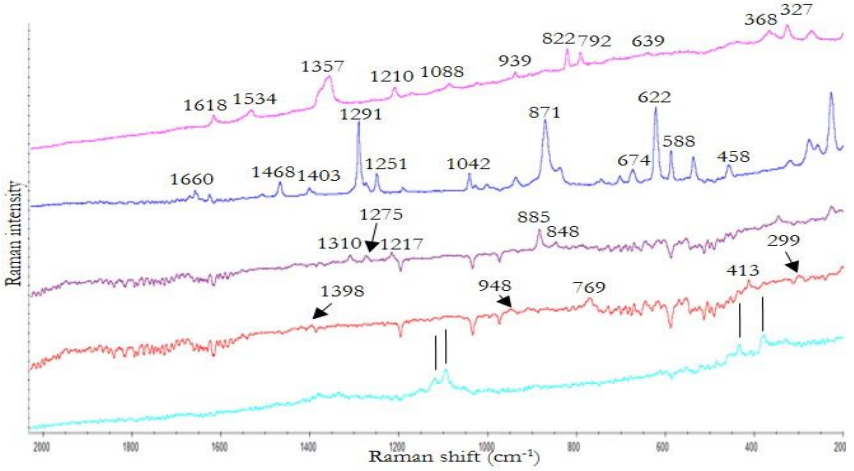

Appendix 29. Raman spectra of (a) ammonal (b) black powder (c) chloratite (d) flash powder particles on white cotton fibres (e) white cotton fibres (asterisks indicate white cotton bands) (Portable BWTEK i-Raman Pro, 785 nm, 1% of 320 mW, 1 s exposure, 10 accumulations).

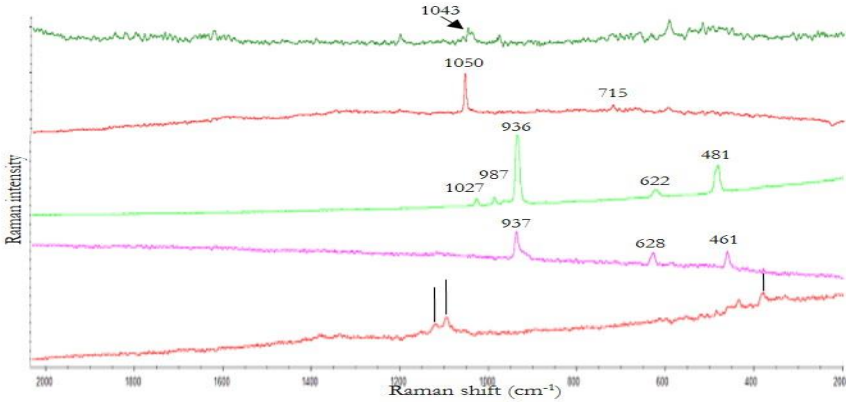

Appendix 30. Raman spectra of (a) ammonium nitrate (b) barium nitrate (c) potassium nitrate (d) sodium nitrate (e) potassium chlorate (f) sodium chlorate (g) potassium perchlorate particles on white polyester B fibres (h) white polyester B fibres (asterisks indicate white polyester B bands) (Portable BWTEK i-Raman Pro, 785 nm, 20% of 320 mW, 0.3 s exposure, 10 accumulations).

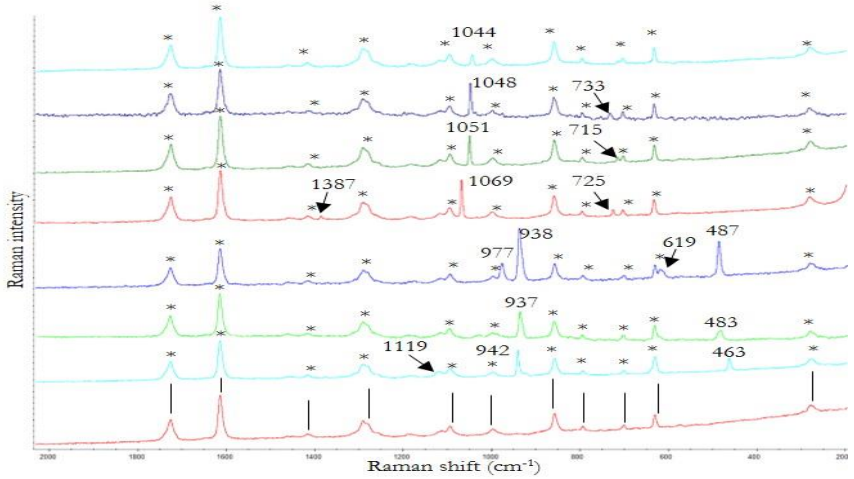

Appendix 31. Raman spectra of (a) TNT (b) PETN (c) RDX (d) HMTD particles on white polyester B fibres (e) white polyester B fibres (asterisks indicate white polyester B bands) (Portable BWTEK i-Raman Pro, 785 nm, 5% of 320 mW, 3 s exposure, 5 accumulations).

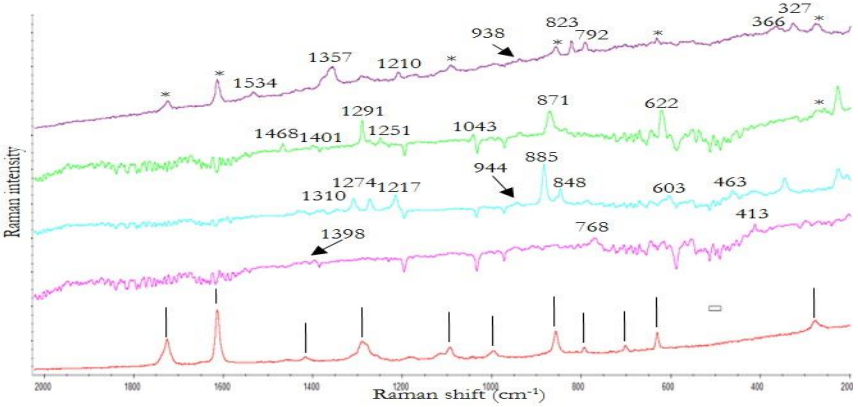

Appendix 32. Raman spectra of (a) ammonal (b) black powder (c) chloratite (d) flash powder particles on white polyester B fibres (e) white polyester B fibres (asterisks indicate white polyester B bands) (Portable BWTEK i-Raman Pro, 785 nm, 1% of 320 mW, 1 s exposure, 10 accumulations).

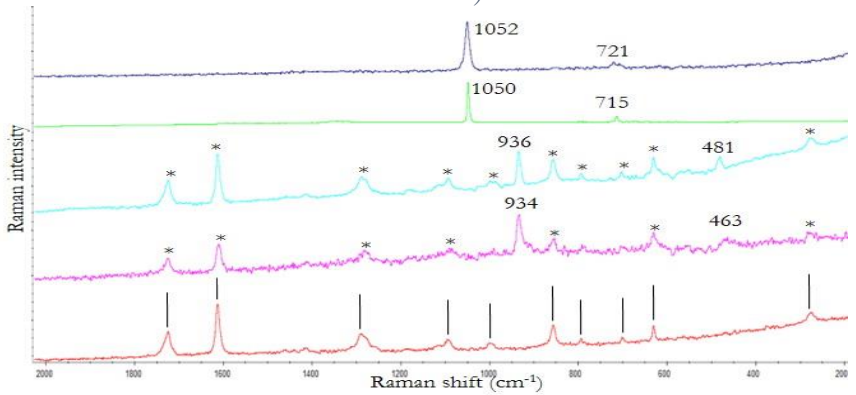

Appendix 33. Raman spectra of (a) ammonium nitrate (b) barium nitrate (c) potassium nitrate (d) sodium nitrate (e) potassium chlorate (f) sodium chlorate (g) potassium perchlorate particles on white polyester A fibres (h) white polyester A fibres (asterisks indicate white polyester A bands) (Thermo Scientific DXR Raman microscope, 780 nm, 14 mW, 5 s exposure, 8 accumulations).

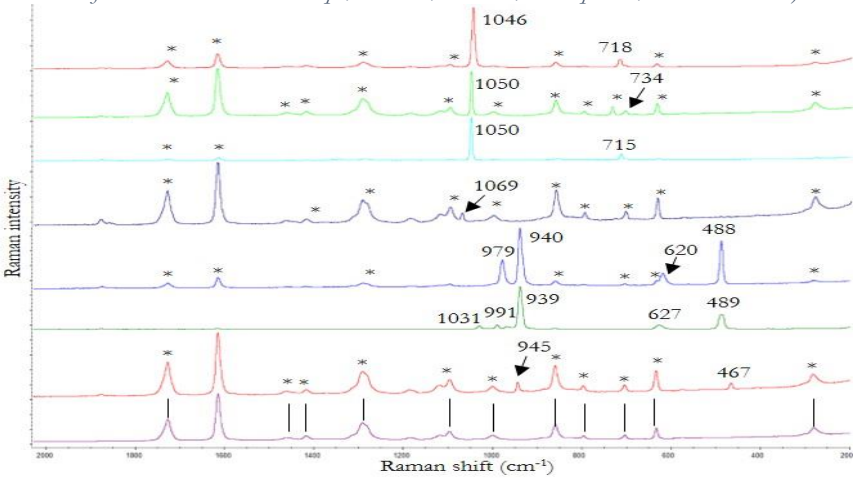

Appendix 34. Raman spectra of (a) TNT (b) PETN (c) RDX (d) HMTD particles on white polyester A fibres (e) white polyester A fibres (asterisks indicate white polyester A bands) (Thermo Scientific DXR Raman microscope, 780 nm, 10 mW, 6 s exposure, 5 accumulations).

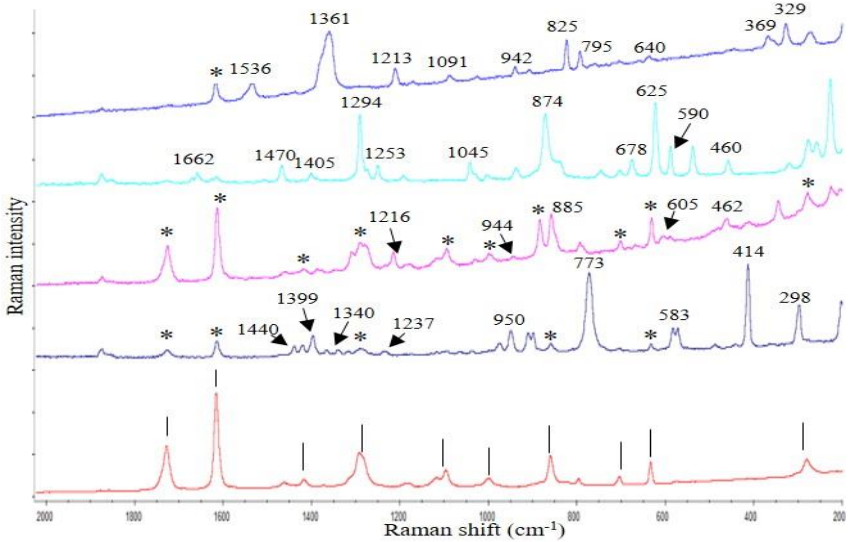

Appendix 35. Raman spectra of (a) ammonal (b) black powder (c) chloratite (d) flash powder particles on white polyester A fibres (e) white polyester A fibres (asterisks indicate white polyester A bands) (Thermo Scientific DXR Raman microscope, 780 nm, 10 mW, 6 s exposure, 5 accumulations).

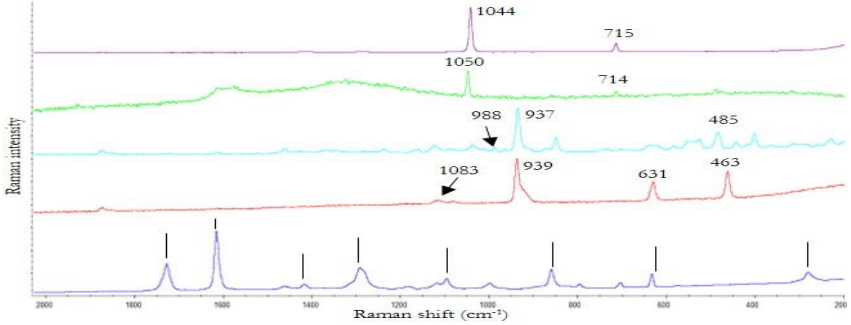

Appendix 36. Raman spectra of (a) ammonium nitrate (b) barium nitrate (c) potassium nitrate (d) sodium nitrate (e) potassium chlorate (f) sodium chlorate (g) potassium perchlorate particles on white polyester A fibres (h) white polyester A fibres (asterisks indicate white polyester A bands) (Portable BWTEK i-Raman Pro, 785 nm, 20% of 320 mW, 0.3 s exposure, 10 accumulations).

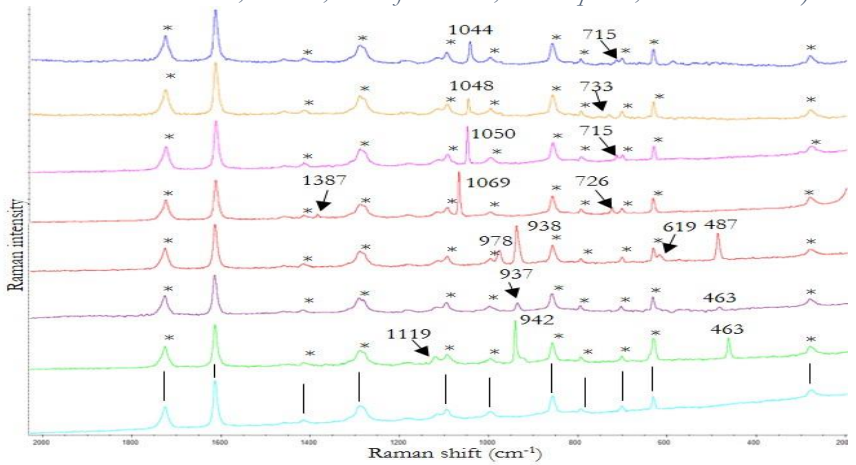

Appendix 37. Raman spectra of (a) TNT (b) PETN (c) RDX (d) HMTD particles on white polyester A fibres (e) white polyester A fibres (asterisks indicate white polyester A bands) (Portable BWTEK i-Raman Pro, 785 nm, 5% of 320 mW, 3 s exposure, 5 accumulations).

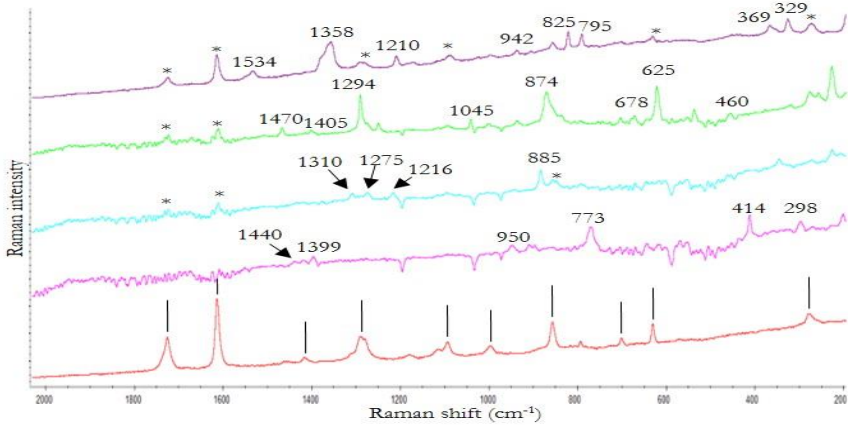

Appendix 38. Raman spectra of (a) ammonal (b) black powder (c) chloratite (d) flash powder particles on white polyester A fibres (e) white polyester A fibres (asterisks indicate white polyester A bands) (Portable BWTEK i-Raman Pro, 785 nm, 1% of 320 mW, 1 s exposure, 10 accumulations).

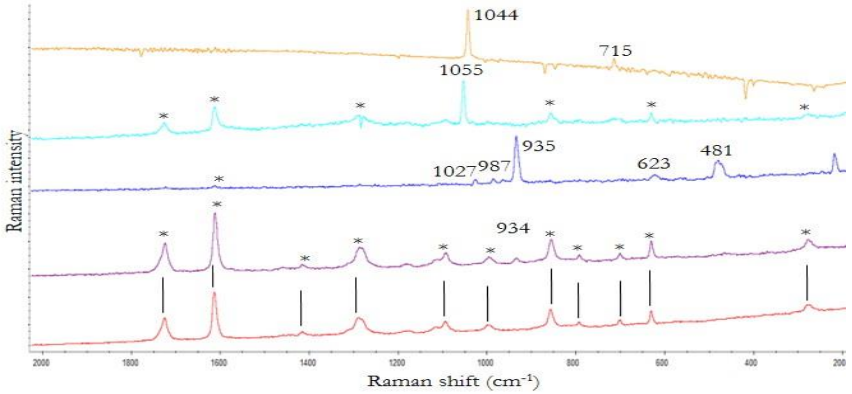

Appendix 39. Raman spectra of (a) ammonium nitrate (b) barium nitrate (c) potassium nitrate (d) sodium nitrate (e) potassium chlorate (f) sodium chlorate (g) potassium perchlorate particles on blue cotton fibres (h) blue cotton fibres (asterisks indicate blue cotton bands) (Portable BWTEK i-Raman Pro, 785 nm, 1% of 320 mW, 0.3 s exposure, 10 accumulations).

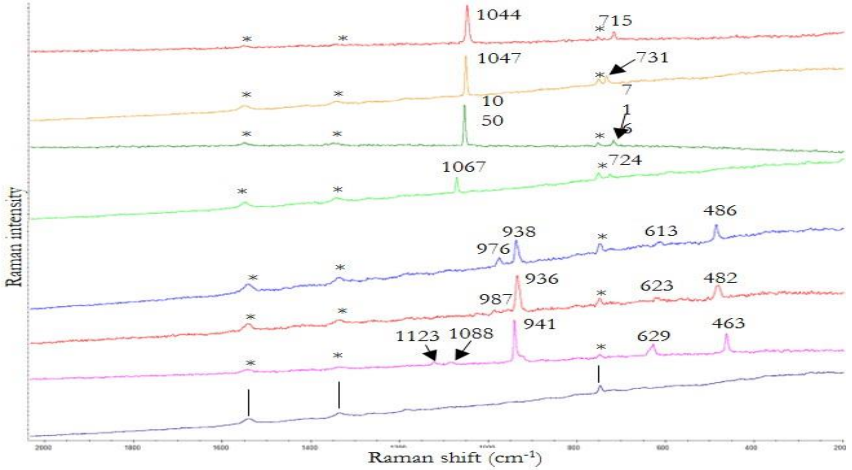

Appendix 40. Raman spectra of (a) TNT (b) PETN (c) RDX (d) HMTD particles on blue cotton fibres (e) blue cotton fibres (asterisks indicate blue cotton bands) (Portable BWTEK i-Raman Pro, 785 nm, 1% of 320 mW, 3 s exposure, 5 accumulations).

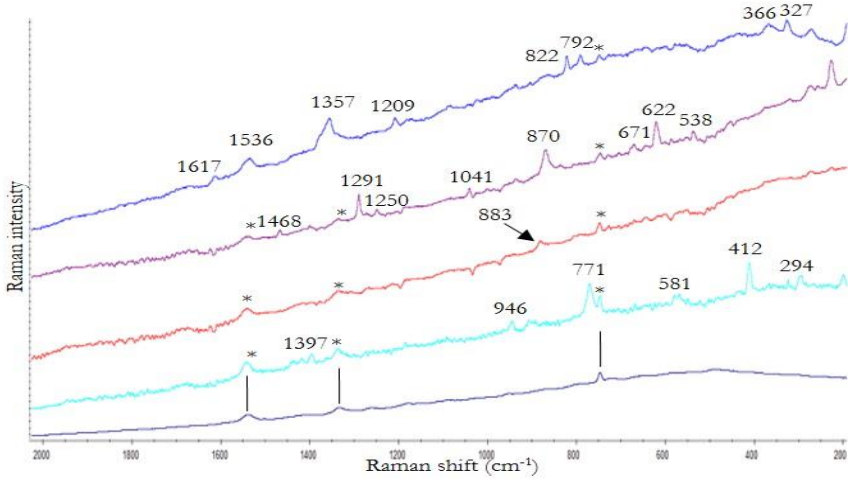

Appendix 41. Raman spectra of (a) ammonal (b) black powder (c) chloratite (d) flash powder particles on blue cotton fibres (e) blue cotton fibres (asterisks indicate blue cotton bands) (Portable BWTEK i-Raman Pro, 785 nm, 1% of 320 mW, 1 s exposure, 10 accumulations).

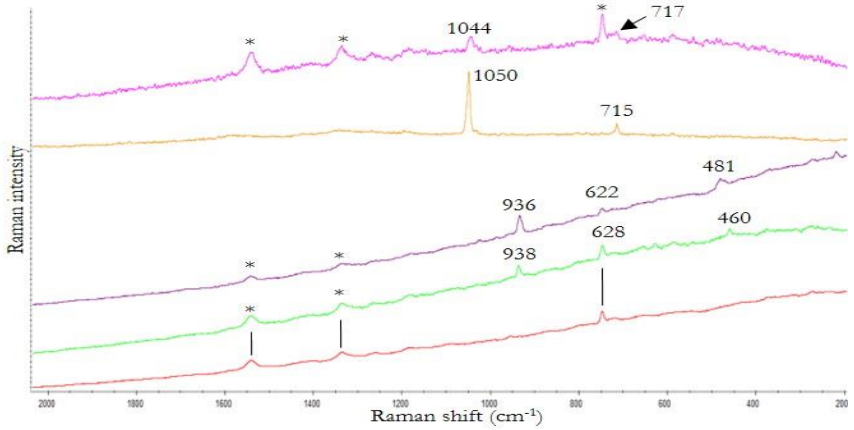

Appendix 42. Raman spectra of (a) ammonium nitrate (b) barium nitrate (c) potassium nitrate (d) sodium nitrate (e) potassium chlorate (f) sodium chlorate (g) potassium perchlorate particles on red cotton fibres (h) red cotton fibres (asterisks indicate red cotton bands) (Thermo Scientific DXR Raman microscope, 780 nm, 14 mW, 5 s exposure, 8 accumulations).

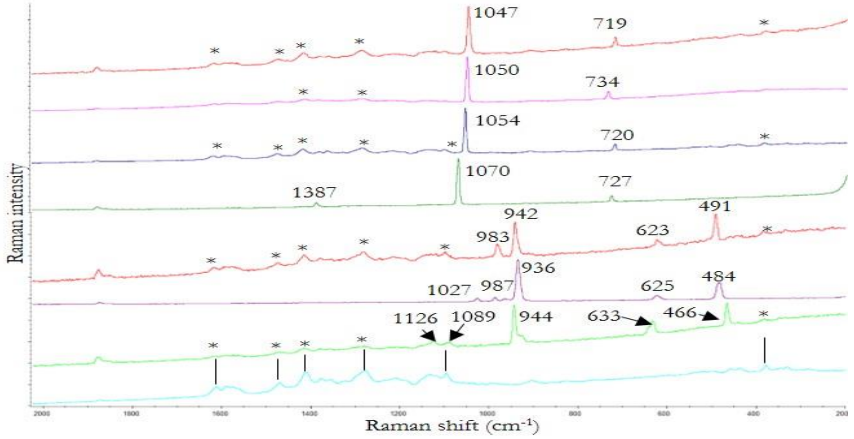

Appendix 43. Raman spectra of (a) ammonium nitrate (b) barium nitrate (c) potassium nitrate (d) sodium nitrate (e) potassium chlorate (f) sodium chlorate (g) potassium perchlorate particles on red cotton fibres (h) red cotton fibres (asterisks indicate red cotton bands) (Portable BWTEK i-Raman Pro, 785 nm, 20% of 320 mW, 0.3 s exposure, 10 accumulations).

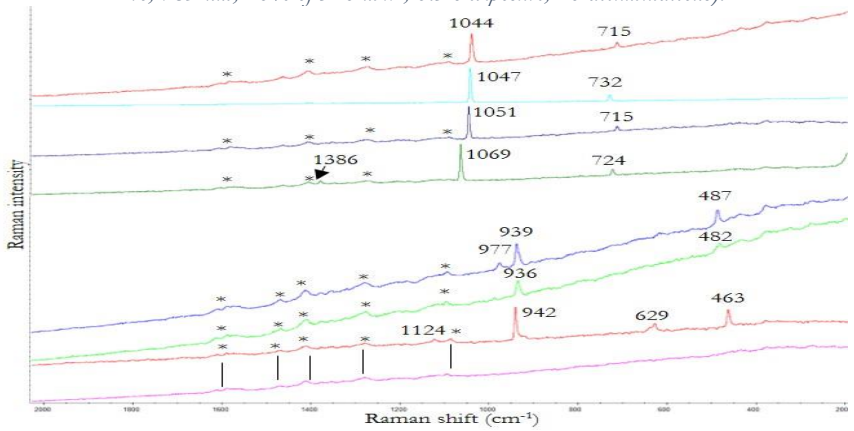

Appendix 44. Raman spectra of (a) TNT (b) PETN (c) RDX (d) HMTD particles on red cotton fibres (e) red cotton fibres (asterisks indicate red cotton bands) (Thermo Scientific DXR Raman microscope, 780 nm, 10 mW, 6 s exposure, 5 accumulations).

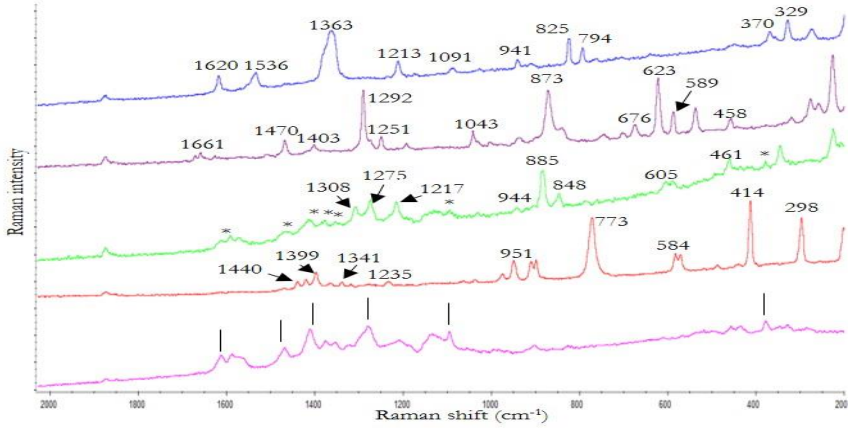

Appendix 45. Raman spectra of (a) TNT (b) PETN (c) RDX (d) HMTD particles on red cotton fibres (e) red cotton fibres (asterisks indicate red cotton bands) (Portable BWTEK i-Raman Pro, 785 nm, 5% of 320 mW, 3 s exposure, 5 accumulations).

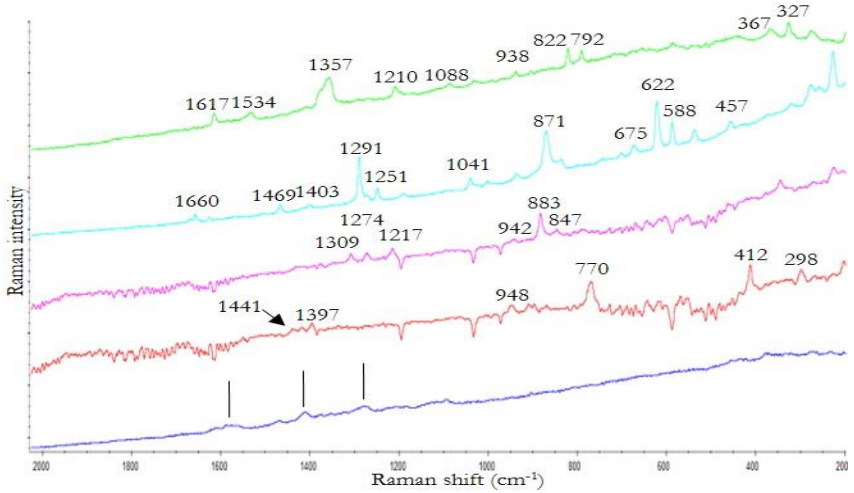

Appendix 46. Raman spectra of (a) ammonal (b) black powder (c) chloratite (d) flash powder particles on red cotton fibres (e) red cotton fibres (asterisks indicate red cotton bands) (Thermo Scientific DXR Raman microscope, 780 nm, 10 mW, 6 s exposure, 5 accumulations).

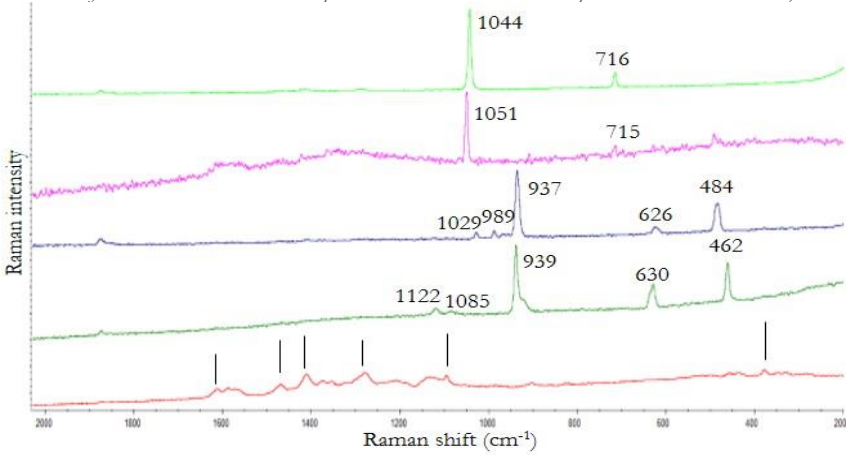

Appendix 47. Raman spectra of (a) ammonal (b) black powder (c) chloratite (d) flash powder particles on red cotton fibres (e) red cotton fibres (asterisks indicate red cotton bands) (Portable BWTEK i-Raman Pro, 785 nm, 1% of 320 mW, 1 s exposure, 10 accumulations).

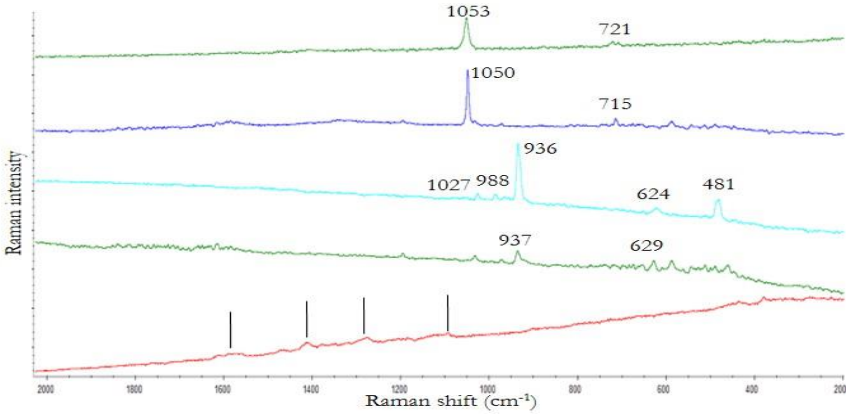

Appendix 48. Raman spectra of (a) ammonium nitrate (b) barium nitrate (c) potassium nitrate (d) sodium nitrate (e) potassium chlorate (f) sodium chlorate (g) potassium perchlorate particles on green cotton fibres (h) green cotton fibres (asterisks indicate green cotton bands) (Thermo Scientific DXR Raman microscope, 780 nm, 14 mW, 5 s exposure, 8 accumulations).

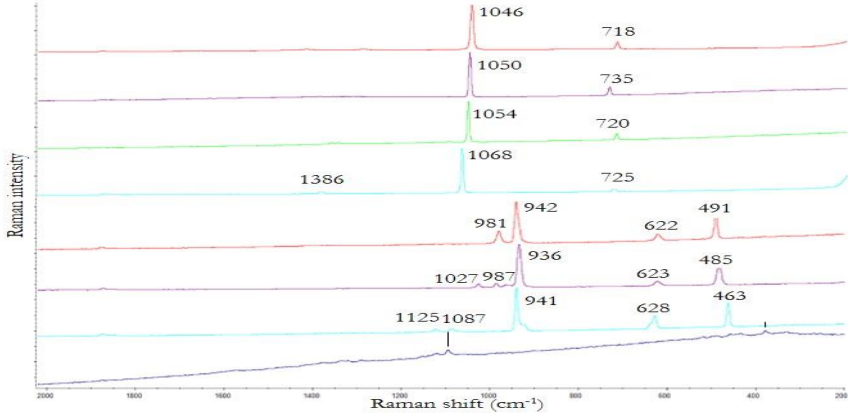

Appendix 49. Raman spectra of (a) ammonium nitrate (b) barium nitrate (c) potassium nitrate (d) sodium nitrate (e) potassium chlorate (f) sodium chlorate (g) potassium perchlorate particles on green cotton fibres (h) green cotton fibres (asterisks indicate green cotton bands) (Portable BWTEK i-Raman Pro, 785 nm, 20% of 320 mW, 0.3 s exposure, 10 accumulations).

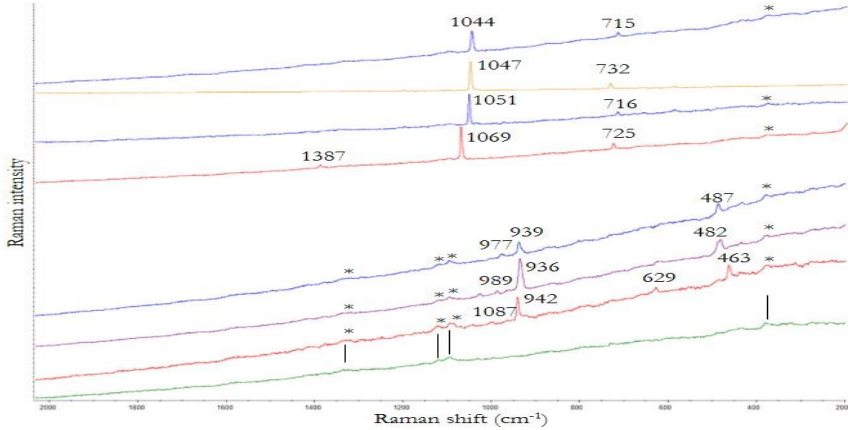

Appendix 50. Raman spectra of (a) TNT (b) PETN (c) RDX (d) HMTD particles on green cotton fibres (e) greeen cotton fibres (asterisks indicate green cotton bands) (Thermo Scientific DXR Raman microscope, 780 nm, 10 mW, 6 s exposure, 5 accumulations).

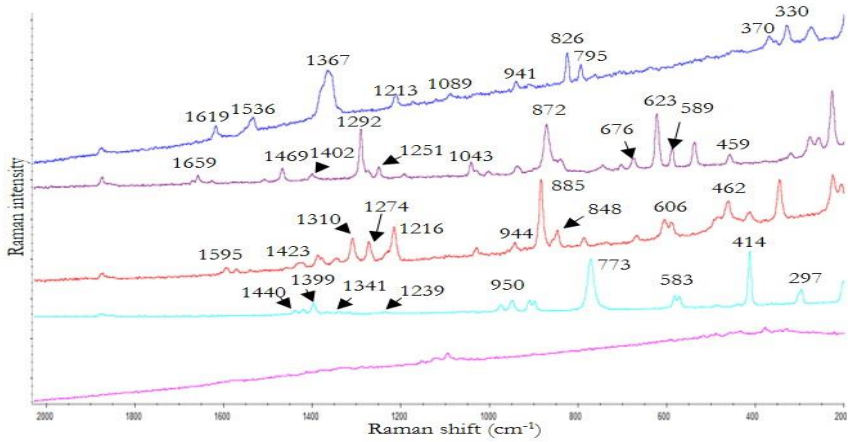

Appendix 51. Raman spectra of (a) TNT (b) PETN (c) RDX (d) HMTD particles on green cotton fibres (e) green cotton fibres (asterisks indicate green cotton bands) (Portable BWTEK i-Raman Pro, 785 nm, 5% of 320 mW, 3 s exposure, 5 accumulations).

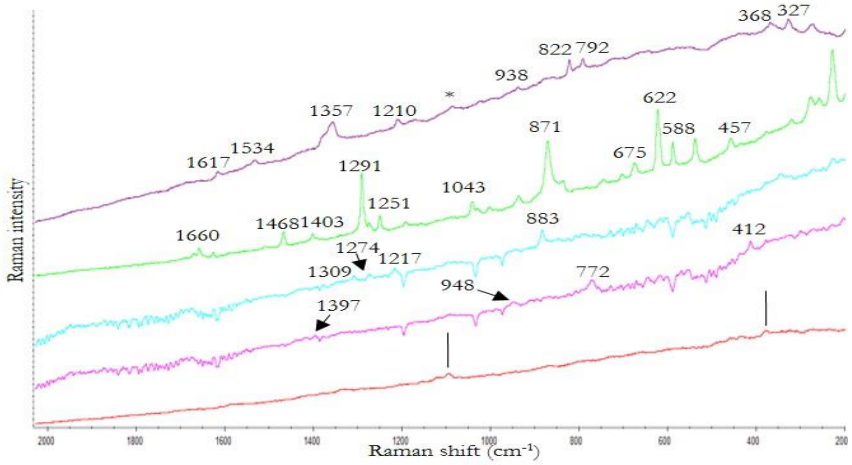

Appendix 52. Raman spectra of (a) ammonal (b) black powder (c) chloratite (d) flash powder particles on green cotton fibres (e) green cotton fibres (asterisks indicate green cotton bands) (Thermo Scientific DXR Raman microscope, 780 nm, 10 mW, 6 s exposure, 5 accumulations).

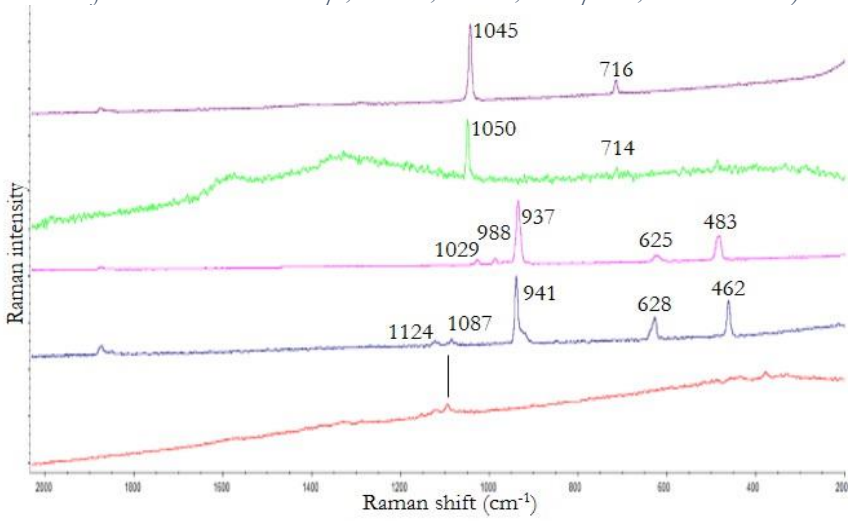

Appendix 53. Raman spectra of (a) ammonal (b) black powder (c) chloratite (d) flash powder particles on green cotton fibres (e) green cotton fibres (asterisks indicate green cotton bands) (Portable BWTEK i-Raman Pro, 785 nm, 1% of 320 mW, 1 s exposure, 10 accumulations).

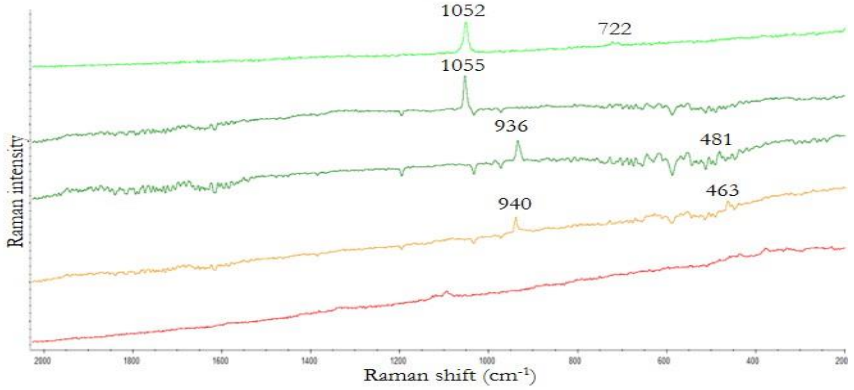

Appendix 54. Raman spectra of (a) ammonium nitrate (b) barium nitrate (c) potassium nitrate (d) sodium nitrate (e) potassium chlorate (f) sodium chlorate (g) potassium perchlorate particles on black cotton fibres (h) black cotton fibres (asterisks indicate black cotton bands) (Thermo Scientific DXR Raman microscope, 780 nm, 14 mW, 5 s exposure, 8 accumulations).

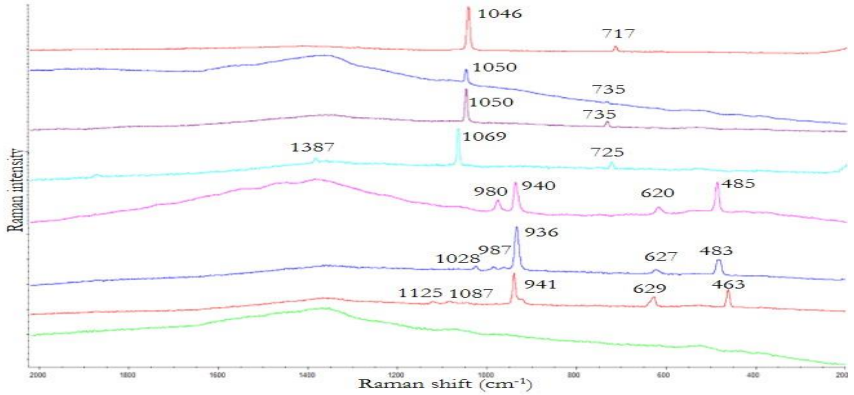

Appendix 55. Raman spectra of (a) ammonium nitrate (b) barium nitrate (c) potassium nitrate (d) sodium nitrate (e) potassium chlorate (f) sodium chlorate (g) potassium perchlorate particles on black cotton fibres (h) black cotton fibres (asterisks indicate black cotton bands) (Portable BWTEK i-Raman Pro, 785 nm, 1% of 320 mW, 0.3 s exposure, 10 accumulations).

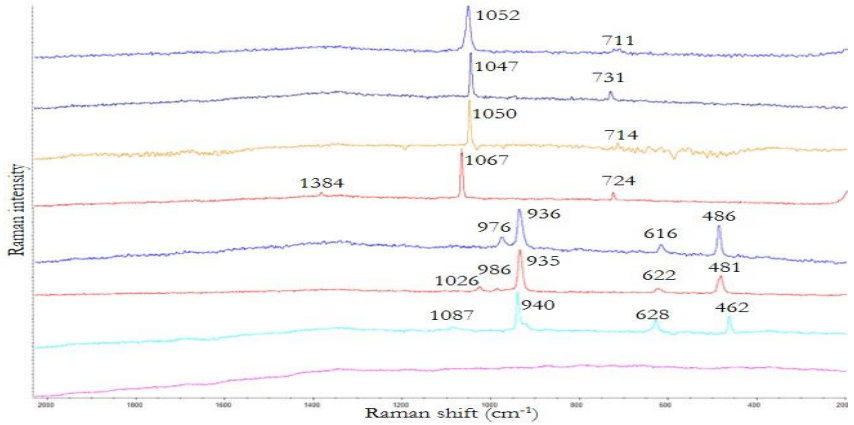

Appendix 56. Raman spectra of (a) TNT (b) PETN (c) RDX (d) HMTD particles on black cotton fibres (e) black cotton fibres (asterisks indicate black cotton bands) (Thermo Scientific DXR Raman microscope, 780 nm, 5 mW, 6 s exposure, 5 accumulations).

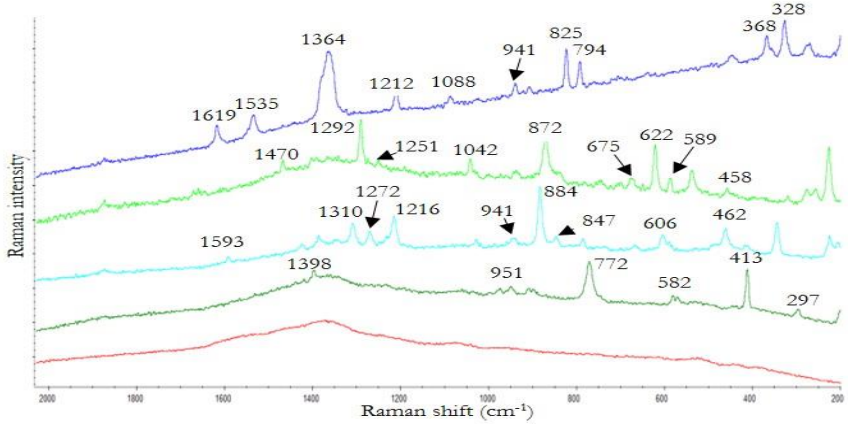

Appendix 57. Raman spectra of (a) TNT (b) PETN (c) RDX (d) HMTD particles on black cotton fibres (e) black cotton fibres (asterisks indicate black cotton bands) (Portable BWTEK i-Raman Pro, 785 nm, 1% of 320 mW, 3 s exposure, 5 accumulations).

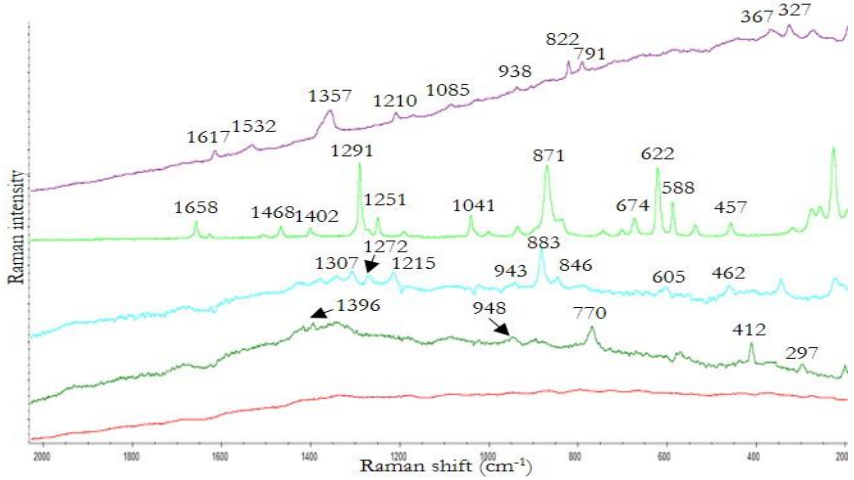

Appendix 58. Raman spectra of (a) ammonal (b) black powder (c) chloratite (d) flash powder particles on black cotton fibres (e) black cotton fibres (asterisks indicate black cotton bands) (Thermo Scientific DXR Raman microscope, 780 nm, 10 mW, 6 s exposure, 5 accumulations).

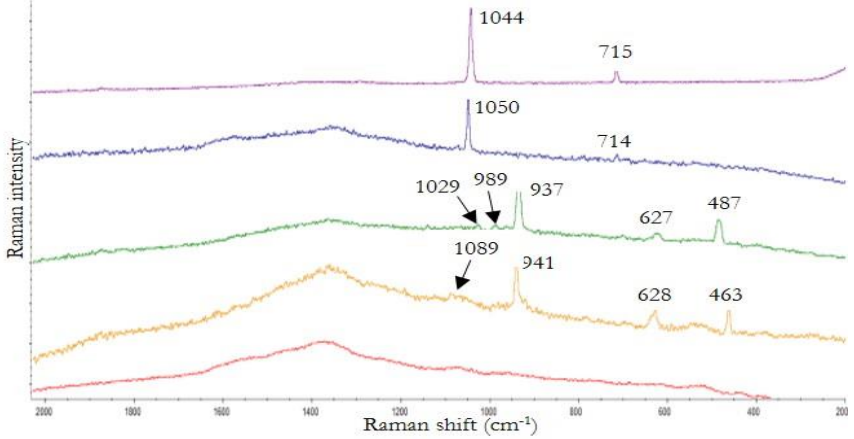

Appendix 59. Raman spectra of (a) ammonal (b) black powder (c) chloratite (d) flash powder particles on black cotton fibres (e) black cotton fibres (asterisks indicate black cotton bands) (Portable BWTEK i-Raman Pro, 785 nm, 1% of 320 mW, 1 s exposure, 10 accumulations).

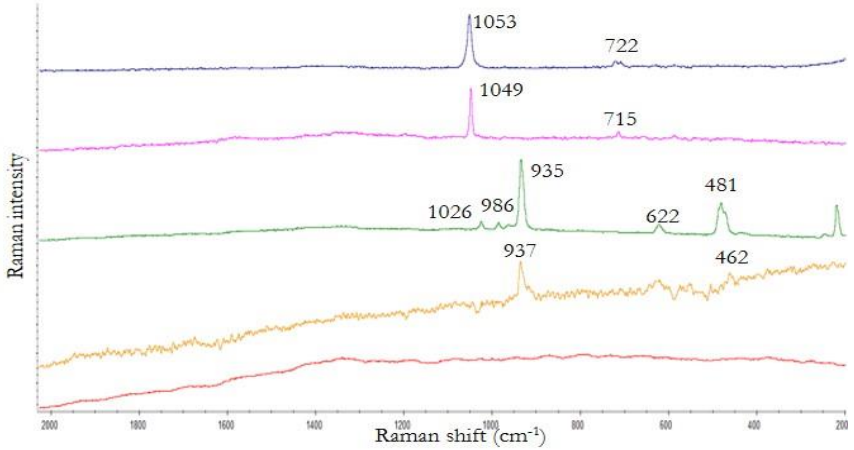

Appendix 60. Raman spectra of (a) ammonium nitrate (b) barium nitrate (c) potassium nitrate (d) sodium nitrate (e) potassium chlorate (f) sodium chlorate (g) potassium perchlorate particles on blue polyester fibres (h) blue polyester fibres (asterisks indicate blue polyester bands) (Portable BWTEK i-Raman Pro, 785 nm, 20% of 320 mW, 0.3 s exposure, 10 accumulations for (a-d), 1% of 320 mW for (h)).

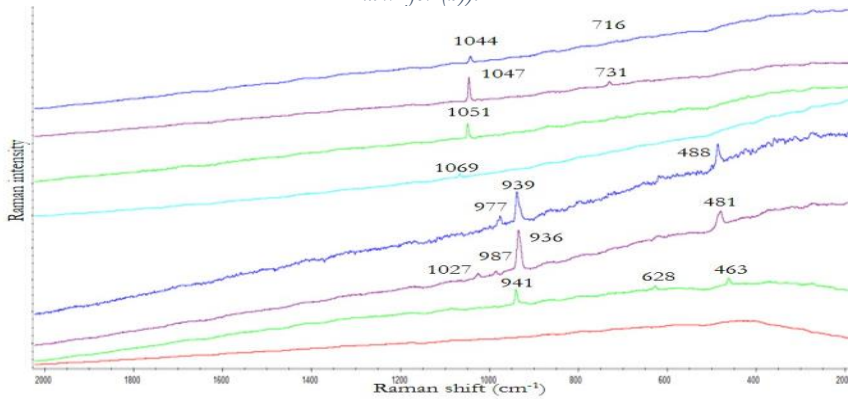

Appendix 61. Raman spectra of (a) TNT (b) PETN (c) RDX (d) HMTD particles on blue polyester fibres (e) blue polyester fibres (asterisks indicate blue polyester bands) (Portable BWTEK i-Raman Pro, 785 nm, 5% of 320 mW, 3 s exposure, 5 accumulations for (a-d), 1% of 320 mW, 0.3 s exposure, 10 accumulations for (e)).

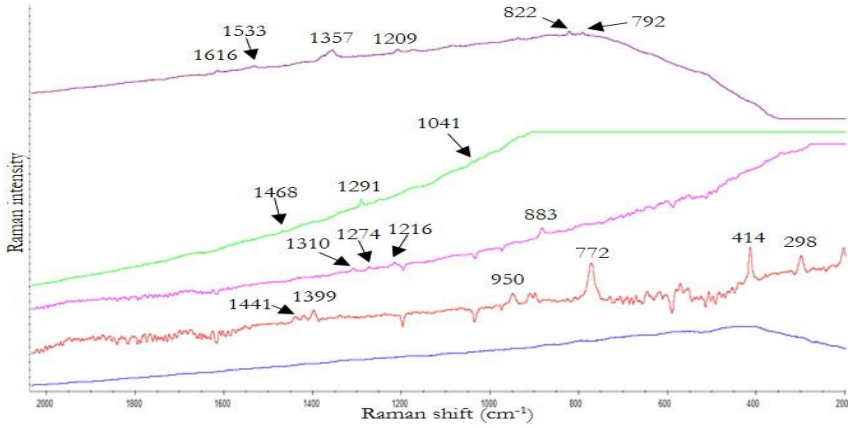

Appendix 62. Raman spectra of (a) ammonal (b) black powder (c) chloratite (d) flash powder particles on blue polyester fibres (e) blue polyester fibres (asterisks indicate blue polyester bands) (Portable BWTEK i-Raman Pro, 785 nm, 1% of 320 mW, 1 s exposure, 10 accumulations for (a-d), 0.3 s exposure for (e)).

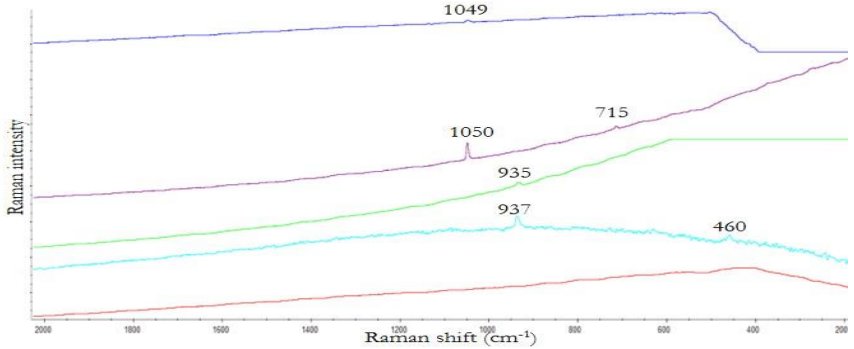

Appendix 63. Raman spectra of (a) ammonium nitrate (b) barium nitrate (c) potassium nitrate (d) sodium nitrate (e) potassium chlorate (f) sodium chlorate (g) potassium perchlorate particles on black polyester fibres (h) black polyester fibres (asterisks indicate black polyester bands) (Thermo Scientific DXR Raman microscope, 780 nm, 14 mW, 5 s exposure, 8 accumulations).

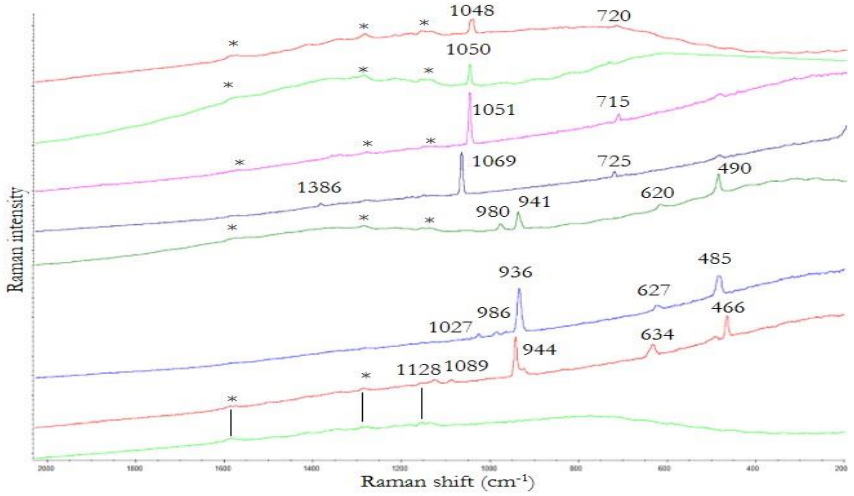

Appendix 64. Raman spectra of (a) ammonium nitrate (b) barium nitrate (c) potassium nitrate (d) sodium nitrate (e) potassium chlorate (f) sodium chlorate (g) potassium perchlorate particles on black polyester fibres (h) black polyester fibres (asterisks indicate black polyester bands) (Portable BWTEK i-Raman Pro, 785 nm, 20% of 320 mW, 0.3 s exposure, 10 accumulations for (a-d), 1% of 320 mW for (h)).

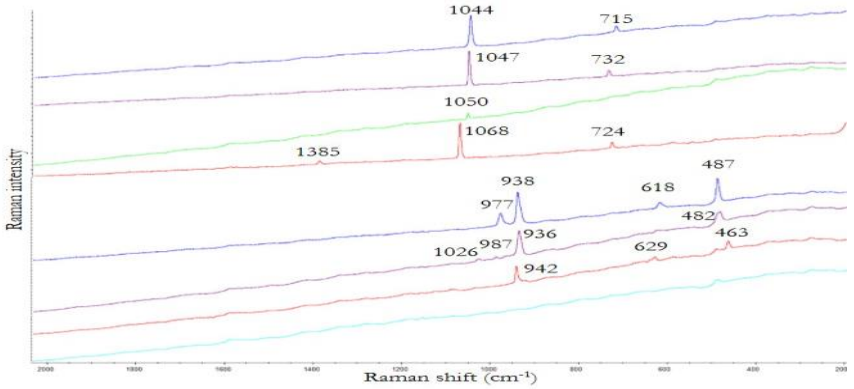

Appendix 65. Raman spectra of (a) TNT (b) PETN (c) RDX (d) HMTD particles on black polyester fibres (e) black polyester fibres (asterisks indicate black polyester bands) (Thermo Scientific DXR Raman microscope, 780 nm, 10 mW, 6 s exposure, 5 accumulations).

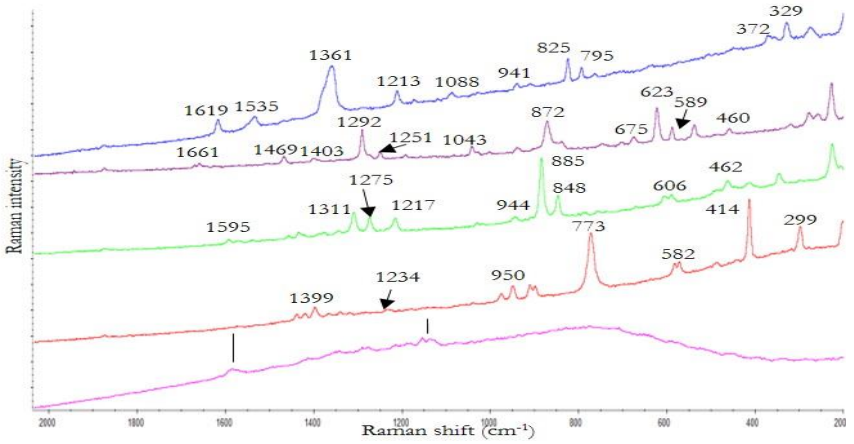

Appendix 66. Raman spectra of (a) TNT (b) PETN (c) RDX (d) HMTD particles on black polyester fibres (e) black polyester fibres (asterisks indicate black polyester bands) (Portable BWTEK i-Raman Pro, 785 nm, 5% of 320 mW, 3 s exposure, 5 accumulations for (a-d), 5% of 320 mW, 1 s exposure, 10 accumulations for (e)).

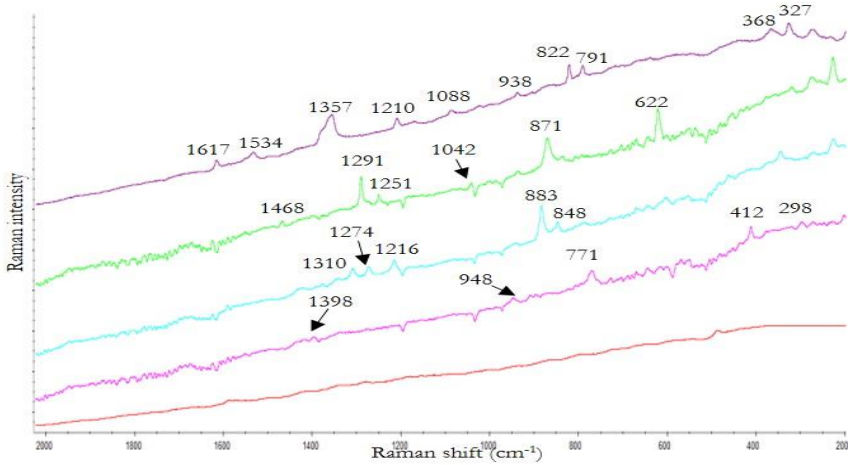

Appendix 67. Raman spectra of (a) ammonal (b) black powder (c) chloratite (d) flash powder particles on black polyester fibres (e) black polyester fibres (asterisks indicate black polyester bands) (Thermo Scientific DXR Raman microscope, 780 nm, 10 mW, 6 s exposure, 5 accumulations for (a-d), 5 mW, 5 s exposure, 8 accumulations for (e)).

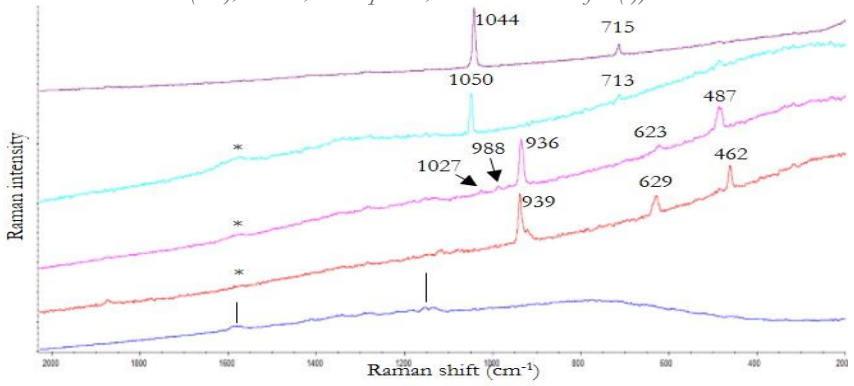

Appendix 68. Raman spectra of (a) ammonal (b) black powder (c) chloratite (d) flash powder particles on black polyester fibres (e) black polyester fibres (asterisks indicate black polyester bands) (Portable BWTEK i-Raman Pro, 785 nm, 1% of 320 mW, 1 s exposure, 10 accumulations).

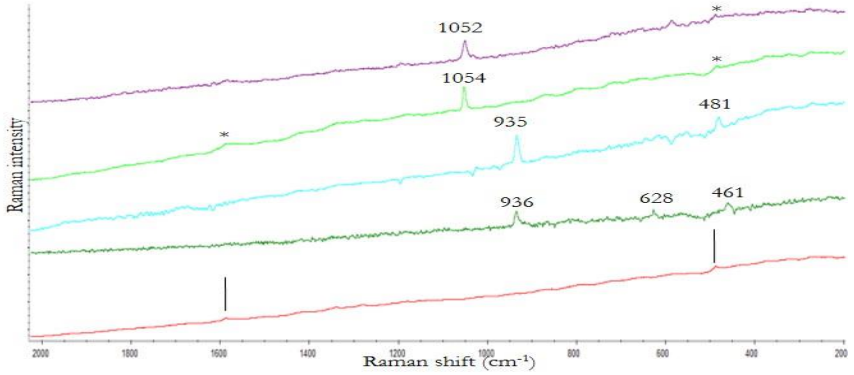

Appendix 69. Raman spectra of (a) ammonium nitrate (b) barium nitrate (c) potassium nitrate (d) sodium nitrate (e) potassium chlorate (f) sodium chlorate (g) potassium perchlorate particles on jeans B fibres (h) jeans B fibres (asterisks indicate jeans B bands) (Portable BWTEK i-Raman Pro, 785 nm, 1% of 320 mW, 0.3 s exposure, 10 accumulations).

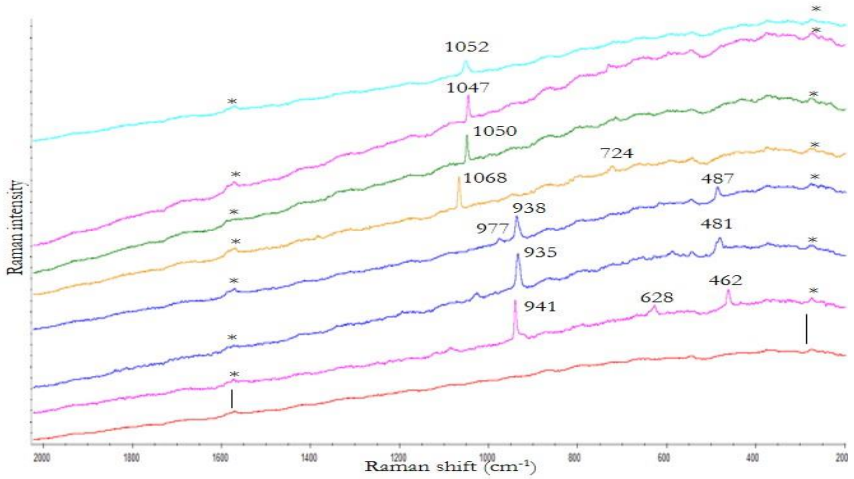

Appendix 70. Raman spectra of (a) TNT (b) PETN (c) RDX (d) HMTD particles on jeans B fibres (e) jeans B fibres (asterisks indicate jeans B bands) (Portable BWTEK i-Raman Pro, 785 nm, 1% of 320 mW, 3 s exposure, 5 accumulations for (a-d), 1% of 320 mW, 1 s exposure, 10 accumulations for (e)).

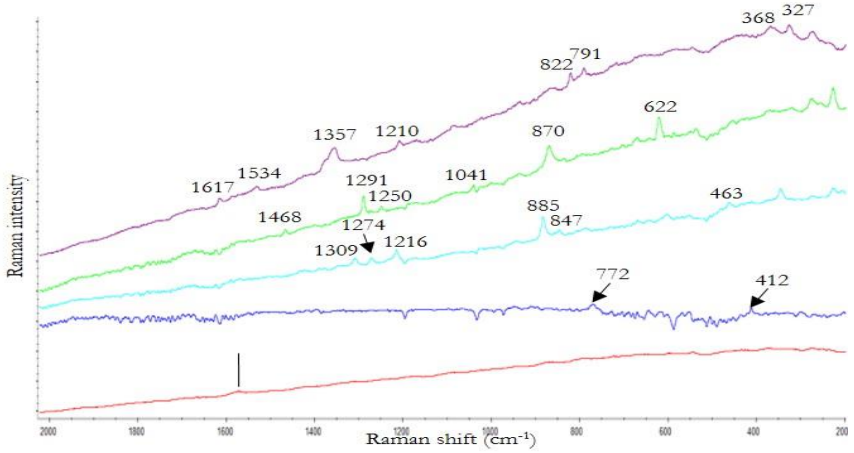

Appendix 71. Raman spectra of (a) ammonal (b) black powder (c) chloratite (d) flash powder particles on jeans B fibres (e) jeans B general fibres (asterisks indicate jeans B bands) (Portable BWTEK i-Raman Pro, 785 nm, 1% of 320 mW, 3 s exposure, 5 accumulations for (a-d), 1% of 320 mW, 1 s exposure, 10 accumulations for (e)).

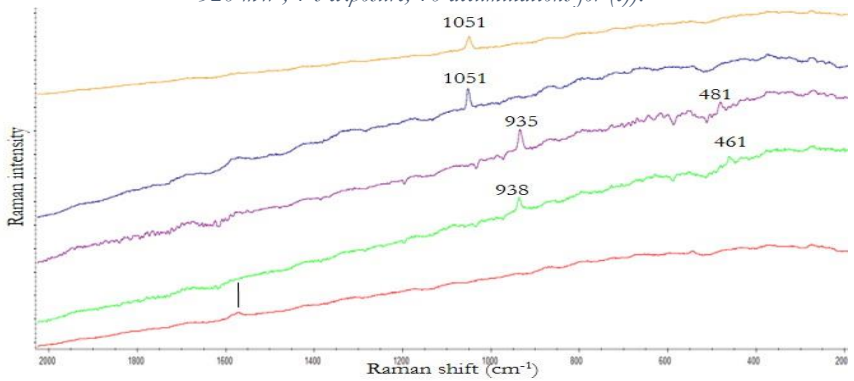

Appendix 72. Raman spectra of (a) ammonium nitrate (b) barium nitrate (c) potassium nitrate (d) sodium nitrate (e) potassium chlorate (f) sodium chlorate (g) potassium perchlorate particles on jeans A fibres (h) jeans A fibres (asterisks indicate jeans A bands) (Thermo Scientific DXR Raman microscope, 780 nm, 14 mW, 5 s exposure, 8 accumulations for (a-g), 1 mW, 6 s exposure, 5 accumulations for (h)).

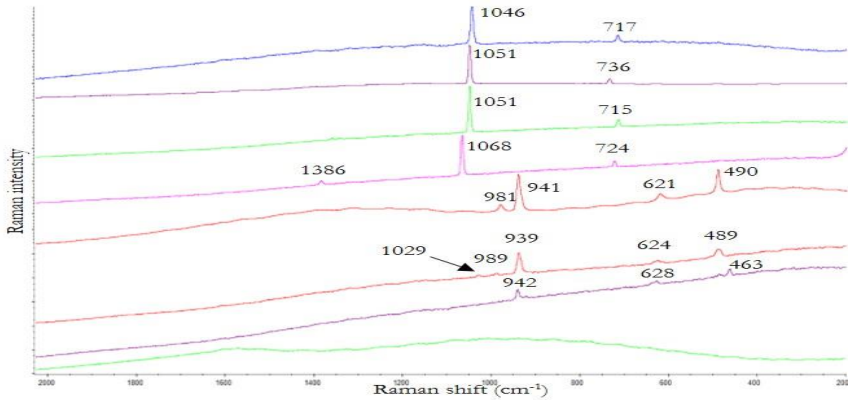

Appendix 73. Raman spectra of (a) ammonium nitrate (b) barium nitrate (c) potassium nitrate (d) sodium nitrate (e) potassium chlorate (f) sodium chlorate (g) potassium perchlorate particles on jeans A fibres (h) jeans A fibres (asterisks indicate jeans A bands) (Portable BWTEK i-Raman Pro, 785 nm, 1% of 320 mW, 0.3 s exposure, 10 accumulations).

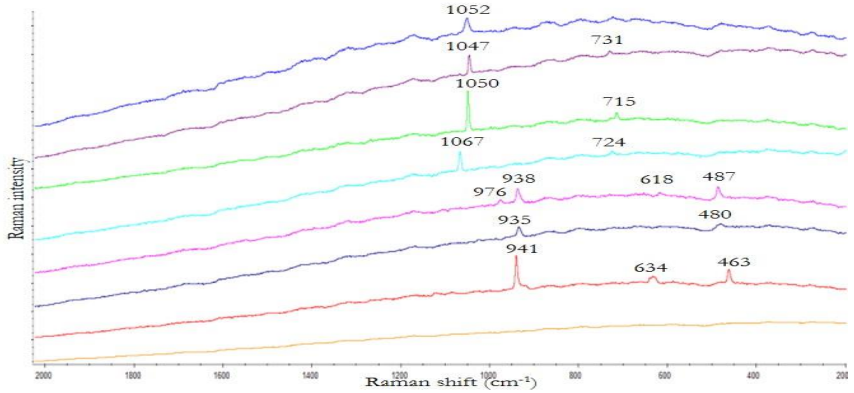

Appendix 74. Raman spectra of (a) TNT (b) PETN (c) RDX (d) HMTD particles on jeans A fibres (e) jeans A fibres (asterisks indicate jeans A bands) (Thermo Scientific DXR Raman microscope, 780 nm, 10 mW, 6 s exposure, 5 accumulations for (a-d), 1 mW, 6 s exposure, 5 accumulations for (e)).

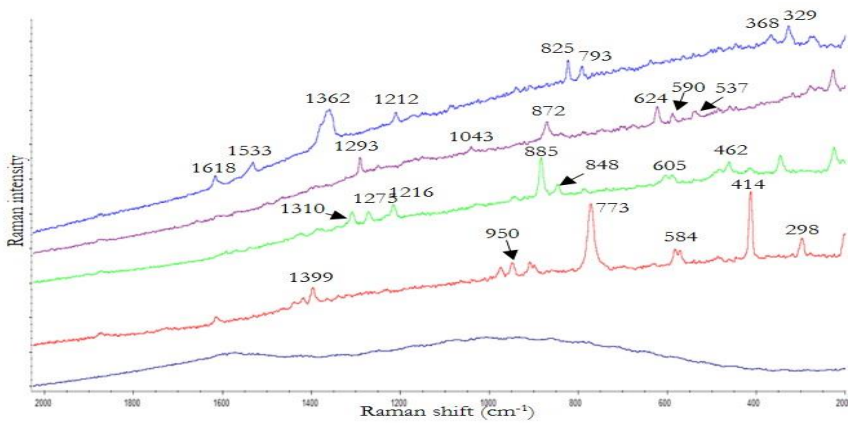

Appendix 75. Raman spectra of (a) TNT (b) PETN (c) RDX (d) HMTD particles on jeans A fibres (e) jeans A fibres (asterisks indicate jeans A bands) (Portable BWTEK i-Raman Pro, 785 nm, 1% of 320 mW, 3 s exposure, 5 accumulations for (a-d), 1% of 320 mW, 0.3 s exposure, 10 accumulations for (e)).

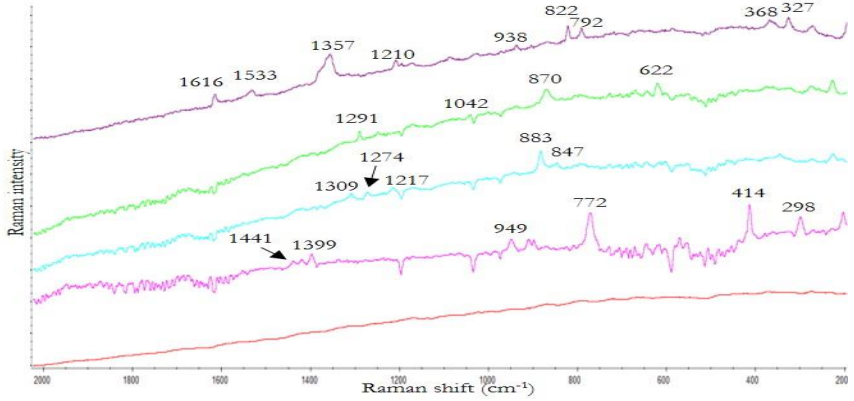

Appendix 76. Raman spectra of (a) ammonal (b) black powder (c) chloratite (d) flash powder particles on jeans A fibres (e) jeans A fibres (asterisks indicate jeans A bands) (Thermo Scientific DXR Raman microscope, 780 nm, 10 mW, 6 s exposure, 5 accumulations for (a-d), 1 mW, 6 s exposure, 5 accumulations for (e)).

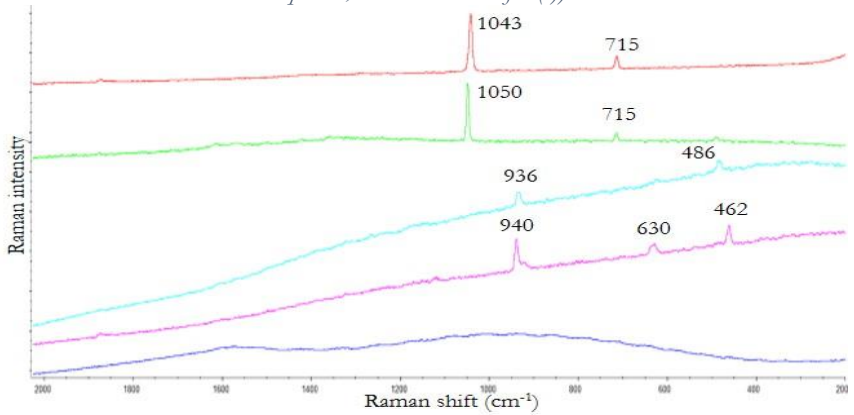

Appendix 77. Raman spectra of (a) ammonal (b) black powder (c) chloratite (d) flash powder particles on jeans A fibres (e) jeans A general fibres (f) jeans A white fibres (asterisks indicate jeans A bands) (Portable BWTEK i-Raman Pro, 785 nm, 1% of 320 mW, 3 s exposure, 5 accumulations for (a-d), 1% of 320 mW, 0.3 s exposure, 10 accumulations for (e), 1% of 320 mW, 1 s exposure, 10 accumulations for (f)).

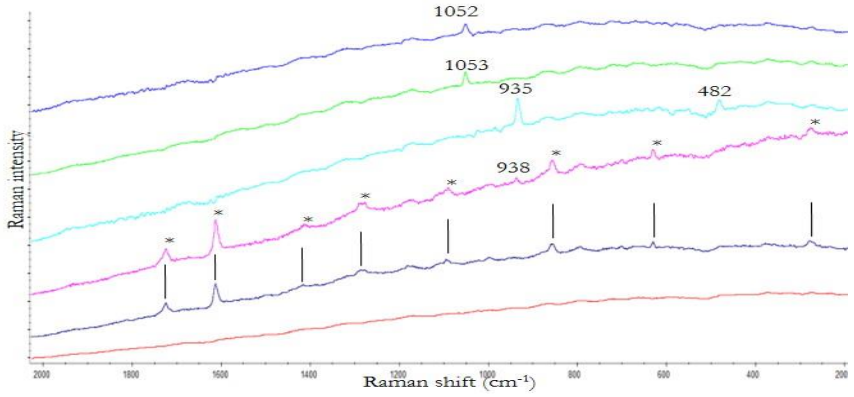

Appendix 78. Raman spectra of (a) ammonium nitrate (b) barium nitrate (c) potassium nitrate (d) sodium nitrate (e) potassium chlorate (f) sodium chlorate (g) potassium perchlorate particles on wool fibres (h) wool fibres (Portable BWTEK i-Raman Pro, 785 nm, 20% of 320 mW, 0.3 s exposure, 10 accumulations).

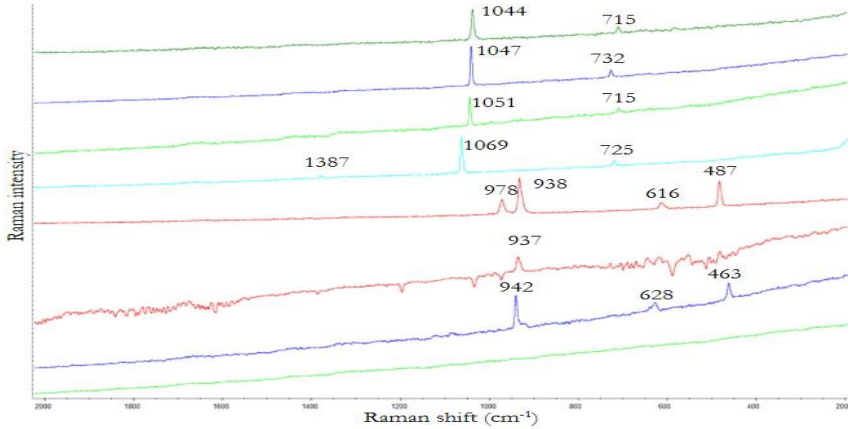

Appendix 79. Raman spectra of (a) TNT (b) PETN (c) RDX (d) HMTD particles on wool fibres (e) wool fibres (Portable BWTEK i-Raman Pro, 785 nm, 5% of 320 mW, 3 s exposure, 5 accumulations).

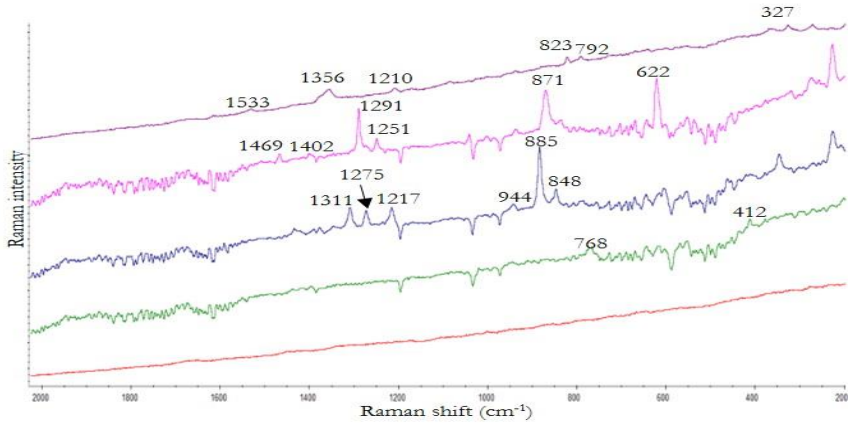

Appendix 80. Raman spectra of (a) ammonal (b) black powder (c) chloratite (d) flash powder particles on wool fibres (e) wool fibres (Portable BWTEK i-Raman Pro, 785 nm, 1% of 320 mW, 1 s exposure, 10 accumulations).

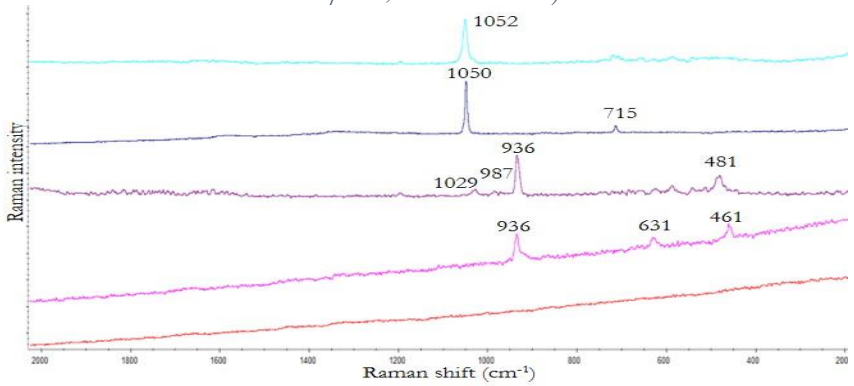

Appendix 81. Raman spectra of (a) ammonium nitrate (b) barium nitrate (c) potassium nitrate (d) sodium nitrate (e) potassium chlorate (f) sodium chlorate (g) potassium perchlorate particles on polyskin fibres (h) polyskin fibres (asterisks indicate polyskin bands) (Thermo Scientific DXR Raman microscope, 780 nm, 1 mW, 5 s exposure, 8 accumulations for (a-g), 1 mW, 6 s exposure, 5 accumulations for (h)).

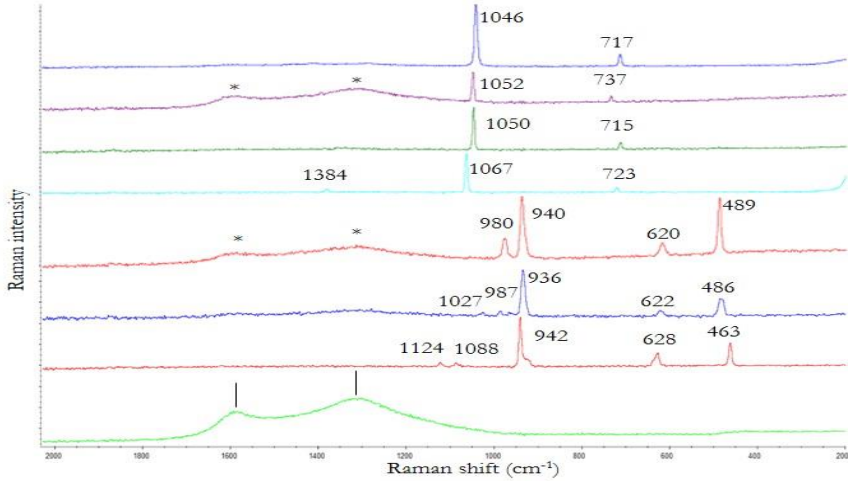

Appendix 82. Raman spectra of (a) TNT (b) PETN (c) RDX (d) HMTD particles on polyskin fibres (e) polyskin fibres (Thermo Scientific DXR Raman microscope, 780 nm, 1 mW, 6 s exposure, 5 accumulations for (a-d), 1 mW, 5 s exposure, 8 accumulations for (e)).

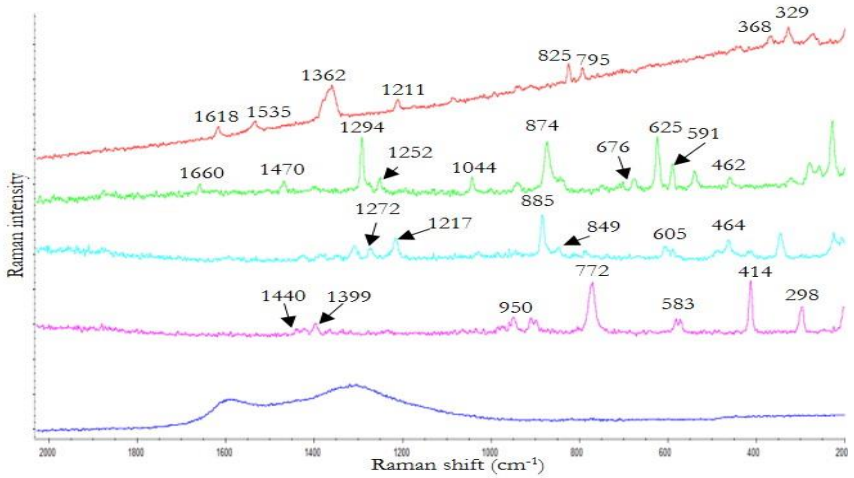

Appendix 83. Raman spectra of (a) ammonal (b) black powder (c) chloratite (d) flash powder particles on polyskin fibres (e) polyskin fibres (Thermo Scientific DXR Raman microscope, 780 nm, 1 mW, 6 s exposure, 5 accumulations for (a-d), 1 mW, 5 s exposure, 8 accumulations for (e)).

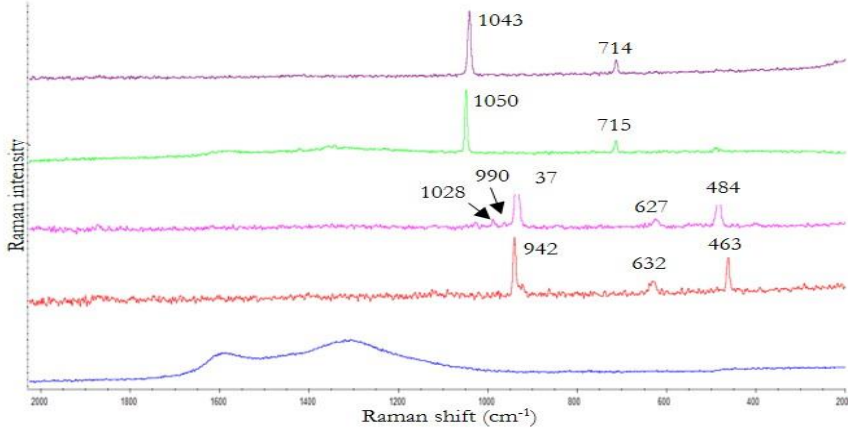

Appendix 84. Raman spectra of (a) ammonium nitrate (b) barium nitrate (c) potassium nitrate (d) sodium nitrate (e) potassium chlorate (f) sodium chlorate (g) potassium perchlorate particles on nitrile A (h) nitrile A (asterisks indicate nitrile A bands) (Portable BWTEK i-Raman Pro, 785 nm, 20% of 320 mW, 0.3 s exposure, 10 accumulations).

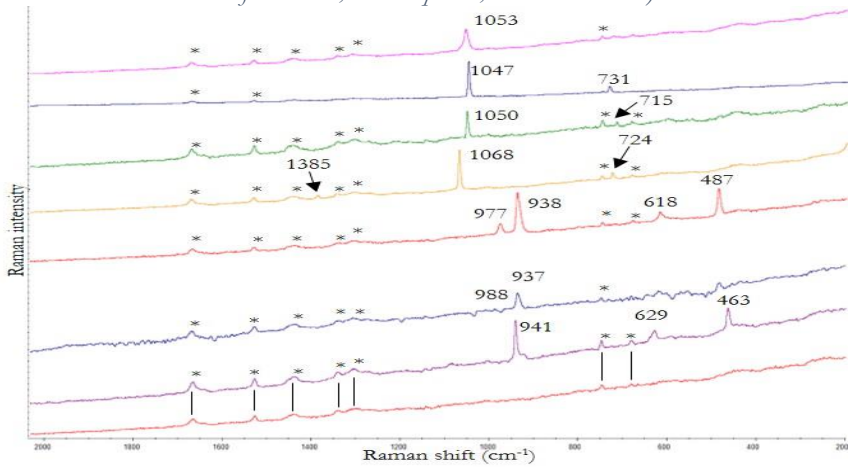

Appendix 85. Raman spectra of (a) TNT (b) PETN (c) RDX (d) HMTD particles on nitrile A (e) nitrile A (asterisks indicate nitrile A bands) (Portable BWTEK i-Raman Pro, 785 nm, 5% of 320 mW, 3 s exposure, 5 accumulations).

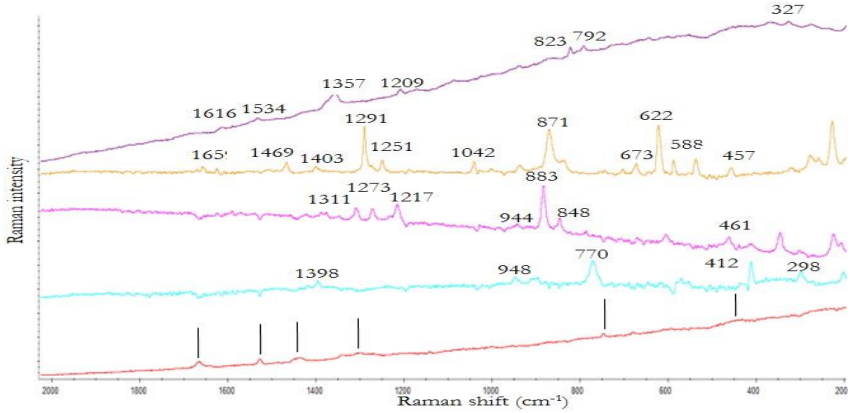

Appendix 86. Raman spectra of (a) ammonal (b) black powder (c) chloratite (d) flash powder particles on nitrile A (e) nitrile A (asterisks indicate nitrile A bands) (Portable BWTEK i-Raman Pro, 785 nm, 1% of 320 mW, 1 s exposure, 10 accumulations for (a-d), 5% of 320 mW for (e)).

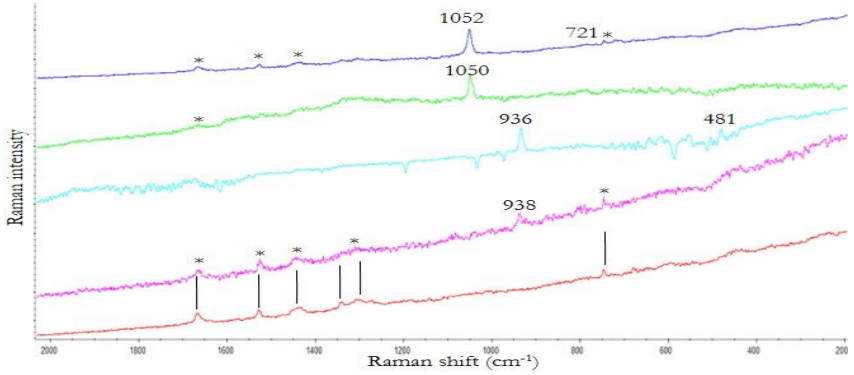

Appendix 87. Raman spectra of (a) ammonium nitrate (b) barium nitrate (c) potassium nitrate (d) sodium nitrate (e) potassium chlorate (f) sodium chlorate (g) potassium perchlorate particles on nitrile B (h) nitrile B (asterisks indicate nitrile B bands) (Thermo Scientific DXR Raman microscope, 780 nm, 14 mW, 5 s exposure, 8 accumulations).

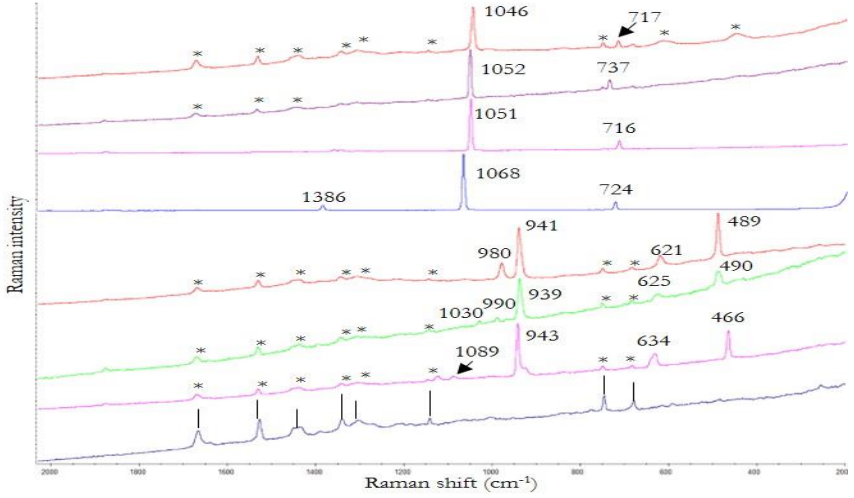

Appendix 88. Raman spectra of (a) ammonium nitrate (b) barium nitrate (c) potassium nitrate (d) sodium nitrate (e) potassium chlorate (f) sodium chlorate (g) potassium perchlorate particles on nitrile B (h) nitrile B (asterisks indicate nitrile B bands) (Portable BWTEK i-Raman Pro, 785 nm, 20% of 320 mW, 0.3 s exposure, 10 accumulations).

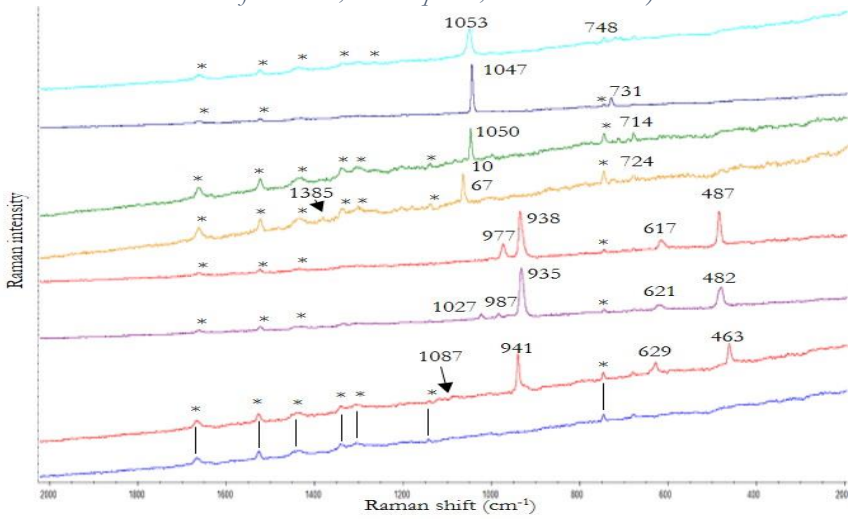

Appendix 89. Raman spectra of (a) TNT (b) PETN (c) RDX (d) HMTD particles on nitrile B (e) nitrile B (asterisks indicate nitrile B bands) (Thermo Scientific DXR Raman microscope, 780 nm, 10 mW, 6 s exposure, 5 accumulations).

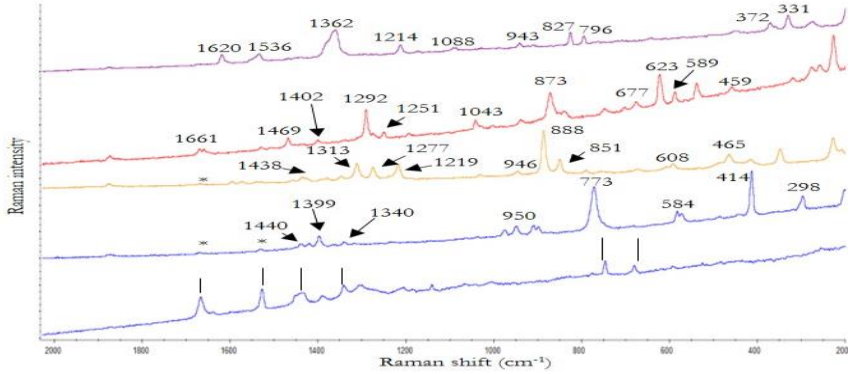

Appendix 90. Raman spectra of (a) TNT (b) PETN (c) RDX (d) HMTD particles on nitrile B (e) nitrile B (asterisks indicate nitrile B bands) (Portable BWTEK i-Raman Pro, 785 nm, 5% of 320 mW, 3 s exposure, 5 accumulations).

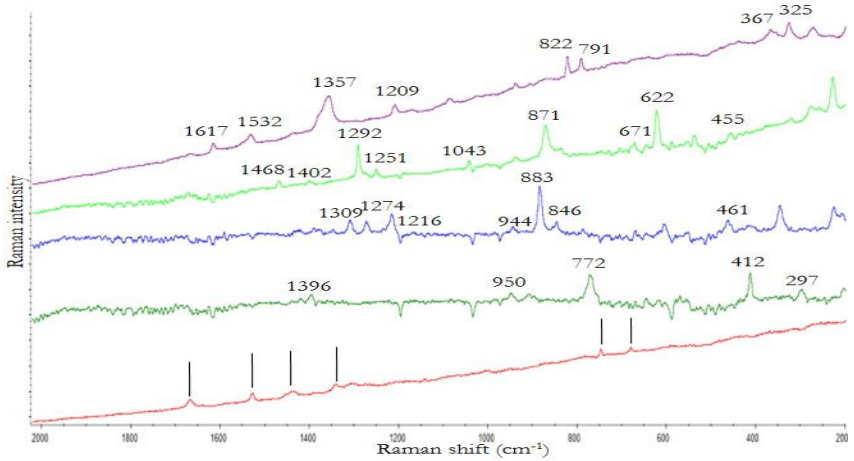

Appendix 91. Raman spectra of (a) ammonal (b) black powder (c) chloratite (d) flash powder particles on nitrile B (e) nitrile B (asterisks indicate nitrile B bands) (Thermo Scientific DXR Raman microscope, 780 nm, 10 mW, 6 s exposure, 5 accumulations).

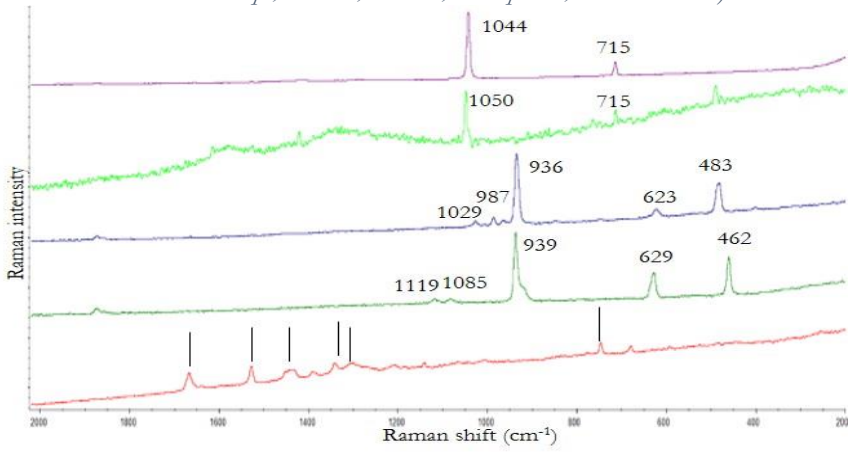

Appendix 92. Raman spectra of (a) ammonal (b) black powder (c) chloratite (d) flash powder particles on nitrile B (e) nitrile B (asterisks indicate nitrile B bands) (Portable BWTEK i-Raman Pro, 785 nm, 1% of 320 mW, 1 s exposure, 10 accumulations for (a-d), 5% of 320 mW for (e)).

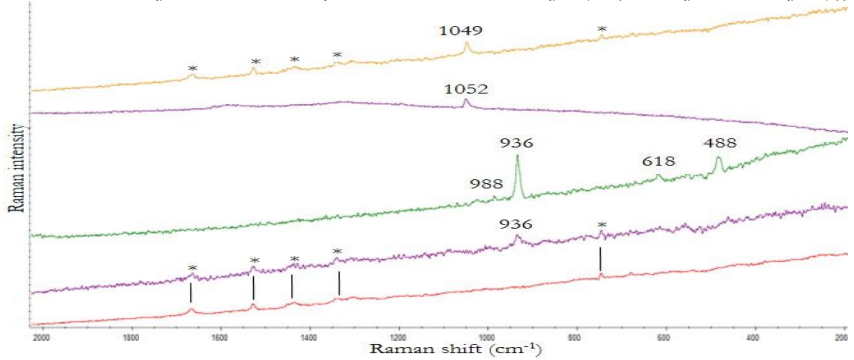

Appendix 93. Raman spectra of (a) ammonium nitrate (b) barium nitrate (c) potassium nitrate (d) sodium nitrate (e) potassium chlorate (f) sodium chlorate (g) potassium perchlorate particles on latex (h) latex (asterisks indicate latex bands) (Portable BWTEK i-Raman Pro, 785 nm, 20% of 320 mW, 0.3 s exposure, 10 accumulations).

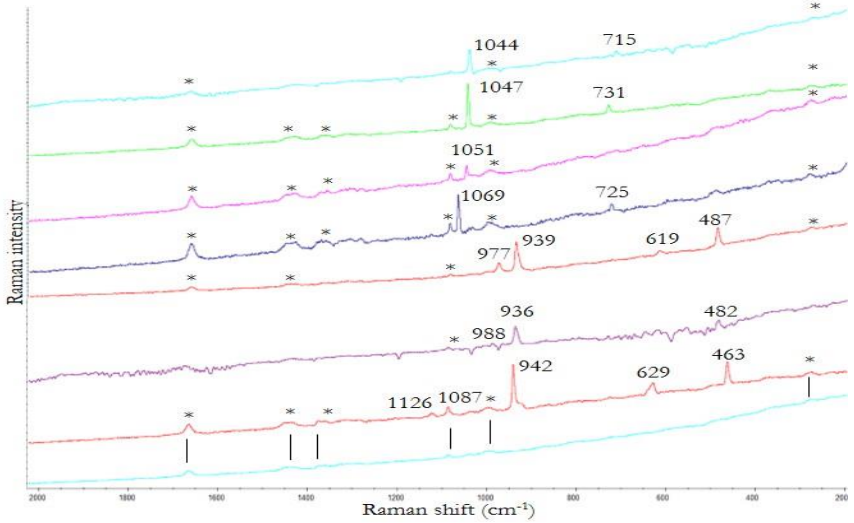

Appendix 94. Raman spectra of (a) TNT (b) PETN (c) RDX (d) HMTD particles on latex (e) latex (asterisks indicate latex bands) (Portable BWTEK i-Raman Pro, 785 nm, 5% of 320 mW, 3 s exposure, 5 accumulations).

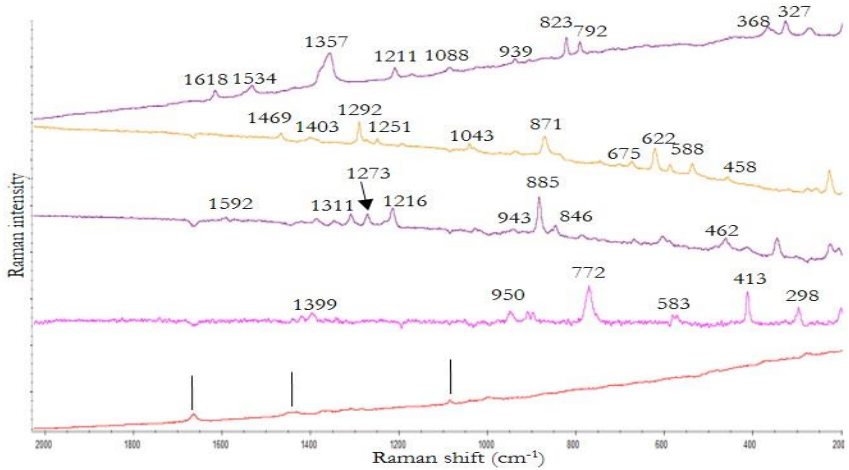

Appendix 95. Raman spectra of (a) ammonal (b) black powder (c) chloratite (d) flash powder particles on latex (e) latex (asterisks indicate latex bands) (Portable BWTEK i-Raman Pro, 785 nm, 1% of 320 mW, 1 s exposure, 10 accumulations for (a-d), 5% of 320 mW for (e)).

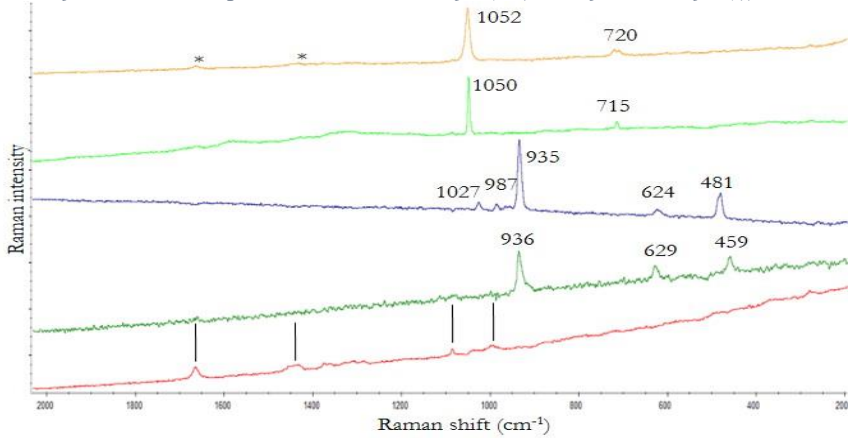

Appendix 96. Raman spectra of (a) ammonium nitrate trapped on blue cotton (b) blue cotton standard (c) ammonium nitrate standard (Portable BWTEK i-Raman pro, 785 nm, 1% of 320 mW, 0.3 s exposure, 10 accumulations).

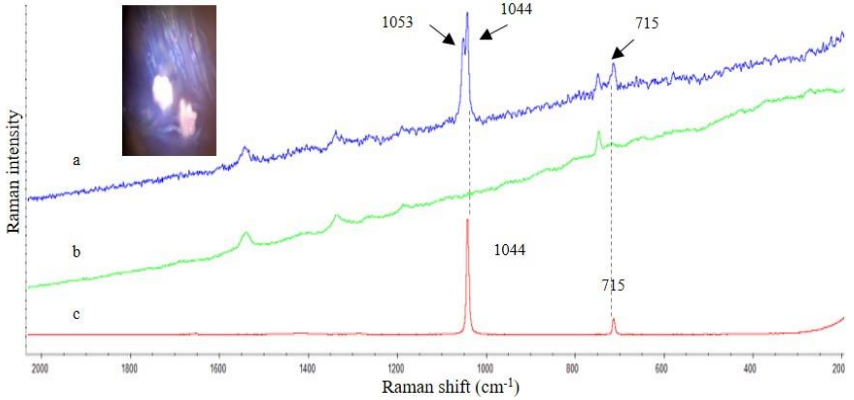

Appendix 97. Burning textile fabrics with the percentages (%) of the Portable BWTEK i-Raman pro laser power (320 mW): black cotton (A.1 – 1%; A.2 – 8%; A.3 – 20%), jeans B (B.1 – 10%, B.2 – 15%, B.3 – 20%), jeans A (C – 20%), blue cotton (D.1 – 10%, D.2 – 20%), and polyskin (E.1 – 1%, E.2 – 20%); (Portable BWTEK i-Raman Pro, 785 nm, 0.3 s exposure, 10 accumulations).

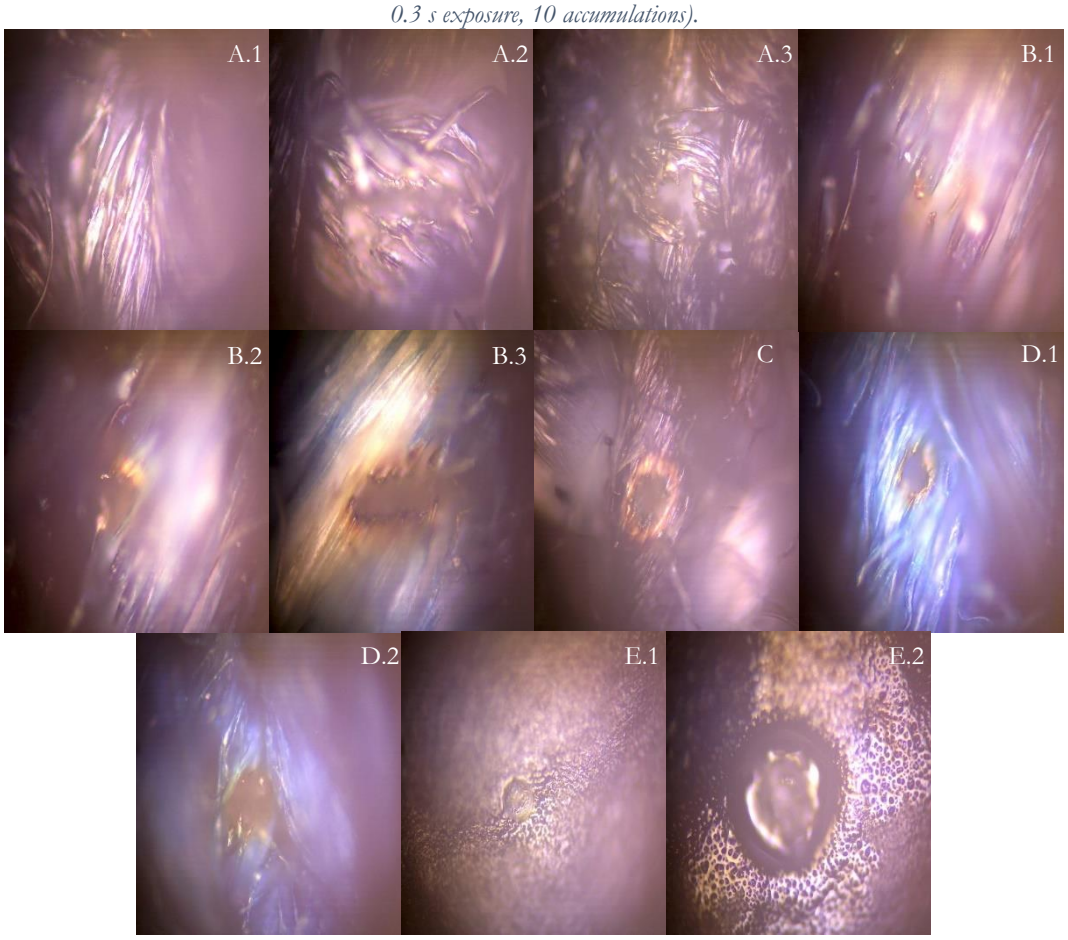

Appendix 98. Database search for the white cotton textile fabric (Thermo Scientific DXR Raman microscope).

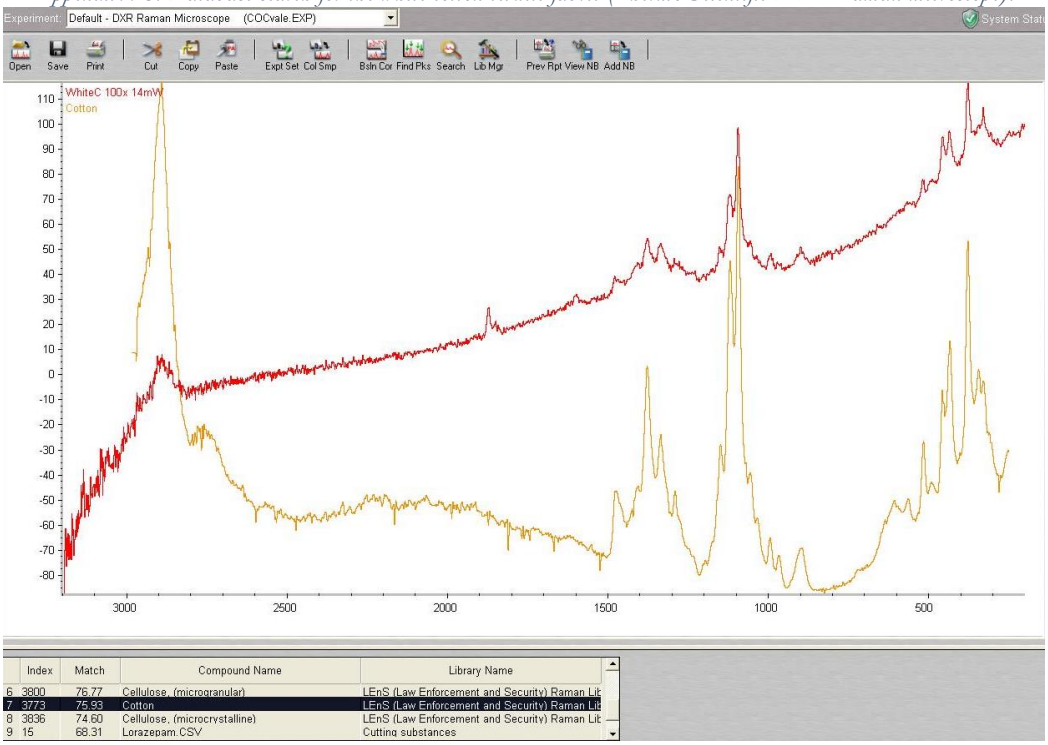

Appendix 99. Database search for the green cotton textile fabric (Thermo Scientific DXR Raman microscope).

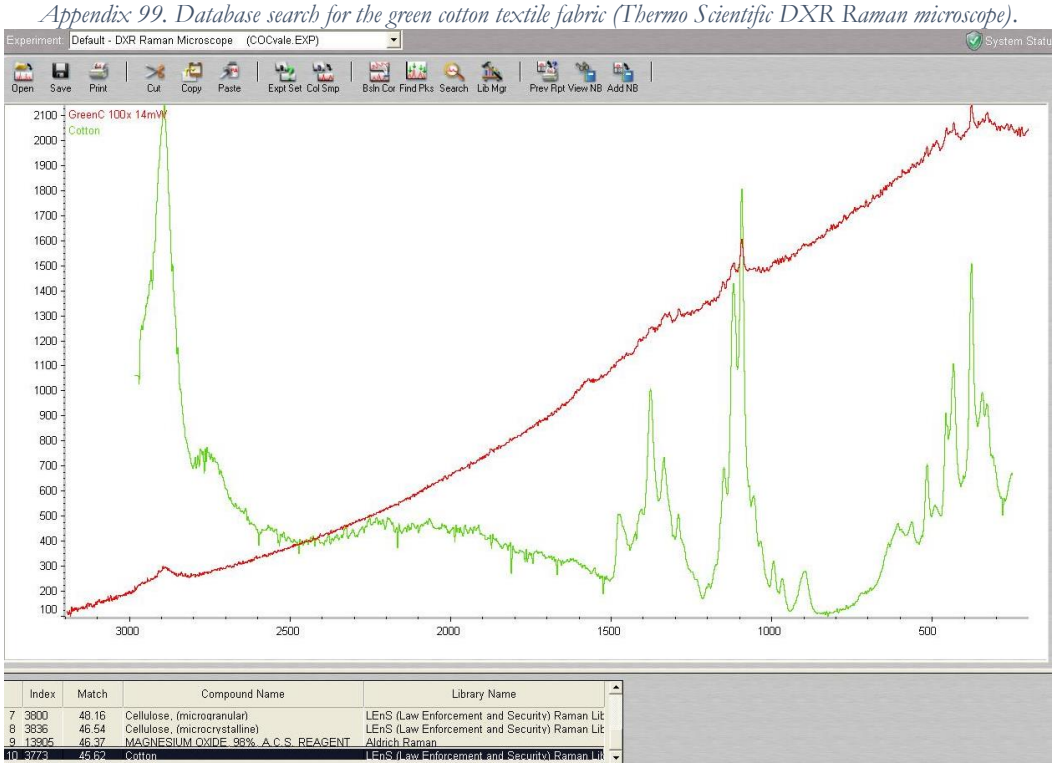

Appendix 100. Database search for the red cotton textile fabric (Thermo Scientific DXR Raman microscope).

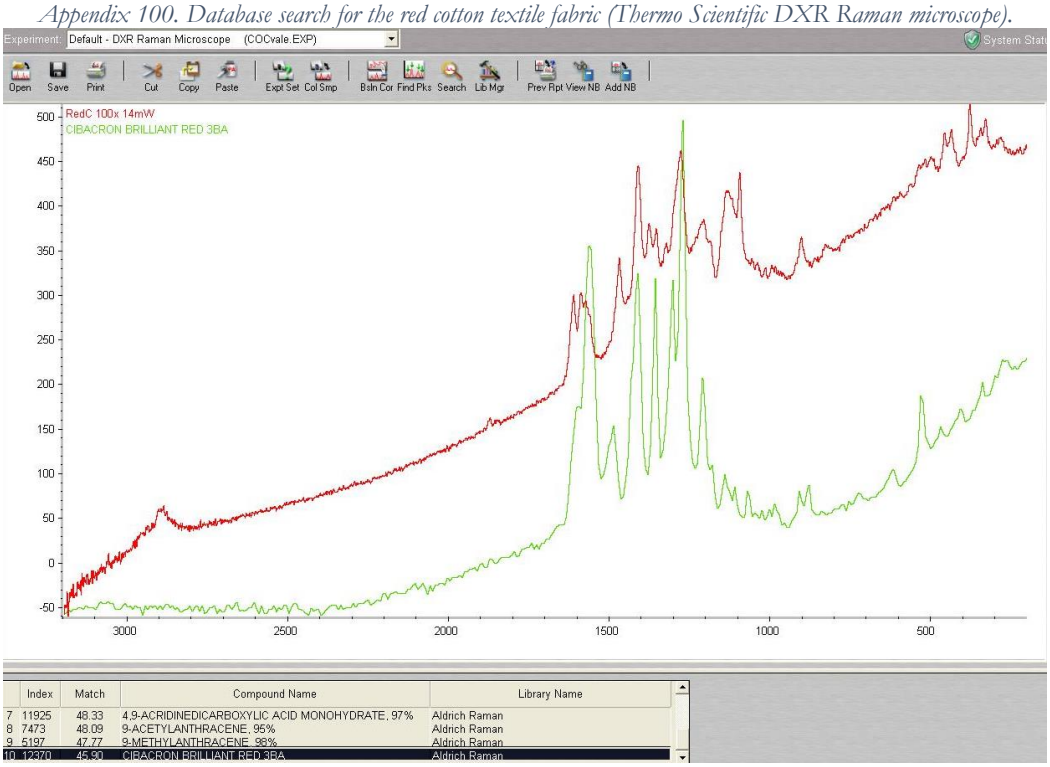

Appendix 101. Database search for the blue denim jeans textile fabric (Thermo Scientific DXR Raman microscope).

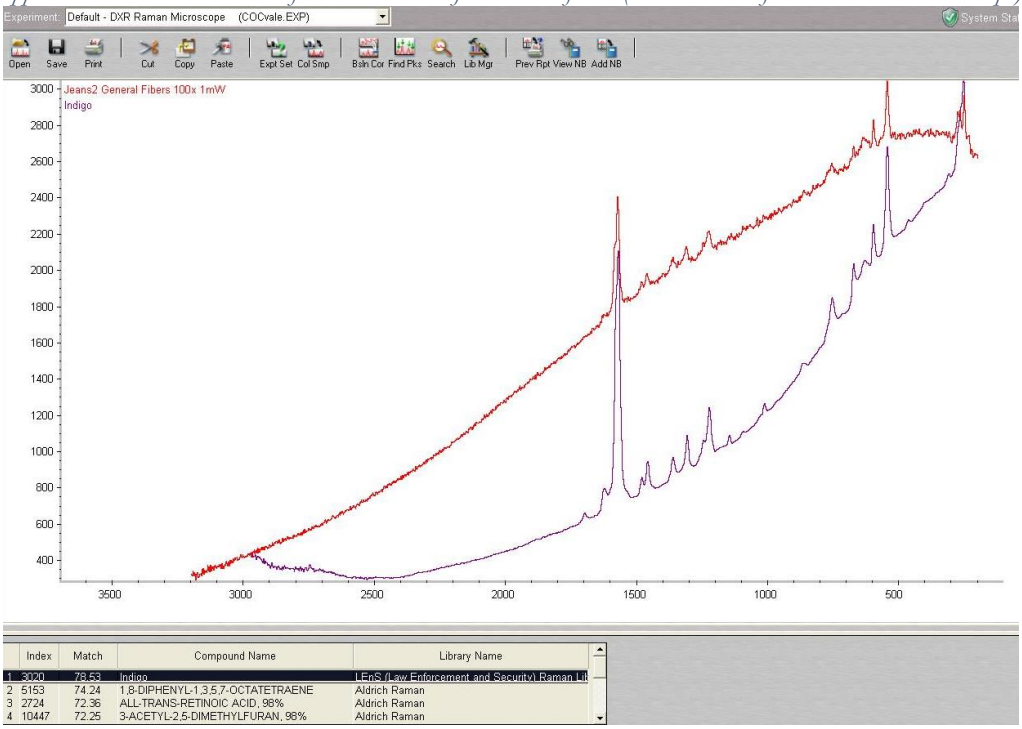

Appendix 102. Scales used for the calculation of the oxidizing salts and explosive particles analysed by the Thermo Scientific DXR Raman microscope.

Thermo Scientific DXR Raman microscope		
Microscope objective	Distance in pixels	Scale (µm)
100x	66,959	10
	68,2845	
	65,6067	
	68,2845	
	68,2845	
Mean (100x - 10 µm)	**67,48384**	
50x	168,7029	50
	167,364	
	171,3808	
	167,364	
	170,0418	
Mean (50x - 50 µm)	**168,9707**	
20x	70,9623	50
	72,3013	
	72,3013	
	70,9623	
	73,6523	
Mean (20x - 50 µm)	**72,0359**	
10x	33,4728	50
	33,4996	
	34,8117	
	34,8117	
	33,4728	
Mean (10x - 50 µm)	**34,01372**	

Appendix 103. Scales used for the calculation of the oxidizing salts and explosive particles analyzed by the Portable BW&TEK i-Raman Pro.

Portable BW&TEK i-Raman Pro		
Microscope objective	Distance in pixels	Scale (µm)
40x	**1704,41392**	1000
20x	848,1698	1000
	855,8972	
	846,6617	
	856,9527	
	853,3534	
Mean (20x - 1000 µm)	**852,207**	

Appendix 104. Raman spectra of the 10 interfering substances: (a) white sugar, (b) powdered sugar, (c) brown sugar, (d) charcoal, (e) aluminium, (f) wheat flour, (g) corn starch ("Maizena"), (h) chocolate cocoa powder "Brand 2" white particles, (i) chocolate cocoa powder "Brand 1" white particles, (j) chocolate cocoa powder "Brand 2" brown particles, (k) chocolate cocoa powder "Brand 1" brown particles, and (l) talc powder (Portable BWTEK i-Raman pro, 785 nm, 20% of 320 mW, 3 s exposure, 10 accumulations for (a), (b), (c), (f), (g), (h), (i), and (l); 1% of 320 mW for (d), (e); 5% of 320 mW for (j) and (k)).

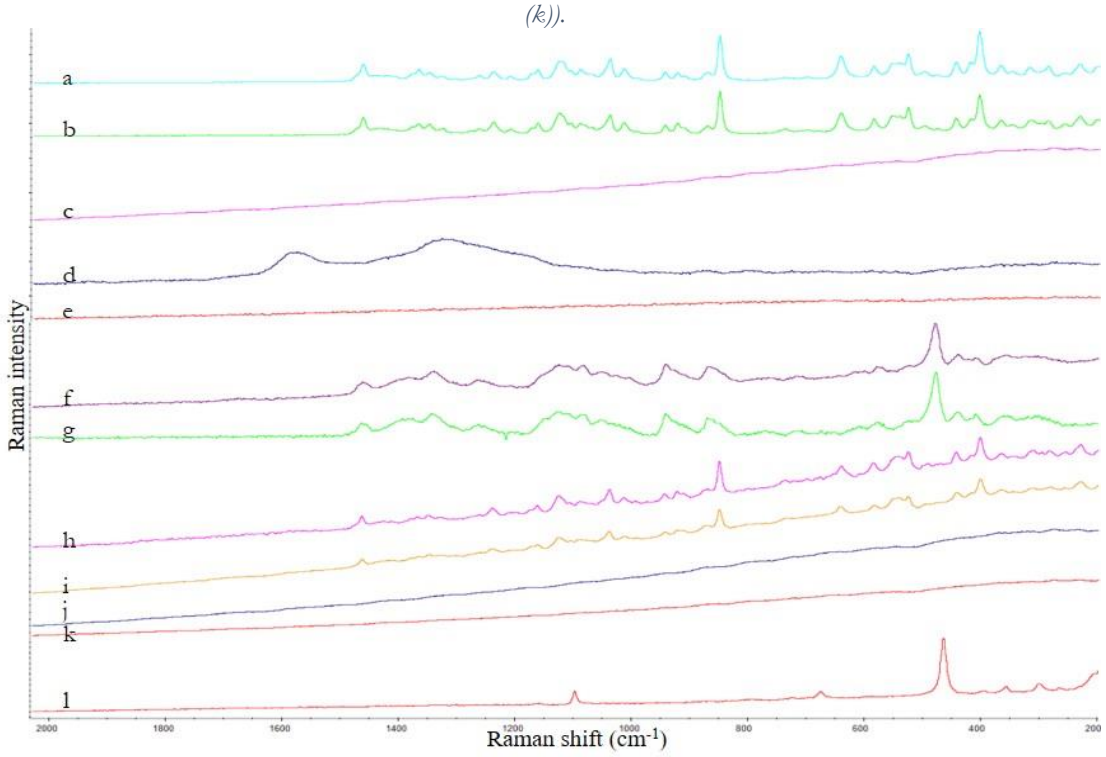

Appendix 105. Images of the interfering substances (fuels); Right to left: white normal sugar (10x), powdered sugar (10x), brown sugar (10x), charcoal (10x), aluminium (10x), wheat flour (10x), corn starch ("Maizena") (10x), chocolate cocoa powder "Brand 1" (10x), chocolate cocoa powder "Brand 1" white particle (50x), chocolate cocoa powder "Brand 1" brown particle (10x), chocolate cocoa powder "Brand 2" (10x), chocolate cocoa powder "Brand 2" white particle (50x), chocolate cocoa powder "Brand 2" brown particle (50x), talc powder (10x) (Thermo Scientific DXR Raman microscope).

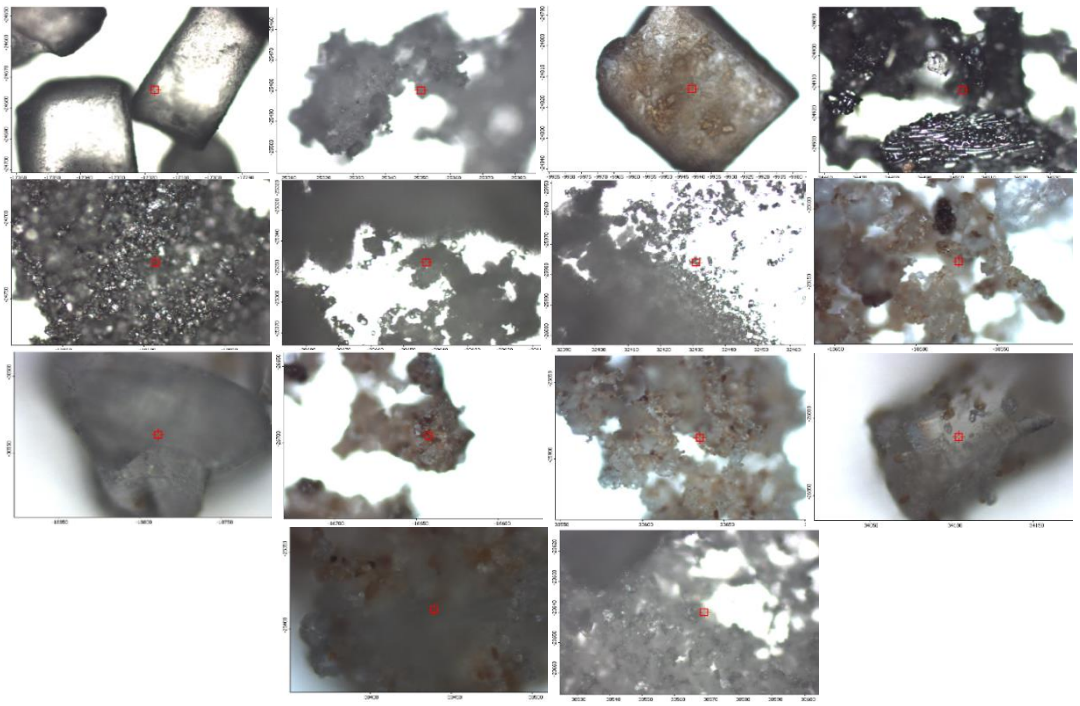

Appendix 106. Database search for the interfering substances (top to bottom): white sugar, powdered sugar, chocolate cocoa powder "Brand 1", and chocolate cocoa powder "Brand 2" (Thermo Scientific DXR Raman microscope).

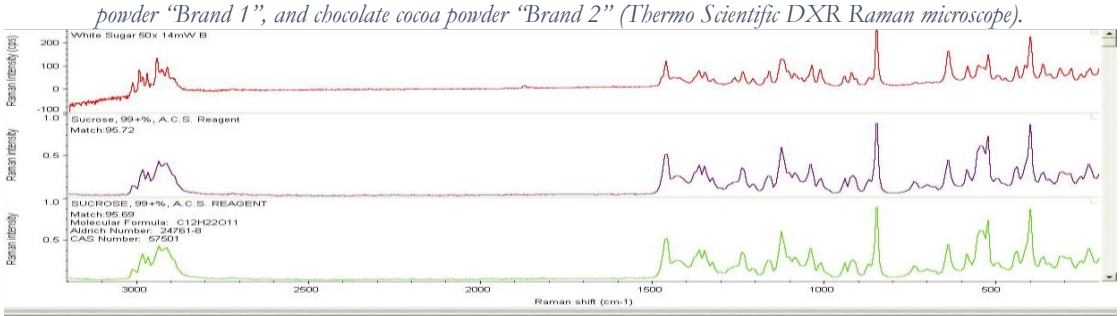

Index	Match	Compound Name	Library Name
1 26	95.72	Sucrose, 99+%, A.C.S. Reagent	Raman Sample Library
2 929	95.69	SUCROSE, 99+%, A.C.S. REAGENT	Aldrich Raman
3 278	91.66	Sucrose	HR Pharmaceutical Excipients FT-Raman Library
4 3065	91.31	Sugar, granulated	LEnS (Law Enforcement and Security) Raman Lit
5 280	91.03	Sugar, Confectioner's	HR Pharmaceutical Excipients FT-Raman Library
6 3071	90.72	Confectioners sugar	LEnS (Law Enforcement and Security) Raman Lit
7 3126	90.42	LIPASE, TYPE II, CRUDE, FROM PORCINE PAI	Aldrich Raman
8 3701	87.47	Sucrose	LEnS (Law Enforcement and Security) Raman Lit
9 5060	68.11	Methyl acetate	LEnS (Law Enforcement and Security) Raman Lit
10 3134	67.74	METHYL ACETATE, 99%	Aldrich Raman

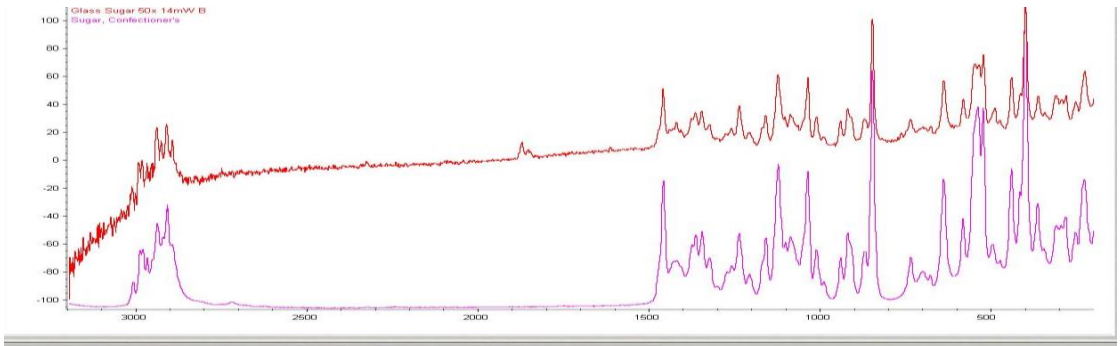

Index	Match	Compound Name	Library Name
3 3126	94.69	LIPASE, TYPE II, CRUDE, FROM PORCINE PAI	Aldrich Raman
4 280	93.96	Sugar, Confectioner's	HR Pharmaceutical Excipients FT-Raman Library
5 278	93.96	Sucrose	HR Pharmaceutical Excipients FT-Raman Library
6 3065	93.11	Sugar, granulated	LEnS (Law Enforcement and Security) Raman Lit

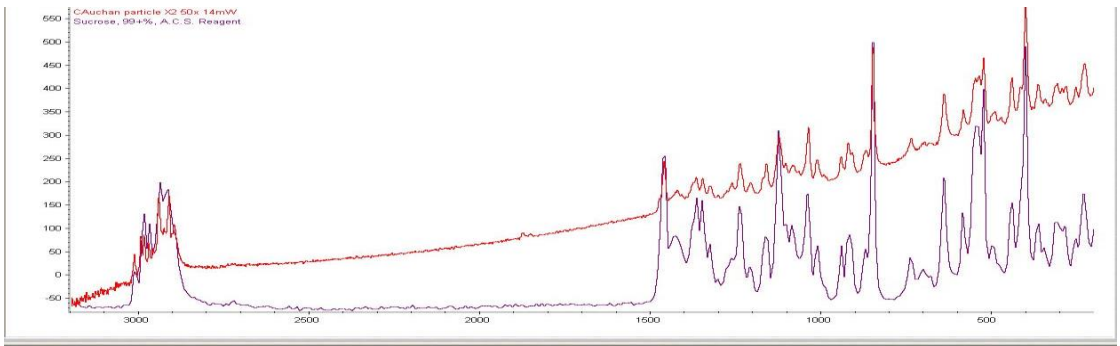

Index	Match	Compound Name	Library Name
1 26	98.03	Sucrose, 99+%, A.C.S. Reagent	Raman Sample Library
2 929	97.96	SUCROSE, 99+%, A.C.S. REAGENT	Aldrich Raman
3 278	94.26	Sucrose	HR Pharmaceutical Excipients FT-Raman Library
4 280	94.24	Sugar, Confectioner's	HR Pharmaceutical Excipients FT-Raman Library

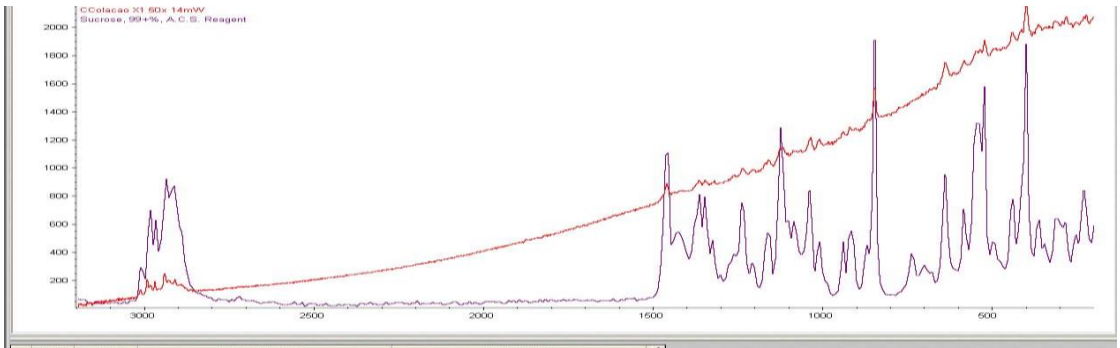

Index	Match	Compound Name	Library Name
1 26	87.24	Sucrose, 99+%, A.C.S. Reagent	Raman Sample Library
2 929	86.78	SUCROSE, 99+%, A.C.S. REAGENT	Aldrich Raman
3 3126	83.36	LIPASE, TYPE II, CRUDE, FROM PORCINE PAI	Aldrich Raman
4 278	82.64	Sucrose	HR Pharmaceutical Excipients FT-Raman Library

Appendix 107. Database search for the interfering substances (top to bottom): wheat flour and corn starch ("Maizena") (Thermo Scientific DXR Raman microscope).

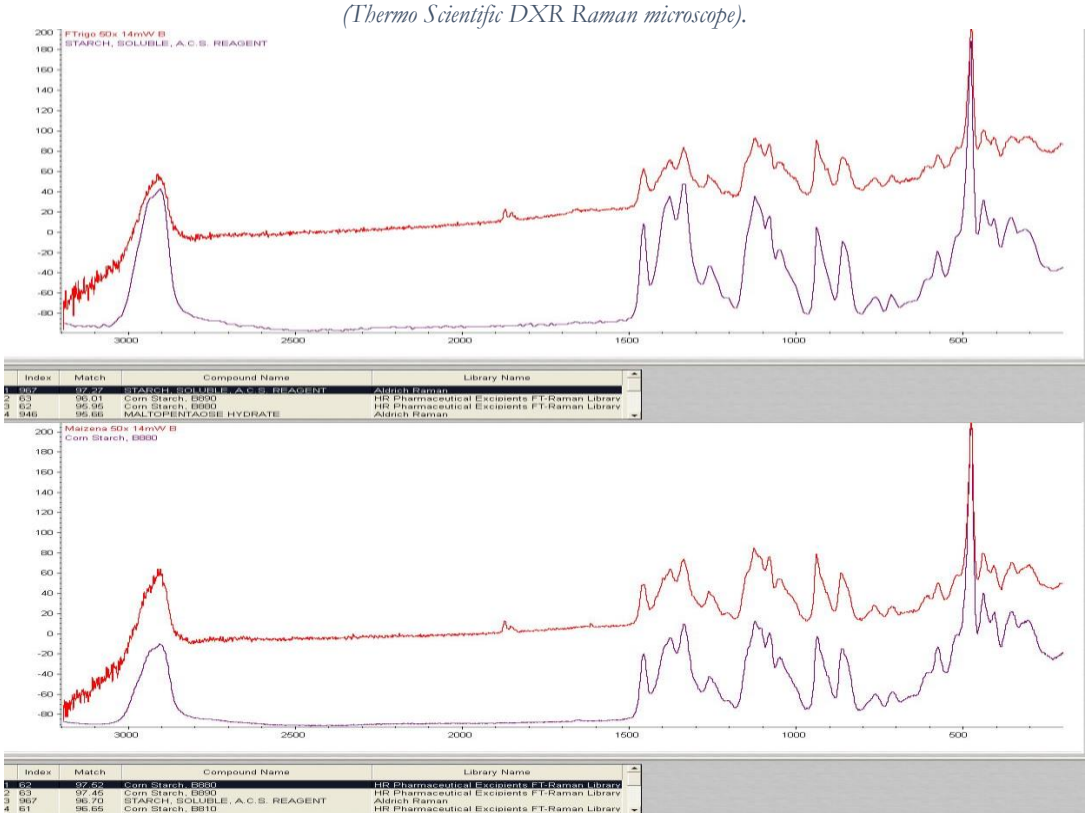

Appendix 108. Raman spectra of (a) PN + white sugar, (b) PN + powdered sugar, (c) PN + brown sugar, and (d) potassium nitrate (PN) (Portable BWTEK i-Raman pro, 785 nm, 20% of 320 mW, 3 s, 10 accumulations, 0.3 s for (d)).

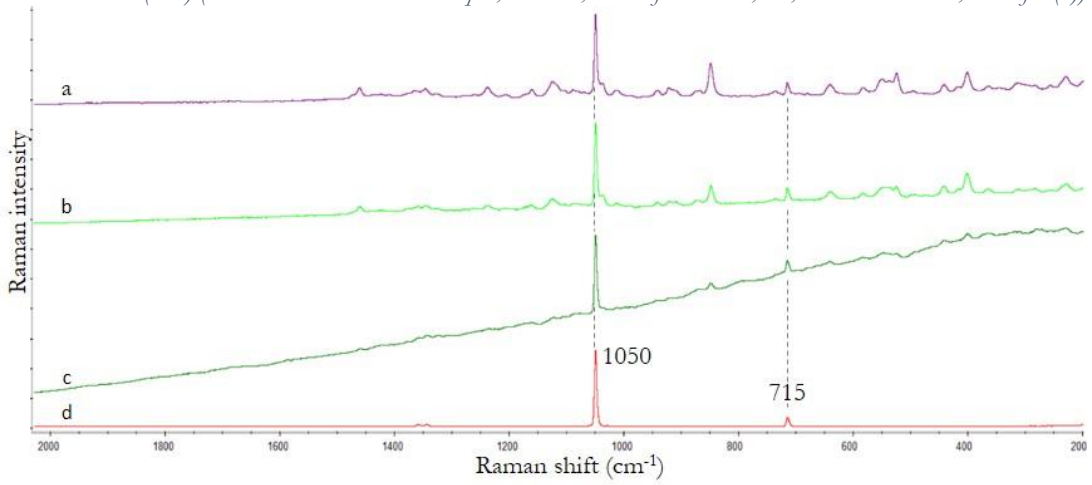

Appendix 109. Raman spectra of (a) PN + wheat flour, (b) PN + corn starch ("Maizena"), (c) PN + talc powder, and (d) potassium nitrate (PN) (Portable BWTEK i-Raman pro, 785 nm, 20% of 320 mW, 3 s, 10 accumulations; 0.3 s for (d)).

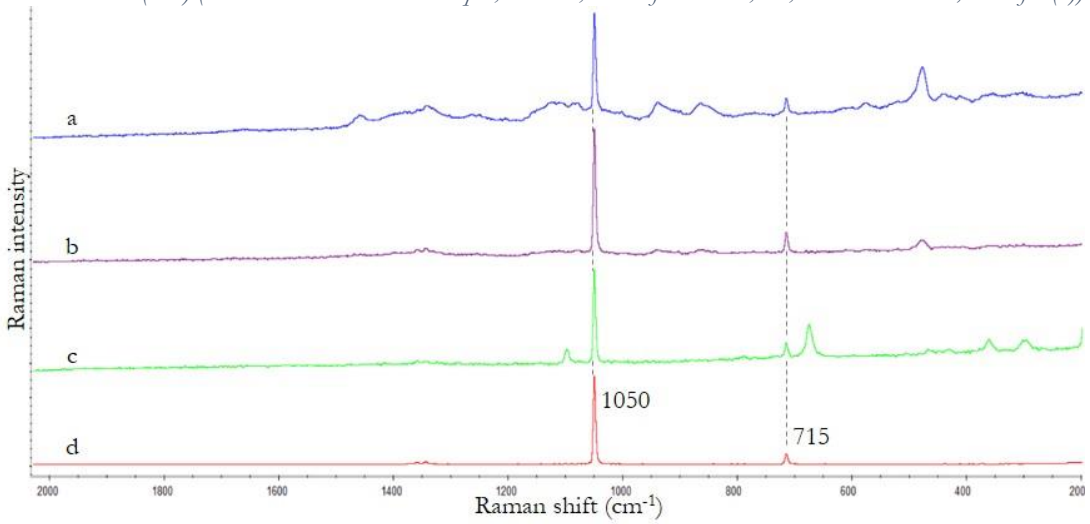

Appendix 110. Raman spectra of (a) PN + chocolate cocoa powder "Brand 1" white particles, (b) PN + chocolate cocoa powder "Brand 2" white particles, (c) potassium nitrate (PN) (Portable BWTEK i-Raman pro, 785 nm, 20% of 320 mW, 3 s, 10 accumulations, 0.3 s for (d)).

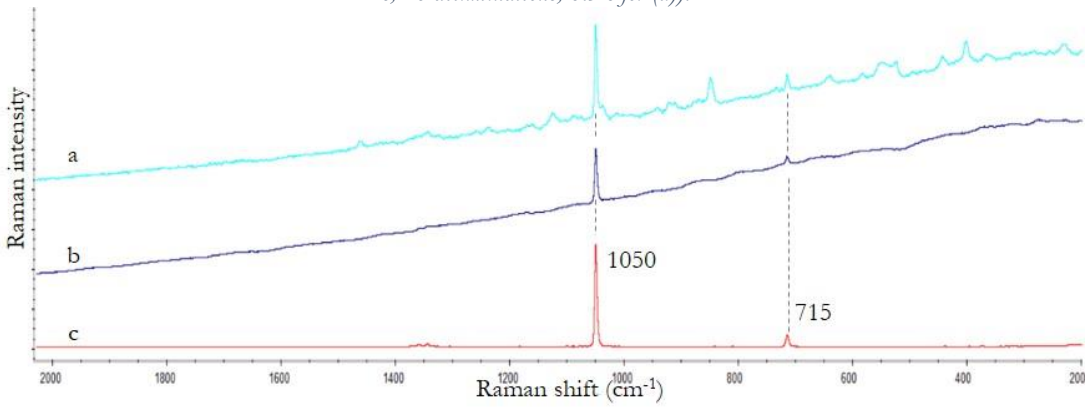

Appendix 111. Raman spectra of (a) PN + aluminium powder, (b) PN + charcoal, (c) potassium nitrate (PN) (Portable BWTEK i-Raman pro, 785 nm, 1% of 320 mW, 3 s, 10 accumulations for (a) and (b); 20% of 320 mW, 0.3 s for (c)).

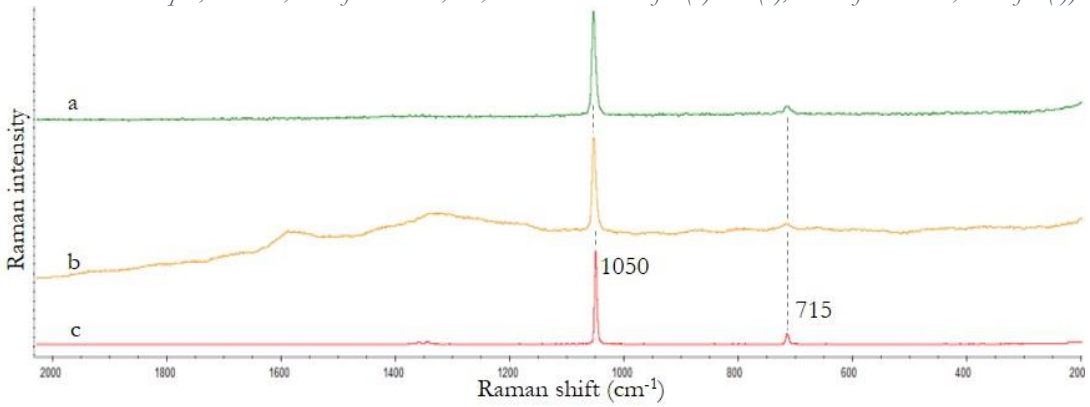

Appendix 112. Raman spectra and images (left to right) of (a) PN + white sugar, (b) PN + powdered sugar, (c) PN + brown sugar, (d) rec cotton fibre, and (e) potassium nitrate (PN) trapped on red cotton fibres (Portable BWTEK i-Raman pro, 785 nm, 20% of 320 mW, 3 s, 10 accumulations; 0.3 s for (e)).

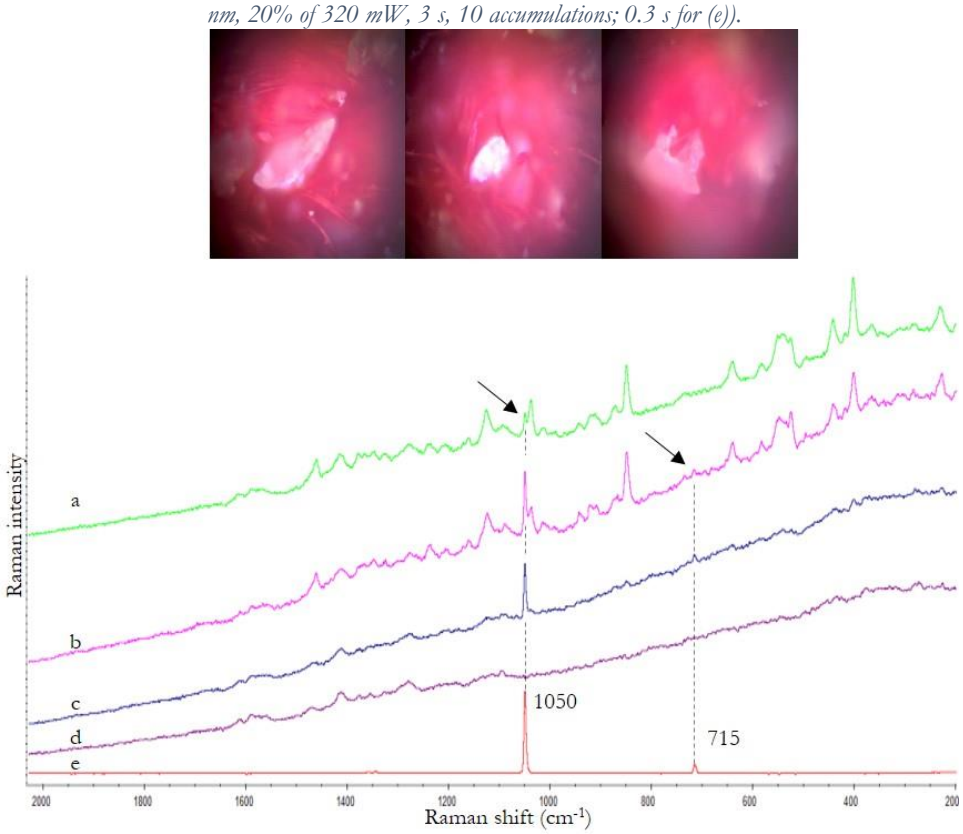

Appendix 113. Raman spectra and images (left to right) of (a) PN + wheat flour, (b) PN + corn starch ("Maizena") (c) PN + talc powder, (d) rec cotton fibre, and (e) potassium nitrate (PN) trapped on red cotton fibres (Portable BWTEK i-Raman pro, 785 nm, 20% of 320 mW, 3 s, 10 accumulations; 0.3 s for (e)).

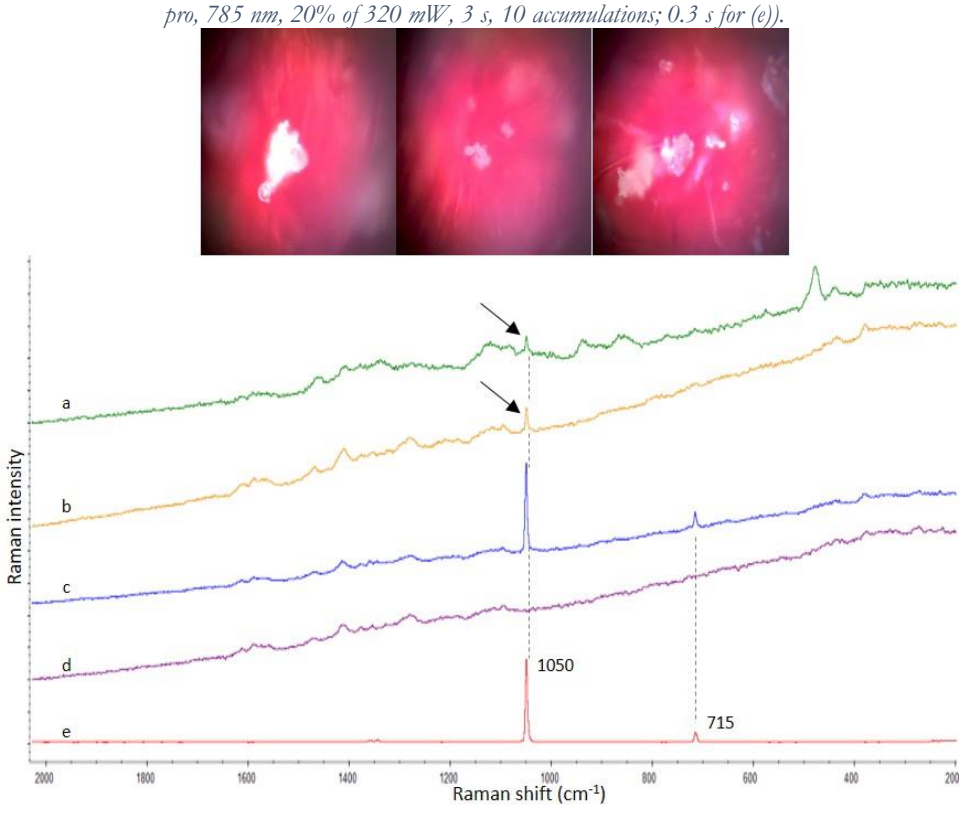

Appendix 114. Raman spectra and images (left to right) of (a) PN + chocolate cocoa powder "Brand 1" white particle, (b) PN + chocolate cocoa powder "Brand 2" white particle (c) rec cotton fibre, and (d) potassium nitrate (PN) trapped on red cotton fibres (Portable BWTEK i-Raman pro, 785 nm, 20% of 320 mW, 3 s, 10 accumulations; 0.3 s for (d)).

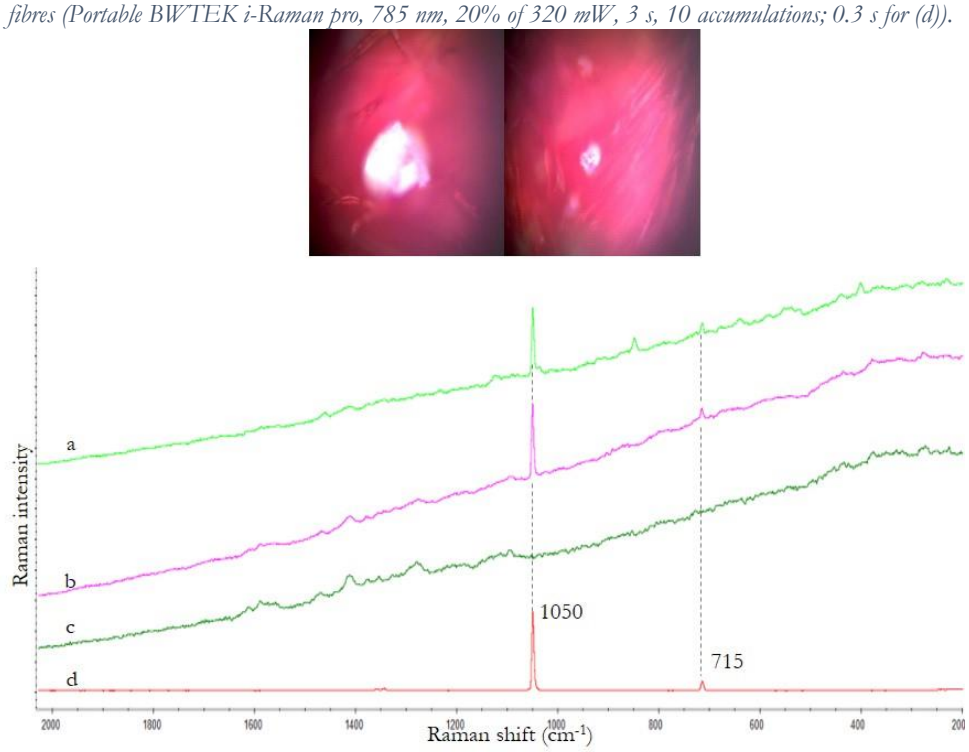

Appendix 115. Raman spectra and images (left to right) of (a) PN + aluminium powder, (b) PN + charcoal (c) rec cotton fibre, and (d) potassium nitrate (PN) trapped on red cotton fibres (Portable BWTEK i-Raman pro, 785 nm, 5% of 320 mW, 3 s, 10 accumulations for (a); 10% of 320 mW for (b); and 20% of 320 mW, 0.3 s for (d)).